HARMONIC WAVELET ANALYSIS OF SURFACE WAVES AT COMPLEX GEOTECHNICAL SITES

A Dissertation

presented to

the Faculty of the Graduate School

at the University of Missouri

In Partial Fulfillment

of the Requirements for the Degree

Doctor of Philosophy

---

by

MOHAMMED KHAN

Dr. Brent L. Rosenblad, Dissertation Supervisor

December 2020

The undersigned, appointed by the dean of the Graduate School, have examined the dissertation entitled

HARMONIC WAVELET ANALYSIS OF SURFACE WAVES AT COMPLEX GEOTECHNICAL SITES

presented by Mohammed Khan,

a candidate for the doctor of philosophy,

and hereby certify that, in their opinion, it is worthy of acceptance.

Professor Brent L. Rosenblad, PhD, PE

Professor John J. Bowders, Jr., PhD, PE

Professor J. Erik Loehr, PhD, PE

Professor Eric Sandvol, PhD

This dissertation is dedicated to

My mother, Jamila, whose love, encouragement, patience, and prayers carried me through the entire dissertation process, My sister, Shamim, who was always available to talk when I most needed it, and My friends who have been true friends.

ACKNOWLEDGEMENTS

All Praise is for Allah, the Lord of All Creation

I would like to express my great thanks and sincerest gratitude to my advisor, Dr. Rosenblad, for his valuable advice, patience, guidance and generous assistance given through the time of preparation of this work. His is truly an expert in the field of surface wave analyses for geotechnical engineering, and it has been an honor to work with him on this research. The pursuit of perfection he expected will greatly benefit me in my professional world. I would like to thank Dr. Rosenblad for his extensive and detailed revisions of my work, which made this dissertation what it is today.

1 must thank the entire faculty and staff members in the department who helped me over the years. Dr. Bowders for his practice, encouragement, enthusiasm for geotechnical engineering, and support during my time at the University of Missouri.

I thank Dr. Loehr for passing his in depth knowledge and experience of geotechnical engineering to me. It is my great pleasure to have them as members of the committee for this dissertation.

I greatly appreciate Dr. Eric Sandvol for taking the time to participate on my dissertation committee and giving me his valuable advice.

Also, I would also like to thank my all of my colleagues who have been there for me over the years. Dr. Ali Hamad, Ibrahim, Nimer, Ghiath, Hashim, provided valuable support either in the classroom or field. They have been good friends and always willing to help.

Finally, I would like to thank my mother and sisters, and the rest of my family and friends who have lent undying love and support to me. They have always been supportive and my biggest fans through everything. I am forever indebted to them for all they have

done for me. Thanks to them cannot be expressed with words.

TABLE OF CONTENTS

LIST OF TABLES

Table **Page**

LIST OF FIGURES

Figure **Page**

HARMONIC WAVELET ANALYSIS OF SURFACE WAVES AT COMPLEX GEOTECHNICAL SITES

Mohammed Khan

Dr. Brent L. Rosenblad, Dissertation Supervisor

ABSTRACT

The use of stress wave-based geophysical methods in geotechnical engineering has continued to grow and is now a routine component of many geotechnical site investigation programs. Surface wave methods, in particular, are now widely used in a variety of applications. Since their introduction in the 1980's, surface wave methods have evolved from the two-channel Spectral-Analysis-of-Surface-Waves (SASW) method to multi-channel, full waveform inversion methods that require hundreds of time records collected using extensive receiver spreads. With these changes, the capabilities of these methods has certainly improved, however, it has come at the cost of greater equipment requirements, increased space requirements, increased data acquisition time, and more complex data processing and interpretation.

In contrast, the SASW method only requires two geophones and a laptop with a data acquisition card. However, there is a need to improve the SASW methodology, as it is both time and labor intensive and has been shown to be ineffective for some geotechnical site conditions. Surprisingly, there has been very little research effort applied to improving simpler surface wave methods. One of the few novel two-channel techniques proposed is the Harmonic-Wavelet-Analysis-of-Surface-Wave (HWAW) method. However, the literature on this method is limited and the method has not been widely adopted.

The goal of this project is to improve the application of surface wave methods in geotechnical practice by evaluating the effectiveness of the HWAW method at complex geotechnical sites and developing guidelines for implementing this method generally. It is hypothesized that the HWAW method can overcome issues associated with applying the SASW method at complex geotechnical sites. Simulated surface wave measurements and experimental verification studies were performed to test this hypothesis.

Simulated surface wave data were used to perform a parametric study of data collection and data processing variables used in the HWAW method. The results from this study showed that using a sufficiently narrow bandwidth was the most important variable for determining an accurate dispersion curve from HWAW processing. The sampling frequency was found to have only a small effect on the accuracy of the dispersion curves. Interestingly, receiver spacing and source offset had no effect on the effectiveness of the HWAW processing for the profiles considered in this study. It was found that data collected using the typical SASW testing arrangement of equal source offset and receiver spacing could be effectively processed with the HWAW method. Simulation results also showed that changing Poisson's ratio of the material (i.e. saturation conditions) did not adversely affect the HWAW results. However, large fluctuations in the dispersion curve were observed for sites with high values of Poisson's ratio when small receiver spacings were used. This was also confirmed from experimental results.

Simulations of surface wave measurements at complex sites, including soft-over-stiff sites, sites with shallow velocity gradients, and sites with velocity inversions due to embedded soft and stiff layers also demonstrated that the HWAW method could effectively recover the dispersion curve for a variety of source and receiver configurations. Of

particular note are soft-over-stiff sites with large impedance contrasts where an abrupt mode transition makes conventional SASW interpretation untenable. For these cases, HWAW processing of the SASW data effectively dealt with the mode transition and recovered the correct dispersion curve. This important finding was validated with experimental measurements.

This research only focused on assessing the consistency between theoretical and HWAW-processed dispersion curves and did not address the inversion of these dispersion curves to determine shear wave velocity (V_S) profiles. Future work should focus on assessing the reliability of V_S profiles determined from the inversion of dispersion curves collected with small source offsets and short receiver spacings, as are used in published HWAW measurements. However, based on the findings from this research it is recommended that the current phase unwrapping approach used in the SASW methodology should be replaced with the automated HWAW processing method using the guidelines presented in this dissertation.

CHAPTER 1 INTRODUCTION

1.1 Overview

The use of stress-wave-based geophysical methods in geotechnical engineering has continued to grow such that they are now a routine component of many geotechnical site investigation programs (Rosenblad and Boeckmann, 2020). Surface wave methods in particular are now widely used in a variety of applications. Since their introduction in the 1980's, surface wave methods have evolved from the two-channel Spectral-Analysis-of-Surface-Waves (SASW) method to three-dimensional, multi-channel, full waveform inversion methods that require hundreds of time records collected using extensive receiver spreads (e.g. Tran et al., 2019). With these changes, the capabilities of these methods has certainly improved, however, it has come at the cost of greater equipment requirements, increased space requirements, increased data acquisition time, and more complex data processing and interpretation. Even fairly simple methods, such as the Multi-Channel Analysis of Surface Waves (MASW) method requires 24 to 48 channel receiver spreads deployed over long distances to be effective (Foti et al.,2017).

There remains a need to develop and improve methods that can be effectively used with minimal equipment costs, acquisition time, and space requirements. For example, in some situations, cost may be a significant barrier to adoption of geophysical methods. The acquisition of 48-channel receiver spreads, seismographs and sources can cost tens of thousands of dollars. In contrast, older methods like the SASW method, only require two inexpensive ($80) geophones and a laptop with a data acquisition card. In fact, there are now free plans online to build low channel count data acquisition systems for surface wave measurements (e.g. Kafadar, 2020). In addition, the limited space requirements of methods

like the SASW method make it more effective for measurements of soil properties over small areas (for example, shallow foundation applications). However, there is a need to improve the SASW methodology, as it has been shown to be ineffective for some geotechnical site conditions (Rosenblad and Li, 2009). Surprisingly, there has been very little research effort applied to the problem of improving these simpler surface wave methods. One of the novel two-channel techniques proposed is the Harmonic-Wavelet-Analysis-of Surface-Wave (HWAW) method, which is the focus areas of this research.

This dissertation presents findings from a study of the HWAW method for geotechnical site characterization. This work is motivated by the need to develop, improve and better understand the capabilities of low-cost geophysical methods with minimal equipment and space requirements. As the use of geophysical methods in geotechnical practice continues to grow, it is important to develop reliable, accurate and economical methods to obtain site properties of engineering interest that can be quickly and reliably obtained. The advantages of the HWAW method are the limited equipment requirements, and the small spatial spread of receivers. These advantages have the potential to expand the usefulness of stress wave-based geophysical methods in geotechnical engineering applications for different scenarios, such as testing in developing countries where equipment may be limited, at remote test sites that are difficult to access, at locations where localized information is needed or in response situations after natural disasters where smaller and portable equipment requirements would be advantageous. However, as detailed in the following chapters, the literature on the HWAW method for geotechnical applications is incomplete in many respects. This research fills a current void in the literature on the implementation

and applicability of the HWAW method at complex geotechnical sites. The specific problems investigated in this work are described below.

1.2 Problem Statement

Surface wave methods are non-intrusive and non-destructive techniques used to determine small-strain shear wave velocity (Vs) profiles at soil and rock sites. The non-intrusive aspect of surface wave measurements makes them economical and less time-consuming as compared to intrusive methods such as downhole and crosshole measurements. Shear wave velocity profiles are used in a variety of geotechnical analyses, including seismic site response analysis (e.g., Foti et al., 2009), liquefaction susceptibility assessment (e.g., Andrus and Stokoe II, 1999), foundation settlement predictions (e.g., Lo Presti et al., 1995, Mayne, 2000, Stokoe et al., 2013), foundation vibration modeling (e.g., Gazetas, 1991), site class determination (e.g., Boore and Brown, 1998), and general site characterization. As the use of V_S in geotechnical practice continues to grow, it is important to develop reliable, accurate and economical methods to determine V_S profiles.

Active-source surface wave methods used in geotechnical engineering consists of three general steps. First, data collection involves placement of a source and sensors in the field to excite and record ground vibrations. Second, data processing involves using the recorded records to develop an experimental dispersion curve relating surface wave velocity to frequency or wavelength. Third, data interpretation involves iteratively matching the experimental dispersion curve with a compatible theoretical dispersion curve to develop the V_S profile for the site.

The original implementation of surface wave methods in geotechnical engineering developed in the 1980's was called the Spectral-Analysis-of-Surface-Waves (SASW)

method (e.g., Stokoe et al., 1994). The SASW approach used an active source and two receivers which were reset for several measurements at the same location to develop an experimental dispersion curve (e.g., Nazarian and Stokoe, 1984). This method has the advantage of simple and portable equipment requirements but some limitations as discussed later in the dissertation. In recent years, multi-channel wavefield transformation approaches, such as the Multichannel Analysis of Surface Waves (MASW) method, have been used extensively (e.g., Park et al., 1999b) and largely supplanted the SASW method as the predominant method in geotechnical engineering practice. The MASW method utilizes an active source and a single multiple-channel array to collect surface wave data (typically 24 to 48 channels). Like SASW, MASW also has limitations, as discussed later in this proposal. There are several other active and passive surface wave methods (e.g., Refraction Microtremor -ReMi and Spatial Auto Correlation - SPAC), but the SASW and MASW techniques remain common active-source methods used in geotechnical practice.

Each surface wave method has advantages and limitations. For simple geotechnical profiles which are characterized by a gradual increase in V_S with depth (so-called normally dispersive sites) both techniques (SASW and MASW) yield reliable results when performed correctly. However, at more complex sites, these methods have limitations that can result in erroneous profiles. Complex sites include: (1) sites with a very strong V_S contrast between layers at shallow depths (e.g., the contact between low-velocity sediments and bedrock), (2) sites with a shallow velocity gradient (3) sites with a low-velocity layer between two high-velocity layers, (4) sites with an embedded high-velocity layer between two lower-velocity layers, and (5) sites with high Poisson's ratio values (saturated sites).

In many applications, the simple equipment and data collection of the SASW method

is beneficial. However, this method has limitations that can lead to erroneous profiles, as discussed in this study. Likewise, the MASW method has weaknesses that can lead to incorrect V_S profiles and ultimately affect design values. To overcome these issues, the MASW approach requires many sensors, long arrays (to separate modes), long source-offset distance (to minimize near-field effects) and hence large sources to generate sufficient energy over these distances (Yoon and Rix, 2009, Rosenblad and Li, 2011).These requirements are often not implemented in practice which can result in erroneous values.

In current practice, both the SASW and multi-channel methods are flawed and may produce erroneous Vs profiles in some cases. Therefore, there is a need to explore other approaches to surface wave measurements and processing that may prove advantageous. A novel approach based on the harmonic wavelet transform analysis (e.g., Newland, 1998) has been proposed and tested (e.g., Kim and Park, 2001, Kim et al., 2015). This approach, termed the Harmonic Wavelet Analysis of Waves (HWAW) by the method's authors, uses a similar two-channel data collection technique as the SASW method, but a distinctly different approach to developing the experimental dispersion curve. Analytical and experimental studies have demonstrated the potential benefits of this method, including: (1) more localized V_S measurements and (2) improved signal-to-noise, allowing for smaller sources (e.g., Park and Joh, 2009, and Hwang and Park, 2014, Kim et al., 2015). Despite these potential advantages, the HWAW method has not been widely adopted in geotechnical practice.

A review of the literature on the HWAW shows that there have been few studies comparing the performance of this technique with established surface wave methods (SASW and MASW) for near-surface characterization. The body of literature on this

method is incomplete in the following ways. First, published studies are predominantly from sites with simple soil profiles where V_S increases do not contain large contrasts in velocity. Studies of the HWAW method over a broad range of more complex sites that have proven problematic to other methods have not been performed. In addition, the susceptibility of this method to variations in Poisson's ratio of the soil (particular soft, saturated soil conditions where Poisson's ratio approaches 0.5) has not been examined yet. Second, most of the published studies of this method have been performed by the method's originators and the methods reliability has not been independently confirmed by other investigators. Third, criteria for implementing this method in practice are not well-defined. Specifically, guidelines on the receiver spacing, source location, bandwidth and sampling rate to be used should be developed, as has been done with the SASW method.

1.3 Objectives and Hypothesis

The overall goal of this research is to improve the application of surface wave methods in geotechnical practice by evaluating the effectiveness of the HWAW method at complex geotechnical sites and developing guidelines for implementing the method. It is hypothesized that the HWAW method can overcome problems encountered by current surface wave methods at complex geotechnical sites. The following research objectives were pursued:

(1) The first objective was to investigate how data collection and data processing parameters affect the reliability of results obtained with the HWAW method for simple site conditions. Specifically, these parameters include: source-receiver offset, receiver spacing, sampling rate of time records, and frequency bandwidth used in HWAW processing.

(2) The second objective was to investigate the applicability and performance of the HWAW method at complex sites by applying data collection and data processing parameters obtained from the parametric study performed on simple profiles. This portion of the study involves simulating surface wave measurements for a variety of complex site conditions. The results were compared with current conventional SASW data collection and processing.

(3) Based on the results from (1) and (2), the third objective was to develop recommendations for implementing the HWAW method in practice. Specifically, guidelines were developed regarding data collection and data processing parameters.

(4) The fourth objective was to validate the findings from the numerical simulations with experimental measurements at field sites with complex site conditions.

1.4 Organization of Dissertation

This dissertation is organized into six chapters. Chapter 2 is a review of common surface wave methods used in geotechnical engineering practice and their advantages and limitations for specific conditions. It also provides a literature review of the HWAW method, including how the methods is applied and past studies of the HWAW method. Chapter 3 presents the methods used in this study. Chapter 4 presents results and analyses of the study performed using simulated surface wave data and includes guidelines and practical limitations of the HWAW method. Chapter 5 presents results from field studies used to validate the observations from Chapter 4. Lastly, Chapter 6 presents a summary of the research, conclusions derived from the results, and recommendations for future research.

CHAPTER 2 BACKGROUND AND LITERATURE REVIEW

2.1 Introduction

In this chapter background on common surface wave methods used in geotechnical engineering practice as well as their advantages and limitations for specific conditions are presented. This chapter also provides a literature review of the harmonic wavelet analysis of waves (HWAW) method and past studies of the HWAW method for developing V_S profiles for geotechnical applications.

2.2 Background on Surface Wave Methods in Geotechnical Engineering

Surface wave methods involve measurement of wave propagation at the ground surface initiated from an active source or ambient noise and recorded using a receiver array. The objective of surface wave measurements is to develop a shear wave velocity (V_S) profile for a site. There are many surface wave methods used in geotechnical practice (e.g Foti et al, 2014), but each follows the same general steps for creating a V_S profile, namely (1) data collection, (2) data processing, and (3) data inversion.

The two most common active-source surface wave methods used in geotechnical practice are the Spectral-Analysis-of-Surface-Waves (SASW) and the Multichannel Analysis of Surface Waves (MASW). These methods are described below.

2.2.1 Spectral-Analysis-of-Surface-Waves (SASW) Method

The Spectral-Analysis-of-Surface-Waves (SASW) method is a non-destructive and non-intrusive seismic method for evaluation of V_S profiles of geotechnical and pavement systems. An overview of this method along with the implementation limitations are presented below.

2.2.1.1 Overview of SASW

The original widespread implementation of surface wave methods in geotechnical engineering began in the early 1980's using a method called the Spectral-Analysis-of-Surface-Waves (SASW) method (Nazarian and Stokoe, 1984). The SASW measurement consists of an active source, two-receiver spread of vertically-oriented geophones and a signal analyzer, as shown in Figure 2.1.

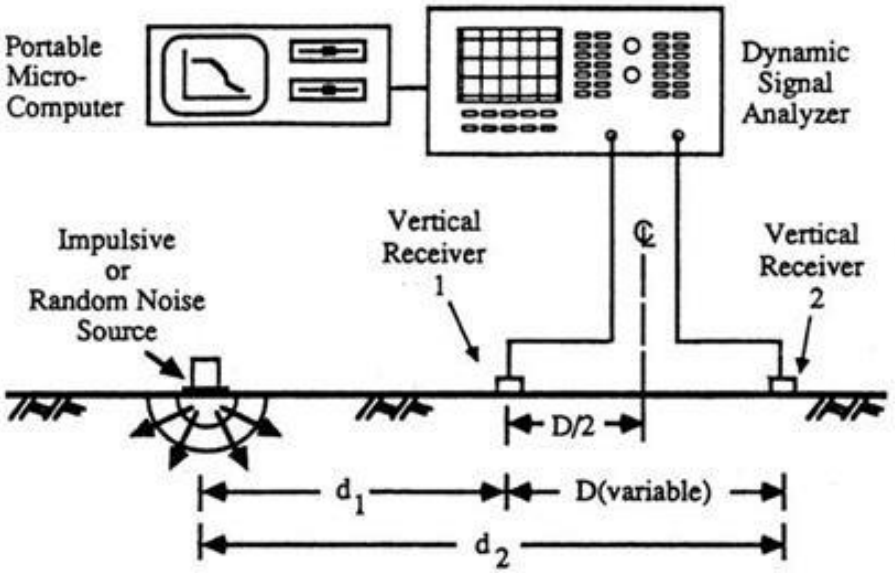

Figure 2.1 Data collection arrangement for Spectral Analysis of Surface Waves (SASW) testing (Rix and Stokoe, 1990).

Energy is excited using an impact source or shaker and the response at the ground surface is recorded with the geophones. The processing steps involved in the SASW method are shown in Figure 2.2. The time records collected from each receiver pair (Figure 2.2a), are converted to the frequency domain using the Fast Fourier Transform (FFT) algorithm (Figure 2.2b). The wrapped phase difference (lead or lag of $\pm$ 180 degrees) between the two receivers is determined from the cross power spectrum or transfer function calculated between the receiver pair and plotted as a function of frequency, as shown in Figure 2.2c. Portions of the phase plot that contain significant noise or do not follow a saw-

tooth phase pattern are masked out and not used in the analysis. In addition, close to the source, near-field effects due to non-planar wave propagation and coupled interactions of body and surface waves affect the wavefield. This portion is typically removed (i.e. masked) within accepted filtering criteria (Sanchez-Salinero et al., 1987; Gucunski and Woods, 1992; Joh, 1996). The cumulative phase shift between receivers (Figure 2.2d) is then determined from manually "unwrapping" the phase plot by identifying 360-degree "jumps" in the wrapped phase. For each frequency, the wavelength is calculated from the unwrapped phase and receiver spacing using:

$$\lambda = d\left(\frac{360^o}{\phi_{unwrapped}}\right) \tag{2.1}$$

And the effective phase velocity is calculated from the frequency and wavelength from:

$$V = \lambda f \tag{2.2}$$

Measurements are repeated with progressively larger source offset and receiver spacing to develop a dispersion curve covering the desired range of wavelengths, as illustrated in Figure 2.2e. The final step is determination of the V_S profile by using an inversion procedure to fit a theoretical dispersion curve to the experimental dispersion curve. Early implementation of the SASW method used a modal theoretical dispersion curve (so called 2D method), while more recent approaches have used an "effective mode" dispersion curve developed from simulation of all wave contributions at the receiver locations to fit to an average dispersion curve.

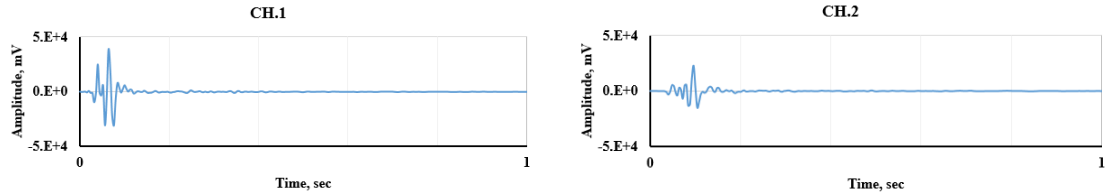

(a) Experimental time record data

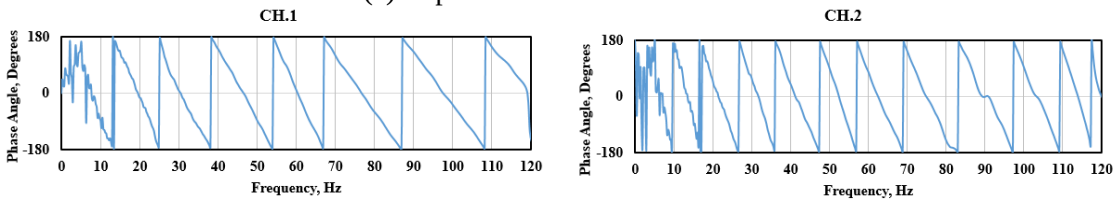

(b) Frequency domain conversion using FFT

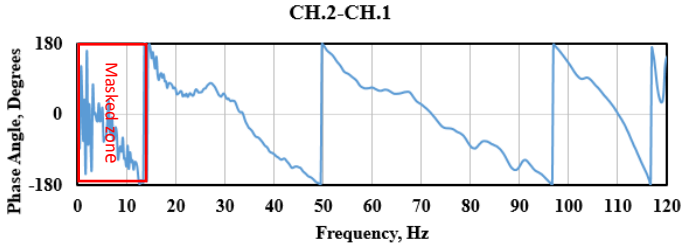

(c) Wrapped phase difference between two receivers

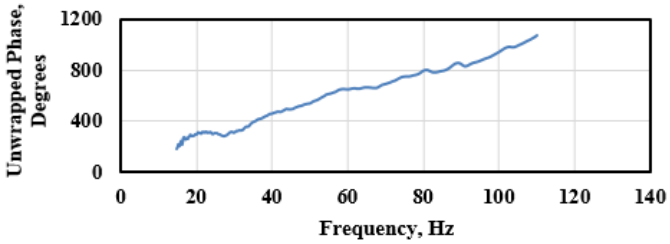

(d) Unwrapped phase difference between two receivers

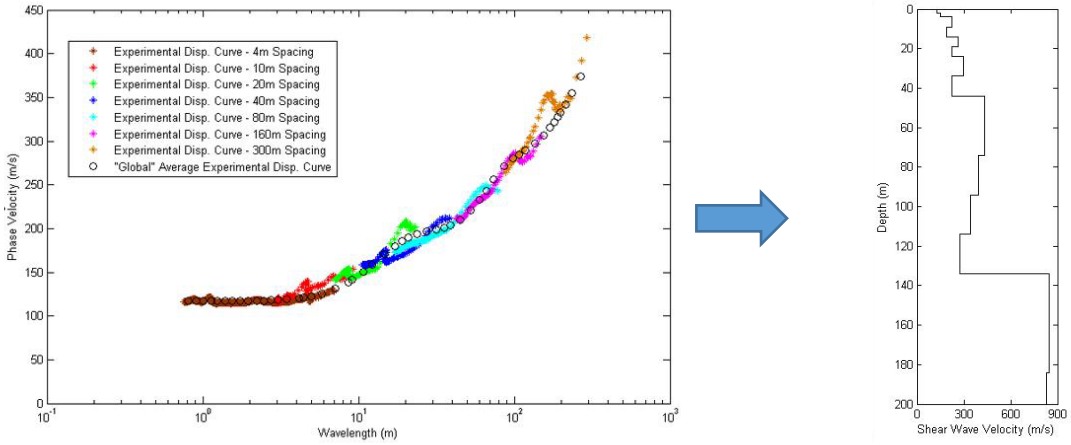

(e) Compute dispersion curve from multiple receiver pairs

(f) V_S profile determined from inversion of dispersion data

Figure 2.2 SASW processing flow illustrating conversion of time-series data to an experimental dispersion curve.

Historically, three different theoretical models (termed “2D Global”, “3D Global”, and “3D Array”) have been used to perform the inversion analysis. The term “Global” refers to the fact that the theoretical model is fit to a single average experimental dispersion curve determined in the data processing stage (i.e. a single composite curve determined from all receiver pairs). The “2D global” theoretical model, also known as the far-field or plane wave solution, produces a theoretical dispersion curve composed solely of (two-dimensional) plane Rayleigh waves. The dispersion curve generated by this approach is considered to correspond to the fundamental mode of Rayleigh wave propagation. With the 2D global approach, experimental data must be collected in the far-field to be compatible with the model and yield an accurate inversion of the V_S profile.

The theoretical model utilized in both the “3D global” and “3D array” approaches accounts for three-dimensional wave propagation effects and the presence of body waves by means of a Green’s function solution. The Green’s function provides the complete response at a given location relative to the source due to all wave types. This is also considered to be an “effective mode” solution, since fundamental and higher modes from multiple wave types (body waves and surface waves) are superposed, producing a phase velocity that may not correspond to any single Rayleigh mode. The theoretical dispersion curve from the 3D global is still a single global experimental dispersion curve created by averaging the individual dispersion curves. Since this dispersion curve does not correspond to any single receiver location, the typical approach is to compute the Green’s function response at distances corresponding to 2 and 4 wavelengths from the source (at each frequency). This inconsistency between experimental data collection and the theoretical model led to the development of the 3D array approach proposed by Joh (1996). With the

array approach, multiple individual experimental dispersion curves are produced (instead of a single global dispersion curve) – one for each receiver pair used in the data collection stage. Theoretical dispersion curves are simultaneously calculated and fit to the individual experimental curves, such that the theoretical response simulates the in-situ experimental response.

The original SASW source and receiver location setup was developed by Sanchez-Salinero et al. (1987). He performed a parametric study on data collection criteria to identify the best configuration of source and receivers to provide consistency between the measured dispersion curve and the 2D solution used at the time. He ultimately recommended the SASW setup with equal source-receiver and receiver pair spacing and used a limiting source offset to wavelength (d/λ) ratio of at least 2.0 (first 720 degrees of phase plot omitted) to completely avoid the near-field for. He noted, however, that a d/λ of 1.0 (first 360 degrees of phase plot omitted) or greater could be used if more low-frequency data were required. Current practice is to omit the first 180 degrees of phase (d/λ of 0.5) from the analysis when the 3D Global or 3D array implementation is used.

2.2.1.2 Limitations of the SASW Method

Although the SASW method has been used successfully for many years, there are several limitations inherent to this method, as described below.

Dispersion Curve Incompatibility

For complex site conditions (e.g. large velocity contrasts, velocity inversions), multiple surface wave modes are often present (Park et al., 2001a). A two-channel receiver spread does not allow for separation of modes if multiple modes are present. Therefore, use of a modal theoretical dispersion curve is not appropriate except at simple sites where a single

fundamental mode of propagation dominates. Instead, an "effective mode" dispersion curve calculated from the simulation of all wave contributions at the specific receiver locations must be used. However, since several receiver pair locations are used to develop the dispersion curve, there is not a single "effective mode" dispersion curve. The original solution to this issue was to calculate a representative "effective mode" dispersion curve determined at specific wavelengths from the source (e.g. 2λ-4λ), as noted above. Although this approach has been successfully used for years, in some cases it may lead to an inconsistency between the average experimental dispersion and the theoretical dispersion curves. The more recent approach using multiple individual theoretical dispersion curves proposed by Joh (1996) to fit each individual experimental dispersion curve addresses this problem, but can be computational intensive and time consuming, which limits the type of inversion schemes that can be used.

Noise Contamination

Data collection using the SASW method requires a long time acquisition to obtain sufficient frequency resolution. Background noise can be a significant problem (e.g. Gucunski and Shokouhi, 2004) which can degrade the quality of the phase plots and present difficulties when unwrapping the phase. Time domain filtering can be used to minimize this issue or a higher energy source may be required to overcome the noise effects, which makes the equipment requirements more significant.

Phase Unwrapping Difficulty

The most significant issue with the SASW method is phase unwrapping ambiguities. The SASW method is predicated on an assumption of a single continuous dispersion curve. Under some field conditions, where multiple modes propagate and the dominant

propagation mode shifts with frequency (i.e. modes transitions), wrapped phase plots are rather complex and difficult to unwrap correctly. Therefore, the usual manual phase unwrapping method can lead to erroneous dispersion curves, (e.g. Al-Hunaidi, 1993; Joh, 1996; Rosenblad and Bertel, 2008), as illustrated in Figure 2.3. This figure shows a comparison between the experimental dispersion curve developed from the multi-channel f-k method and the SASW method performed at a deep soil site in northern Arkansas. The multi-channel dispersion curve shows an abrupt transition to a higher mode in the frequency range of approximately 2.4 Hz to 4.0 Hz. However, the SASW results show a dispersion curve exhibiting a lower phase velocity than the multichannel measurement over the frequency range of 2.4 Hz to 4.0 Hz. This problem is due to the abrupt transition between modes where unwrapping the phase plot as a single continuous dispersion curve is invalid (Rosenblad and Bertel, 2008).

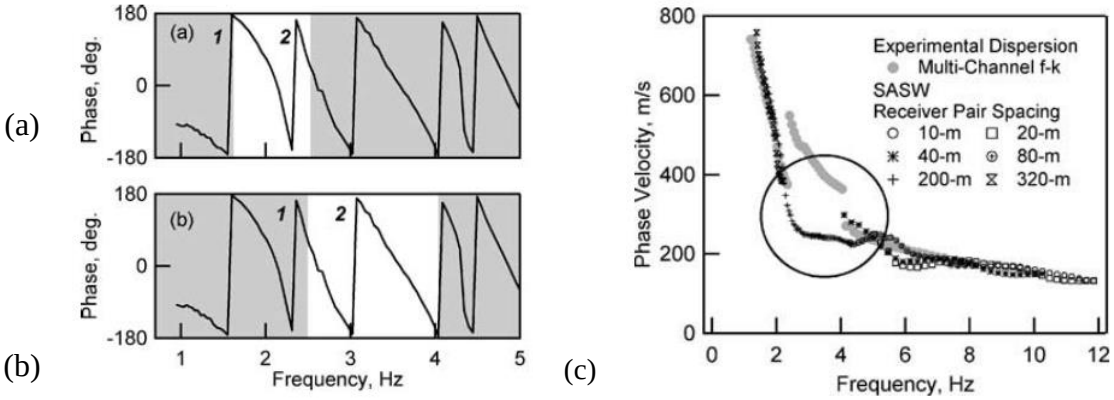

Figure 2.3 Experimental dispersion curves developed from f-k multi-channel analysis and conventional SASW phase unwrapping: (a) phase unwrapping of the lower mode (b) phase unwrapping of higher mode (c) Comparison of experimental dispersion curves (Rosenblad and Bertel, 2008).

Near-field Effects

If the modal approach or single "effective mode" model is used in the inversion, near-field contributions to the wave field can be a problem. When the source is too close to the

first receiver, contributions from body waves and non-planar surface wave propagation result in changes to the measured phase velocity (Mera, 1995, and Joh, 1996). The non-planar wave propagation produces an underestimation of the phase velocity and the body waves contributions produce oscillations in the dispersion curve (Chai et al., 2011). This results in an inconsistency between the plane wave theoretical dispersion curve and the measured dispersion curve. To overcome this issue, either the source has to be located far away from the receivers (to approximate a plane wave), which requires a bigger source, or one needs to model the actual ground deformations including the body waves and cylindrical wave spreading at the actual receiver locations, as is done in the 3D array inversion approach (Joh, 1996). The theoretical model used by Joh (1996) involves computing the complete response due to all wave contributions at each receiver location (Figure 2.4b). Therefore, the near-field contributions can be modeled and do not need to be totally avoided in the data collection stage, as shown in Figure 2.4. However, this approach is computational time consuming and difficult to implement in some inversion methods.

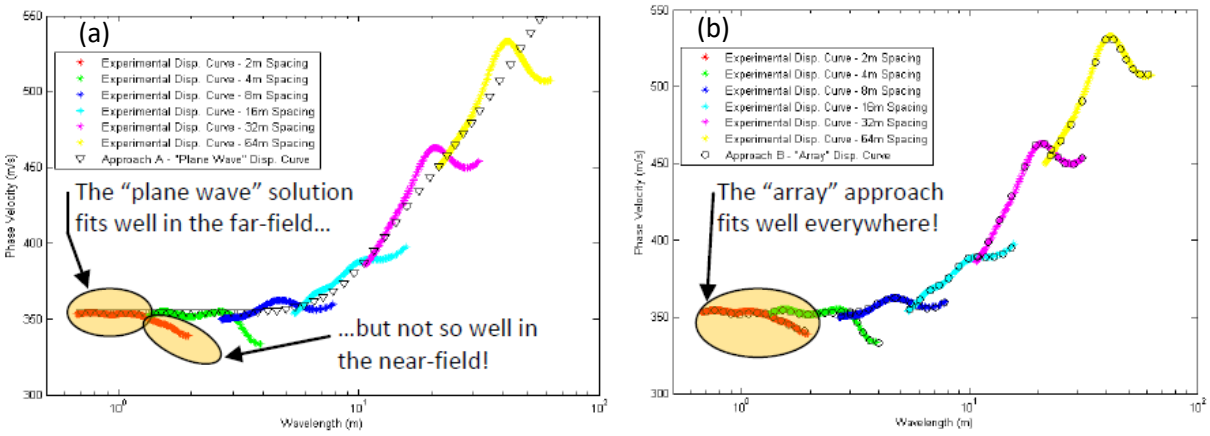

Figure 2.4 A comparison between the far-field plane wave solution (black triangles, at left) and the "array" inversion approach (black circles, at right) (McCaskill, 2014).

2.2.2 Multi-channel Surface Wave Methods

In the late 1990's, multi-channel surface wave methods were proposed and implemented to overcome some of the limitations of the SASW method. These methods used a large number of closely spaced sensors, typically 24-48, and wavefield transformation processing to develop the dispersion curve (Park et al. 1999). Although these methods overcome some limitations of the SASW method, they also have significant limitations as described below.

2.2.2.1 Overview of Multi-channel Methods

The Multi-channel Analysis of Surface Wave (MASW) method (Park, 1999) is the most common active source method used in geotechnical engineering practice today. The MASW method is one implementation of several multi-channel surface wave analysis approaches. MASW and other multi-channel methods involve the same three general steps as SASW. First, data collection involves placement of a source and a multiple-channel receiver spread, typically consisting of 24 to 48 closely-spaced (e.g. 2 m) receivers, as shown in Figure 2.5.

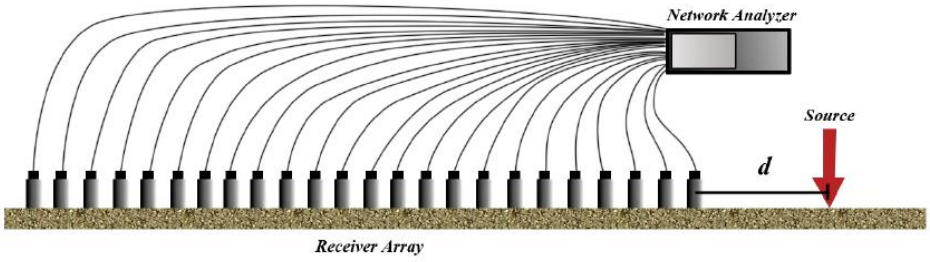

Figure 2.5 Typical data collection arrangement for multi-channel surface wave testing (McCaskill, 2014).

Second, processing of the data typically involves developing a dispersion curve from the recorded ground vibrations using one of several possible wavefield transformation

techniques such as frequency-wavenumber (*f-k*) transform. Third, data interpretation involves identifying the fundamental mode in the dispersion plot and fitting a fundamental mode, plane wave theoretical dispersion curve to the experimental dispersion curve, as shown in Figure 2.6. Although, some advanced methods utilize higher modes in the inversion, the most common implementation uses only the fundamental mode.

The advantages of the MASW method over the SASW method include, improved performance in noisy environments and use of a simple theoretical solution (fundamental mode plane wave) in the inversion step. However, there are several limitations to this approach as described in the following section.

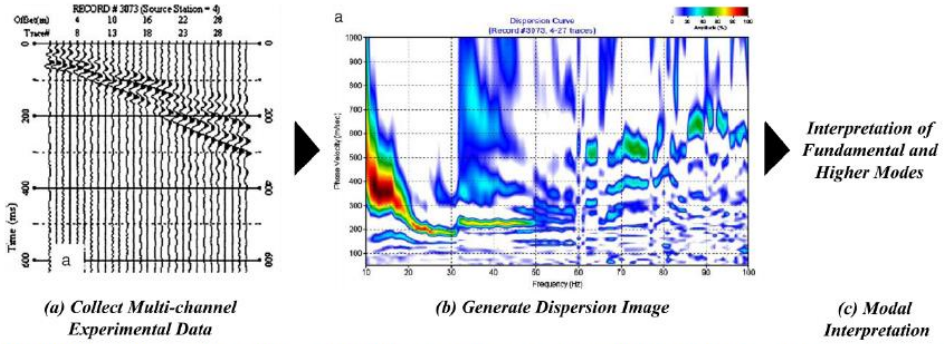

Figure 2.6 Processing flow for multi-channel data, including (a) time-series receiver data, (b) dispersion image generation and (c) interpretation of modes (Xu et al. (2006).

2.2.2.2 Limitations of Multi-channel Analysis of Surface Waves (MASW)

Mode Separation Issues

As noted above, multi-channel methods use a simple, fundamental mode theoretical dispersion curve which requires that the fundamental mode is correctly identified in the experimental data. However, when energy is carried on multiple modes, separation of closely spaced modes can be problematic and requires a long receiver array (i.e. aperture) to obtain the necessary resolution (Zywicki, 1999). If the array is not long enough, a

combined “effective mode” can be unknowingly measured and when fit to a fundamental mode solution produces an erroneous V_S profile. To overcome this problem, long receiver spreads and, therefore, a larger source to generate sufficient energy are needed to produce a correct V_S profiles.

Near-field Effects

Use of a planar, Rayleigh wave theoretical modal requires that the experimental data are collected with the source located far enough away from the receiver array so that near-field contributions are negligible. When the source is too close, the measured dispersion curve deviates significantly from the planar, fundamental mode solution. This was shown to be a more significant issue when Poisson’s ratio is large, such as at saturated soil sites (Rosenblad and Li, 2011).

A good example of how the near-field effects can produce different dispersion curves and ultimately erroneous V_S profiles is illustrated in Figure 2.7. It is clear that the dispersion curve with near-field effects deviates from the dispersion curve with no field effects. Therefore, the source must be located far enough from the receiver array which resulting in very long offsets and the necessity for large sources. In practice, these requirements are often not met, which may produce erroneous V_S profiles.

Non-localized Measurements

One of the consequences of requiring a long array and large source offset is that the measurement values reflects more global soil properties averaged over the spread length instead of local properties. This can be particularly problematic when these methods are used to identify a small subsurface feature, to characterize soil over a small region for

foundation design applications, or when developing a 2-D profile by combining multiple measurements.

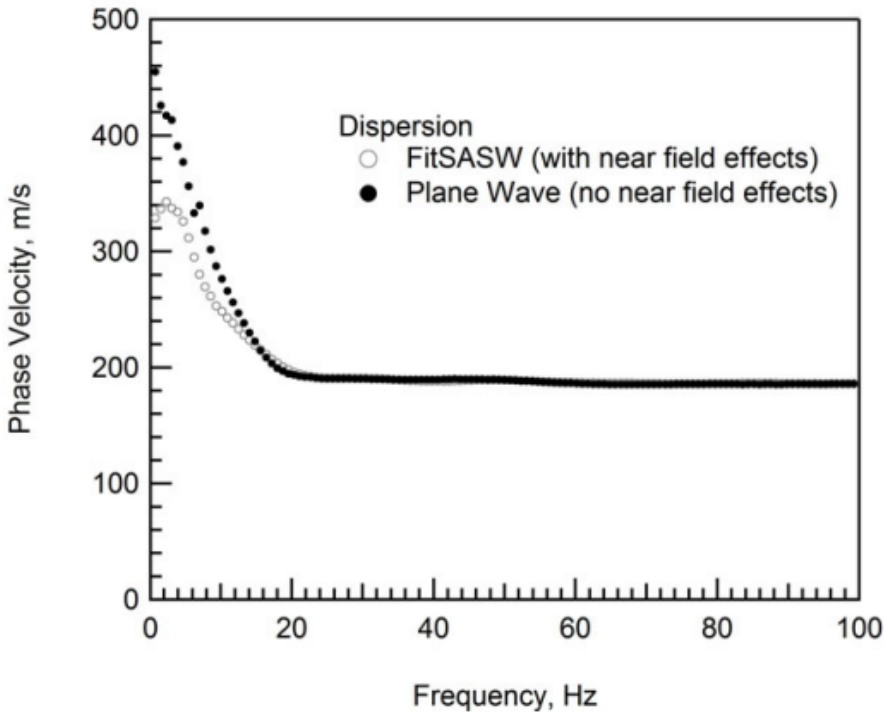

Figure 2.7 Example dispersion curves determined form FitSASW and plane wave model for the soil profile with source offset of 7 m, Rosenblad and Li (2011).

2.3 Harmonic Wavelet Analysis of Waves (HWAW)

Despite the limitations of the SASW and MASW methods, these methods remain the most commonly used active-source methods in geotechnical practice. More recently, a novel approach utilizing the Harmonic Wavelet Transform (Newland, 1997) has been proposed. Wavelet transform methods have become common analysis tools in various signal processing applications, (e.g. Rioul and Vetterli, 1991). The reason for their popularity among many fields and science disciplines is that the wavelet transform overcomes the difficulties associated with the traditional time-frequency analysis methods such as the windowed or short-time Fourier transform (STFT), and the Wigner- Ville

Distribution (WVD) (e.g. Newland, 1997). It provides a time-frequency representation of a signal based on a double series of basic functions called "wavelets" (small waves). A variety of wavelet types have been applied. Newland (1993) introduced the harmonic wavelet transform which has been applied to a broad range of applications, including: acoustics (Newland, 1997), image processing (Antonini et al., 1992), and damage detection in structural members (Hou et al., 2000; Spanos et al., 2006). Kim and Park (2001, 2002) proposed using the harmonic wavelet for processing of surface waves, which is the focus of this research. The harmonic wavelet transform and the approach used to process surface wave data are described below.

2.3.1 Overview of Harmonic Wavelet Transform

The following description of the Harmonic Wavelet Transform is adapted from Newland (1997). The wavelet analysis is a fundamental correlation method. The wavelet coefficient, $a(t)$, provides information concerning the structure of the signal and the relationship between the signal $s(t)$ and the shape of the analyzing wavelet, $w(t)$. The wavelet coefficient $a(t)$ is defined by the following equation:

$$a(t) = \int_{-\infty}^{\infty} s(\tau)\, w^*(\tau - t) d\tau \tag{2.3}$$

Where:

τ is the separation time,

t is the absolute time, and

$w^*(t)$ is the complex conjugate of $w^*(\tau - t)$.

When $s(\tau)$ correlates well with $w(t)$, $a(t)$ will be large. However, $a(t)$ will be small when they do not correlate.

The harmonic wavelet as defined by Newland (1997) is an orthogonal wavelet represented as follows in the frequency and time domains:

$$W_{m,n}(\omega) = \frac{1}{2\pi(n-m)} \qquad \text{for } 2\pi m \le \omega < 2\pi n \tag{2.4}$$

$$W_{m,n}(t) = \frac{e^{jn2\pi t} - e^{jm2\pi t}}{(n-m)2\pi t} \qquad \text{for } 2\pi m \le \omega < 2\pi n \tag{2.5}$$

Here, n and m are real but not necessarily integers, and $j = \sqrt{-1}$. Each harmonic wavelet can be related to an ideal bandpass filter as it has a constant real value inside the band of frequency while it is zero elsewhere. The harmonic wavelet has localized harmonic characteristic in the time domain. By taking the Fourier transform on both sides of Eq. (1), the convolution integral in the time domain in Eq. (1) becomes a multiplication operation in the frequency domain as follows:

$$A(\omega) = S(\omega)W^*(\omega) \tag{2.6}$$

$A(\omega)$, $S(\omega)$, and $W^*(\omega)$ are the Fourier transform of the harmonic wavelet coefficient $a(t)$, input signal $s(t)$, and harmonic wavelet $w(t)$. The harmonic wavelet coefficients are generally determined by applying the algorithm explained step-by-step in the schematic diagram shown in Figure 2.8.

First, the time record of the signal, $s(t)$, is transformed into the frequency domain using a Fast Fourier Transform (FFT). Next, the frequency domain, $S(\omega)$, is multiplied by a band limited boxcar window, $W^*(\omega)$ where the values are retained within that window $A(\omega)$ and assigned zero elsewhere. Last, the inverse of FFT is applied to $A(\omega)$ to get the harmonic wavelet transform coefficient in the time domain, $a(t)$. These steps are repeated using a shifted window to cover the whole signal, $s(t)$.

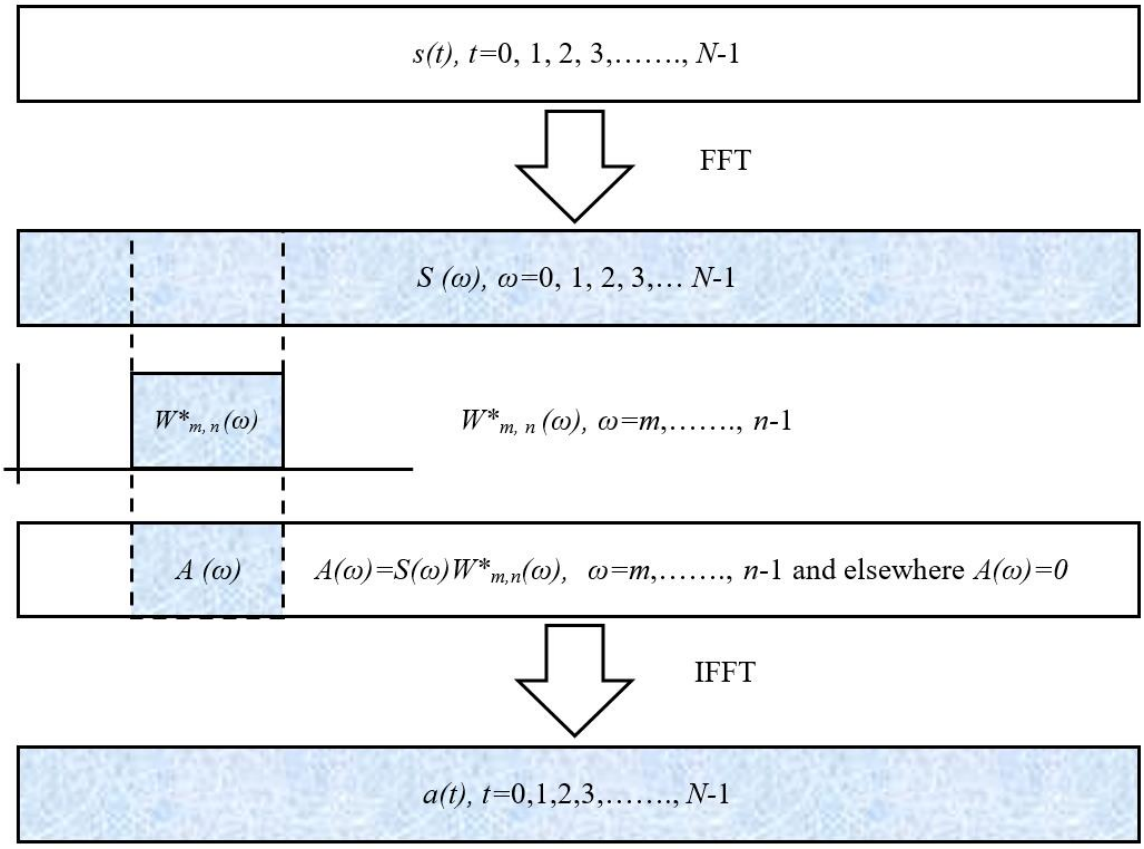

Figure 2.8 FFT algorithm to calculate harmonic wavelet coefficients for wavelets in the frequency band $\boldsymbol{2\pi m \leq \omega < 2\pi n}$ (Newland, 1998).

Decomposition of the time record by the harmonic wavelet transformation into frequency components is illustrated in Figure 2.9.

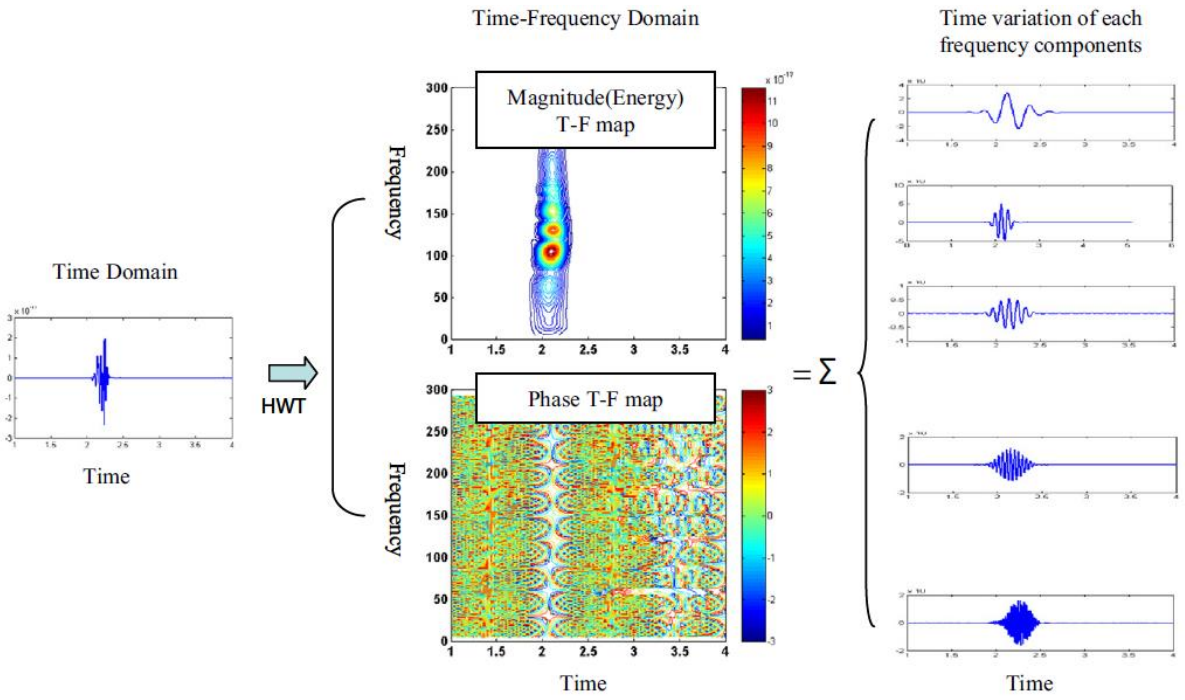

Figure 2.9 Decomposition of the time record by the harmonic wavelet transform (Hwang and Park, 2014).

2.3.1.1 Phase and Group Velocities from Harmonic Wavelet Analysis

Kim and Park (2001) proposed using the harmonic wavelet transform as a means to determine the dispersion curve from surface wave measurements using only a single pair of receivers. A detailed explanation of their interpretation of the meaning of the harmonic wavelet coefficient, $a_{m,n}(t)$, defined by $W_{m,n}(\omega)$, can be found in Kim and Park (2001).

Kim and Park (2001) proposed the following procedure to determine the phase and group velocities for a pair of time domain signals. Their approach is based on the assertion that the harmonic wavelet transform acts as an ideal bandpass filter so that harmonic wavelet coefficient, $a_{m,n}(t)$ for wavelet $W_{m,n}(\omega)$ contains information only in the selective frequency band $(m2\pi, n2\pi)$. They state that if the bandwidth of $W_{m,n}(\omega)$, $(n-m)2\pi$, is sufficiently narrow (which they do not define), then the soil system approximately acts as an ideal bandpass filter in the frequency band $(m2\pi, n2\pi)$, thus the

group delay, t_g and phase delay, t_{ph} calculated by their method have sensible meaning. Their proposed approach uses a two-channel data collection method, similar to the SASW method. The group and phase delays between Receivers 1 and 2 are obtained from magnitude and phase information of $a^1_{m,n}(t)$ and $a^2_{m,n}(t)$ and the group and phase velocities are calculated from these delays. Based on the interpretation concept introduced by Kim and Park (2001), the following procedure is used to determine group and phase velocities:

1. Compute the harmonic wavelet transform of signals from Receivers 1 and 2 where the frequency band of each wavelet is sufficiently narrow.
2. At frequency $(n+m)\pi$ which is the center frequency of arbitrary harmonic wavelet $W_{m,n}(\omega)$, the group delays (t_g^1 and t_g^2) are the time corresponding to the maximum magnitude of $a^1_{m,n}(t)$ and $a^2_{m,n}(t)$ at Receivers 1 and 2 respectively, as shown in Figures 2.10 and 2.11.
3. From the phase information of $a^1_{m,n}(t)$, θ_1 is taken as a phase corresponding to time t_g^1 (Figure 2.12).
4. t_L and t_R are obtained from the phase information of $a^2_{m,n}(t)$. t_L is the time corresponding to θ_1 which is the closest to t_g^2 on the left side of t_g^2 and t_R is the time corresponding to θ_1 which is the closest to t_g^2 on the right side of t_g^2 (Figure 2.13).
5. t_{ph}^1 is defined as t_g^1 and t_{ph}^2 is either t_L or t_R depending upon which is closer to t_g^2 (Figure 2.13).
6. The phase and group delays for all frequencies are determined by repeating procedures (2, 3, 4, and 5) for all harmonic wavelet coefficients.

7. By knowing the distance, (D) between Receivers 1 and 2, the group velocity V_{gr} and phase velocity V_{ph} at each frequency are calculated from:

$$V_{gr} = \frac{D}{t_g^2 - t_g^1} \tag{2.7}$$

$$V_{ph} = \frac{D}{t_{ph}^2 - t_{ph}^1} \tag{2.8}$$

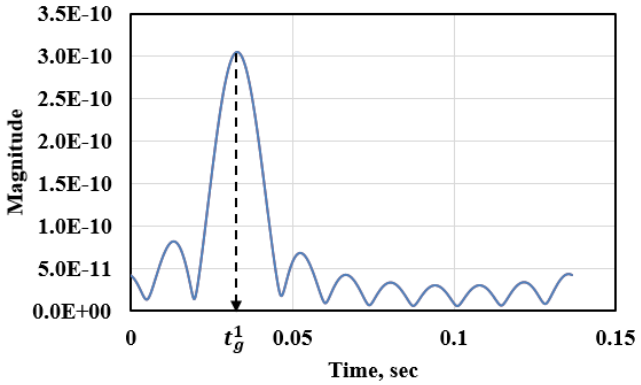

Figure 2.10 Determination of group delay from magnitude of $a_{m,n}^1(t)$ at Receiver 1 for frequency$(n+m)\pi$ using the HWAW method.

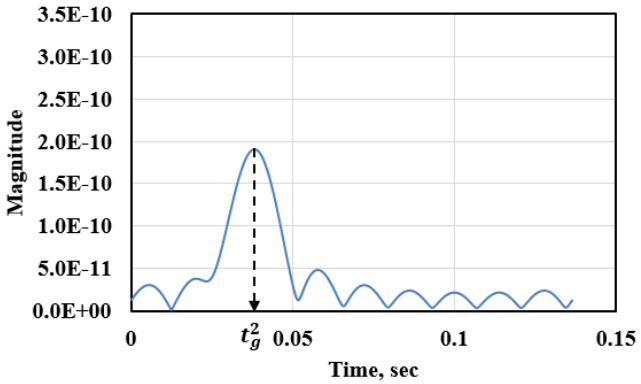

Figure 2.11 Determination of group delay from magnitude of $a_{m,n}^2(t)$ at Receiver 2 for frequency$(n+m)\pi$ using the HWAW method.

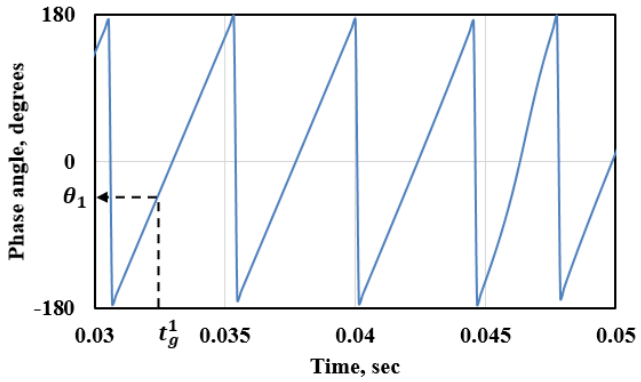

Figure 2.12 Determination of θ_1 from phase of $a_{m,n}^1(t)$ at Receiver 1 for frequency$(n+m)\pi$ using the HWAW method.

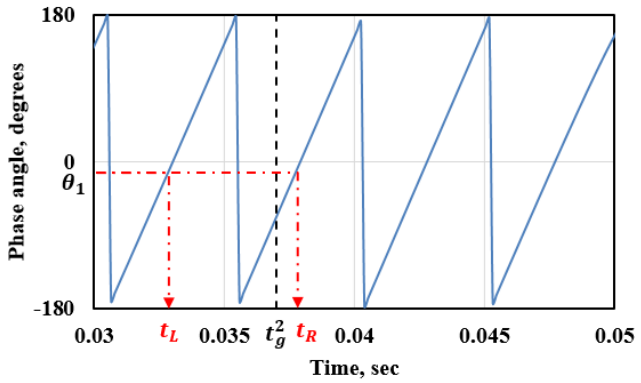

Figure 2.13 Determination of phase delay, t_{ph}^2 at Receiver 2 for frequency$(n+m)\pi$ using the HWAW method.

2.3.2 Literature Review of HWAW for V_S Profiling using Surface Waves

The HWAW method was first proposed in 2001 by Kim and Park. Since then several studies (mostly by the same authors) have been performed using both numerical simulations and field studies. These studies are summarized in the following sections.

2.3.2.1 Numerical Simulation Studies of HWAW Method

Kim and Park (2002) conducted a numerical simulation study of the HWAW method as an alternative method to the conventional phase unwrapping method used in SASW and to improve the signal-to-noise ratio (SNR), as shown in Figure 2.14. The five soil profiles

used in this study are shown in Table 2.1. The simulated experimental setups were divided into three categories: regular profile (Case1), irregular profiles (Cases 2-4), and stiff-over-soft pavement site (Case 5).

Table 2.1 Material properties for simulated profiles (Kim and Park, 2002).

Layer No.	Thickness (m)	V_S(m/s) Case No.				Density (t/m^3)	ν*	Thickness (m)	Case 5		
		1	2	3	4				V_S (m/s)	Density (t/m^3)	ν*
1	1	200	300	200	400	1.7	0.333	0.1	1570	2.2	0.333
2	1	300	200	400	300			0.4	127	1.83	0.314
3	-	400	400	300	200			-	122	2.0	0.474

*: Poisson's ratio

Simulated time records were developed for two receivers located 1 m and 2 m from the impact source for Cases 1 to 4, while for Case 5, the time records are simulated at distances of 2 m and 4 m from the impact source. The results using the simulated soil profiles to develop the dispersion curve with the HWAW method were in good agreement (Figure 2.14) with the theoretical dispersion curve indicating that the use of this method is promising as an alternative means of V_S profiling. The potential benefits of this method, including: (1) limited instrumentation (2 receivers) (2) implicit small spatial spread of receivers and (3) one setup configuration to get the shear wave velocity dispersion curve.

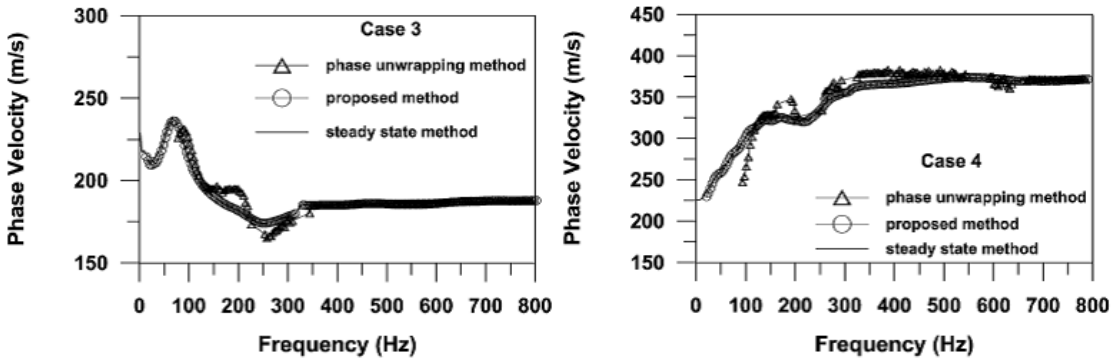

Figure 2.14 Comparison of phase velocity for Case 3 and Case 4 used in Kim and Park (2002).

Park and Joh (2009) also proposed the harmonic wavelet transform method to determine the frequency domain phase spectrum used in SASW with improved signal-to-

noise. Their numerical simulation was carried out on three different soil profiles. The first soil profile was a regular profile in which velocity stiffness gradually increases with depth (Case 1: V_S= 100, 200 and 300 m/s). The second and the third profiles were irregularly soil profiles in which stiffness varies irregular with depth (Case 2: V_S= 200, 400 and 300 m/s, Case 3: V_S= 400, 300 and 200 m/s). The experimental setup for these profiles consisted of three layers with Poisson's ratio of 0.333, density of 1.9 t/m^3, and damping ratio 0.02%. Regarding the test setup, a source was simulated at the surface and the time domain signals were simulated at two receivers located at 2 m and 4 m from the source.

The study showed that the proposed method is a better approach than the conventional cross power spectrum for developing wrapped phase plots (Figure 2.15) due to the reduction of noise contamination of the phase plots.

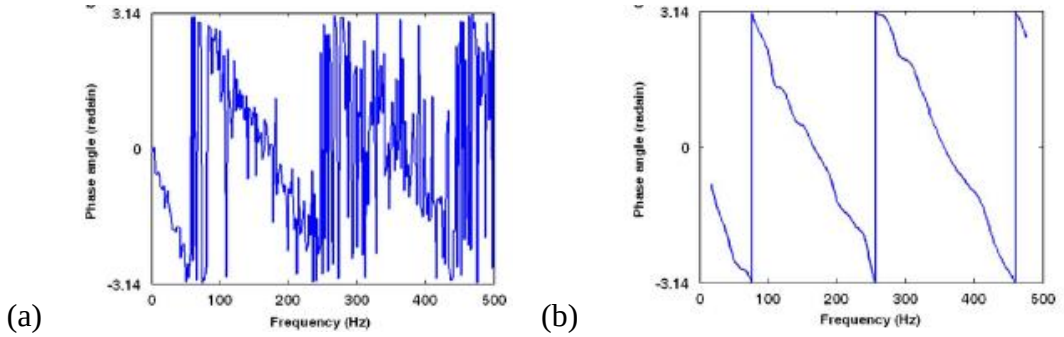

Figure 2.15 Phase spectrum for Case 3 with noise by: (a) cross power spectrum (b) HWAW.

Hwang and Park (2014) used the HWAW method to evaluate the condition of a gravel ballast layer using shallow shear wave velocity values. Numerical simulations and field applications of the proposed method were conducted. For the numerical simulation, a two-layered system was used to mimic the gravel ballast layer, as shown in Table 2.2. The thickness of the first layer was the depth of the concrete sleeper, and the stiffness of the second layer was greater than that of the first layer.

Table 2.2 Material properties for simulated model (Hwang and Park, 2014).

Layer No.	Thickness (m)	V_S(m/s)	Unit weight(kN/m^3)	Poisson's ratio
1	0.2	100	17.66	0.25
2	0.3	200		

The time domain signals were simulated at receivers located 0.3 m and 0.4 m respectively from the impact source. To simulate the effect of noisy field conditions generated by the train, random white noise was added to the time domain signals. Figures 2.16(a) and 2.16(b) show the good agreement between the theoretical dispersion curve and the dispersion curve determined with the HWAW method in term of frequency-phase velocity and wavelength- phase velocity respectively.

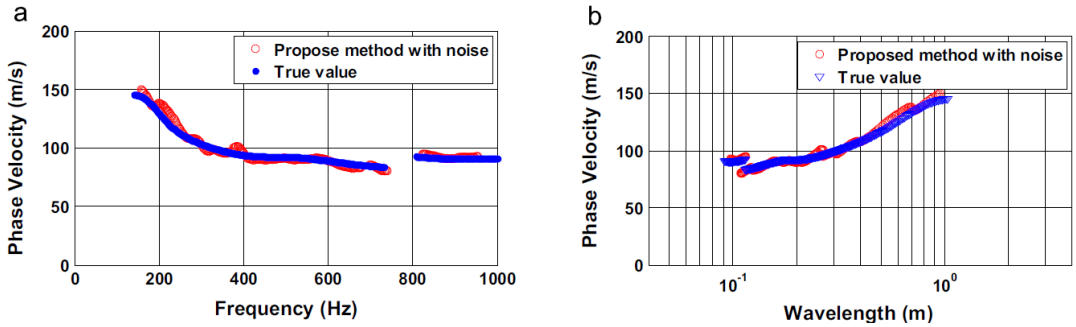

Figure 2.16 Comparison of the theoretical dispersion curve and that obtained by HWAW method. (a) Frequency-phase velocity. (b) Wavelength-phase velocity (Park and Joh, 2014).

2.3.2.2 Field and Model Studies of the HWAW Method

Gucunski and Shokouhi (2004) adopted the HWAW approach, introduced by Kim and Park (2001), to evaluate the elastic moduli and layer thicknesses of multi-layer systems such as pavement layers, with a strong shear wave velocity stiffness decrease with depth. Time records data were collected using a Seismic Pavement Analyzer (SPA) which is typically used for SASW measurements. The spacing between the accelerometers was 0.6 m and the time records and the harmonic wavelet time frequency maps for the pavement response recorded by accelerometer 4 and 5. Results of the comparative analysis of the

collected data by the SPA using the conventional SASW and HWAW methods showed that the dispersion curve obtained by HWAW was more reliable than the one calculated by the SASW method. The authors concluded that the frequency-time analysis using wavelet transforms provides a more efficient tool for surface wave data interpretation and a reliable approach for pavement systems characterization (Gucunski and Shokouhi, 2005).

Park et al. (2007) performed field studies of the application of the HWAW method to determine V_S profiles with comparisons to other conventional methods. To examine the applicability of the proposed method, field tests were performed at four sites. Two sites were used for evaluating the accuracy of the test method and others were used for estimating the applicability of 2-D imaging with the HWAW method. Through field applications and comparison with other test results (SASW, MASW, P-S suspension logging, and downhole test), the accuracy and applicability of the proposed method were verified, as shown in Figure 2.17. The field test setup used for each site was not the same. For Site 1, the source-receiver offset was 12.9 m and receiver spacing was 1.8 m while for Site 2, the source-receiver offset was 6.9 m and receiver spacing was 1.8 m. There were no specific criteria or guidelines provided for selecting suitable source-receiver offsets and receiver spacings. Also, the velocity contrasts in these profiles were small, as shown in Figure 2.17.

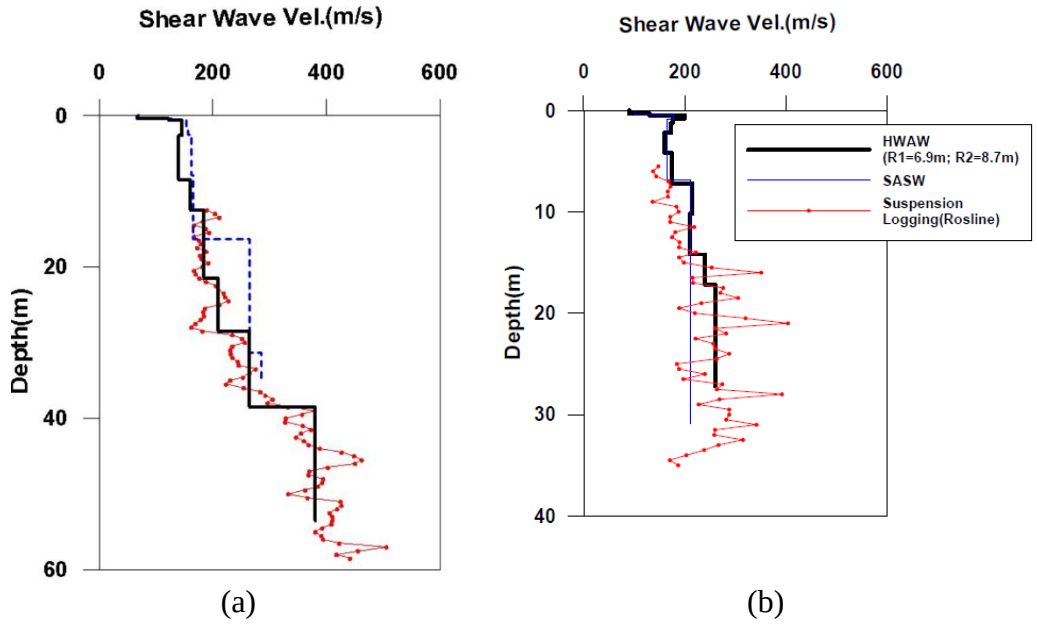

Figure 2.17 Comparison of V_S profiles determined by short receiver spacing HWAW (Black line), SASW (Blue), and PS suspension logging (Red) tests for: (a) Site 1 short receiver spacing (R1=12.9 m, and R2=14.7 m) HWAW and (b) Site 2 short receiver spacing (R1=6.9 m, and R2=8.7 m) HWAW (Park et al., 2007).

Hwang and Park (2014) used the Harmonic Wavelet Analysis of Waves (HWAW) method to numerically and experimentally evaluate the condition of s gravel ballast layer, on a high-speed railway from the indication of shear wave velocity values. Numerically simulated conditions of the gravel ballast layer were discussed in the numerical simulation studies of HWAW method (Section 2.3.2.1). In this test setup, as shown in Figure 2.18, the distance from the source to receiver 1 was between 0.3 m and 0.6 m, and the receiver spacing was between 0.1 m and 0.3 m for Bridge Site 1 (Ca#1). However, for Bridge Site 2 (Ba#1), the distance from the source to receiver 1 was between 0.1 m and 0.3 m, and the receiver spacing was between 0.1 m and 0.3 m.

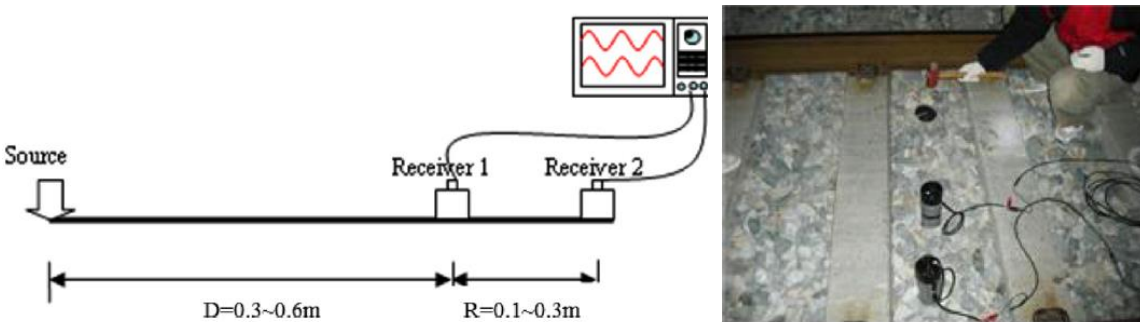

(a) Test setup configuration (b) Field test

Figure 2.11 Test setup for evaluating shear wave velocity profile of ballast layer: (a) Range of test setup configurations for Bridge Site 1(Ca#1) and Bridge Site 2 (Ba#1) (b) Field test between the concrete sleepers (Hwang and Park, 2014).

Figure 2.19a shows the phase spectrum determined by typical 2-channel surface wave methods using the time domain signals measured at two Bridge Sites Ca#1 and Ba#1 respectively. This figure shows that the phase spectra were distorted and hard to determine a reliable dispersion curves from the conventional SASW phase unwrapping method. However, Figure 2.19b depicts the dispersion curves obtained by HWAW method using the same signals as those used for the phase spectrum. It is clear that HWAW method can determine the dispersion curve under noisy field conditions (Hwang and Park, 2014).

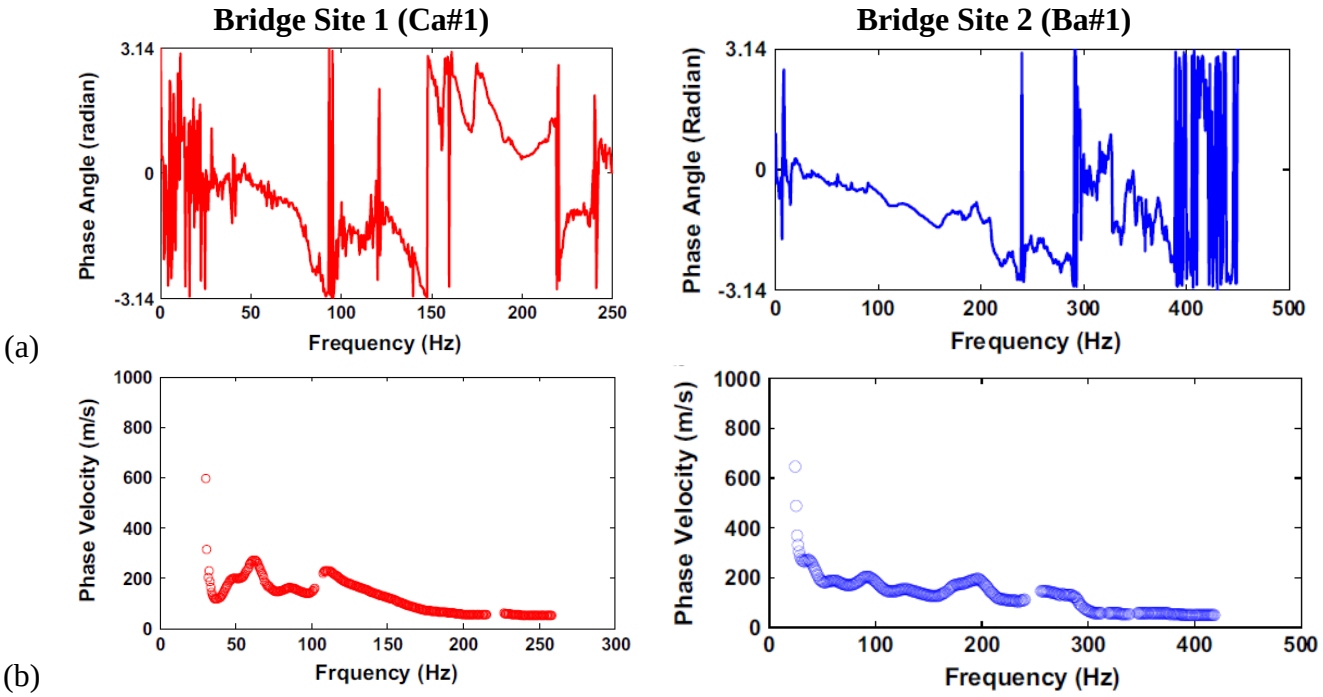

Figure 2.19 Comparison between typical 2-channel surface wave method and HWAW method performed at Bridge Site 1 (Ca#1) and Bridge Site 2 (Ba#1). (a) Phase spectrum by typical 2-channel surface wave method (b) Dispersion curve determined by HWAW method (Hwang and Park, 2014).

Kim et al. (2015) conducted a large-scale model study of the feasibility of the HWAW method for evaluating the lateral variation of V_S profiles (two-dimensional shear wave velocity image). The HWAW, SASW, and down-hole methods were performed on a constructed model testing site, and the test results were compared to reference values obtained from wave propagation measurements between 104 embedded geophones in the constructed model. The HWAW method was performed with a short receiver spacing test setup. This setup consisted of a single pair of receiver arrangement, where the source to receiver spacing (S–R1) was 6 m and the receiver to receiver spacing (R1–R2) was 2 m.

To obtain data covering the model test site, repeated short receiver spacing tests were performed where the source and receivers locations were shifted in parallel at 7 tests locations from 0 m to 15 m as shown in Figure 2.20. Based on the verification done by this study, it was concluded that the HWAW method is a viable approach to determine a 2-D

V_S image (lateral variation of shear wave velocity profiles) by interpolating the 1D profiles of local fields subdividing the entire field in a lateral direction. However, it should be noted that the velocity contrasts for these profiles were very small, with V_S values were in the range of 200 m/s and 300 m/s.

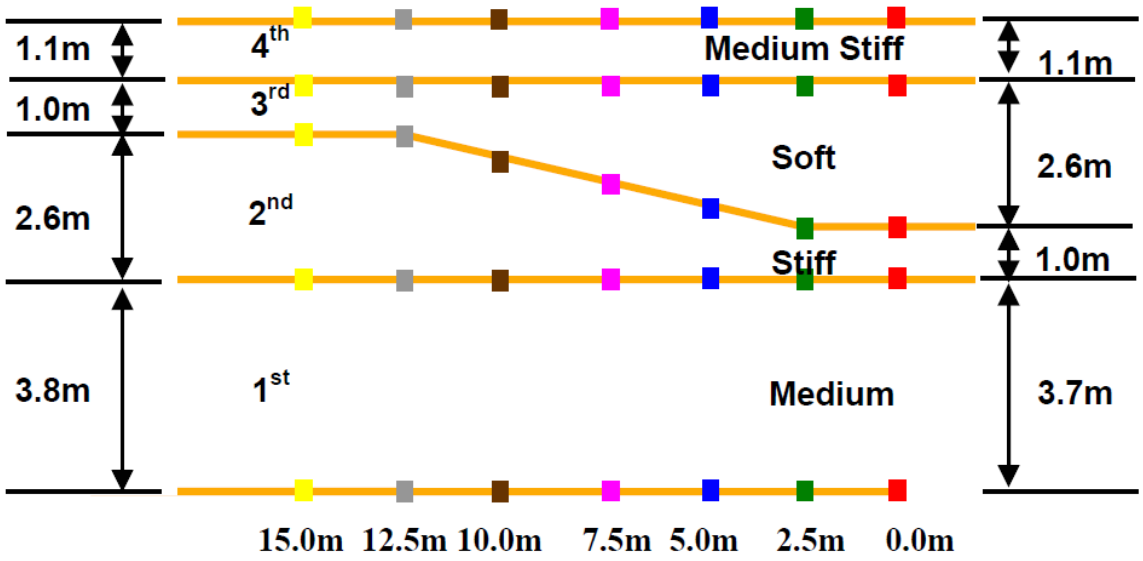

Figure 2.20 Vertical cross section of the model testing site (Park et al., 2007, and Kim et al., 2015).

2.3.3 Summary of Limitations of Past Studies

In summary, a review of published studies using the HWAW method, shows it to be an effective alternative method to obtain surface wave dispersion curves which overcomes some of the limitations of the SASW and MASW methods. However, there are two primary exclusions in the body of literature on this subject.

First, as noted in the studies described above, all of the V_S profiles tested both numerically and experimentally involve relative small changes in velocity between adjacent layers (ratio of 2 or less typically). It has been shown in other studies that sites with large velocity contrasts (in excess of about 3) are especially problematic do to mode transformations (Stokoe et al., 1994). Also only a few sites included velocity inversion due

to embedded soft or stiff layers. Therefore, there is currently no published information on the performance of this method at complex sites where processing of surface wave data is more problematic. In addition, all of the studies were performed at real or simulated sites where Poisson's ratio values were 0.2 to 0.33. These values represent unsaturated soil conditions. Under saturated conditions, Poisson's ratio can approach 0.5. No examples of HWAW applied at soft saturated soil sites (i.e. Poisson's ratio values approaching 0.5) are presented. These sites have been shown to be problematic for other surface wave methods in previous studies. Table 2.3 shows the material properties for simulated profiles from the published studies.

Secondly, as observed in the literature review presented above, implementation of the HWAW method, specifically how the data were collected and processed in terms of: (1) receiver spacing, (2) source location, (3) wavelet bandwidth and (4) sampling rate, were not consistent between the sites and no explanations for how and why these changes were made was provided. Surface wave methods such as SASW and MASW have developed general implementation guidelines based on research and field testing of the methods. Therefore, the proposed study will seek to fill this existing void in the current literature on this method.

Table 2.3 Material properties for simulated profiles from the published studies.

Study type	Reference	Layer No.	Thickness (m)	Vs(m/s) Case No. 1	Case No. 2	Case No. 3	Case No. 4	Density (t/m^3)	Poisson's ratio	Receiver spacing, m	Source offset, m	Profiled depth, m
Numerical simulation studies of HWAW method	Kim and Park (2001,2002)	1	1	200	300	200	400	1.7	0.333	1.0	1.0	~ 2-3
		2	1	300	200	400	300					
		3	-	400	400	300	200					
		Layer No.	**Thickness (m)**	**Vs(m/s) Case No.5**				**Density (t/m^3)**	**Poisson's ratio**	**Receiver spacing, m**	**Source offset, m**	**Profiled depth, m**
		1	0.1	1570				2.2	0.333	2.0	2.0	1.0
		2	0.4	127				1.83	0.314			
		3	-	122				2.0	0.474			
	Park and Joh (2009)	Layer No.	Thickness (m)	Vs(m/s) Case No. 1	Case No. 2	Case No. 3		Density (t/m^3)	Poisson's ratio	Receiver spacing, m	Source offset, m	Profiled depth, m
		1	1	100	200	400		1.9	0.333	2.0	2.0	~ 2-3
		2	1	200	400	300						
		3	-	300	300	200						
	Hwang and Park (2014)	Layer No.	Thickness (m)	Vs(m/s)				Density (kN/m^3)	Poisson's ratio	Receiver spacing, m	Source offset, m	Profiled depth, m
		1	0.2	100				17.66	0.25	0.1	0.3	1.0
		2	0.3	200								
	Hwang and Park (2014)	Layer No.	Thickness (m)	Vs(m/s)				Density (kN/m^3)	Poisson's ratio	Receiver spacing, m	Source offset, m	Profiled depth, m
		1	2	610				17.66	0.25	4.0	12.0	~ 40.0
		2	27	1150								
		3	-	1900								
Field and model studies of the HWAW method	Park et al. (2007)	Site No.		Velocity range, Vs(m/s)				Density (kN/m^3)	Poisson's ratio	Receiver spacing, m	Source offset, m	Profiled depth, m
		1		100~400				-	-	1.8	12.9	~ 45-50
		2		100~275				-	-	1.8	6.9	~ 25-27
		3*		200~300				-	0.23-0.41	2.0	6.0	8.5
		4		125~1000				-	-	2.0	6.0	~ 30-35
	Hwang and Park (2014)	1		60~200				-	-	0.1-0.3	0.3-0.6	~ 1.0
	Park and Joh (2009)	1		-				-	-	4.0	6.0	-
	Kim et al. (2015)	1*		200~300				-	-	1.0-3.0	6.0-12.0	8.5

*: Model testing site

CHAPTER 3 METHODOLOGY

3.1 Introduction

The primary objectives of this research are to: (1) investigate how data collection and processing parameters used in the HWAW method affect the reliability of the results of simple profiles, (2) investigate the performance of the HWAW method at complex geotechnical sites by applying the data collection and data processing obtained from the parametric study performed on simple profiles (3) develop guidelines for implementing the HWAW method in geotechnical practice and (4) validate the performance of the method at field sites.

Objectives 1, 2 and 3 were achieved by simulating wave propagation time records for simple and complex shear wave velocity (V_S) profiles and processing the data using the HWAW algorithm. Simple sites (i.e. V_S profiles) are defined as those with a gradual and small transition in shear wave velocity such that a single, continuous dispersion curve is measured. Complex sites are defined as V_S profiles that are often problematic to other common surface wave methods (e.g. SASW and MASW), as identified in the literature. These sites include: (1) sites with strong impedance (ρV) contrasts (i.e. factor of 2 or more) (2) sites with high Poisson's ratio values (i.e. fully saturated sites), (3) sites with a near-surface gradient in shear wave velocity and (4) sites with embedded stiff or soft layers. The HWAW data processing was performed using a MATLAB algorithm developed for this study. Experimental surface wave data from several field sites were also analyzed in this study as part of Objective 4. This chapter presents details of the analytical and experimental methods used in this research.

3.2 Ground Motion and Dispersion Curve Simulations

Ground motions recorded from surface wave measurements include cylindrically spreading surface wave modes as well as spherically spreading body wave contributions. To mathematically simulate the ground motions, it is necessary to calculate the Green's function relating the ground displacements at a given receiver location to a dynamic load.

In this research, time records were simulated for a variety of V_S profiles and data collection methods and then processed using the HWAW methodology to develop a dispersion curve relating V_S to frequency (or wavelength). The resulting dispersion curve was then compared to the true theoretical dispersion curve calculated directly from the computer simulation. The simulated time records and theoretical dispersion curves were obtained using the program FitSASW, which was developed at the University of Texas and later updated at Chung-Ang University in Korea (Joh, 2003).

An example of simulated time records and a theoretical dispersion curve obtained using the program FitSASW is shown in Figure 3.1. The soil profile used in this example was adopted from Hwang and Park (2014) as tabulated in Table 3.1. This program simulates wave propagation in a one-dimensional (1-D) layered soil profile due to a vertically oriented, surface source using the discrete stiffness matrix analysis, as described in Kausel and Roesset (1981) and Kausel (1981). The dynamic stiffness approach relates displacements ($\bar{U}$) and forces (P) as:

$$K\bar{U} = P \tag{3.1}$$

where K is the dynamic stiffness matrix for a 1-D layered profile with an underlying halfspace.

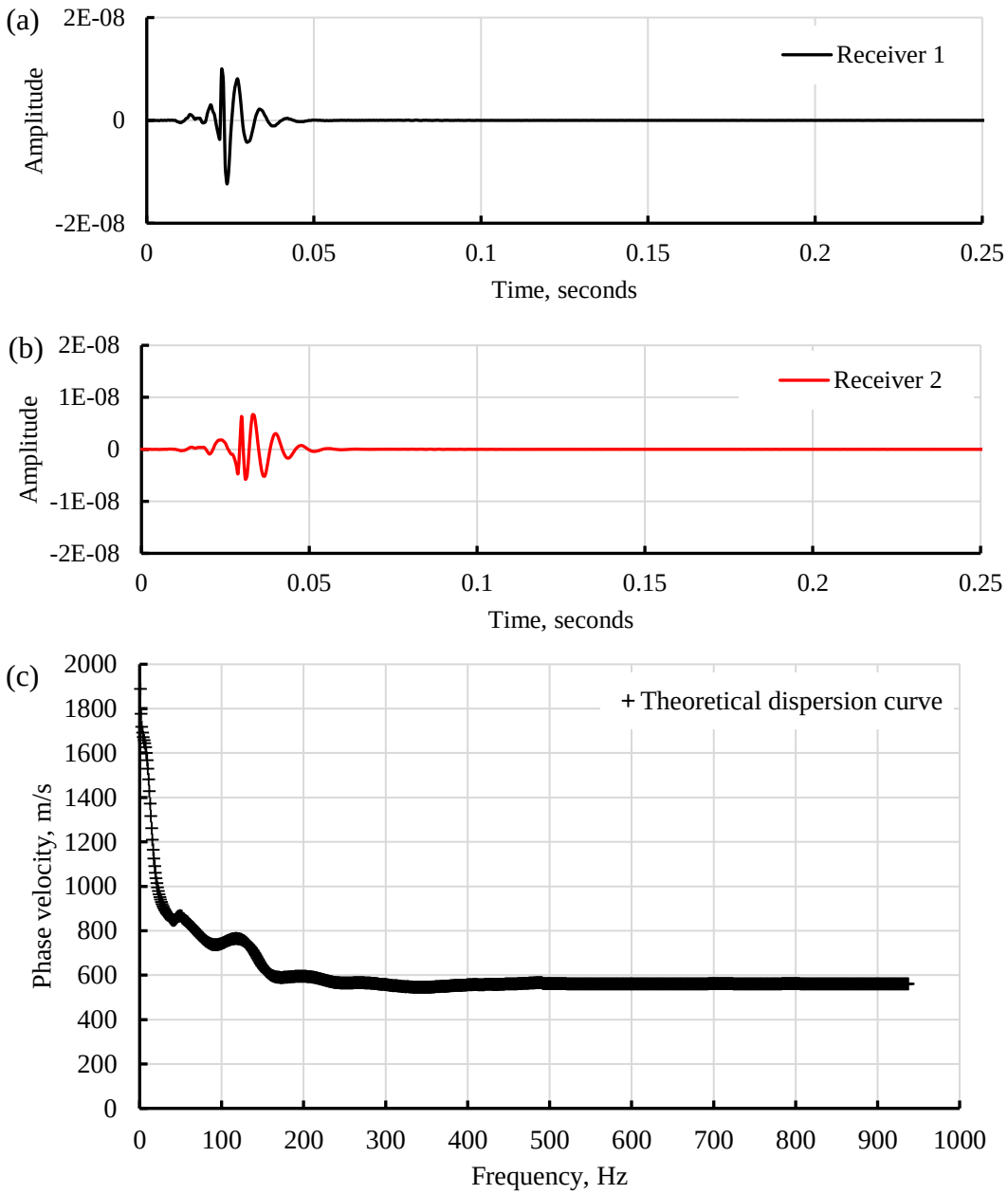

Figure 3.1 Time records simulated at 12 m (top) and 16 m (middle) from the source, and the theoretical dispersion curve (bottom) generated from FitSASW for the soil profile shown in Table 3.1.

Table 3.1 Individual layer characteristics of profile from Hwang and Park (2014).

Layer	Depth, z(m)	Thickness (m)	V_S (m/sec)	ν	Density (gm/cm^3)
1	0	2	610	0.25	1.766
2	2	27	1150	0.25	1.766
3	29	10	1900	0.25	1.766

In the continuous formulation the in-plane radial and vertical displacements U and W at the ground surface can be calculated as:

$$U = qR \int_0^\infty \bar{u}\, \mathrm{J}_1(kR)\mathrm{J}_1(kr)dk \tag{3.2}$$

$$W = \int_0^\infty \bar{w}\, \mathrm{J}_1(kR)\mathrm{J}_0(kr)dk \tag{3.3}$$

where J_0 and J_1 are the zero and first order Bessel function, k is the wave number, r is the radial distance from the source to the receiver location, R is the radius of the source, and q is the magnitude of the uniformly distributed surface load. The displacements $\bar{u}$ and $\bar{w}$ are functions of wavenumber, k.

The solution requires assembling the stiffness matrix, K, of the layered medium, solving the system of Equation 3.1 for a range of wavenumbers, k, and numerically evaluating the integrals of Equations 3.2 and 3.3 (Foinquinos, 1995). The continuous formulation is computationally expensive and not practical for a system with many layers, so an alternative approach is to use the discrete formulation or so-called thin-layer method (TLM). In the discrete formulation, terms of the dynamic stiffness matrix (K) are expanded in a Taylor series, keeping only up to second degree terms. This approach is equivalent to the assumption that the displacements have a linear variation with depth over each layer. Therefore, formulation of the solution requires a subdivision of layers into sufficiently thin layers to accurately reproduce the displacements.

The solution from FitSASW includes contributions from surface wave and body wave modes. The required profile input parameters are: number of layers, layer thickness, $\mathrm{V_S}$, Poisson's ratio (or p-wave velocity), mass density, and damping ratio. Receiver locations relative to the source are specified along with the sampling frequency. The program outputs time records at the chosen receiver locations and the theoretical phase velocity dispersion

curve calculated between a pair of receivers. It is important to note that the dispersion curve produced by FitSASW is not a modal Rayleigh wave dispersion curve, but is instead an "effective" or "apparent" phase velocity dispersion curve produced by multiple modes of cylindrically spreading Rayleigh waves and spherically spreading body waves. Therefore, the simulated data includes near-field contributions to the dispersion curve which are often attributed to body wave contributions and non-planar Rayleigh waves, (Chai et al., 2011). This approach to modeling the displacements from a surface load has been used and verified under different conditions of receiver location and Poisson's ratio for analytical studies of the Falling Weight Deflectometer (FWD) test in pavement applications (e.g. Foinquinos, 1995) and simulation of SASW measurements (e.g. Foinquinos, 1995; Sanchez-Salinero, 1987). Yoon and Rix (2009) used the same approach implemented in the program PUNCH (Kausel, 1981) to perform their numerical study of near-field effects in multiple-channel surface wave measurements.

3.3 Processing of Time Records with HWAW Method

The simulated time records developed from FitSASW and the experimental field data were processed using the HWAW method, which was implemented in a MATLAB algorithm developed for this research. Details of the HWAW procedure are described in Chapter 2. The steps involved in processing data using the MATLAB algorithm are described below. A walk through of how to determine the phase velocity, V_{ph} is illustrated in the following example and shown in Figures 3.1(a), 3.1(b) through 3.2(f) using data simulated for the soil profile from Hwang and Park (2014), as shown in Table 3.1. The processing procedure is performed as follows:

(1) The user uploads simulated or experimentally recorded time record files (ASCII or Excel files) collected from two receiver locations. Each time record contains two-column data (time, amplitude), as shown in Figures 3.1(a) and 3.1(b).

(2) To compute the harmonic wavelet transform (Figure 3.2) of signals from Receivers 1 and 2 the user inputs the frequency bandwidth of the harmonic wavelet, the increment by which the function moves along the frequency axis and the spacing between the receivers, D. The red lines in Figure 3.2 represent the time of group delays (t_g^1 and t_g^2) for each frequency value at Receivers 1 and 2 respectively (described below).

(3) At the center frequency of the wavelet, the group delays (t_g^1 and t_g^2) are identified as the time corresponding to the maximum magnitude of $a_{m,n}^1(t)$ and $a_{m,n}^2(t)$ at Receivers 1 and 2 respectively, as shown in Figure 3.3.

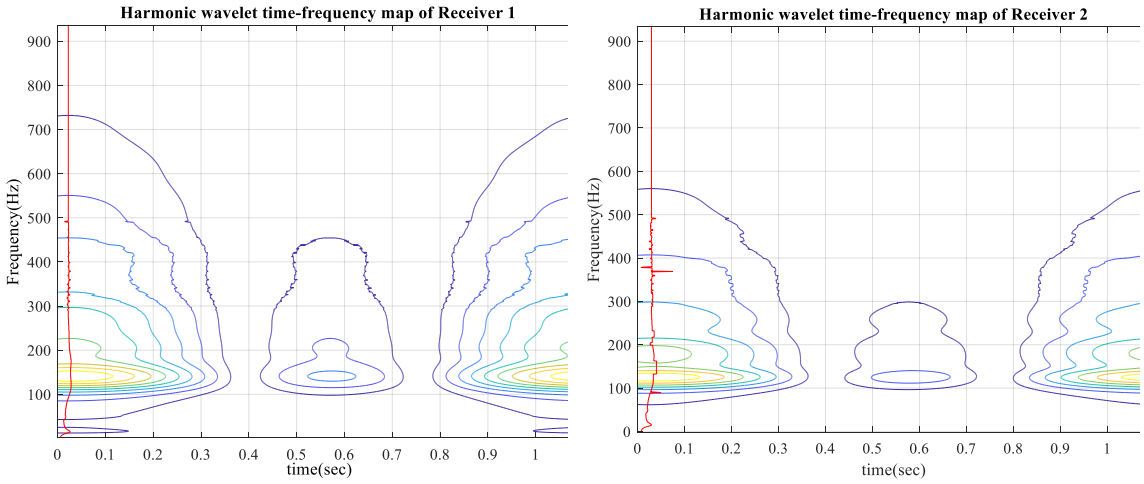

Figure 3.2 Harmonic wavelet time-frequency maps for wave signals at Receivers 1 and 2.

(4) From the instantaneous phase information of $a_{m,n}^1(t)$, θ_1 is identified as the wrapped phase angle corresponding to time t_g^1 (Figure 3.4).

(5) From the instantaneous phase information of $a^2_{m,n}(t)$, t_L and t_R are obtained, where t_L is the time corresponding to θ_1 which is the closest to t_g^2 on the left side of t_g^2 and t_R is the time corresponding to θ_1 which is the closest to t_g^2 on the right side of t_g^2 (Figure 3.4).

(6) t_{ph}^1 is defined as t_g^1 and t_{ph}^2 is either t_L or t_R depending upon which is closer to t_g^2 (Figure 3.4). The phase value is interpolated using a linear fit between time sampled points.

(7) Using the distance, (D) between Receivers 1 and 2, the group velocity V_{gr} and phase velocity V_{ph} at each frequency are calculated from:

$$V_{gr} = \frac{D}{t_g^2 - t_g^1} \tag{3.4}$$

$$V_{ph} = \frac{D}{t_{ph}^2 - t_{ph}^1} \tag{3.5}$$

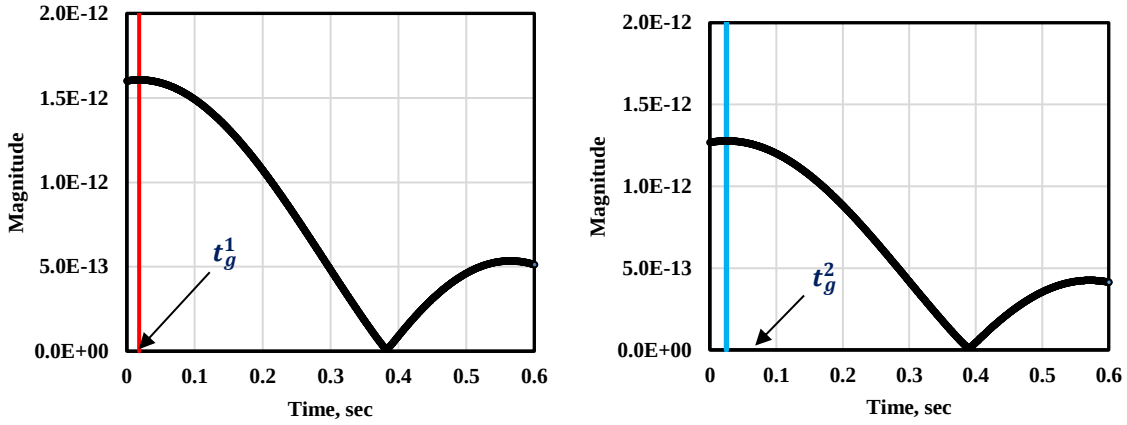

Receiver 1 Receiver 2

Figure 3.3 Determination of group delay, t_g^1 from magnitude of $a^1_{m,n}(t)$ and group delay, t_g^2 from magnitude of $a^2_{m,n}(t)$ at Receivers 1 and 2.

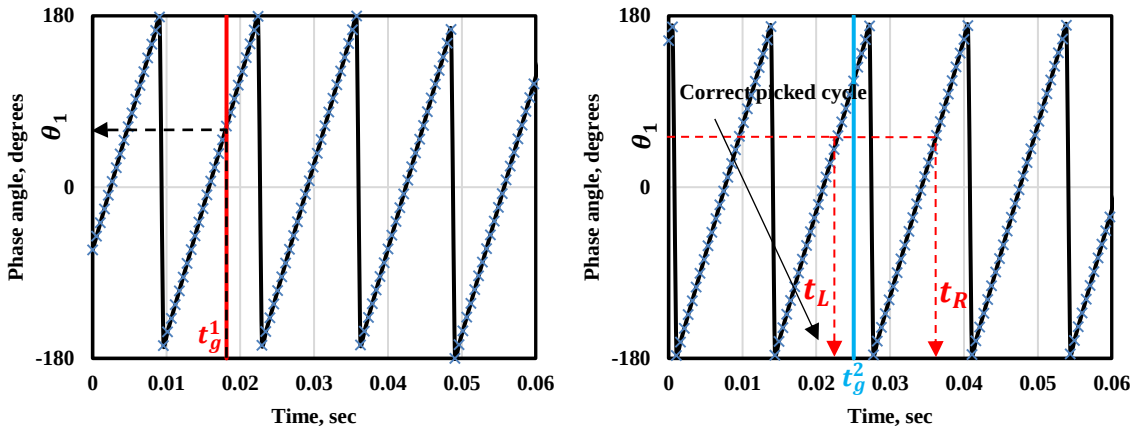

Determination of θ_1 from phase of $a_{m,n}^1(t)$ at Receiver 1.

Determination of t_{ph}^2 from phase at Receiver 2.

Figure 3.4 Determination of phase delay, t_{ph}^2 at Receiver 2.

(8) The phase and group delays for all frequencies are determined by repeating procedures (3, 4, 5, 6, 7 and 8) over a range of frequency values to develop a phase velocity dispersion, as shown in Figure 3.5 which depicts the dispersion curve from HWAW processing and the theoretical dispersion curves obtained from FitSASW using the soil profile adopted from Hwang and Park (2014). The basic processing flow is summarized in Figure 3.6.

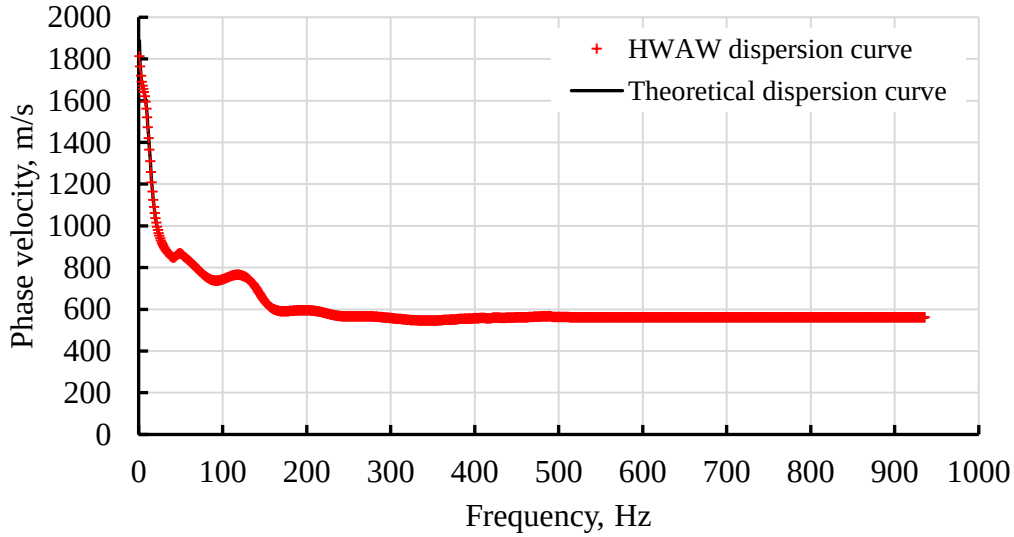

Figure 3.5 HWAW and theoretical phase velocity dispersion curve versus frequency for the profile adopted from Hwang and Park (2014).

The MATLAB algorithm developed for the HWAW method was tested and verified using V_s profiles and dispersion curves published in the literature, as discussed and presented in Chapter 4, Section 4.2.

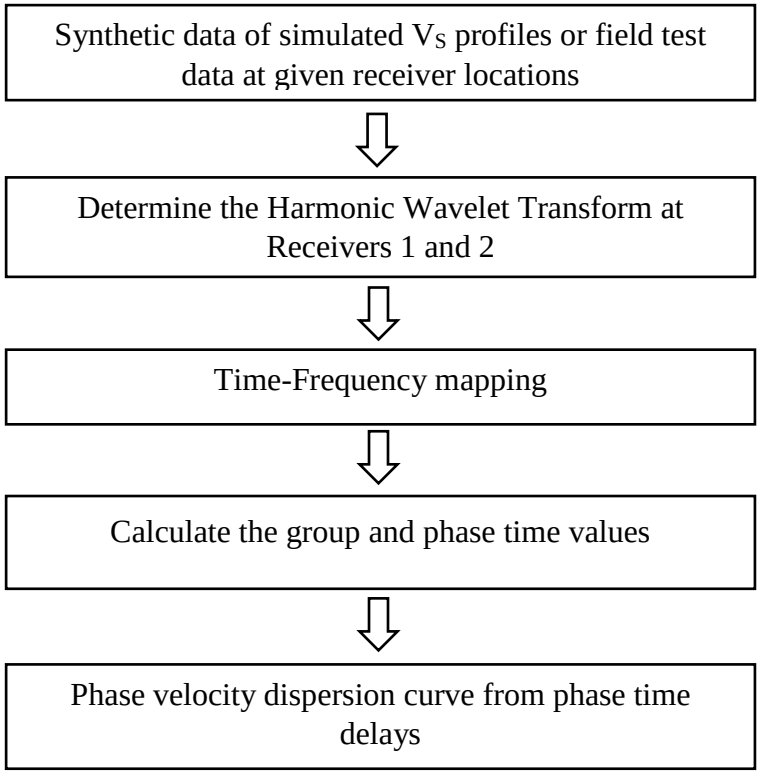

Figure 3.6 Flow chart for developing dispersion curves from simulated or field data.

The simulated data and MATLAB algorithm were used to assess the influence of V_S profile complexity, data collection procedures, and data processing parameters on the reliability and accuracy of the dispersion curve generated from HWAW processing. The data collection and processing variables that were studied include: source-receiver offset distance, receiver spacing, sampling rate of time records, and bandwidth frequency of HWAW wavelet.

Figure 3.7 depicts the flow chart summarizing the calculations and data generation involved in conducting this study. Section 3.4 provides details on the specific profiles that were modeled and the data collection and processing parameters that were used for each

profile. Conventional SASW data collection and processing was also performed for both the simulated profiles and the experimental field data.

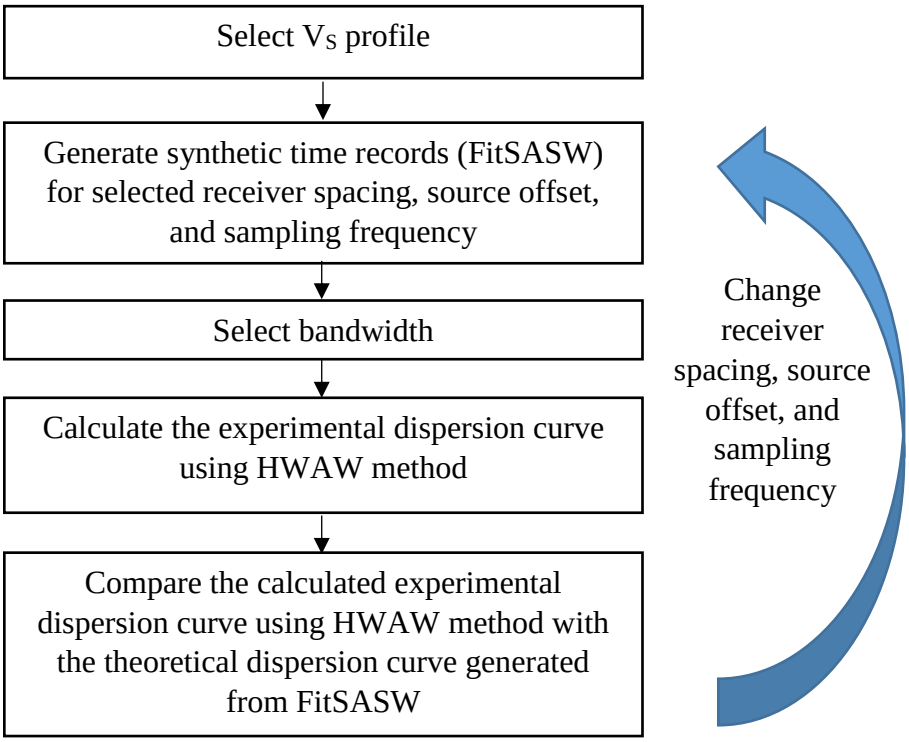

Figure 3.7 Flowchart showing the progression of data generation and data processing for a selected V_S profile using the HWAW method.

3.4 Processing of Simulated Data with SASW Method

The simulated time records developed from FitSASW and the experimental field data were processed using the SASW method, which was implemented in the program WinSASW (Joh, 1996). WinSASW is a windows-based surface wave analysis program developed at the University of Texas. The steps for surface wave data processing and analysis procedures applied in WinSASW, and used in this study, are described below.

(1) Experimental data were imported into WinSASW in the form of a wrapped phase plot showing the phase difference between receivers as a function of frequency for each receiver pair, as shown in Figure 3.8.

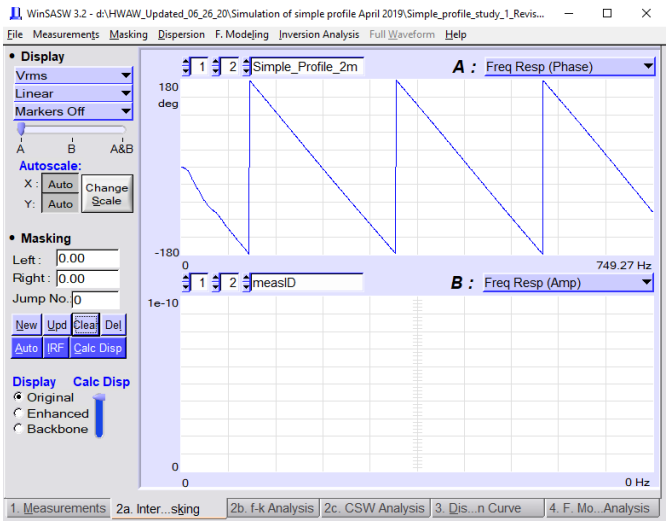

Figure 3.8 Example of wrapped phase plot imported into WinSASW with receiver pairs of 2-4 m.

(2) The next step was to mask out portions of the phase plot corresponding to regions affected by near-field effects, noisy regions, or portions that do not follow the characteristic saw-tooth pattern. The near-field criterion of wavelengths longer than twice the source-to-receiver spacing was applied, which requires that the first 180° of the wrapped phase plot be masked out. An example of phase plot masking is shown in Figure 3.9. The number of "jumps" from -180° to + 180° contained by each "masked out" region must be specified during the masking process to produce the correct experimental dispersion curve.

(3) Once the masking process was complete, the next step was to determine the unwrapped phase and produce a dispersion curve. The unwrapping process, itself, was performed internally in WinSASW. A dispersion curve produced from the masked wrapped phase data (Figure 3.9) is shown in Figure 3.10. The masking and unwrapping processes were repeated with data from several different receiver spacings to produce the individual segments of the "composite" dispersion curve

shown in Figure 3.11.

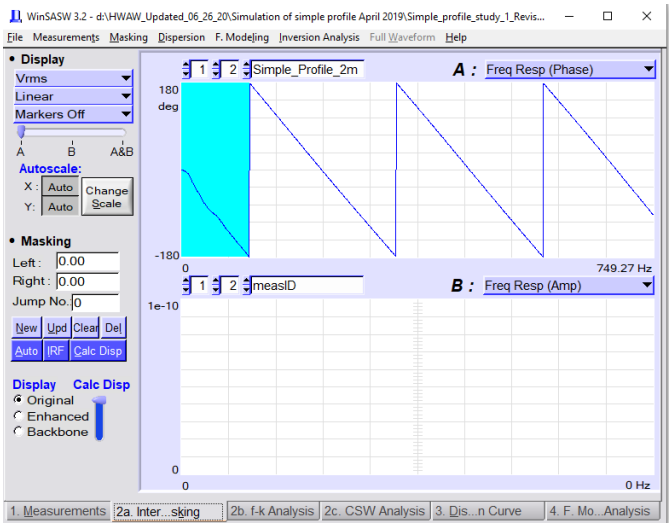

Figure 3.9 Example of "masking out" near-field effects (the blue shaded area in left side) in WinSASW with receiver pair of 2m-2m.

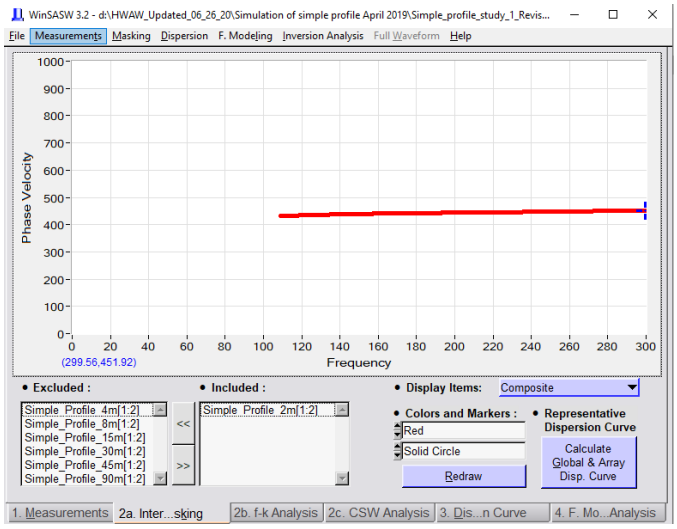

Figure 3.10 Single dispersion curve from a 2m SASW spacing, as calculated from the wrapped phase plot of Figure 3.3.

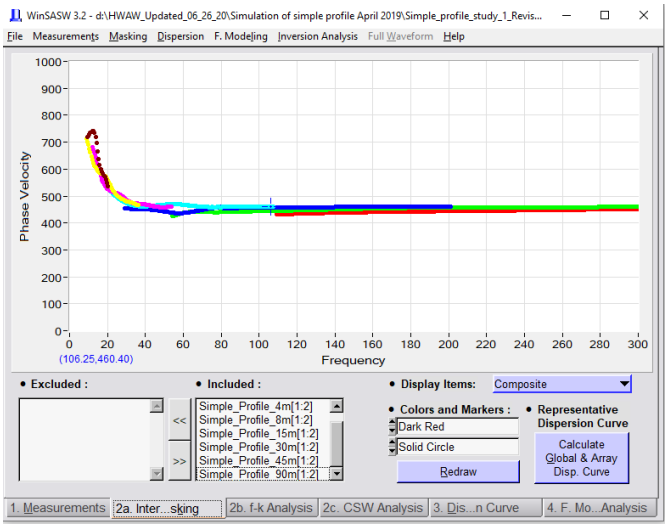

Figure 3.11 Composite dispersion curve generated from SASW spacings of 2m, 4m, 8m, 15m, 30m, 45m, and 90m.

Data collected with the SASW testing arrangement were also processed using the HWAW approach which described in Section 3.3.

3.5 Shear Wave Velocity Profiles used in Simulation Studies

In this study shear wave velocity (V_S) profiles where categorized as either simple or complex, as defined below. A variety of simple and complex V_S profiles were selected for the simulation study to study the effect of data collection and data processing on the reliability of the HWAW method. The soil profiles used in this study are described and illustrated in the following sections.

3.5.1 Simple V_S Profiles

Simple profiles are defined in this study as V_S profiles with no velocity inversion (i.e. normally dispersive) and a gradual change in shear wave velocity (specifically, the change in velocity between adjacent layers is a factor of 2 or lower) such that the resulting dispersion curve follows a single dominant mode. The simple profiles were also initially assumed to have a Poisson's ratio of 0.25 which is indicative of unsaturated conditions in

the field. These simple sites are generally well-handled by conventional SASW testing as well as MASW measurements.

The reasoning behind choosing simple V_S profiles was to avoid complications associated with complex sites when studying the effects of various data collection and data processing procedures. These complications include issues such as abrupt mode transformations and large body wave contributions associated with high Poisson's ratio conditions.

Three simple profiles, identified as Profiles 1, 2, and 3, were selected for presentation in this dissertation and are shown in Table 3.2 and Figure 3.12. These three profiles were chosen to represent typical ranges of V_S encountered in geotechnical practice. Profile 1 represents a soft to stiff soil site, Profile 2 represents stiff soil to soft rock and Profile 3 represents conditions associated with weathered to intact rock. A consistent profile depth of 30 m was chosen for these profiles, as this is a common profile depth for geotechnical applications. However, the results from the simulations can be generalized for different profile depths. Also, surface wave wavelengths of two to three times the target profile depth should be measured for an effective inversion. Therefore, the wavelength range of interest in this study is 60 m to 90 m.

Table 3.2 Individual layer characteristics of Profiles 1, 2, and 3.

Profile No.	Layer	Depth, z(m)	Thickness (m)	Shear velocity, V_S, (m/sec)	Poisson's Ratio, ν	Density (kg/m^3)
1	1	0	10	200	0.25	1700
	2	10	10	300	0.25	1700
	3	20	10	400	0.25	1700
2	1	0	10	500	0.25	1766
	2	10	10	750	0.25	1766
	3	20	10	1000	0.25	1766
3	1	0	10	1000	0.25	1766
	2	10	10	1500	0.25	1766
	3	20	10	2000	0.25	1766

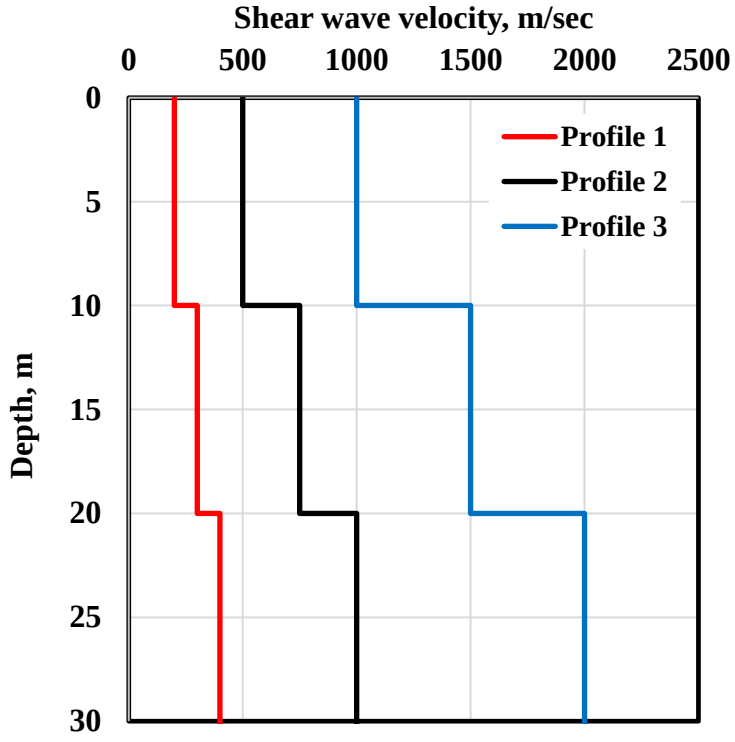

Figure 3.12 V_S Profiles 1 through 3 representing simple site conditions.

3.5.2 Changes in Poisson's Ratio Values

One of the interesting properties of soil is that the value of Poisson's ratio can change considerably due to saturation conditions. Under dry conditions, Poisson's ratio will typically fall in the range of 0.2 to 0.3. However, when fully saturated Poisson's ratio of soft soils can approach 0.5. The partitioning of energy between surface and body waves

and the resulting time records change with Poisson's ratio. The effect of soil saturation was studied by varying Poisson's ratio values of the subsurface layers and repeating the simulations of SASW and HWAW processing.

To investigate the effect of different Poisson's ratio values on the HWAW method, simulations of Profiles 1, 2 and 3 were performed using Poisson's ratio values of 0.25, 0.33, 0.40, and 0.45 to represent a range of soil types and site conditions, as shown in Figures 3.13. Therefore, nine additional profiles were analyzed in this portion of the study. These profiles are indicated by the same profile number but with an extension of P-XX to indicate the Poisson's ratio value. For example Profile 2-P45, indicates Profile 2 with a Poisson's ratio of 0.45.

Results and discussions of the effect of variable Poisson's ratio values relative to the base case of Poisson's ratio of 0.25 are presented in Chapter 4, Section 4.3.3.

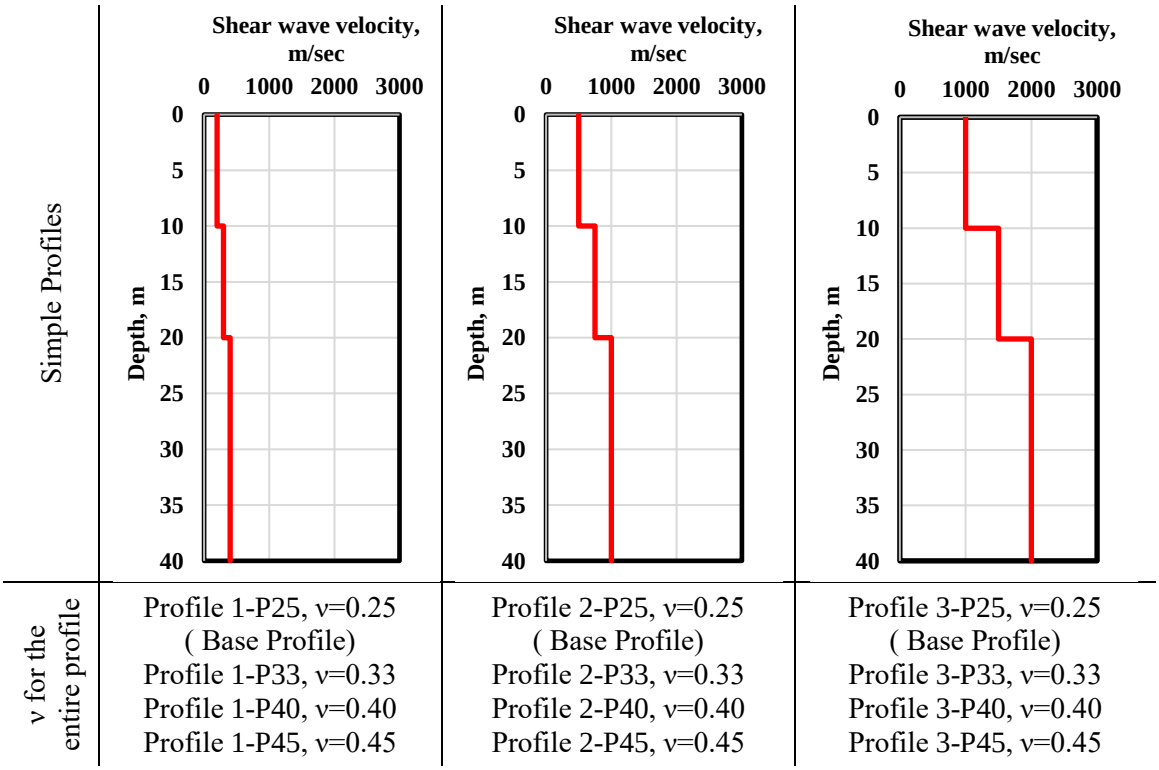

Figure 3.13 Profiles 1, 2 and 3 with different Poisson's ratio values.

3.5.3 Complex Profiles

As noted in Chapter 2, the main limitation of existing literature on the HWAW method is the lack of measurements at complex sites. Based on a literature review of problematic site conditions for SASW and MASW data processing, several complex soil profiles were identified and investigated in this study, namely: (1) sites with a large contrast (3 or greater) in impedance between layers, (2) sites with shallow velocity gradients (3) sites with an embedded low-velocity layer between two higher-velocity layers, (4) and sites with an embedded high-velocity layer between two lower-velocity layers.

To study the performance of HWAW at complex sites, a selection of canonical V_S profiles were identified and adopted from Foti et al. (2017), which was a product of the InterPACIFIC (Intercomparison of methods for site parameter and velocity profile characterization) project. This project was aimed at the comparison of the most common techniques for surface wave analysis in order to evaluate their performance and reliability.

In this research, the canonical soil profiles from Foti et al. (2017) have been scaled down to a depth of 30 m from the 100 m depth used in the InterPACIFIC project study. Thirty meters was selected as the maximum depth for this study because it is a common depth range for geotechnical investigations and is also the depth used to determine site classification (based on $V_{S,\,30}$) which is used in several building codes, including the IBC and EC8.

The following eight baseline soil profiles were used to simulated and analyze data using the conventional SASW procedures and the HWAW method to obtain phase velocity dispersion curves. The study was aimed at evaluating the ability to recover the correct dispersion curve from two-channel recordings. These complex V_S profiles are: (1) two-

layer models with high and very high impedance contrasts, (2) models with shallow linear velocity gradients over different depths (3) three-layer models with a thin and thick low velocity inversion in layer 2, and (4) three-layer models with a thin and thick high velocity inversion in layer 2. A constant Poisson's ratio of 0.25 was assumed for all profiles at all depths which simulates unsaturated soil conditions. These profiles, designated as Profiles 4 through 11, are described in detail in the following sections.

3.5.3.1 Soft-over-Stiff Sites with Large Impedance Contrast

Complex profiles, Profiles 4, 5A, 5B, and 5C are soft-over-stiff profiles. They consist of soil underlain by a stiff halfspace. The depth to the stiff layer in Profile 4 is 6 m while for Profiles 5A, 5B, and 5C, the depths to the stiff layer is varied from 3, 6, and 9 m respectively.

The V_s ratio between the soil and the halfspace for Profile 4 is 3 (V_{S2}/V_{S1}=600/200=3). A constant mass density of the soil was assumed so this ratio is also the impedance ratio. Profiles 5A, 5B, and 5C represent cases with a larger impedance contrast of 4 (V_{S2}/V_{S1}=800/200=4). Table 3.3 shows the individual layer characteristics for Profiles 4, 5A, 5B, and 5C. Profile 4 is presented in Figure 3.14 (a) and Profiles 5A, 5B, and 5C are shown in Figure 3.14(b). As noted in Chapter 2, this is an especially problematic site condition for SASW data processing. Results and discussions of soft-over-stiff sites with large impedance contrasts are presented in Chapter 4, Section 4.4.2.

Table 3.3 Individual layer characteristics of Profile 4 and Profiles 5A, 5B, and 5C.

Profile No.	Layer	Depth, z(m)	Thickness (m)	Shear velocity, V_S, (m/sec)	Poisson's ratio, ν	Density (kg/m^3)
4	1	0	6	200	0.25	2000
	2	6	24	600	0.25	2200
5A	1	0	3	200	0.25	2000
	2	6	27	800	0.25	2200
5B	1	0	6	200	0.25	2000
	2	3	24	800	0.25	2200
5C	1	0	9	200	0.25	2000
	2	9	21	800	0.25	2200

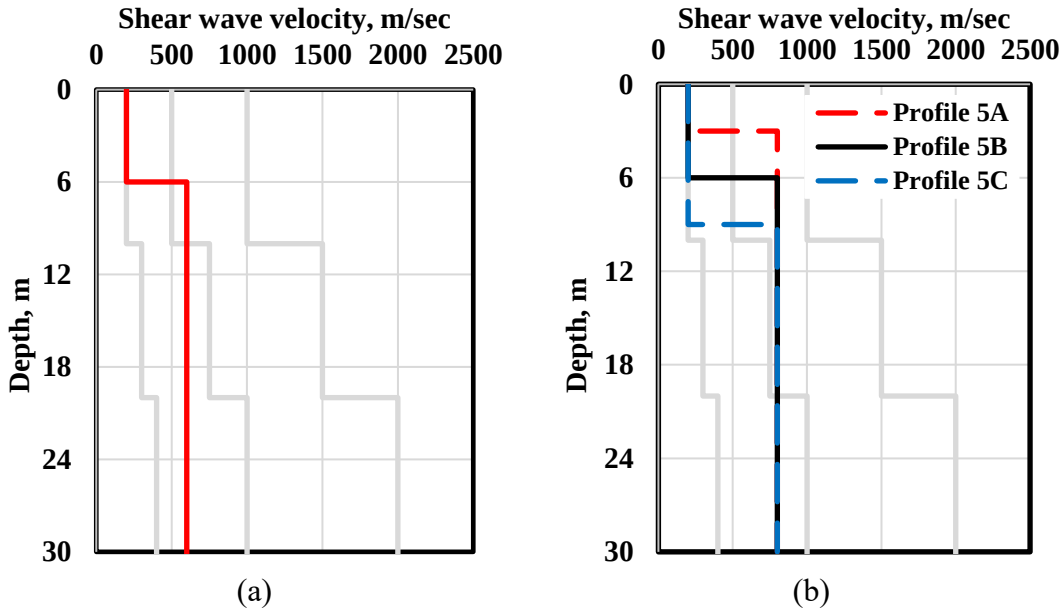

Figure 3.14 Soft-over-stiff soil profiles used for simulations (a) Profile 4 (high contrast), (b) Profiles 5 (very high contrast). Simple profiles are shown in gray for comparison.

3.5.3.2 Linear Velocity Gradient Profiles

The transition between two layers is often of great interest in geotechnical engineering. For example, in earthquake engineering, site response amplification can be quite different for the case of an abrupt transition (with a large impedance contrast) versus a gradual transition. The individual layer characteristics for two complex soil profiles, Profile 6 and 7, with a shallow linear velocity gradient and a deeper linear velocity gradient are shown in Table 3.4 and presented in Figure 3.15. Results and discussions of the linear gradient profiles are presented in Chapter 4, Section 4.4.3.

Table 3.4 Individual layer characteristics of Profile 6 and Profile 7.

Profile No.	Layer	Depth, z(m)	Thickness (m)	Shear velocity, V_S, (m/sec)	Poisson's ratio, ν	Density (kg/m^3)
6	1	0	1	200	0.25	2000
	2	1	1	300	0.25	2000
	3	2	1	400	0.25	2000
	4	3	1	500	0.25	2000
	5	4	1	600	0.25	2000
	6	5	1	700	0.25	2000
	7	6	24	800	0.25	2200
7	1	0	1	200	0.25	2000
	2	1	2	250	0.25	2000
	3	2	3	300	0.25	2000
	4	3	4	350	0.25	2000
	5	4	5	400	0.25	2000
	6	5	6	450	0.25	2000
	7	6	7	500	0.25	2000
	8	7	8	550	0.25	2000
	9	8	9	600	0.25	2000
	10	9	10	650	0.25	2000
	11	10	11	700	0.25	2000
	12	11	12	750	0.25	2000
	13	12	24	800	0.25	2200

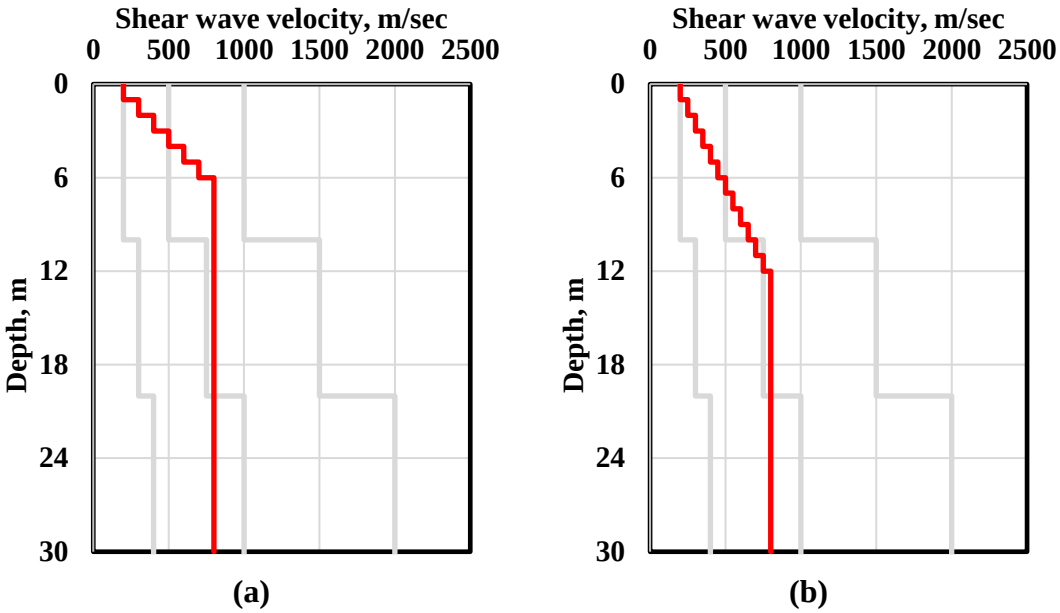

Figure 3.15 Linear velocity gradient soil profiles used for simulations (a) Profile 6 (shallow velocity gradient), (b) Profile 7 (deeper velocity gradient). Simple profiles are shown in gray for comparison.

3.5.3.3 Velocity Inversion (Embedded Lower Velocity Layer)

Profiles 8 and 9 are profiles with an embedded soft layer at a depth of 6 m. The thickness of the soft layer in Profiles 8 and 9 is 3 and 9 m, respectively. Table 3.5 shows the individual layer characteristics for Profiles 8 and 9. Profile 8 is presented in Figure 3.16 (a) and Profile 9 is shown in Figure 3.16 (b). Results and discussions of embedded lower velocity layer profiles are presented in Chapter 4, Section 4.4.4.

Table 3.5 Individual layer characteristics of Profile 8 and Profile 9.

Profile No.	Layer	Depth, z(m)	Thickness (m)	Shear velocity, V_S, (m/sec)	Poisson's ratio, ν	Density (kg/m^3)
8	1	0	6	350	0.25	2000
	2	6	3	250	0.25	2000
	3	9	21	463	0.25	2200
9	1	0	6	350	0.25	2000
	2	6	9	250	0.25	2000
	3	15	15	463	0.25	2200

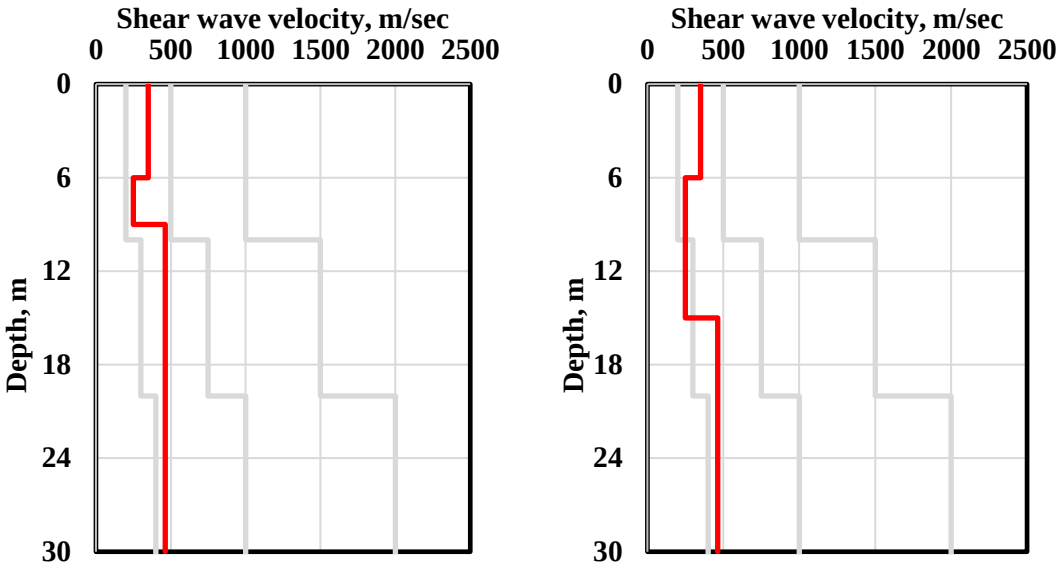

Figure 3.16 Embedded soft layer soil profiles used for simulations (a) Profile 8 (velocity inversion, low-velocity thin layer) (b) Complex Profile 9 (velocity inversion, low-velocity thick layer). Simple profiles are shown in gray for comparison.

3.5.3.4 Velocity Inversion (Embedded Higher Velocity Layer)

Profiles 10 and 11 are profiles with an embedded stiff layer at a depth of 6 m. The thickness of the soft layer in Profiles 10 and 11 is 3 and 9 m respectively. Table 3.6 shows the individual layer characteristics for Profiles 10 and 11. Profile 10 is presented in Figure 3.17 (a) and Profile 11 is shown in Figure 3.17 (b). Results and discussions of embedded higher velocity layer profiles are presented in Chapter 4, Section 4.4.5.

Table 3.6 Individual layer characteristics of Profiles 10 and 11.

Profile No.	Layer	Depth, z(m)	Thickness (m)	Shear velocity, V_S, (m/sec)	Poisson's ratio, ν	Density (kg/m^3)
10	1	0	6	350	0.25	2000
	2	6	3	550	0.25	2000
	3	9	21	463	0.25	2200
11	1	0	6	350	0.25	2000
	2	6	9	550	0.25	2000
	3	15	15	463	0.25	2200

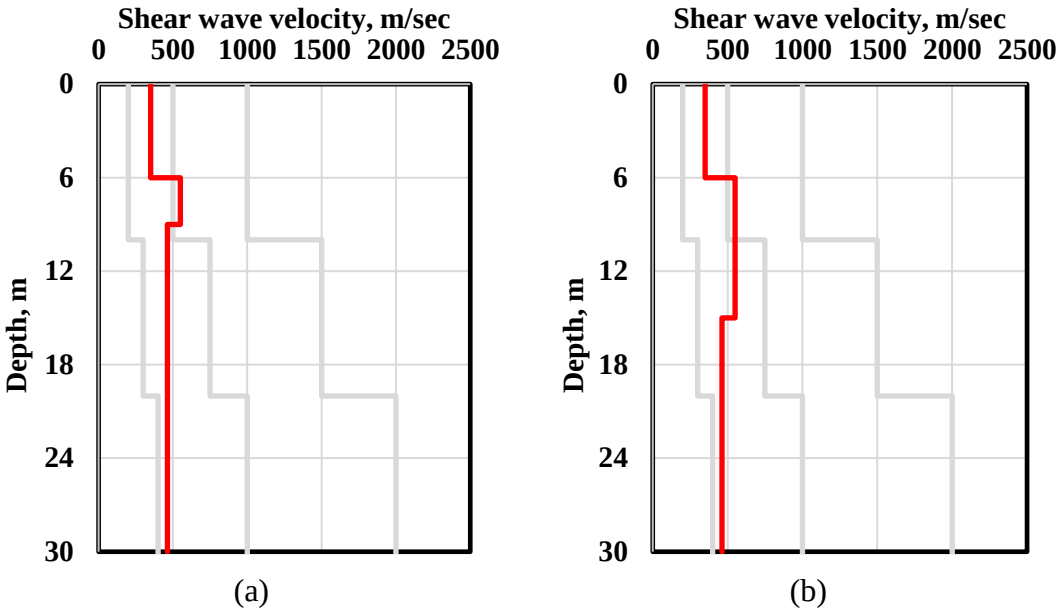

Figure 3.17 Embedded stiff layer soil profiles used for simulations (a) Profile 10 (velocity inversion, high-velocity thin layer) (b) Profile 11 (velocity inversion, high-velocity thick layer). Simple profiles are shown in gray for comparison.

3.6 Data Collection Procedures

The following data collection and processing parameters were varied in this study: (1) sampling frequency, (2) bandwidth of wavelet (3) spacing between receivers and (4) source offset distance. The experimental dispersion curve was then compared to the true theoretical dispersion curve from the FitSASW program.

For the study of the simple profiles, the following four sampling frequencies were used to generate the time records: 1875 Hz, 3750 Hz, 7500 Hz, and 15000 Hz. The number of sample points, N, frequency resolution, Δf, and time length, t are listed in Table 3.7.

Table 3.7 Values of data collection parameters used for simple profiles simulations.

Sampling frequency, f_s, Hz	Number of points, N	Frequency resolution, Δf, Hz	Time length, t, sec
1875	2048	0.91	1.09
3750	2048	1.83	0.55
7500	2048	3.66	0.27
15000	2048	7.32	0.14

A range of bandwidths were used in the HWAW processing, depending on the sampling frequency used. Table 3.8 lists the bandwidth values used for the sampling frequencies of 1875, 3750, 7500, and 15000 Hz. Results and discussions of the effect of sampling frequency and bandwidth are presented in Chapter 4, Section 4.3.1.

Table 3.8 Bandwidths' values used for different sampling frequencies.

Bandwidth frequency, b_w, Hz			
f_s=1875 Hz	f_s=3750 Hz	f_s=7500 Hz	f_s=15000 Hz
1.83	3.66	7.32	14.65
3.66	7.32	14.65	29.30
5.49	10.99	21.97	43.95
8.24	16.48	32.96	65.92
12.82	25.63	51.27	102.54
26.55	53.10	106.20	212.40

The HWAW method is notable for the use of one setup of closely spaced receivers. Receiver spacings of 2 m and 4 m were chosen to be generally consistent with the spacings used in published studies of HWAW method, but some longer receiver spacings from 8 m to 32 m were also simulated.

The source offset was chosen based on the desired profiling depth. The use of a 30 m offset is consistent with the guidelines used in SASW testing (longest wavelength is two times source to receiver distance). Shorter offsets were also simulated for cases where more of the near-field may be used. Data collection procedures that use more of the near-field require shorter arrays and smaller sources, resulting in more efficient data collection, (Kim and Park, 2002, McCaskill, 2014).The source and receiver pair combinations used to create the dispersion curve from the HWAW measurements are presented in Table 3.9.

Table 3.9 Source offsets (S-R1) and receiver spacings (R1-R2) used in the HWAW method.

S-R1, m	R1-R2, m	S-R1, m	R1-R2, m	S-R1, m	R1-R2, m	S-R1, m	R1-R2, m	S-R1, m	R1-R2, m
14	2	12	4	16	8	16	16	32	32
18	2	16	4	24	8	24	16	-	-
22	2	20	4	32	8	32	16	-	-
26	2	24	4	-	-	-	-	-	-
30	2	28	4	-	-	-	-	-	-

SASW data collection were also simulated for each soil profile. Synthetic SASW data were simulated for the different receiver spacings and source offsets listed in Table 3.10. The SASW data were processed using both manual phase unwrapping in WinSASW and HWAW processing.

Table 3.10 Source offsets and receiver spacings used in the SASW method.

Source to first receiver, (S-R1), m	Receiver spacing, (R1-R2), m
2	2
4	4
8	8
15	15
30	30
45	45
60	60

3.7 Field Studies

To verify the findings from the study performed with simulated data, field data were analyzed from selected sites which represent some of the site conditions studied in the simulated data portion of this research. Sites were chosen that had reliable ground truth data of the site conditions based on boring logs or other geophysical measurements.

The objectives of the field portion of this research were to: (1) verify that reliable dispersion curves could be developed using the HWAW procedures under real world conditions, (2) verify that the HWAW processing approach could effectively deal with

mode transformations observed at soft-over-stiff sites, (3) verify observations of HWAW measurements at high Poisson's ratio sites (i.e. saturated soil conditions) and (4) perform automated phase unwrapping using the HWAW methodology on data collected using conventional SASW procedures.

Three sites were selected for this study. Site 1 is a soft-over-stiff, very high-impedance contrast site located on the campus of the University of Missouri. Site 2 is a soft, saturated soil site located in Christchurch New Zealand. Site 3 is a profile site with a moderate increase in shear wave velocity located in Boise, Idaho. Field measurements at Site 1 were performed by the author, while data from Sites 2 and 3 were collected by other investigators and made available for shared-use. Results and discussion of field studies for each of the following sites are presented in Chapter 5.

3.7.1 Site 1: Shallow High Impedance Contrast– University of Missouri

3.7.1.1 Site Location and Experimental Procedure

Site 1 is located on the campus of the University of Missouri west of Virginia Avenue and north of Hospital Drive in Columbia, Missouri as shown in Figure 3.18. The site is the future home of the Next Generation Precision Health Initiative building. Measurements were performed at a location adjacent to borehole B7 as indicated by the yellow line in Figure 3.18. Measurements at B7 were performed in September, 2020.

This site was chosen because it is characterized by soil over shallow stiff rock. Based on the borehole log of B7 (Figure 3.19), limestone is encountered at a depth of 2.68 m.

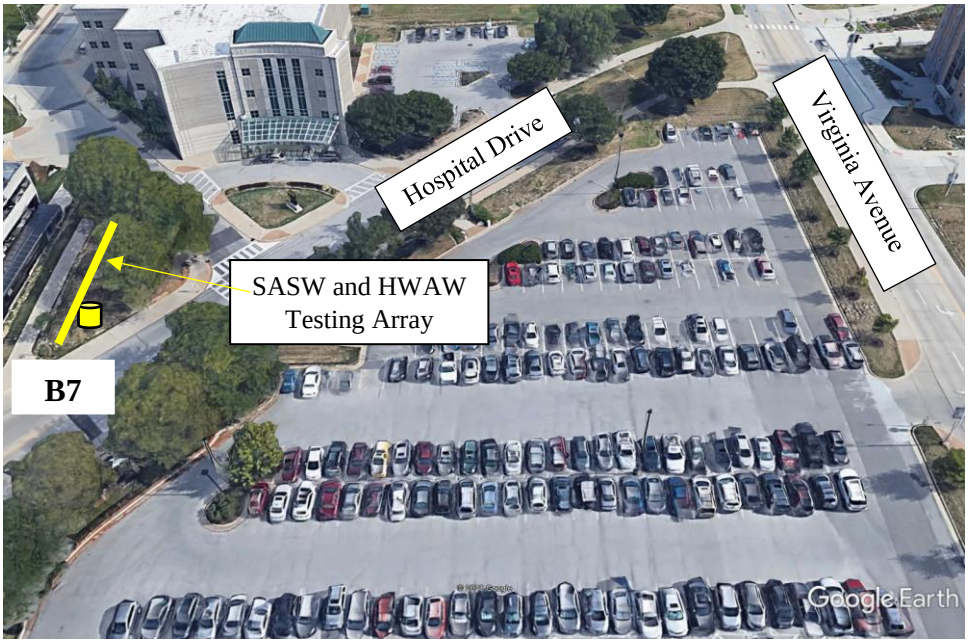

Figure 3.18 Google Earth image and top view of the future home of Next Generation Precision Health Initiative building and borehole location, B7, Columbia, Missouri.

According to the field exploration and laboratory testing report conducted by Crockett Geotechnical Labs (Geotechnical Engineering Report, No.CP190721) and based on borehole log of B7, the encountered subsurface conditions are described as topsoil, ranging in thickness from 8 to 15-cm, or asphalt pavement underlain by base rock ranging in thickness from 5 to 30-cm. Underlying the surficial materials, native soils consisted generally of lean to fat clay to a depth of 2.68 m. Underlying the above mentioned native soils, hard limestone was identified at depths of 2.68 m. The complete soil stratigraphy for B7 is presented in Figure 3.19. Soil velocities are expected to be on the order of 100 to 200 m/s and the velocity of the limestone is expected to be at least 1500 m/s based on lab measurements of limestone cores. Therefore, a very high impedance contrast exists at this site.

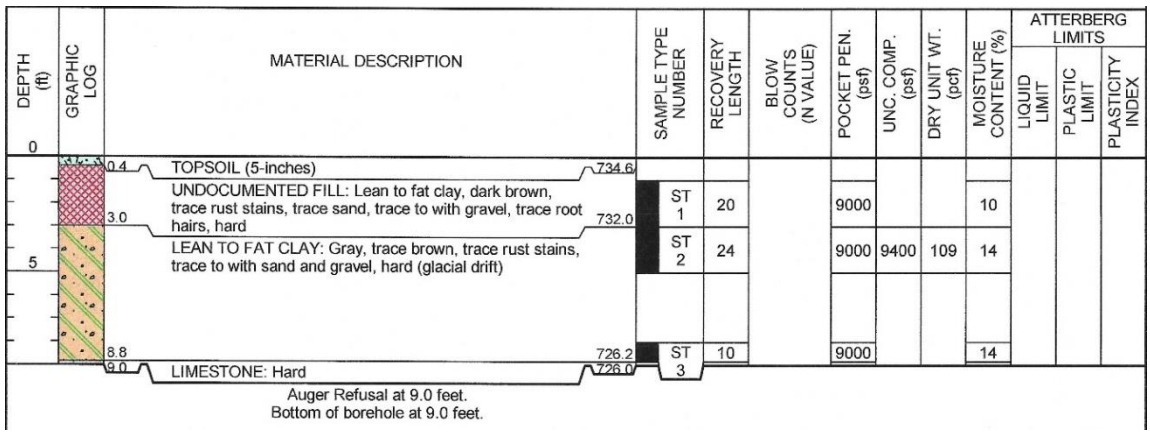

Figure 3.19 Estimated soil stratigraphy of B7 based on geotechnical logs (from Engineering Report, No.CP190721, conducted by Crockett Geotechnical Lab).

HWAW and SASW measurements were performed at the B7 location shown in Figure 3.18. The primary objective of this work was to verify that the HWAW processing approach could effectively handle the mode transformation observed at soft-over-stiff sites, as compared with the SASW method.

Both measurements for the HWAW and SASW methods were conducted using two, 1-Hz geophones manufactured by Sercel Incorporated (Model Number L-4, Serial Numbers: 3835, and 3836). Three impacts from a 4.5 kg (10-lb) sledgehammer were used to excite surface wave energy for SASW measurements and only a single impact was used for the HWAW method. The source offset, receiver spacing, and sampling frequencies used to collect data for the SASW and HWAW measurements for B7 are presented in Table 3.11.

Table 3.11 Data collection and data processing used in the SASW and HWAW methods.

Test method	Source offset to first receiver, (S-R1), m	Receiver spacing, (R1-R2), m	Sampling frequency, f_s, Hz	Time length, sec
SASW	0.61(2 ft)	0.61(2 ft)	1280	1.6
	1.22 (4 ft)	1.22 (4 ft)	1280	1.6
	2.44 (8 ft)	2.44 (8 ft)	1280	1.6
	4.57 (15 ft)	4.57 (15 ft)	256 and 640	8 and 3.2
	9.14 (15 ft)	9.14 (15 ft)	256	8
	12.20 (30 ft)	12.20 (30 ft)	128	16
	15.24 (50 ft)	15.24 (50 ft)	128	16
HWAW	8	4	2560	0.8
	12	4	2560	0.8
	16	4	2560	0.8

After the geophones were in place, the data were recorded using a 4-channal "Quattro" Dynamic Signal Analyzer manufactured by Data Physics. The data were collected in the form of time records for the HWAW method and a transfer function (a wrapped phase plot showing the difference between receivers as a function of frequency) for the SASW method. Figure 3.20 shows the test setup used for B7 using a pair of 1-Hz geophone receiver and a sledgehammer.

For SASW measurements data, as described in Section 3.4, the WinSASW program was used to create a composite experimental dispersion curve from manual phase unwrapping of the phase plots. For the HWAW measurements and HWAW processing of the SASW data, the MATLAB algorithm was used to produce the phase velocity dispersion curve. Results and discussions from the analysis performed using the SASW and HWAW methods are presented in Chapter 5 Section 5.2.

Figure 3.20 Test setup and equipment used for SASW and HWAW methods for Site 1.

3.7.2 Site 2: High Poisson's Ratio Site – Christchurch, New Zealand

3.7.2.1 Site Location and Experimental Procedure

A data set of surface wave measurements (termed the UTexas1 Surface Wave Dataset) was collected at Queen Elizabeth II Park (QEII Park) in Christchurch, as part of an NSF project performed by other investigators. This data set was used in a prior study of surface wave interpretation variability and the data were made available for shared-use (Cox et al., 2014). The QEII Park is located approximately 1.5 km west of the eastern coast of Pegasus Bay on the South Island of New Zealand.

This site consists of loose, interbedded sand and gravels (Figure 3.21) with a shallow water table. This site was chosen to verify the observations of HWAW measurements at high Poisson's ratio sites where soft, saturated soil conditions exist.

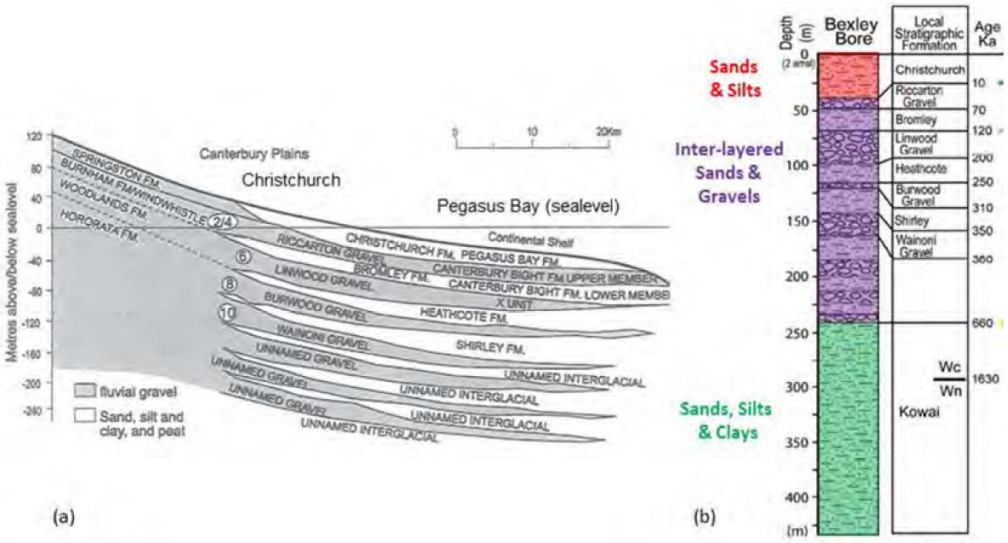

Figure 3.21 (a) Geology beneath Christchurch and Pegasus Bay showing a sequence of deep inter-layered gravel and sand formations, and (b) simplified representation of the geologic layering from Bexley Well2 (modified from Barnes et al. 2011), adopted from Cox et al. (2014).

The surface wave dataset collected at QEII in Christchurch, New Zealand used both active and passive surface wave energy. This research only used the active source measurements. The first phase of the active-source measurements utilized a sledgehammer source and a linear-array of receivers. The sledgehammer linear-array data were collected using a spread of 48, 4.5-Hz vertical geophones with a uniform spacing of 2 m, resulting in a total array length of 94 m. Four separate source-offset distances of 5, 10, 20 and 40 m from the northern-most receiver were used. At each source-offset location, 10 blows of a 4.5 kg sledgehammer on an aluminum strike-plate, overlain by a rubber damping pad, were recorded in the time domain as separate shots. Each shot was sampled at 250 Hz for a total of 4 seconds. These data were collected to allow investigators to use MASW or SASW processing of the data. In this research, selected time records from the receiver spread were used to perform the SASW and HWAW measurements.

A second set of active-source measurements were also performed with a higher energy source to generate low frequency energy. A large Vibroseis truck (Figure 3.22) was

positioned at source-offset distances from the first receiver of 20-m, 40-m and 80-m. For each source-offset location, the Vibroseis was stepped from 10 Hz to 1 Hz in 0.1 Hz increments (91 points total). These data were not analyzed in this study, but the low frequency dispersion curve generated from this data by other researchers was used for comparison purposes.

Active source measurements data using sledgehammer (single impact data) and vibroseis were used in the analysis of SASW method. Data is interpreted using the conventional phase unwrapping procedures.

The same time records from SASW method performed by sledgehammer were also processed using the HWAW method as described in Chapter 3. Data collection and processing parameters used in the processing are presented in Table 3.12.

Figure 3.22 Low-frequency NEES vibrator (from: http://nees.utexas.edu/Equipment-Liquidator.shtml).

The selected data from active source measurements using sledgehammer were analyzed using the HWAW method with different source offsets and receiver spacing pairs, as summarized in Table 3.12.

The resulted dispersion curves for different test setups using the HWAW method were compared with Rayleigh wave dispersion curves (Figure 3.23) analyzed using a variety of

different methods by other investigators, as reported in Cox et al. (2014). Example dispersion curves from this site show that the surface wave velocities are very low (100 m/s). For comparison plots, the Rayleigh wave dispersion curves versus frequency were extracted using an online plot digitizer software namely, WebPlotDigitizer, version 4.3. Results and discussions from the analysis performed using the SASW and HWAW methods are presented in Chapter 5 Section 5.3.

Table 3.12 Data collection and processing parameters used in the SASW and HWAW methods.

Test method	Sampling frequency, f_s, Hz	Total time, seconds	Number of samples	sampling period, milliseconds	Source offset, S-R1, m	Receiver spacing, R1-R2, m
SASW (Sledgehammer)	250	4	1000	4	5	4
					10	10
					20	20
					40	40
SASW (Vibroseis)	10	9.1	91	0.05	40	40
HWAW	250	4	1000	4	5	2
					5	4
					7	2
					7	4
					7	8
					9	2
					9	4
					9	10
					10	2
					10	4
					10	10
					11	2
					11	4
					11	12

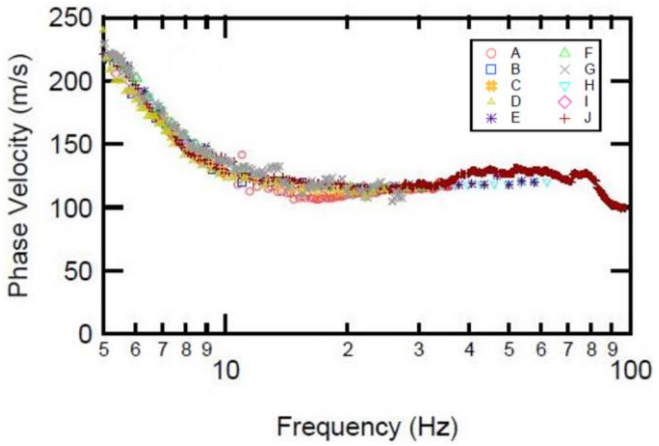

Figure 3.23 Comparison of mean Rayleigh wave dispersion estimates analyzed using a variety of different methods by multiple investigators, Cox et al. (2014).

3.7.3 Site 3: Moderate Impedance Contrast – Capital Station, Boise, Idaho

3.7.3.1 Location and Experimental Procedure

The site was chosen because it represents a two layer profile with a moderate impedance contrast of about two. The surface wave data at this site were collected by Dr. Paul Michaels from the University of Idaho (retired) and made available for shared use on the ASCE GI Geophysical Engineering Committee website. (https://www.geoinstitute.org /committees/ technical-committees/ geophysical-engineering).

Ground truth at this location consists of downhole measurements that were performed by Boise State University, Center for Geophysical Investigation. The V_S profile generated from the downhole data to a depth of 11 m is shown in Figure 3.24. Based on the moderate contrast in velocity, this site should be a normally dispersive profile.

Surface wave data were collected at the Capital Station project in Boise, Idaho using different linear arrays. Multiple lines were tested and the notation of the line which was used in this analysis was Line c015 (ID 8).

A sledgehammer source located 5 m from the first receiver was used at Line c015 and recorded using an array of 48, 4.5-Hz vertical geophones with a uniform spacing of 2 m,

resulting in a total array length of 94 m. Only eleven selected receivers were used for the SASW and HWAW test setups from the Line c015, as shown in Figure 3.25 where R001 to R011 represents Receiver 1 through Receiver 11.

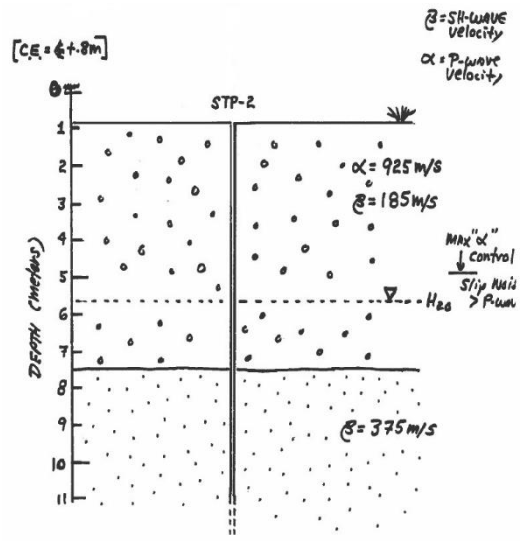

Figure 3.24 Interpretation of downhole velocity measurements near the study area performed by Boise State University, Center for Geophysical Investigation of the shallow Subsurface.

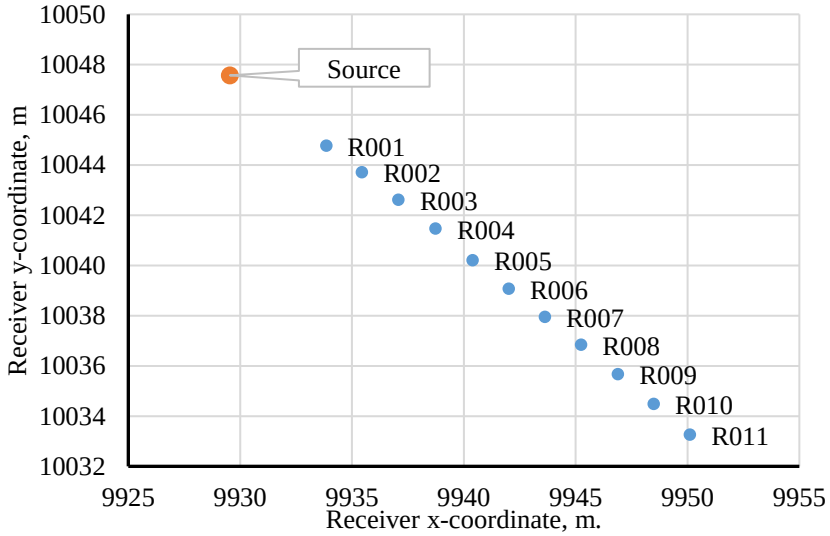

Figure 3.25 Layout of the linear array used in the SASW and HWAW methods showing the source and receivers locations for Site 3.

Time records were collected at each receiver location and each shot was sampled at 2000 Hz for a time of 1.25 seconds (sampling period = 0.0005 seconds and number of samples, N=2500).

The selected time records data were used in the analysis of SASW method and interpreted using the phase unwrapped technique. Also, same time records were processed by the HWAW method. Table 3.13 summarizes the selected data used for the HWAW and SASW measurements.

Table 3.13 Data collection and processing parameters used in the SASW and HWAW methods.

Test method	Sampling frequency, f_s, Hz	Total time, seconds	Number of samples	sampling period, milliseconds	Source offset, S-R1, m	Receiver ID	Receiver spacing, R1-R2, m	Receiver ID
SASW	2000	1.25	2500	0.5	5	R001	6	R003
					7	R002	8	R005
					11	R003	12	R007
					13	R004	14	R009
					15	R005	16	R011
					17	R006	18	R013
HWAW	2000	1.25	2500	0.5	5	R001	2	R002
					5	R001	4	R003
					7	R002	2	R003
					7	R002	4	R004
					9	R003	2	R004
					9	R003	4	R005
					11	R004	2	R005
					11	R004	4	R006
					13	R005	2	R006
					13	R005	4	R007
					15	R006	2	R007
					17	R007	4	R009
					21	R009	2	R010
					21	R009	4	R011

The time records from this site were also selected using an HWAW-type arrangement consisting of a single array with short receiver spacings and source offsets as shown in Table 3.13. Results and discussions from the analysis performed using the SASW and HWAW methods for this site are presented in Chapter 5 Section 5.4.

CHAPTER 4 RESULTS AND DISCUSSIONS FROM STUDY OF HWAW METHOD USING SIMULATED DATA

4.1 Introduction

This chapter presents results and discussion from the processing of simulated surface wave data using the HWAW method at simple and complex geotechnical profiles. In Section 4.2 results are presented from a validation study of the HWAW algorithm developed for this research and corrections applied to the dispersion curve are described. In Section 4.3 results obtained from applying the HWAW algorithm to simple geotechnical profiles (Profiles 1-3) using various data collection and data processing parameters are presented. The effect of these parameters on the accuracy of the dispersion curve is discussed and acceptable values for the parameters are identified. Section 4.3 also includes results from a study of the effect of Poisson's ratio values on the effectiveness of the HWAW method. In Section 4.4results obtained from applying the HWAW method at complex geotechnical profiles (Profiles 4 – 12) are presented. The use of HWAW processing on data collected using conventional SASW data collection procedures is investigated in Section 4.5. Finally, in Section 4.6 the results from this portion of the research are synthesized to develop recommended procedures for applying the HWAW method at geotechnical sites. A summary of the chapter is provided in Section 4.7.

4.2 Validation of HWAW Algorithm

An algorithm to perform HWAW processing of two-channel surface wave data was developed in MATLAB as part of this research. This algorithm was tested and validated by simulating time records for V_S profiles found in the HWAW literature, processing the data with the HWAW algorithm, and comparing the dispersion curves to published dispersion

curves. Specifically, V_S profiles and dispersion curves presented in Kim and Park (2001) and Hwang and Park (2014) were used in this portion of the study. These profiles are shown in Chapter 2, Tables 2.1 and 2.2 respectively. For both the published studies and this study, the program FitSASW was used to compute the simulated time records as discussed in Chapter 3, Section 3.2. Comparisons between the dispersion curves are shown in Figure 4.1, where the published dispersion curves were recreated from digitized values generated from the published figures. It should also be noted that the Hwang and Park (2014) study included simulated noise in the time records, which was not simulated in this study. As can be seen in Figure 4.1, the dispersion curves from this study are in very good agreement with the theoretical dispersion curves for the profile and in good agreement with the results found in the literature. Some of the differences may be attributable to the added noise, errors from digitization of the dispersion curves, or differences in processing parameters that were not identified in the paper.

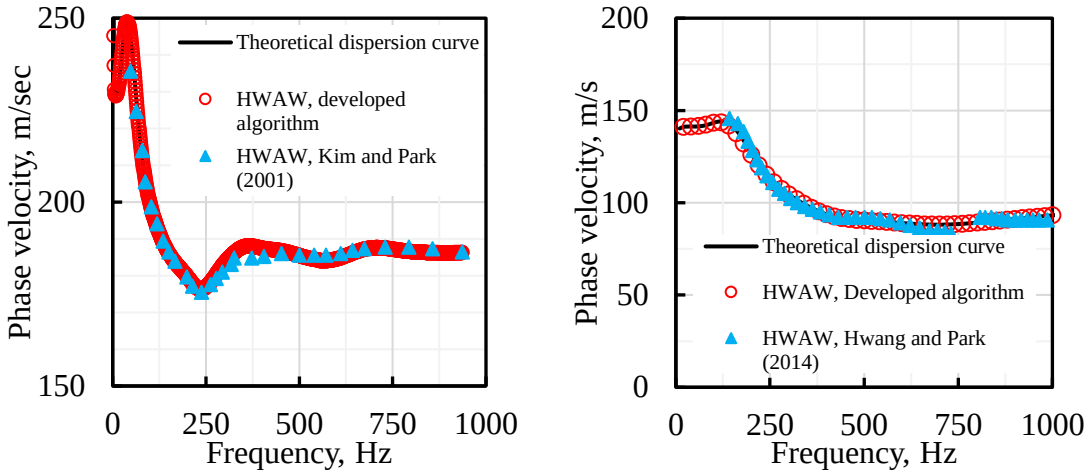

Figure 4.1 Comparison of dispersion curves found in the literature and those obtained using the developed algorithm, (a) Case 1 from Kim and Park, 2001 (b) Gravel ballast layer from Hwang and Park (2014).

Although the HWAW algorithm developed in this study provided consistent results with the published results, it was found that for some V_S profiles, several of the processed

points were not consistent with the theoretical dispersion curve. An example of this is shown in Figure 4.2 for another published profile presented in Hwang and Park (2014), as shown in Table 4.1.

Table 4.1 Material properties for shear wave velocity profile from Hwang and Park, (2014).

Layer No.	Thickness (m)	Shear velocity, V_S, (m/s)	Unit weight(kN/m^3)	Poisson's ratio
1	2	610	17.66	0.25
2	27	1150		
3	11	1900		

In this case, the data analysis procedure described in Chapter 2, Section 2.2.4 did not work correctly in some frequency bands (specifically, 133 to 163 Hz, 218 to 232 Hz, 289 to 320 Hz, and 452 to 480 Hz) as shown in Figure 4.2. In these frequency ranges, the wrong phase cycle (see Figure 2.10d) is identified resulting in an incorrect phase velocity. This issue was noted in the published paper by Hwang and Park (2014) and attributed to differences in the waveform envelope shape at Receivers 1 and 2, however, the authors did not provide a clear explanation as to how to correct this issue.

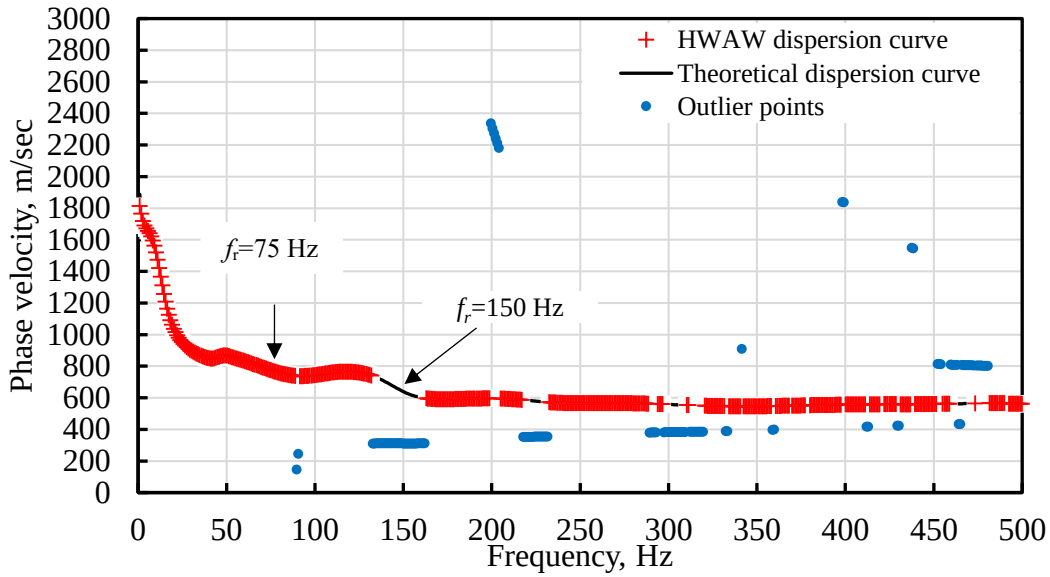

Figure 4.2 Dispersion curve generated from HWAW processing of profile adopted from Hwang and Park (2014) showing outlier points which do not following the theoretical dispersion curve.

Examples of correctly and incorrectly identified phase cycles are shown using two points on the HWAW dispersion curve (Figure 4.2) for the soil profile adopted from Hwang and Park (2014). An example of correct identification is shown in Figure 4.3 for the frequency value of 75 Hz and an example of an incorrect identification of phase velocity is shown in Figure 4.4 for the frequency value of 150.15 Hz. From Figure 4.3 it is observed that the procedure described in Chapter 2 results in identification of the phase time at Receiver 2 that produces the correct phase velocity. However, from Figure 4.4, it is observed that the phase time identified at Receiver 2 using the same procedure results in a phase velocity that significantly underestimates the true value. The phase time at Receiver 2 that corresponds to the correct phase velocity is located at a different cycle. Possible phase time values are located at times shifted from the previously calculated t_{ph}^2 by an amount equal to the period corresponding to the inverse of the frequency component (in this case 1/150.15 sec) multiplied by *N*, where *N* is an integer. Therefore, the possible correct t_{ph}^2 values are calculated as:

$$t_{ph,possible}^2 = period \times N + t_{ph}^2 \tag{4.1}$$

To correct these erroneous points, the $t_{ph,possible}^2$ values were obtained for different values of integer *N*. Then, the phase velocity value corresponding to each $t_{ph,possible}^2$ was calculated and plotted as shown in Figure 4.5. This figure shows the HWAW dispersion curves with possible values based on *N*. When an *N* value of 1 is applied to the 150 Hz point, for example, the resulting phase velocity is in agreement with the theoretical value, as shown in Figure 4.5. To automate this correction process, a MATLAB script was developed to search for the correct value of V_{ph} among all the possible values of V_{ph} corresponding to $t_{ph,possible}^2$. The only input required of the user is to identify a point on

the correct dispersion curve. As seen in Figure 4.2, the red points clearly identify the correct dispersion curve. The algorithm then searches for the V_{ph} points (developed from different N value) that are consistent with the correct dispersion curve. This was done by calculating the absolute difference ratio between each point on the HWAW dispersion curve and all other calculated $V_{ph,possible}$ corresponding to $t^2_{ph,possible}$ at the same frequency. The corrected dispersion curve after applying this procedure is in agreement with the theoretical dispersion curve, as shown in Figure 4.6. This procedure was used throughout this research to automatically correct outlier points and recover the correct dispersion curve.

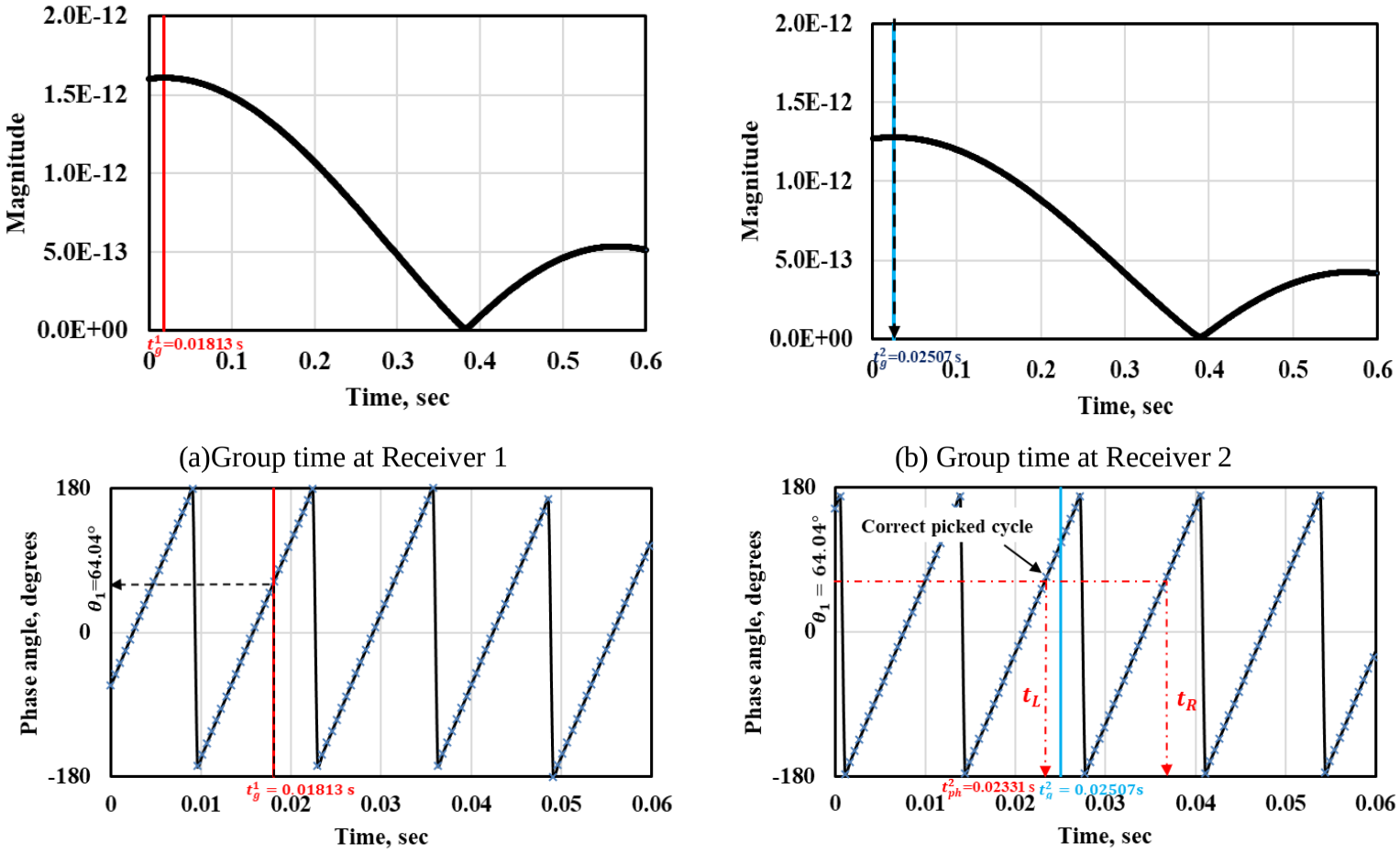

(a)Group time at Receiver 1

(b) Group time at Receiver 2

(c) Phase time at Receiver 1

(d) Phase time at Receiver 2

Figure 4.3 Group and phase times at Receivers 1 and 2 showing correctly identified values for the frequency value of 75 Hz.

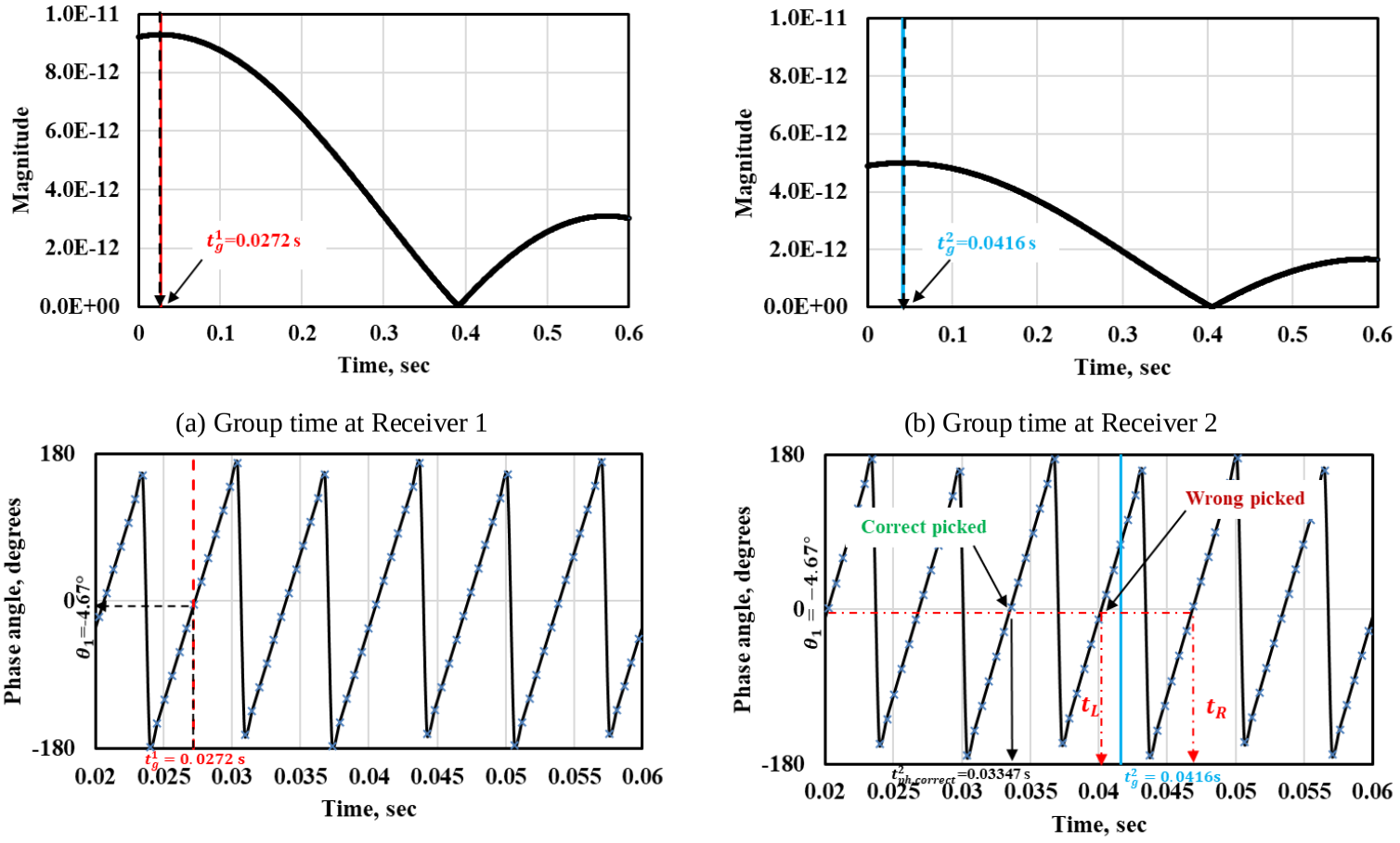

(a) Group time at Receiver 1

(b) Group time at Receiver 2

(c) Phase time at Receiver 1

(d) Phase time at Receiver 2

Figure 4.4 Group and phase times at Receiver 1 and 2 showing the incorrectly identified cycle for the frequency value of 150.15 Hz.

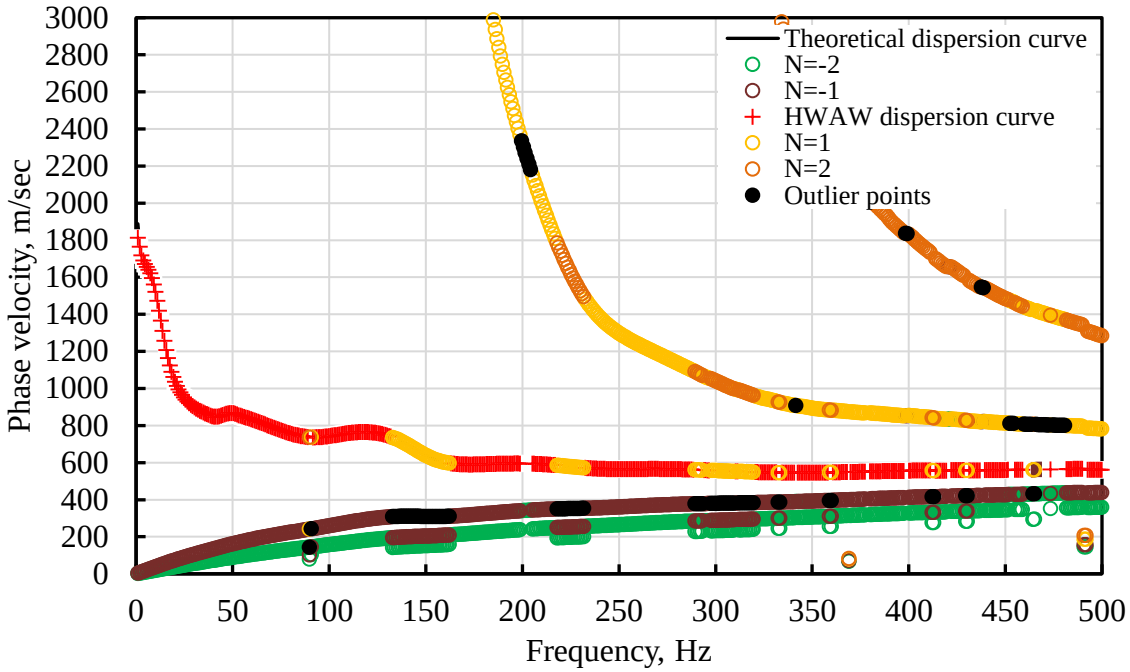

Figure 4.5 Dispersion curve from HWAW processing of the profile adopted from Hwang and Park (2014) showing the outlier points which do not follow the theoretical dispersion curve along with possible values based on different values of *N*.

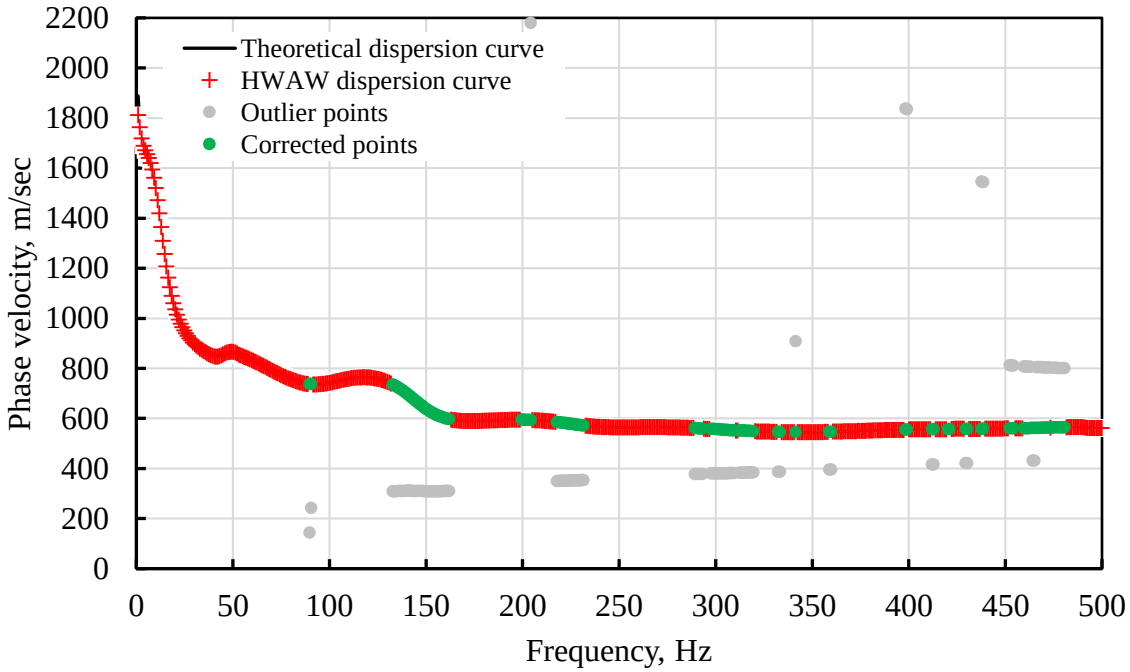

Figure 4.6 Result of automated process for determining the corrected HWAW dispersion curve for the soil profile adopted from Hwang and Park (2014).

4.3 Data Collection and Processing of Simple Profiles

This section presents and discusses the effect of signal processing and data collection parameters, such as sampling frequency, bandwidth, source offset distance, and receiver pair spacing on the accuracy of dispersion curves obtained using the HWAW processing method. The study was performed by simulating time records using a variety of data collection arrangements for the simple profile conditions (Profiles 1-3) followed by processing of the data with the HWAW method using different processing parameters. The effect of the data collection and processing parameters are quantified and discussed. Section 4.3.1 presents the effect of sampling frequency and bandwidth, Section 4.3.2 presents the effect of source and receiver arrangement, and Section 4.3.3 presents the effect of Poisson's ratio on simple profiles.

4.3.1 Study of Sampling Frequency and Bandwidth

4.3.1.1 Introduction

The first decision when collecting surface wave data is what sampling frequency (i.e. digitized samples per second) should be used to record the time records. In SASW measurements the sampling frequency is selected to provide the best resolution in the frequency range of interest. However, for HWAW processing this may not be the best approach. Because HWAW processing requires determination of the time interval between arrivals at Receiver 1 and 2, the time resolution may also be an important parameter. The sampling frequency, f_s, is related to the time resolution, Δt as:

$$\Delta t = \frac{1}{f_s} \tag{4.2}$$

Further, the sampling rate will control the highest measurable frequency (i.e. Nyquist frequency), f_{Ny}, which is equal to half of the sampling frequency. This frequency will

control the shortest wavelength and hence the shallowest profiling depth. Importantly, f_s and the number of time sampling points, determines the length of the time record and the frequency resolution, Δf, as:

$$\Delta f = \frac{f_s}{number\ of\ points} \tag{4.3}$$

The frequency resolution will control the lowest measured frequency (i.e. longest wavelength) which will determine the maximum profiling depth. Typically, surface wave measurements are performed such that the longest wavelength is 2 to 3 times the desired profiling depth. The frequency resolution will also control the minimum bandwidth that can be applied in HWAW processing.

For example, if the sampling frequency, f_s, is 7500 samples/sec and the number of time domain points is 2048, the highest frequency (i.e. Nyquist frequency) is $f_{Ny} = \frac{f_s}{2} = 3750$ Hz (1024 points), and the frequency resolution, Δf is:

$$\Delta f = \frac{f_s}{\text{Number of points}} = \frac{7500}{2048} = 3.66 \text{ Hz}$$

The time resolution, Δt is:

$$\Delta t = \frac{1}{f_s} = \frac{1}{7500} = 0.133\ msec$$

And the time span or duration of the recording, t is:

$$t = \text{number of points} \times \frac{1}{f_s} = 2048 \times \frac{1}{7500} = 0.27\ sec$$

Therefore, one of the research questions addressed in this study is, how does the sampling frequency used in HWAW data collection and the related bandwidth values affect the accuracy of the calculated dispersion curve? To investigate this question, HWAW data

collection procedures were simulated for a range of simple V_S profiles covering typical shear wave velocity values and profiling depths encountered in geotechnical engineering applications. The V_S profiles studied are presented in Chapter 3 Section 3.5.

4.3.1.2 Results of the Effect of Sampling Frequency and Bandwidth on Simple Profiles

The results presented in this section were generated by varying sampling frequency and bandwidth values in the collection and processing of HWAW data. For this portion of the study it was necessary to establish values for the source offset and receiver spacing that remained constant for all cases presented here. A source offset of 20 m and receiver spacing of 4 m were chosen based on an examination of existing HWAW literature and choosing values that were consistent (relative to profiling depth) with those used in published studies. The effect of changing these parameters is studied and presented later in Section 4.3.2.

Four sampling frequencies were selected for this study: 1875 Hz, 3750 Hz, 7500 Hz, and 15000 Hz. The same number of sampling points (2048) was used in each case. The values of the Nyquist frequency, f_{Ny}, number of sampling points, frequency resolution, Δf, time resolution, Δt, and time length, t are summarized in Table 4.2.

For example as shown in Table 4.2, the sampling frequency of 1875 Hz produces excellent frequency resolution and poor time resolution, while the sampling frequency of 15000 Hz produces poor frequency resolution and excellent time resolution. Simulated time records were generated using these four sampling frequencies for the simple soil Profiles 1-3 (Figure 4. and processed with the HWAW method.

Table 4.2 Values of data collection parameters used for simulations of Profiles 1-3.

Sampling frequency, f_s, Hz	Nyquist frequency, f_{Ny}, Hz	Number of points	Frequency resolution, Δf, Hz	Time resolution, Δt, msec	Time length, t, sec
1875	937.5	2048	0.91	0.533	1.09
3750	1875	2048	1.83	0.267	0.55
7500	3750	2048	3.66	0.133	0.27
15000	7500	2048	7.32	0.067	0.14

Profiling depths of 30 m were assumed for Profiles 1, 2, and 3. The maximum wavelength needed to profile to these depths was assumed to be equal to 2 to 3 times the profiling depth (60 to 90 m).

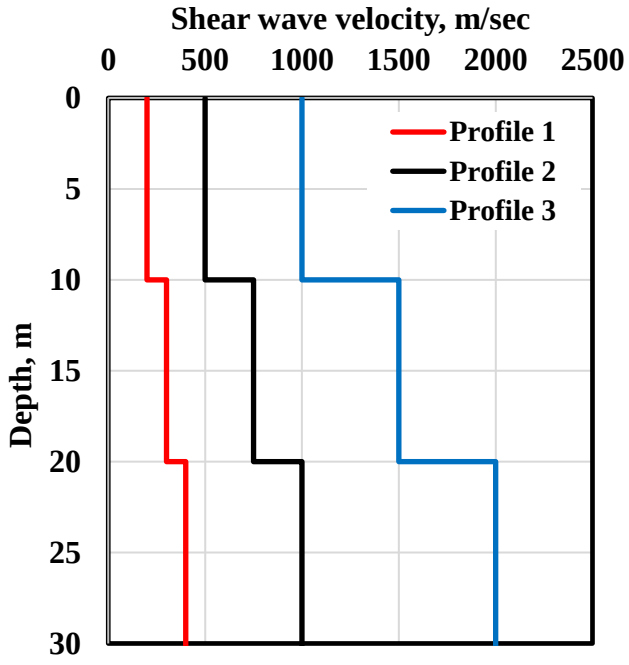

Figure 4.7 Simulated simple V_S profiles with Poisson's ratio=0.25.

Time domain data were generated using FitSASW for each of the simple V_S profiles using four different sampling frequencies, 1875, 3750, 7500, and 15000 Hz. A three-point bandwidth centered at each frequency was initially used in the processing of the data. In all cases, Poisson's ratio was held constant at a value of 0.25 for all depths. Also, the source

and receiver spacing were kept constant with a source offset of 20 m and receiver spacing of 4 m.

An example of the effect of sampling frequency on phase velocity dispersion curves generated from HWAW processing is shown using Profile 2 data in Figures 4.8 and 4.9 where it is plotted in terms of frequency and wavelength, respectively. When comparing the derived dispersion curves to the theoretical dispersion curve (shown in black) it is apparent that the lowest sampling frequency, f_s=1875 Hz, produced a good match between the theoretical and HWAW dispersion curves over all frequency ranges. However, for the higher sampling frequencies, and especially the highest sampling frequency of 15000 Hz, a poor match is observed between the theoretical and the HWAW dispersion curve, especially at frequencies below about 30 Hz.

These low frequencies are required to generate long wavelengths for deep shear wave velocity profiles. In this case, the velocities begin to deviate from the true values at wavelengths of about 30 m, which would only allow for V_S profiles to depths of 10 or 15 m. Similar figures for Profile 1 and 3 are shown in Appendix A.

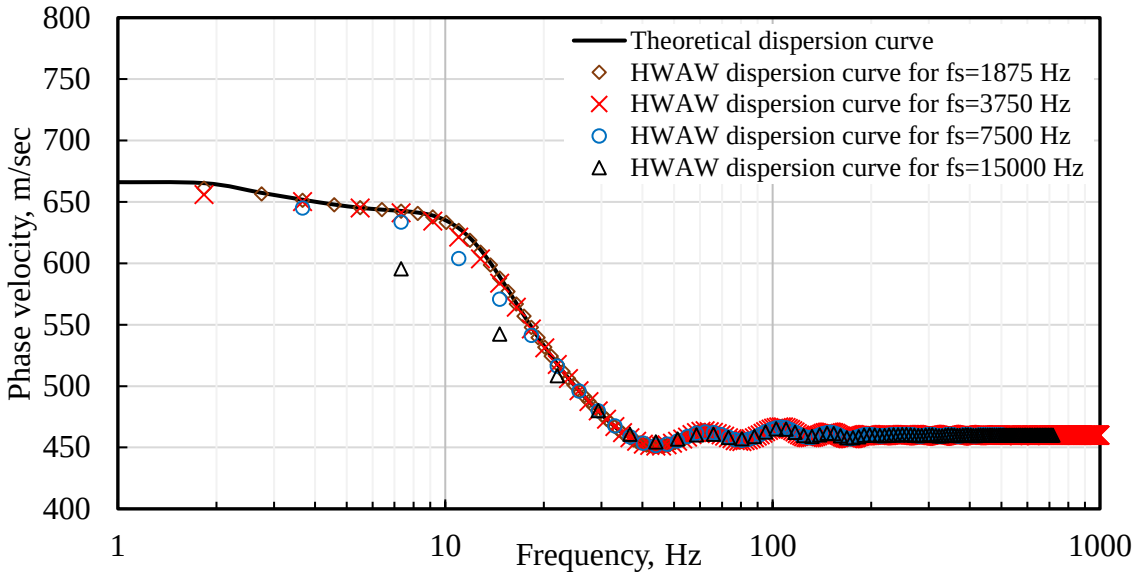

Figure 4.8 Comparison of phase velocity dispersion curves generated for Profile 2 (plotted in terms of frequency) using different sampling frequencies and a three-point bandwidth. Receiver spacing is 4 m and Source offset is 20 m.

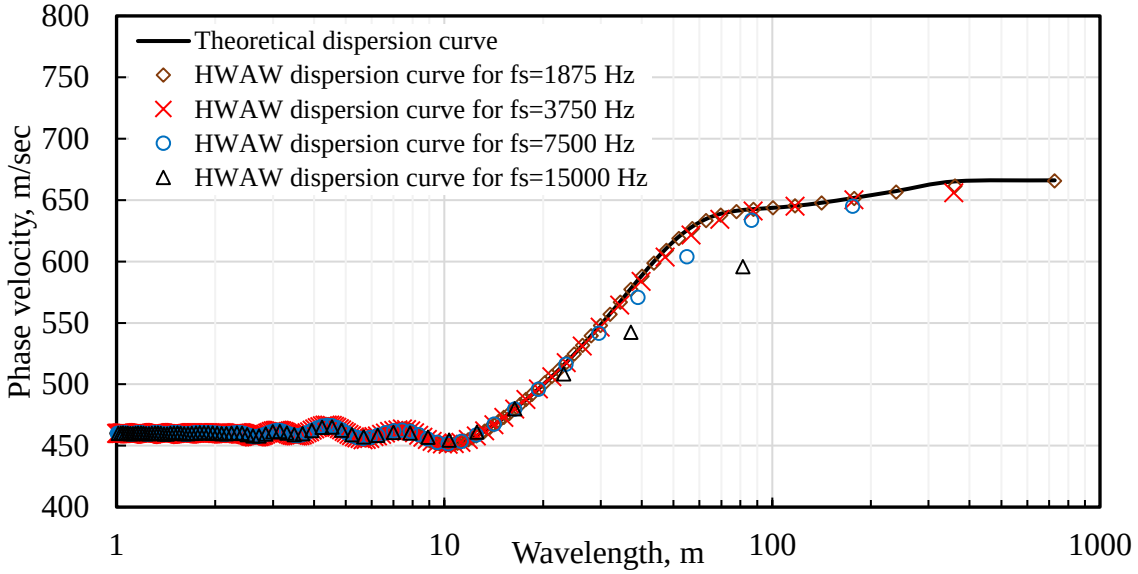

Figure 4.9 Comparison of phase velocity dispersion curves generated for Profile 2 (plotted in terms of wavelength) using different sampling frequencies and a three-point bandwidth. Receiver spacing is 4 m and Source offset is 20 m.

The example above clearly shows that the choice of sampling frequency has an important effect on the reliability of the interpreted dispersion curve. Increasing the sampling frequency improves the time resolution, but decreases the frequency resolution (using the same number of sample points) and for the case of a fixed-point bandwidth (as

used above) it also changes the bandwidth of the wavelet. To isolate the effect of bandwidth on the phase velocity dispersion curve, comparisons are made using different bandwidths for each of sampling frequencies, 1875, 3750, 7500, and 15000 Hz, by changing the number of points used. Table 4.3 lists the bandwidth values used for the sampling frequency of 1875 Hz where m and n represent the starting and ending frequency points. For other sampling frequencies, 3750, 7500, and 15000 Hz, the results are shown in Appendix A.

Table 4.3 Bandwidth values used for the sampling frequency of 1875 Hz.

m	Frequency(m), Hz	n	Frequency(n), Hz	Bandwidth, (Frequency(n) - Frequency(m)), Hz
1	0	3	1.83	1.83
1	0	5	3.66	3.66
1	0	7	5.49	5.49
1	0	10	8.24	8.24
1	0	15	12.82	12.82
1	0	30	26.55	26.55

The effect of different bandwidths on the compatibility between the theoretical and the HWAW dispersion curves for the sampling frequency of 1875 Hz is shown in Figure 4.10. It is obvious that as the bandwidth increases, the HWAW dispersion curves deviates from the true theoretical dispersion curve and the lowest frequency that can be reliably measured increases. The same behavior was observed for other sampling frequencies, which are shown in the Appendix A.

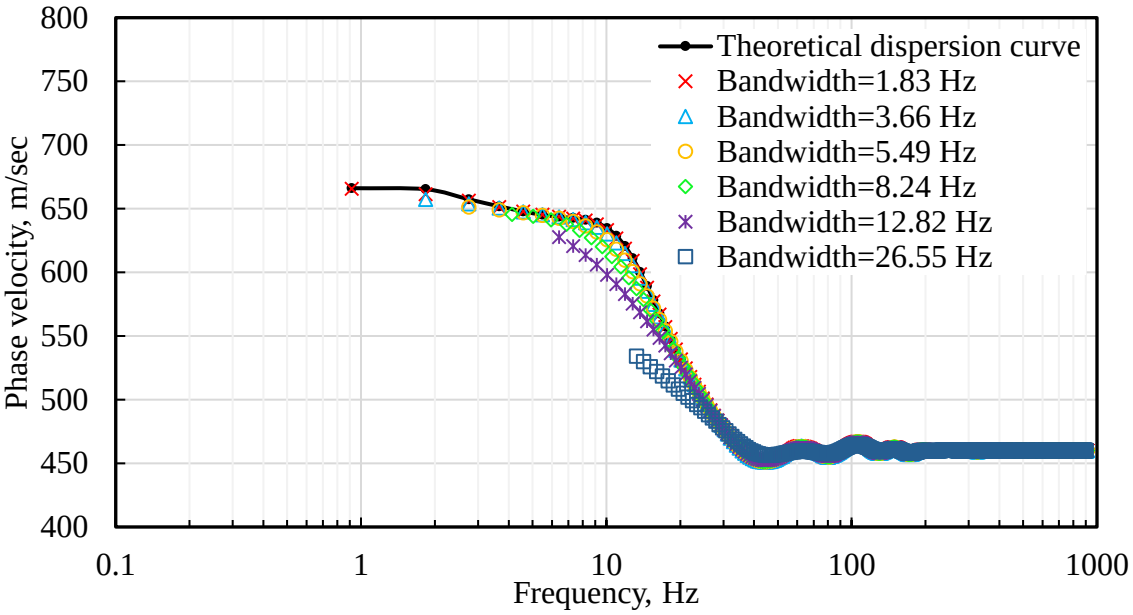

(a)

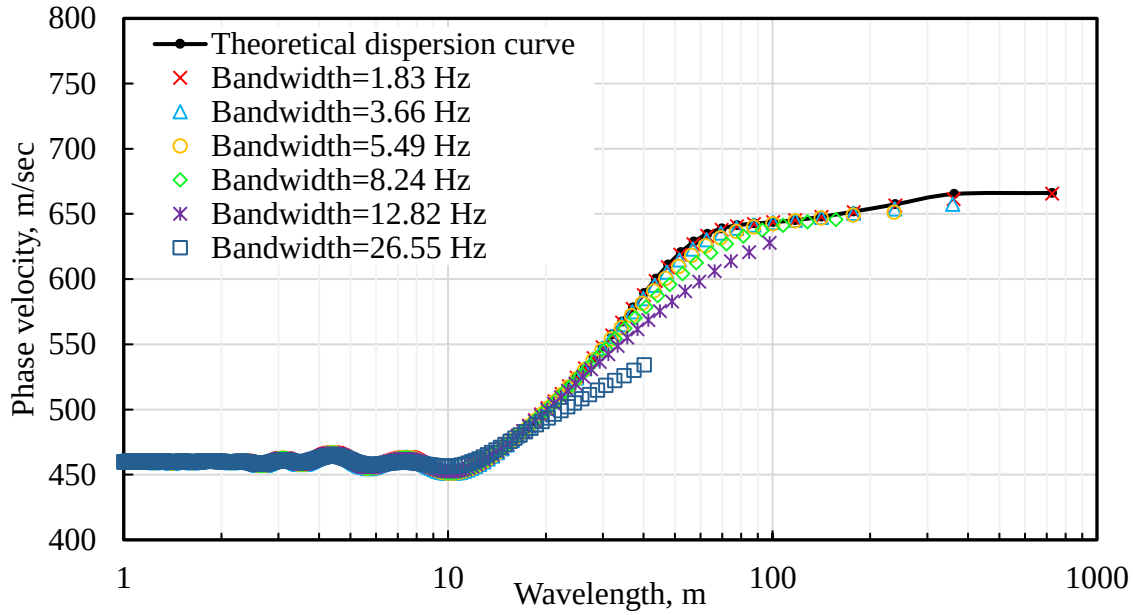

(b)

Figure 4.10 Comparison of dispersion curves using variable bandwidths in HWAW processing of Profile 2 (a) phase velocity versus frequency (b) phase velocity versus wavelength. Sampling frequency=1875 Hz, receiver spacing=4 m, source offset=20 m.

To isolate the effect of sampling frequency on dispersion curve accuracy, comparisons were made using the same bandwidths with different sampling frequencies, as explained and illustrated in Table 4.4 and Figures 4.11, 4.12, and 4.13 respectively.

Table 4.4 Selected bandwidths used for the simulations of the same bandwidths with different sampling frequencies.

Sampling frequency, fs, Hz	Frequency resolution, Δf , Hz	m	Frequency(m), Hz	n	Frequency(n), Hz	Bandwidth, (Frequency(n) - Frequency(m)), Hz
1875	0.915	1	0	5	3.66	3.66
3750	1.83	1	0	3		
1875	0.915	1	0	9	7.32	7.32
7500	3.66	1	0	3		
1875	0.915	1	0	17	14.6484	14.648
15000	7.32	1	0	3		

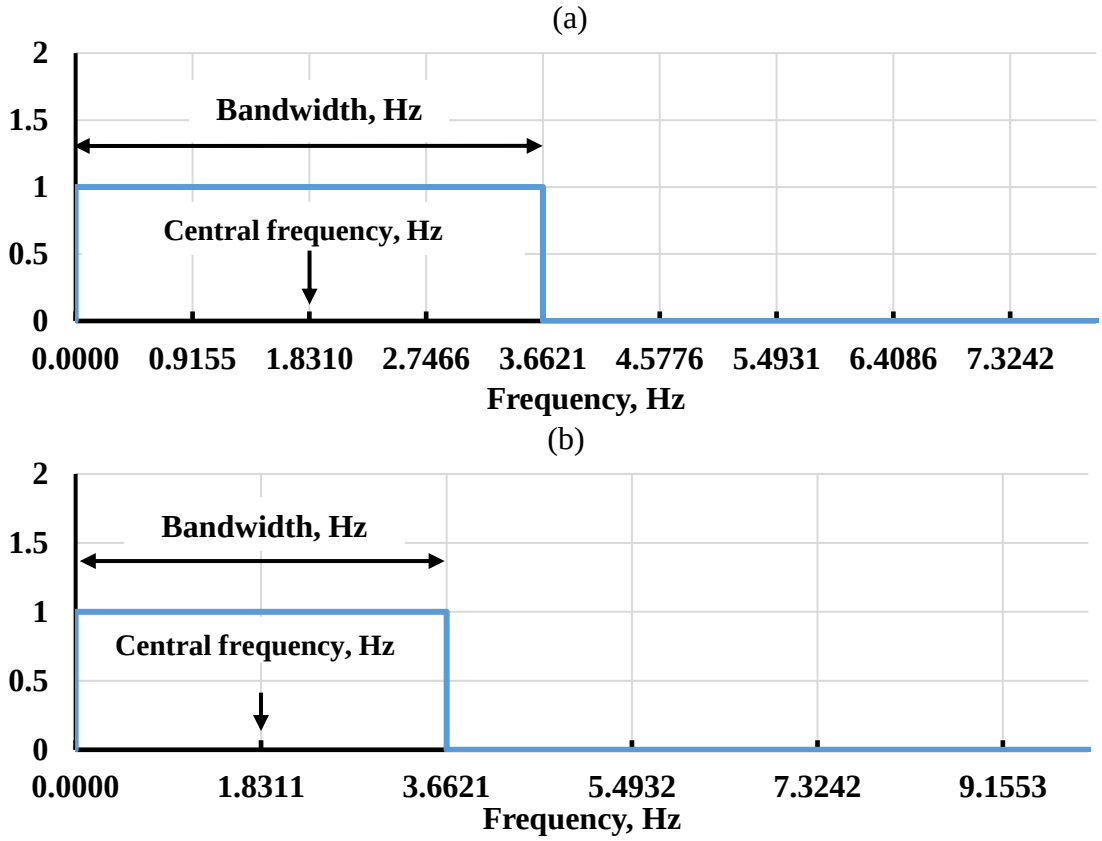

Figure 4.11 Frequency span showing the same bandwidth and the central frequency for receiver spacing of 4 m and source offset of 20m using (a) sampling frequency = 1875 Hz (using 5 points) (b) sampling frequency =3750 Hz (using 3 points).

(a)

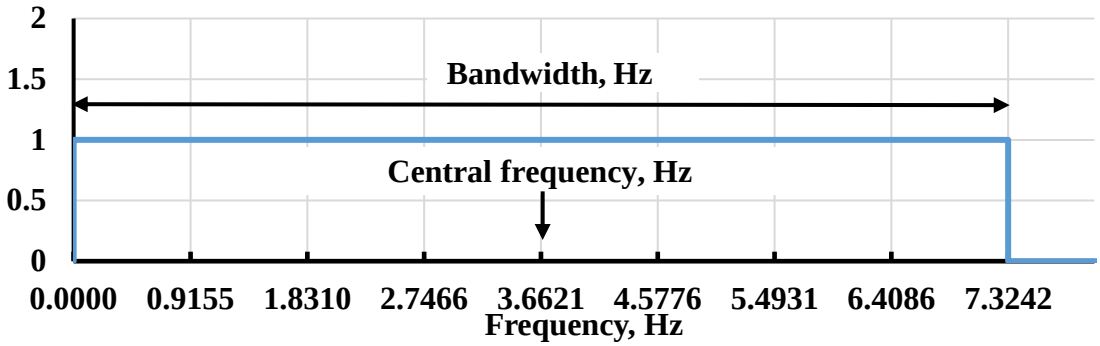

(b)

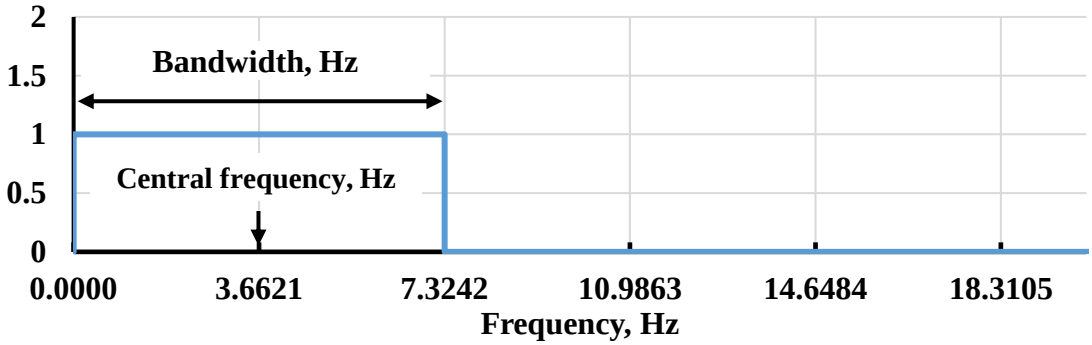

Figure 4.12 Frequency span showing the same bandwidth and the central frequency for receiver spacing of 4 m and source offset of 20m (a) sampling frequency = 1875 Hz (using 9 points) (b) Sampling frequency = 7500 Hz (using 3 points).

(a)

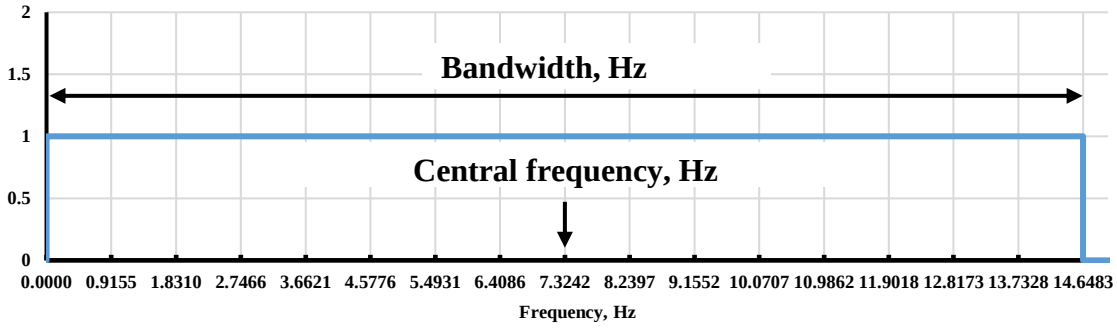

(b)

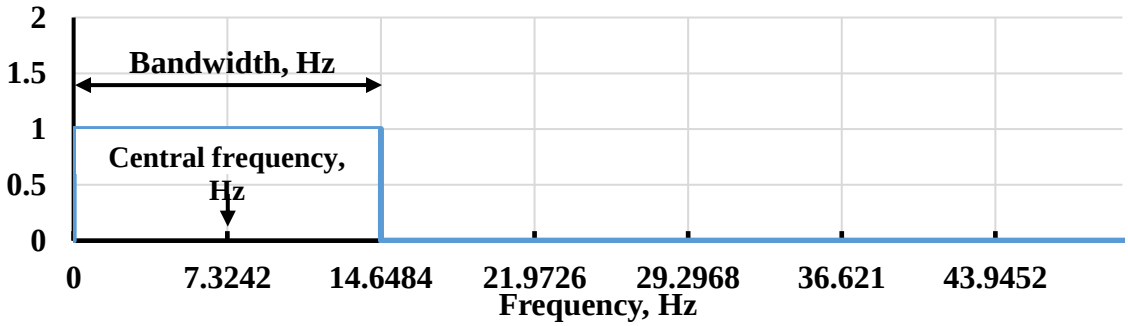

Figure 4.13 Frequency span showing the same bandwidth and the central frequency for receiver spacing of 4 m and source offset of 20m (a) sampling frequency = 1875 Hz (using 17 points) (b) sampling frequency =15000 Hz (using 3 points).

Phase velocity dispersion curves versus frequency for Profile 2 using the same bandwidth value with different sampling frequencies are presented in Figures 4.14, 4.15, and 4.16.

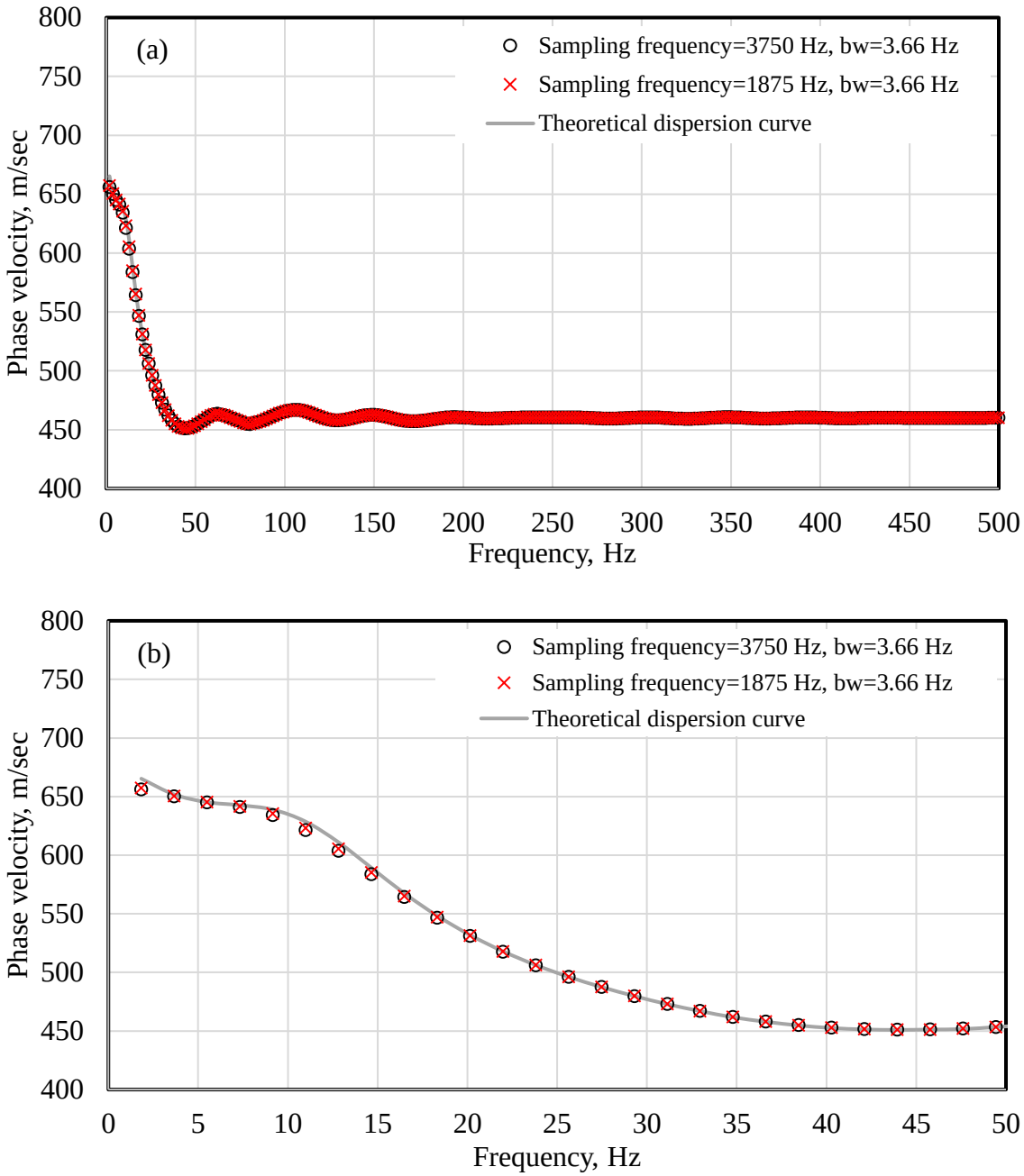

Figure 4.14 Dispersion curves for Profile 2 obtained from HWAW method for receiver spacing of 4 m and source offset of 20 m using same bandwidth (b_w) frequency of 3.66 Hz for sampling frequencies 1875 Hz and 3750 Hz (a) full frequency range (b) frequency range from 0 to 50 Hz.

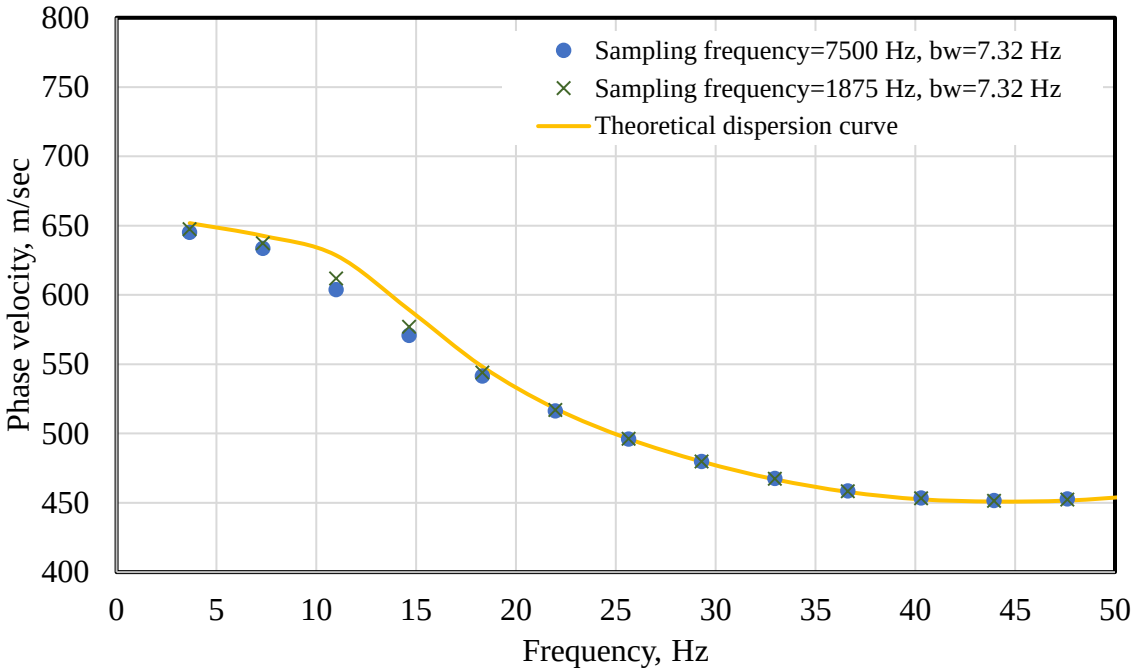

Figure 4.15 Phase velocity versus frequency dispersion curves for Profile 2 obtained from HWAW method for receiver spacing of 4 m and source offset of 20 m using same bandwidth (b_w) of 7.32 Hz for sampling frequencies 1875 Hz and 7500 Hz.

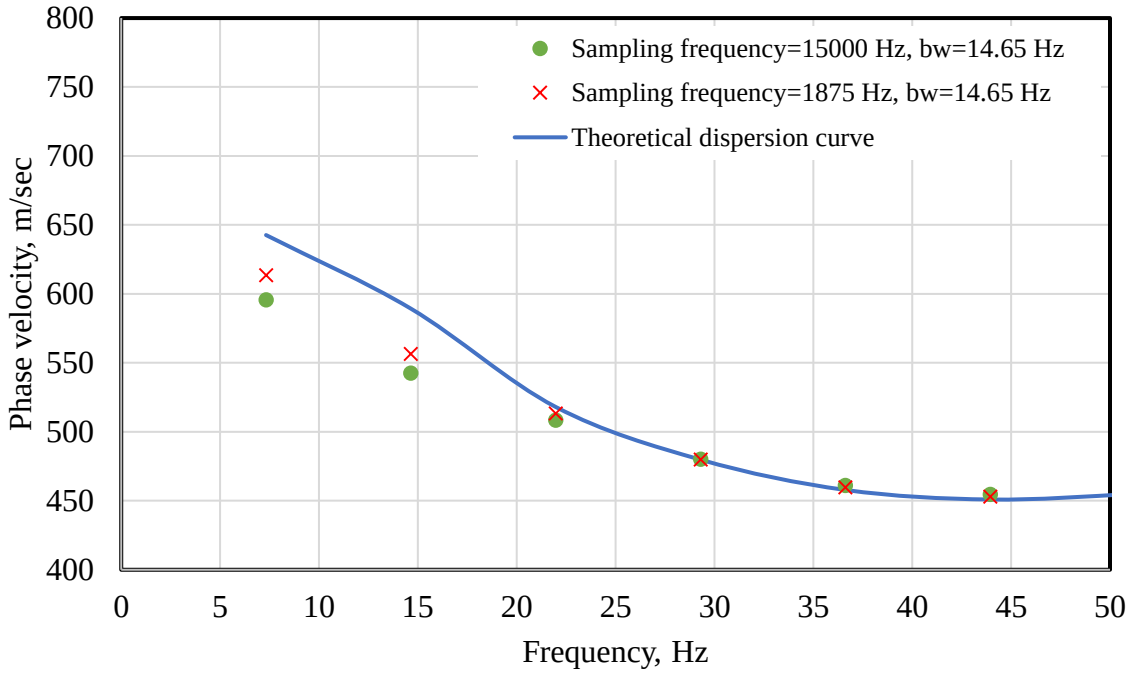

Figure 4.16 Phase velocity versus frequency dispersion curves for Profile 2 obtained from HWAW method for receiver spacing of 4 m and source offset of 20 m using same bandwidth (b_w) of 14.65 Hz for sampling frequencies 1875 Hz and 1500 Hz.

By looking at the consistency between the theoretical dispersion curve and HWAW processed dispersion curve in Figures 4.14, 4.15 and 4.16, some important observations can be made. First, when the bandwidth is sufficiently narrow, a good match between the dispersion curves is achieved and sampling frequency does not appear to have a significant impact on the results, as shown in Figure 4.14. In this case, a good match between the theoretical dispersion curve and processed dispersion curve is observed with an absolute maximum difference error of 1.4% or less. However, as the bandwidth increases, as shown in Figure 4.15 and Figure 4.16, the dispersion curves compare poorly with the theoretical dispersion curves with absolute maximum errors as high as 4% and 8% for bandwidths of 7.32 and 14.65, respectively. The sampling frequency has only a small effect on the results. Similar observations were made for Profiles 1 and 3, as shown in Appendix A.

The same dispersion curves from Figures 4.14, 4.15, and 4.16 are presented in terms of wavelength in Figures 4.17, 4.18, and 4.19. The typical range of wavelengths needed to profile to 30 m are also shown in these figures. These figures show that for this V_S profile, a bandwidth of 3.66 Hz provides an accurate dispersion curve over the wavelength range needed to profile to 30 m. However, use of a larger bandwidth, regardless of sampling frequency significantly underpredicts the phase velocity over the wavelength range of interest, which would result in an underpredicted V_S profile to 30 m. Similar plots for Profile 1 and Profile 3 are presented in Appendix A.

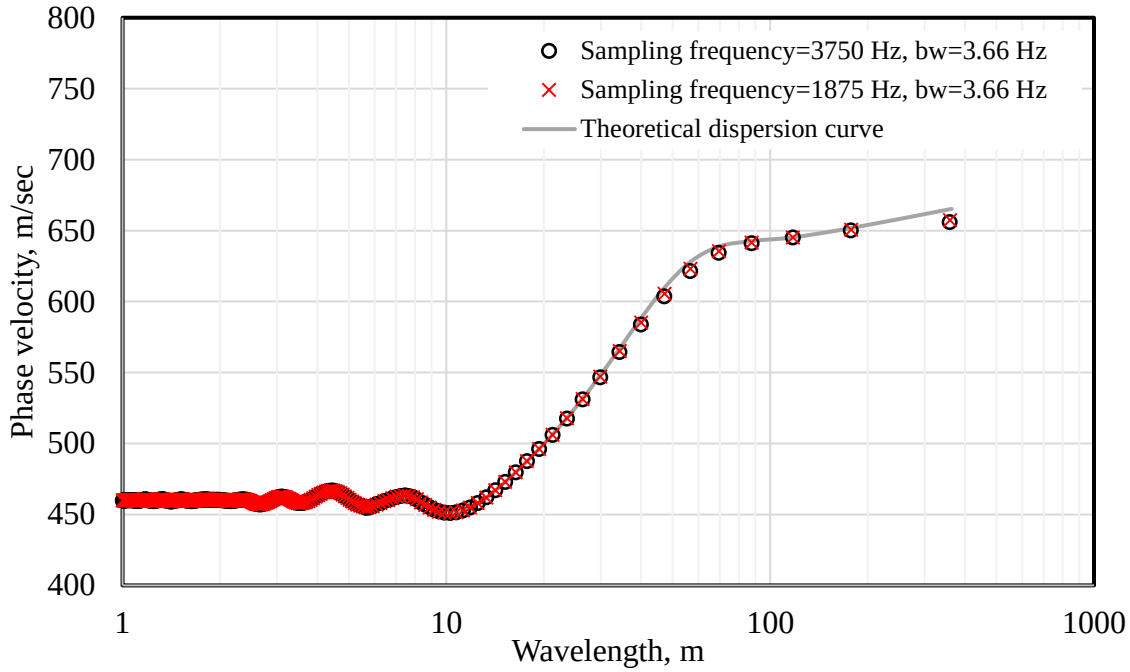

(a)

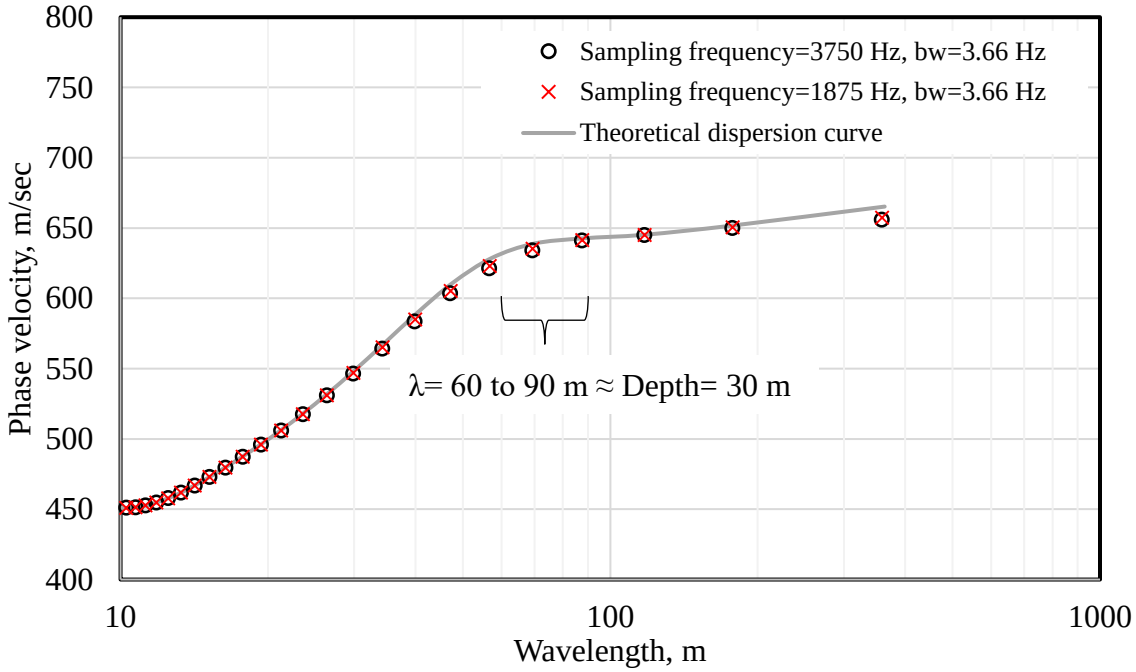

(b)

Figure 4.17 Dispersion curves for Profile 2 obtained from HWAW method for receiver spacing of 4 m and source offset of 20 m using same bandwidth (b_w) frequency of 3.66 Hz for sampling frequencies 1875 Hz and 3750 Hz (a) full wavelength range (b) wavelength range from 10 to 360 m.

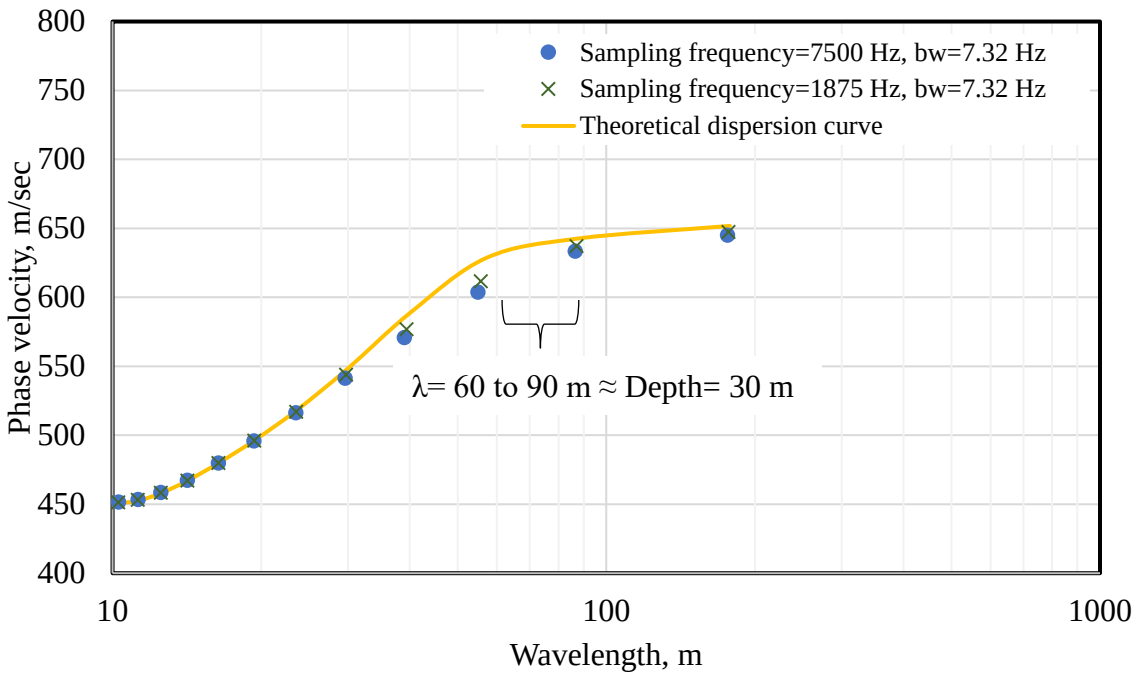

Figure 4.18 Phase velocity versus wavelength dispersion curves for Profile 2 obtained from HWAW method for receiver spacing of 4 m and source offset of 20 m using same bandwidth (b_w) of 7.32 Hz for sampling frequencies 1875 Hz and 7500 Hz.

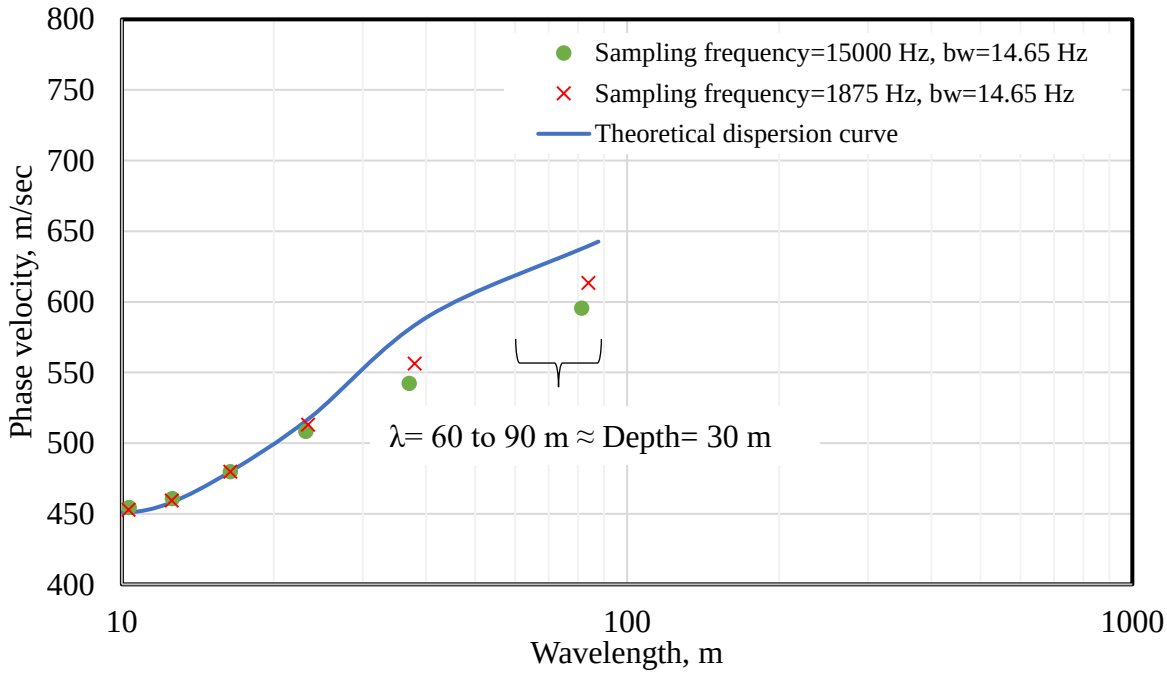

Figure 4.19 Phase velocity versus wavelength dispersion curves for Profile 2 obtained from HWAW method for receiver spacing of 4 m and source offset of 20 m using same bandwidth (b_w) of 14.65 Hz for sampling frequencies 1875 Hz and 1500 Hz.

4.3.1.3 Discussion of the Effect of Sampling Frequency and Bandwidth on Simple Profile

The main observation from this portion of the study is that as the bandwidth increases, the HWAW dispersion curve deviates from the theoretical dispersion curves. Changes in the sampling frequency with the same bandwidth does not have a significant effect on the compatibility between the HWAW and the theoretical dispersion curves. This is apparent from Figures 4.14, 4.15, and 4.16 where the points do not differ greatly when the same bandwidth is used but different sampling frequencies are used.

All bandwidth values produced a good match at high frequencies, but large deviations were observed at low frequencies. To quantitatively study the effect of bandwidth with respect to the frequency on the consistency between the HWAW and the theoretical dispersion curves, the Absolute Difference Error (ADE) percentage between the theoretical and processed dispersion curves was used as a measure of the misfit. The ADE percentage error is calculated as:

$$ADE, \% = \frac{(V_{ph,HWAW} - V_{ph,Theoretical})}{V_{ph,Theoretical}} \times 100 \qquad (4.4)$$

Where:

ADE=Absolute Difference Error percentage

$V_{ph,HWAW}$=Phase velocity calculated from HWAW method

$V_{ph,Theoretical}$=Theoretical phase velocity generated from FitSASW for a specific profile

To generate Figure 4.20, the ratio of the bandwidth to frequency was obtained by dividing the selected bandwidth by each frequency value used in the dispersion curve. This was repeated for each bandwidth studied (Table 4.4).

The ADE percentage was calculated as shown in Equation 4.4. Plots of the ADE percentage versus bandwidth to frequency ratio were generated for Profiles 1, 2, and 3 and are presented in Figures 4.20. These plots show a general trend of larger ADE values for large bandwidth to frequency ratios. Errors of as much as 12% were observed at ratios of 2. However, when the bandwidth to frequency ratio was less than 0.25, ADE of less than 1% were observed for Profiles 1, 2, and 3 and for all sampling frequencies.

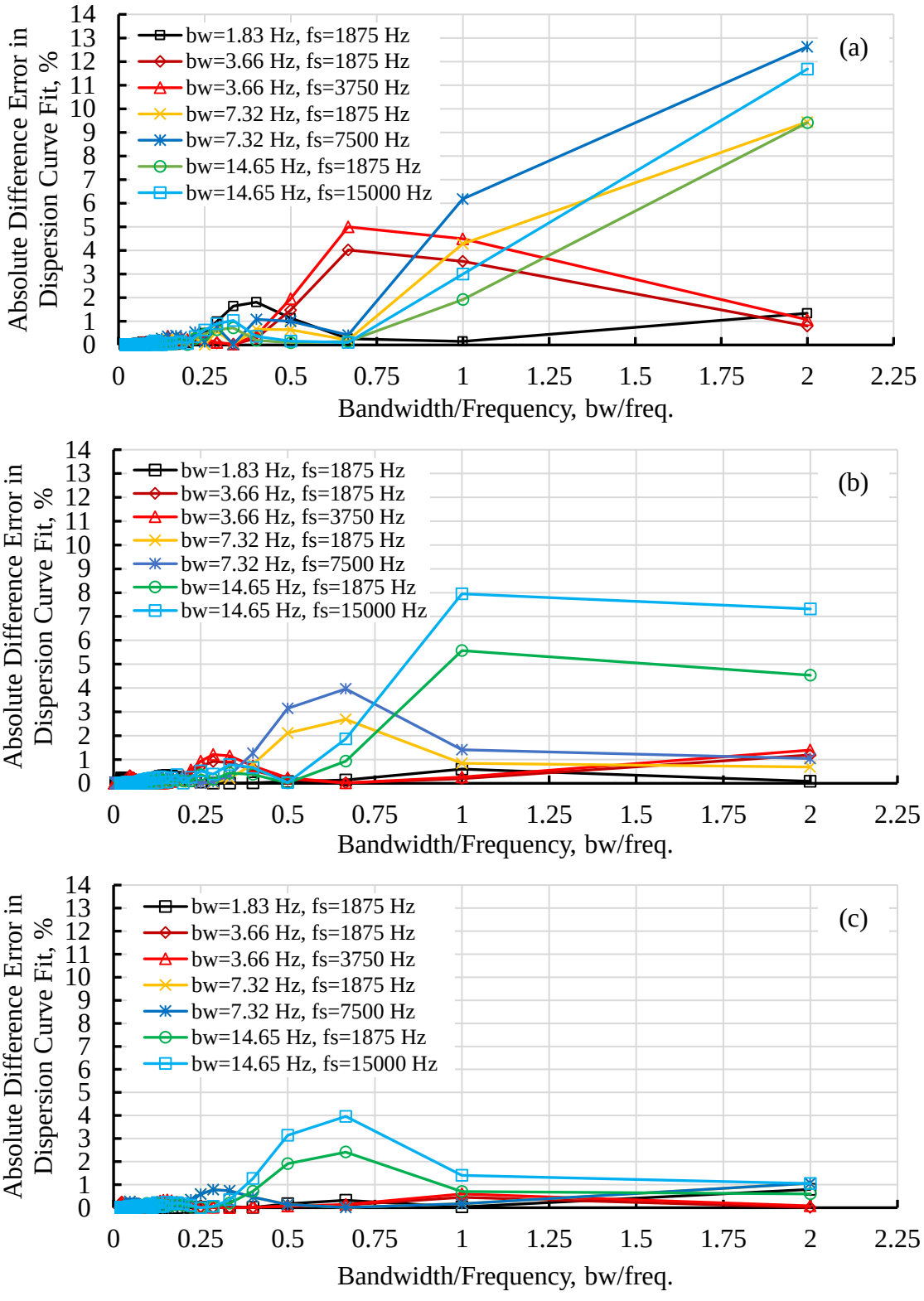

Figure 4.20 Absolute difference error percentage between theoretical and HWAW processed dispersion curves versus bandwidth to frequency ratio for (a) Profile 1, (b), Profile 2 and (c) Profile 3.

Based on this observation, it was concluded that selection of the bandwidth equal to 0.25 or less of the lowest frequency to be measured provides reliable results at simple geotechnical profiles. This criteria is investigated for complex geotechnical sites in Section 4.4.5.4.

4.3.1.4 Discussion of the Effect of Sampling Frequency on the Dispersion Curve Accuracy

As previously mentioned, the sampling frequency appears to have only a minor effect on the agreement between the theoretical and HWAW processed dispersion curves (all else being equal). This result is somewhat unexpected considering the calculation of phase velocity in the HWAW method depends on identifying the time interval between phase delays at Receivers 1 and 2, as described in Chapter 3, Section 3.3. It should be expected that lower sampling frequencies and hence longer time intervals would produce errors in the phase velocity values.

To better understand this observation, simulations of the soil profile taken from Hwang and Park (2014) were repeated using lower sampling frequencies. The dispersion plot from Figure 4.2 is shown again in Figure 4.21 and the profile values are shown in Table 3.1. Different sampling frequencies were simulated over a range from 1875 Hz down to 117.2 Hz, as shown in Table 4.5. The number of points recorded was also adjusted to maintain the same frequency resolution and allow for use of the same bandwidth in each case.

Low-Frequency Phase Velocity: It is expected that the digitization error due to poor time resolution would be most pronounced for this profile at the lowest frequency where the highest phase velocity occurs. For example, at a frequency of 1.83 Hz the phase velocity is 1763 m/s (Figure 4.21). Using the receiver spacing of 4 m, the expected time interval is

2.27 msec. A sampling frequency of 1875 Hz corresponds to a time interval of 0.53 msec. Therefore, there are only about 4 sample points in the interval recorded by the receivers. However, at a sampling frequency of 117 Hz the time interval is 8.55 msec, which is longer than the expected measurement interval. Recording with such a low sampling frequency should not produce meaningful results.

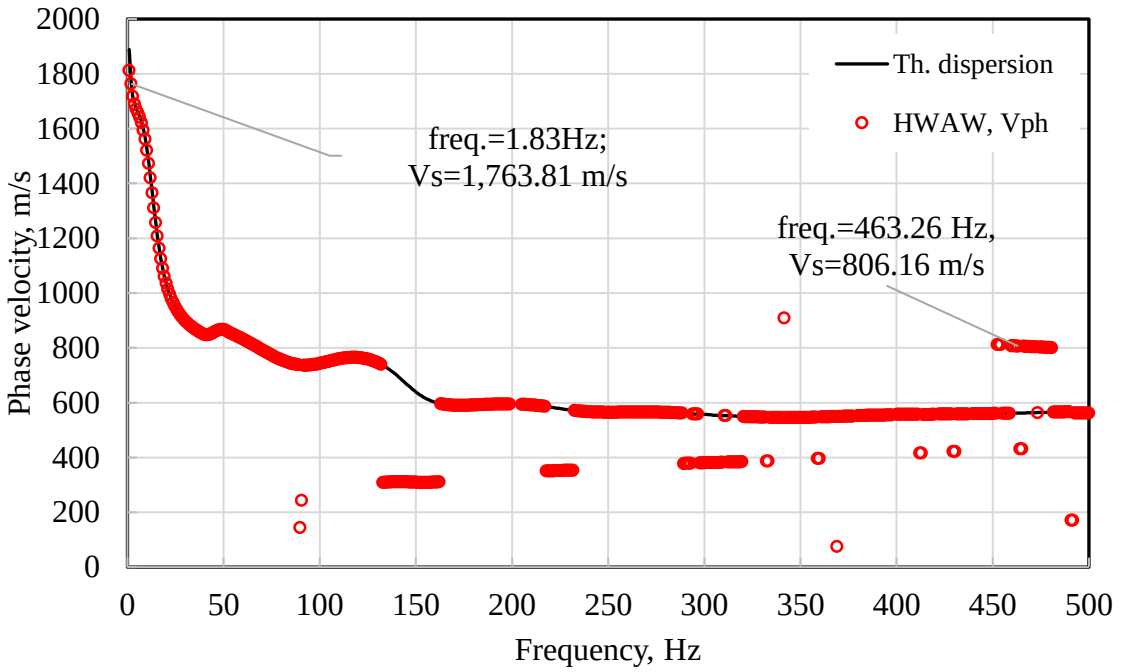

Figure 4.21 HWAW and theoretical dispersion curves for soil profile adopted from Hwang and Park (2014) showing the low and high selected frequencies on the dispersion curve.

Table 4.5 Individual layer characteristics of Profile adopted from Hwang and Park (2014).

Sampling frequency, f_s, Hz	Time interval, Δt, sec	Number of points in the time domain, N	Time length, sec
1875	5.33×10^{-4}	2048	1.092
937.5	1.07×10^{-3}	1024	1.092
468.75	2.13×10^{-3}	512	1.092
234.375	4.27×10^{-3}	256	1.092
117.1875	8.53×10^{-3}	128	1.092

The group and phase plots at Receivers 1 and 2 for the frequency value of 1.83 Hz using high and low values of sampling frequencies of 1875 Hz and 117.2 Hz are presented in Figures 4.22 and 4.23 respectively.

For the frequency value at 1.83 Hz and sampling frequency f_s of 1875 Hz, there are only four points between the maximum magnitudes of the group velocities at Receivers 1 and 2, as shown in Figures 4.22. However, the phase value at Receiver 2 could still be reliably recovered by interpolating between the data points in the linear phase plot. This is shown in an expanded view in Figure 4.22. Interesting, this also works reasonably well even in the extreme case where the separation between group times cannot be determined, as is the case with a sampling frequency of 117.2 Hz. In this case, the first group time is identified but the second falls within the same sampling interval. However, because there is no ambiguity in the phase cycles at this low frequency the phase value at the second receiver can again be reliably recovered from the linear interpolation between points, as shown in Figure 4.23. Table 4.6 compares the velocity values obtained at a frequency of 1.83 using the five sampling frequencies shown in Table 4.5. In all cases the error is less than 1% and does not vary significantly with sampling frequency.

Table 4.6 Percentage error for the velocity obtained at a frequency of 1.83 using the five sampling frequencies

Sampling frequency, f_s, Hz	Actual value of the phase velocity at f_r=1.83 Hz,	Calculated value of the phase velocity at f_r =1.83 Hz,	Error percentage,%
1875	1776.59	1763.81	-0.719
937.5		1764.20	-0.697
468.75		1764.23	-0.696
234.375		1764.24	-0.695
117.1875		1761.02	-0.876

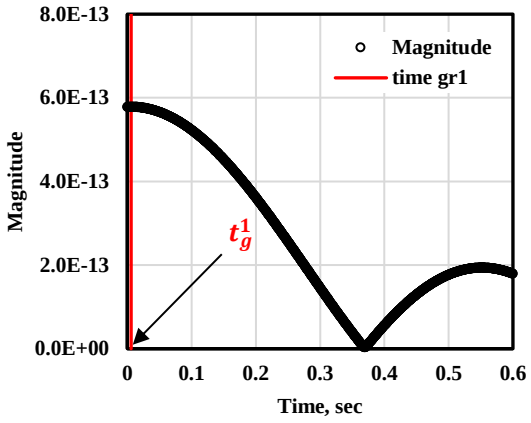

Determination of group delay, t_g^1 at Receiver 1

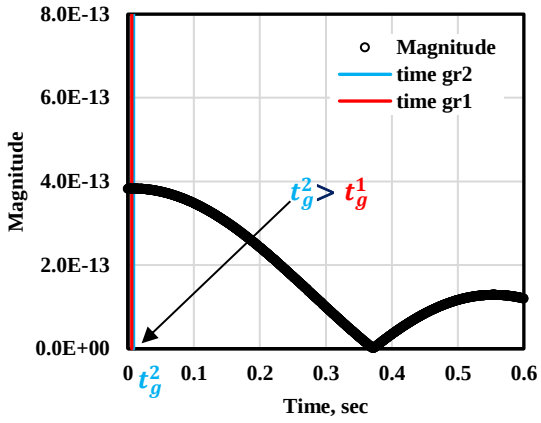

Determination of group delay, t_g^2 at Receiver 2

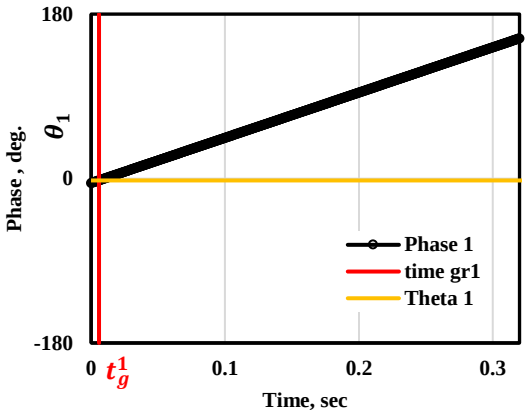

Full view

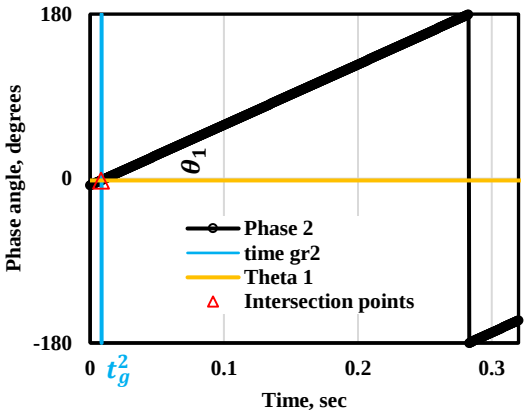

Full view

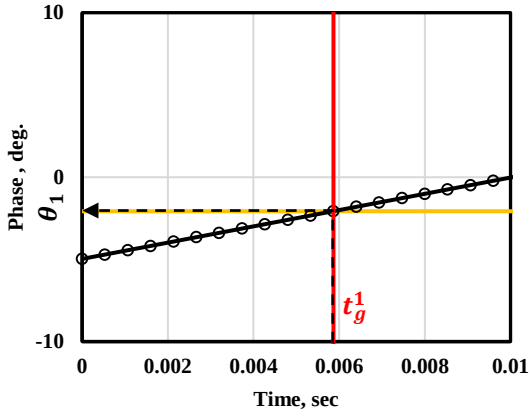

Expanded view
Determination of θ_1 at Receiver 1

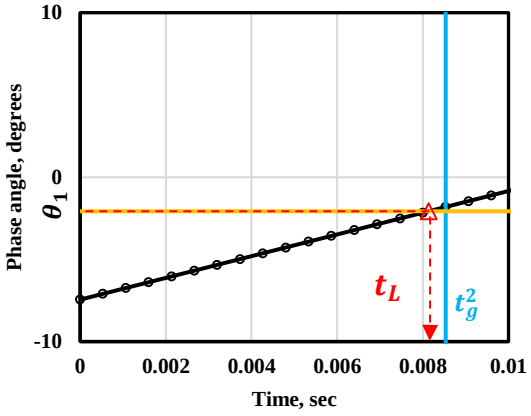

Expanded view
Determination of t_{ph}^2 at Receiver 2

Figure 4.22 Determination of group and phase delays at Receivers 1 and 2 for frequency =1.83 Hz and f_s=1875 Hz.

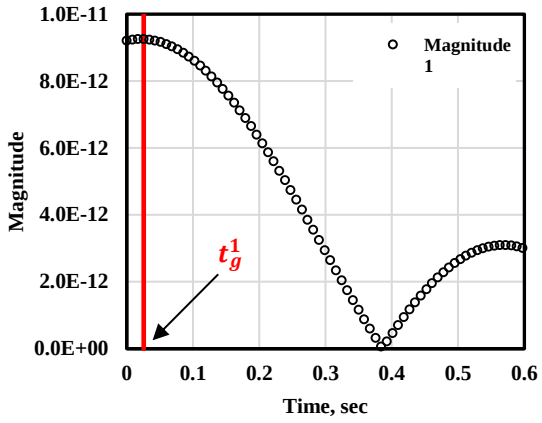

Determination of group delay, t_g^1 at Receiver 1

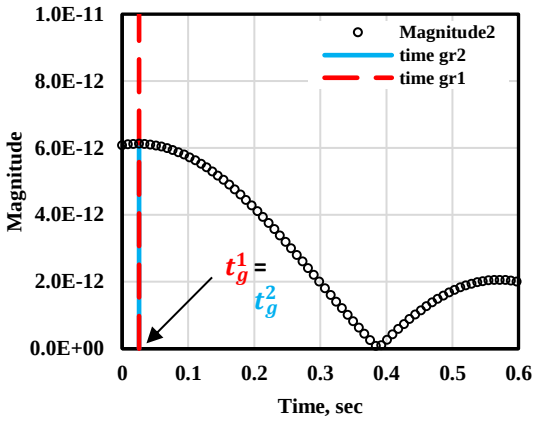

Determination of group delay, t_g^2 at Receiver 2

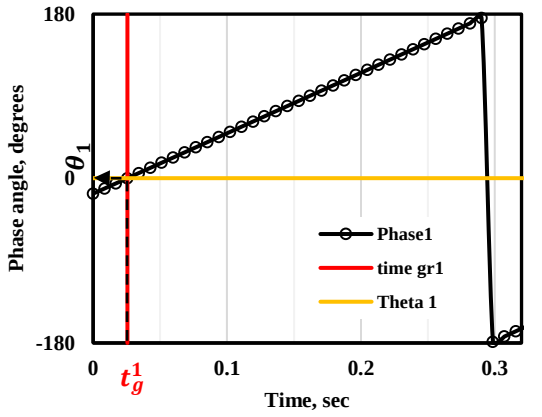

Full view

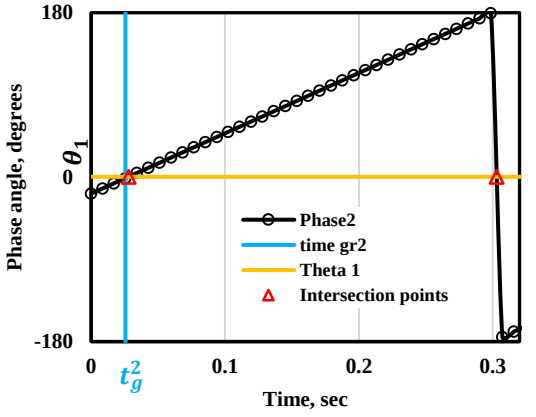

Full view

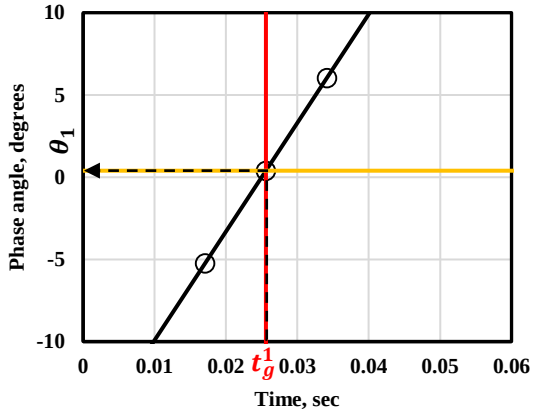

Expanded view
Determination of θ_1 at Receiver 1

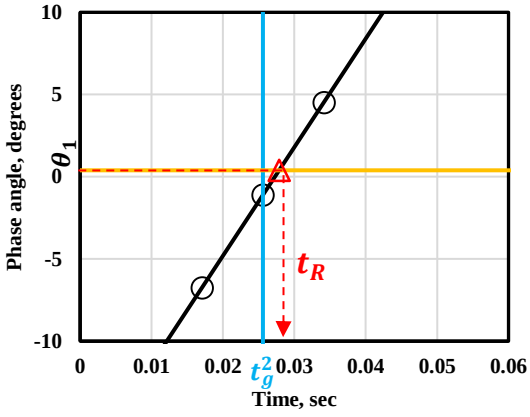

Expanded view
Determination of t_{ph}^2 at Receiver 2

Figure 4.23 Determination of group and phase delays at Receivers 1 and 2 for frequency =1.83 Hz and f_s=117.2 Hz.

High-Frequency Phase Velocity: At high frequencies, sampling frequency is important to fully cover the 360-degree instantaneous phase cycles. Figures 4.24 and 4.25 compare the instantaneous phase diagrams generated for the frequency point at 469.7 Hz using sampling rates of 1875 Hz and 16875 Hz, respectively. With a sampling rate of 1875 Hz, one phase cycle is defined by only four points and the full 360-degree range is not sampled. Using a very high sampling rate of 16875 Hz produces 36 points over one cycle and fully samples the 360 degree range. In this case, both sampling rates produced the same phase velocity value. However, in some cases, poor resolution of the phase diagram can present problems with correct phase time identification. It is recommended to have at least ten points in one phase cycle. This corresponds to a sampling rate of ten times the highest frequency of interest.

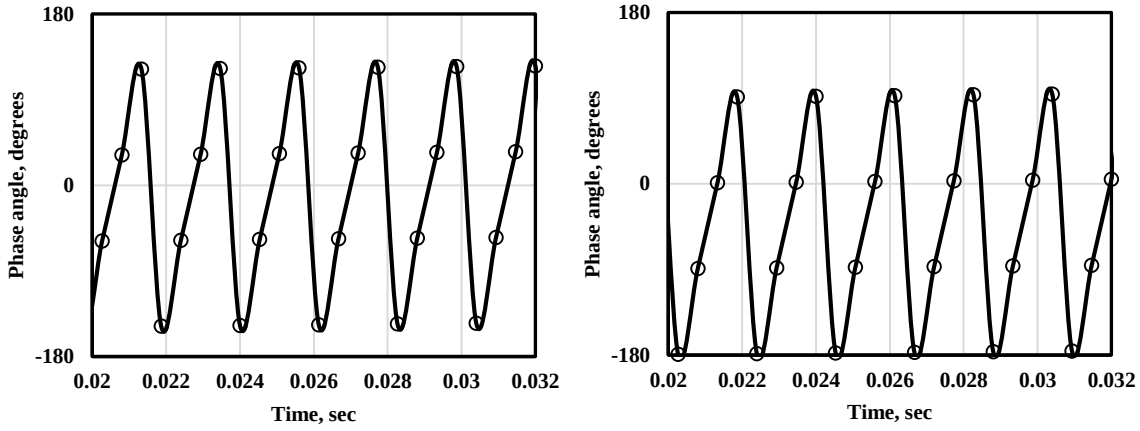

Expanded view of phase diagram at Receiver 1

Expanded view of phase diagram at Receiver 2

Figure 4.24 Expanded view of the instantaneous phase cycles at Receivers 1 and 2 for frequency=469.66 Hz using f_s= 1875 Hz.

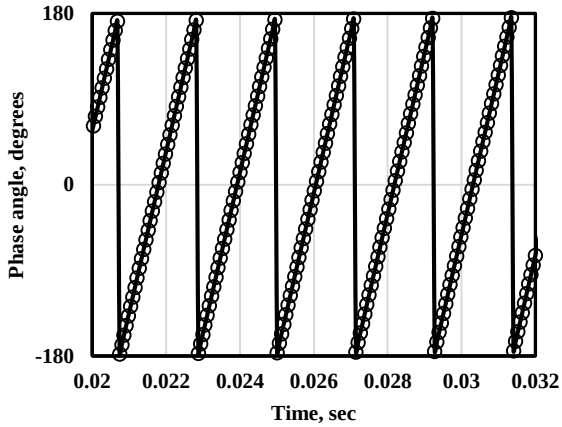

Expanded view of phase diagram at Receiver 1

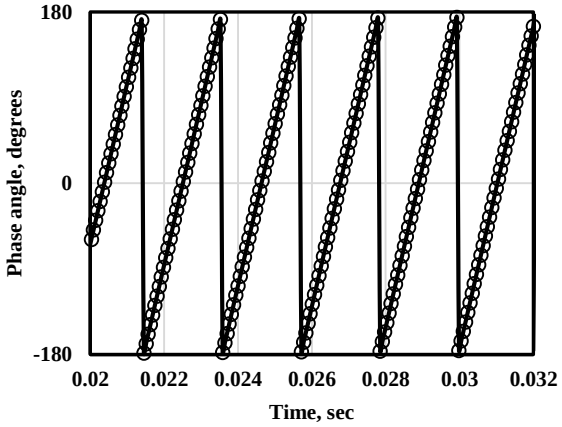

Expanded view of phase diagram at Receiver 2

Figure 4.25 Expanded view of the instantaneous phase cycles at Receivers 1 and 2 for frequency=469.66 Hz using f_s= 16875 Hz.

4.3.2 Study of Source and Receiver Arrangement

4.3.2.1 Introduction

Source-receiver configurations are an important part of data collection procedures for surface wave measurements. Both SASW and MASW have developed procedures describing how to arrange source and receivers in an optimal way based on simulations and field testing of the methods (e.g. Sanchez-Salinero, 1987, and Yoon and Rix, 2009). However, no published procedures exist for the HWAW method.

Published studies of the HWAW method in the literature review, as presented in Chapter 2, used small source-receiver spacings (typically in the range of 1 m to 4 m) which are quite different from the SASW method. The source and receiver spacings were not consistent between the sites and no explanations were provided as to how to select appropriate source and receiver locations.

The objective of this portion of the study is to answer the question, does the source offset and receiver spacing affect the accuracy of the dispersion curves developed with the HWAW method? This section presents results and discussion from a study of the effect of source offset and receiver spacing on HWAW-derived dispersion curves.

4.3.2.2 Results of Source and Receiver Setup at Simple Profiles

In this section, results are presented using simulated data for simple V_S profiles that are processed with the HWAW method. In all cases, a sampling frequency of 1875 Hz and a bandwidth of 1.83 Hz were used based on the successful demonstration of these parameters in Section 4.3.1. Source offset was varied from 12 m to 32 m and the receiver spacing was varied from 2 m to 32 m. The various combinations of source offset and receiver locations are shown in Table 3.9.

The maximum interpretable wavelength in surface wave measurements is a function of source offset. For SASW testing the maximum wavelength is typically taken as twice the source offset. This was established to minimize the effect of near field contributions. Although, other studies such as McCaskill (2014) and the HWAW studies previously referenced (e.g. Kim et al., 2008) have indicated that longer wavelengths could be used (i.e. more of the near field could be included). For this reason a range of source offsets were used in the simulations to generate dispersion curves over a wavelength range from 1 m to 90 m. As previously mentioned, this range of wavelength is appropriate to generate a V_S profile to a depth of 30 m. When short source offsets are used a large portion of the dispersion curve is in the near field and it is expected to deviate from the modal plane wave dispersion curves.

Only results from Profile 2 are presented in this chapter, with the results from Profiles 1 and 3, which showed consistent results, presented in Appendix B. Comparisons between the HWAW derived phase velocity and the theoretical dispersion curves presented in terms of frequency and wavelength for different configurations of source offsets and receiver spacings are presented in Figures 4.26 to 4.30. The fundamental mode dispersion curve for Profile 2 is also presented for comparison.

The main observation from these figures is that for all source offsets and receiver spacings that were simulated the dispersion curves generated from HWAW processing and the theoretical dispersion curves were consistent within an error of less than 1% for all frequency points. The deviations of the theoretical and HWAW dispersion curves from the fundamental mode dispersion curves that are apparent in Figures 4.26 to 4.30 are due to near-field effects. It is important to note that methods that use a modal solution in the

inversion stage must mitigate near-field contributions, but methods that use a theoretical dispersion curve that include near-field effects can tolerate more of the near-field contributions in the measurement.

The largest source offset and receiver spacing simulated were 32 m and 32 m, respectively. This arrangement is consistent with a typical SASW measurement setup for profiling to a depth of 30 m. As shown in Figure 4.30, the dispersion curve was recovered successfully using the HWAW method. Based on this observation, other SASW testing arrangements of 2 m-2 m, 4 m-4 m, 8 m-8 m, 15 m-15 m, 30 m -30 m, 45 m-45 m, and 90 m-90 m for Profile 2 were simulated and processed with the HWAW method. For all of the receiver pairs the dispersion curve was accurately recovered using the HWAW process, as shown in Figure 4.31. The potential for using the HWAW method to automate SASW data interpretation is investigated further for a broader range of profiles in Section 4.5. The same analyses were performed for Profiles 1 and 3 with similar observations. Those figures are presented in the Appendix B.

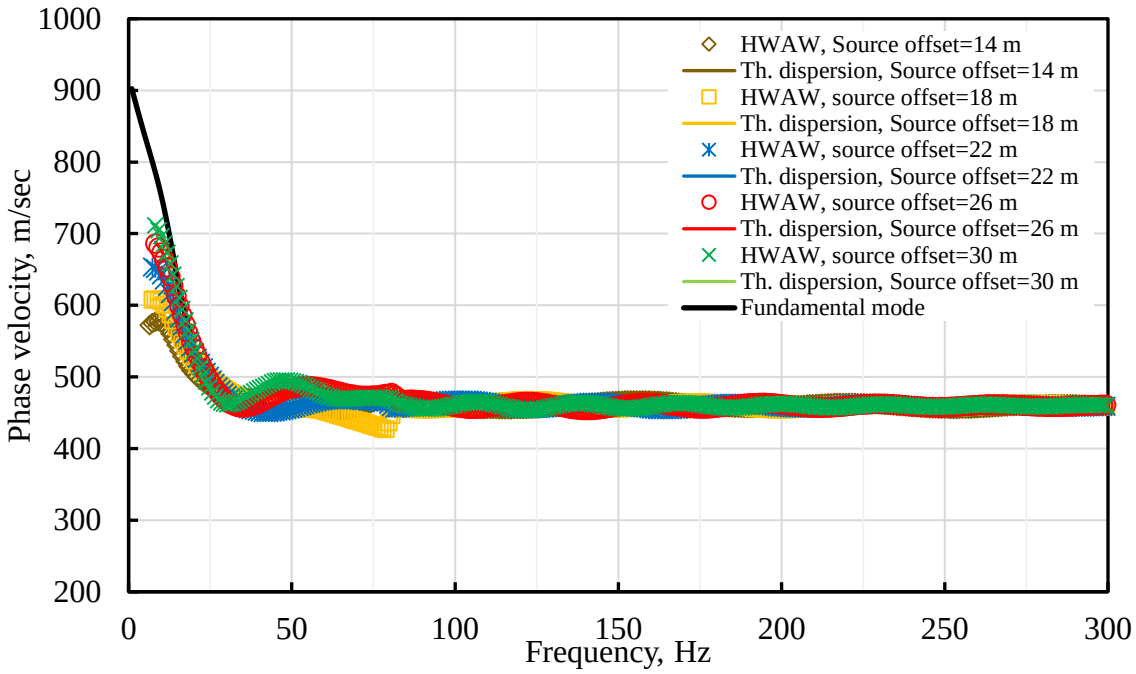

(a)

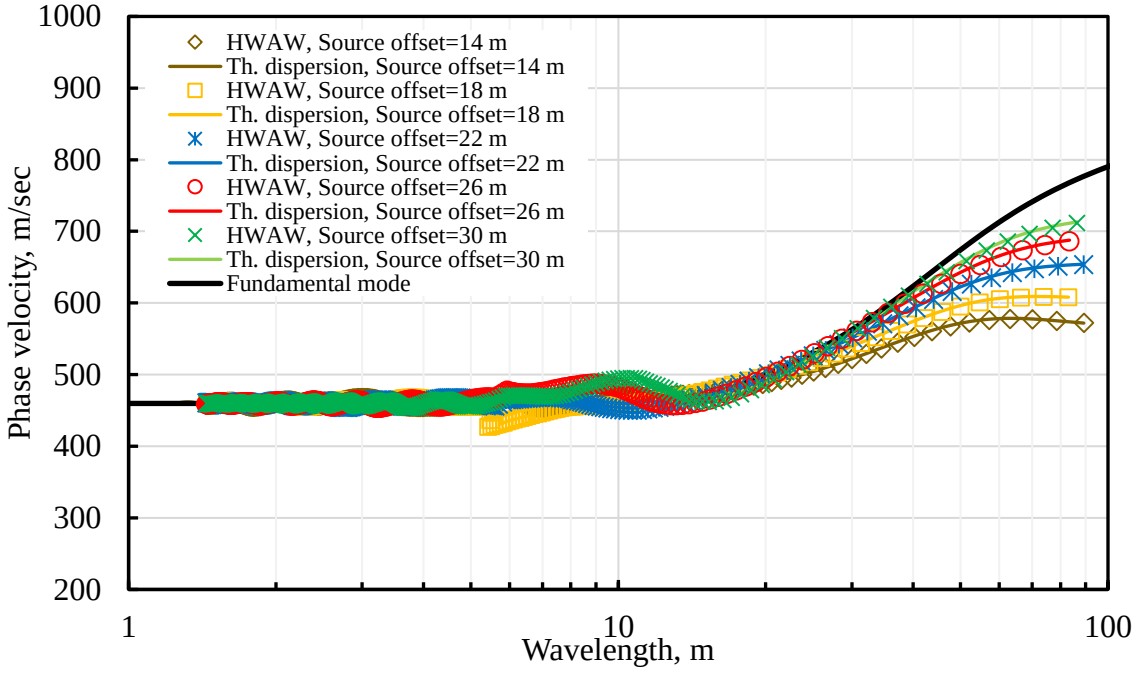

(b)

Figure 4.26 Comparison of theoretical and HWAW processed phase velocity dispersion curves from Profile 2 with receiver spacing of 2 m and different source offsets using f_s=1875 Hz (a) Velocity versus frequency (b) Velocity versus wavelength.

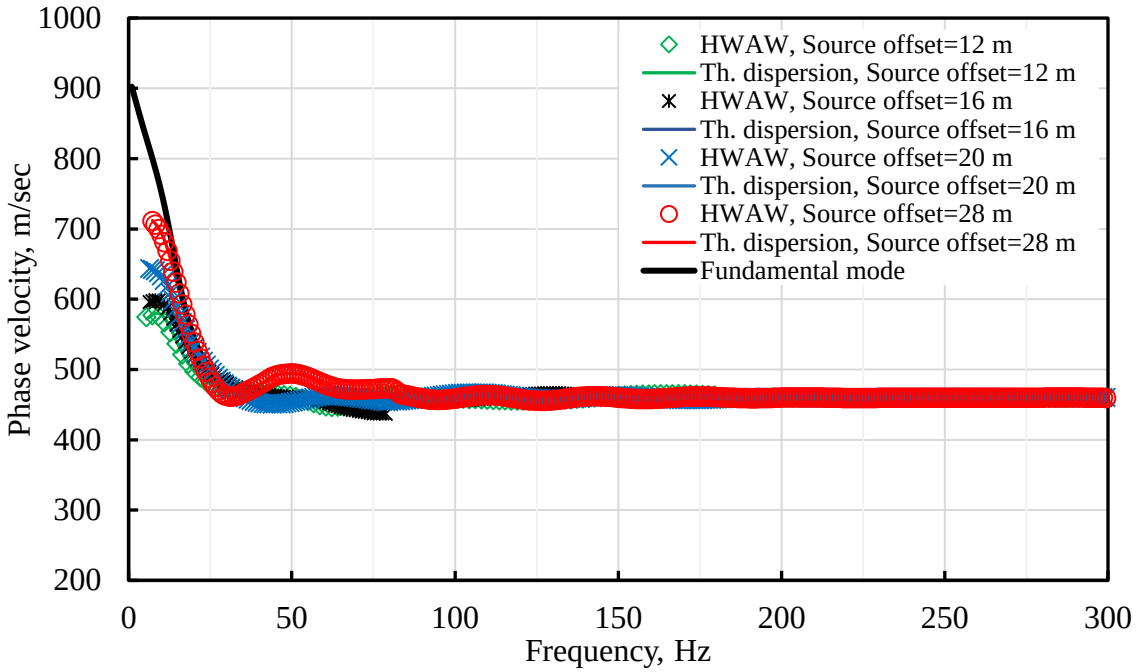

(a)

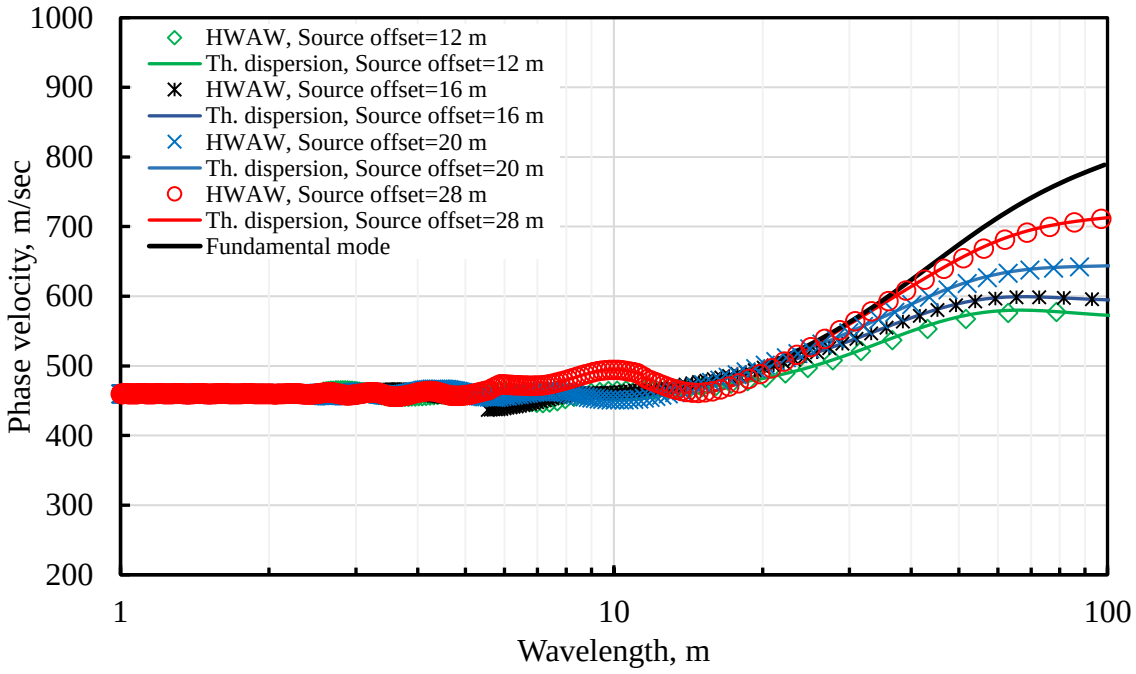

(b)

Figure 4.27 Comparison of theoretical and HWAW processed phase velocity dispersion curves from Profile 2 with receiver spacing of 4 m and different source offsets using f_s=1875 Hz (a) Velocity versus frequency (b) Velocity versus wavelength.

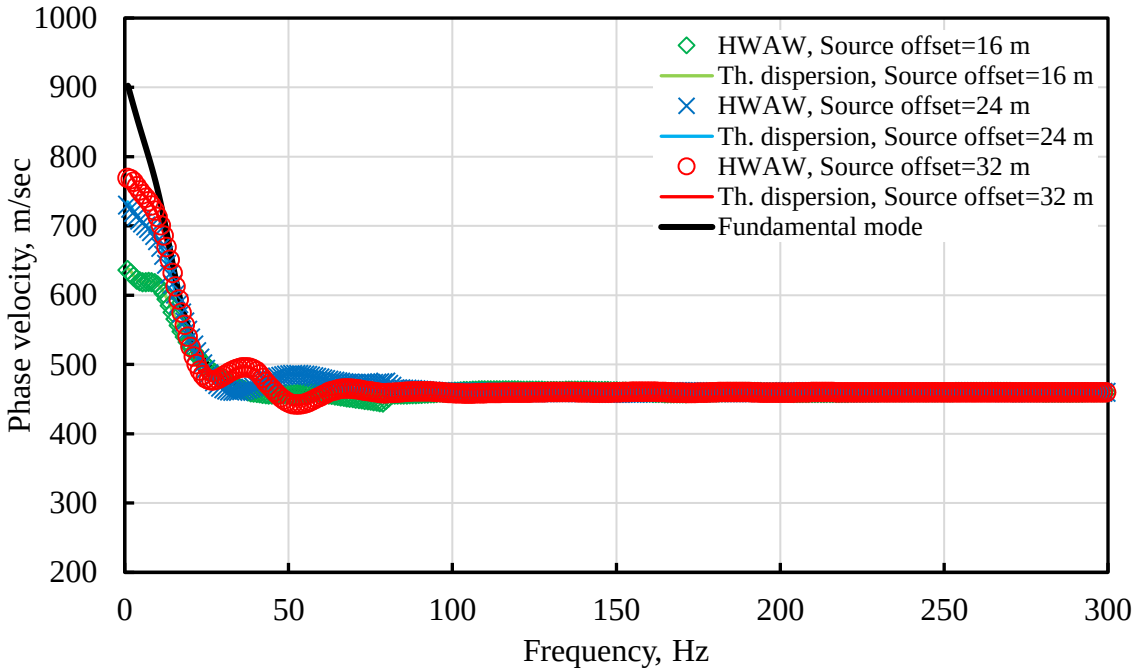

(a)

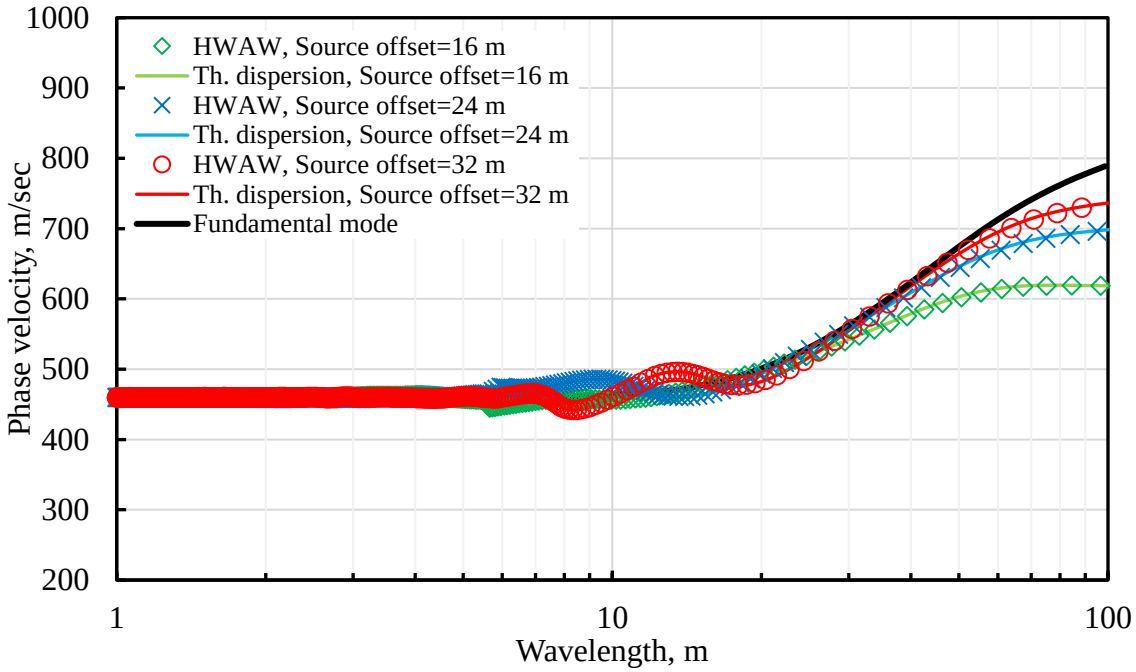

(b)

Figure 4.28 Comparison of theoretical and HWAW processed phase velocity dispersion curves from Profile 2 with receiver spacing of 8 m and different source offsets using f_s=1875 Hz (a) Velocity versus frequency (b) Velocity versus wavelength.

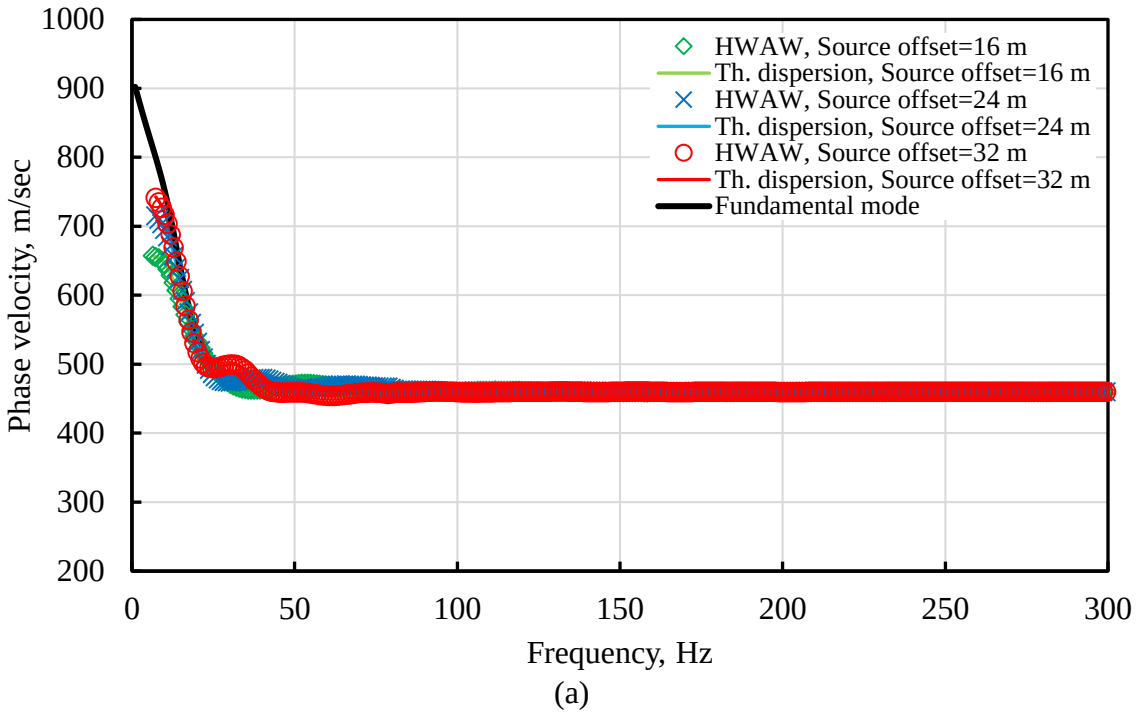

(a)

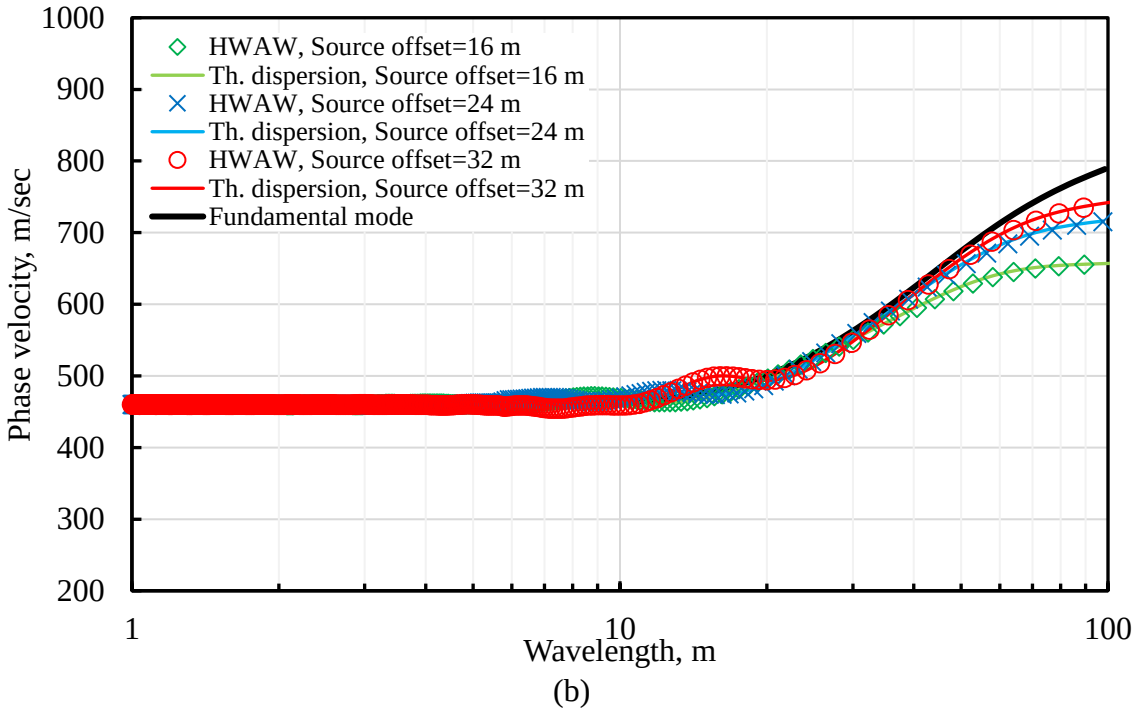

(b)

Figure 4.29 Comparison of theoretical and HWAW processed phase velocity dispersion curves from Profile 2 with receiver spacing of 16 m and different source offsets using f_s=1875 Hz (a) Velocity versus frequency (b) Velocity versus wavelength.

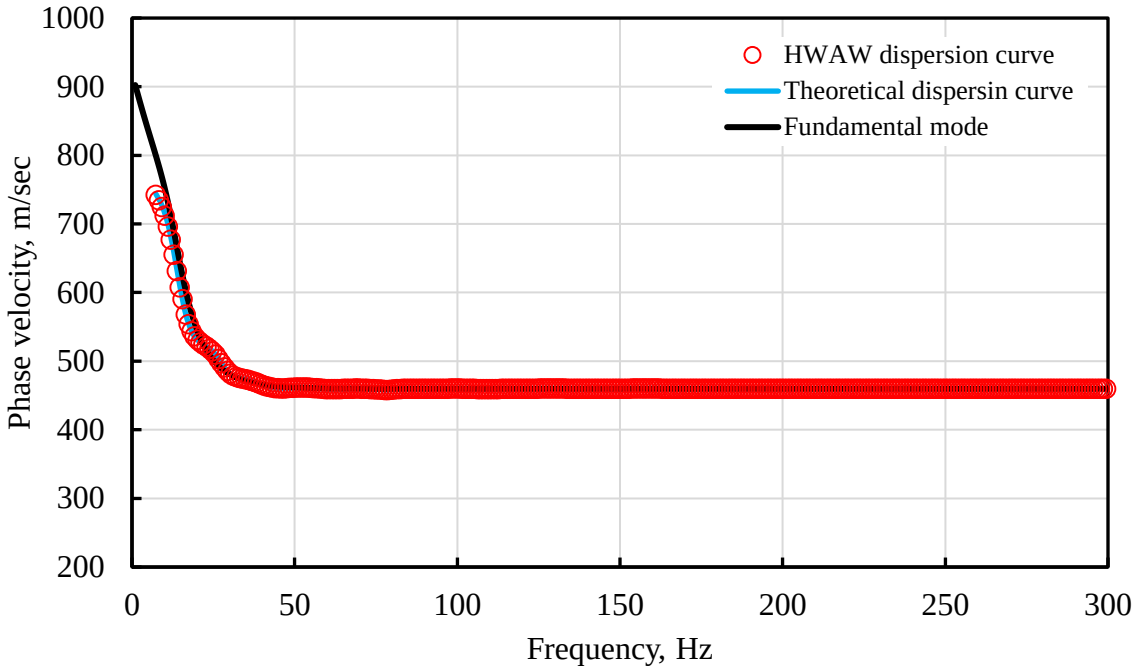

(a)

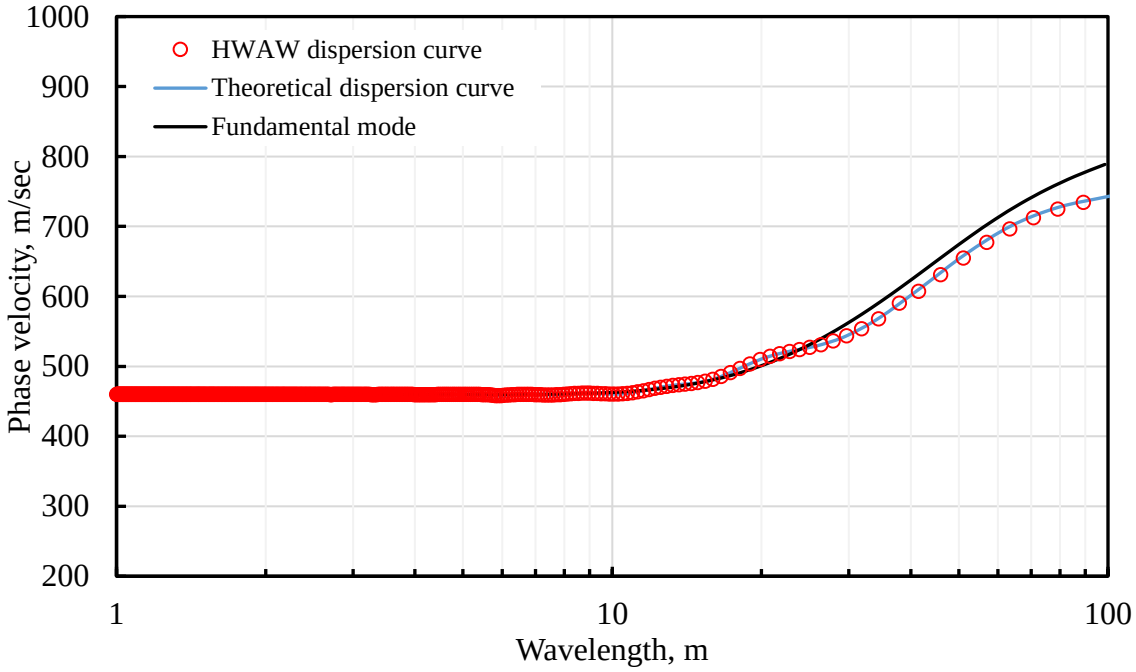

(b)

Figure 4.30 Comparison of theoretical and HWAW processed phase velocity dispersion curves from Profile 2 with receiver spacing of 32 m and different source offsets using f_s=1875 Hz (a) Velocity versus frequency (b) Velocity versus wavelength.

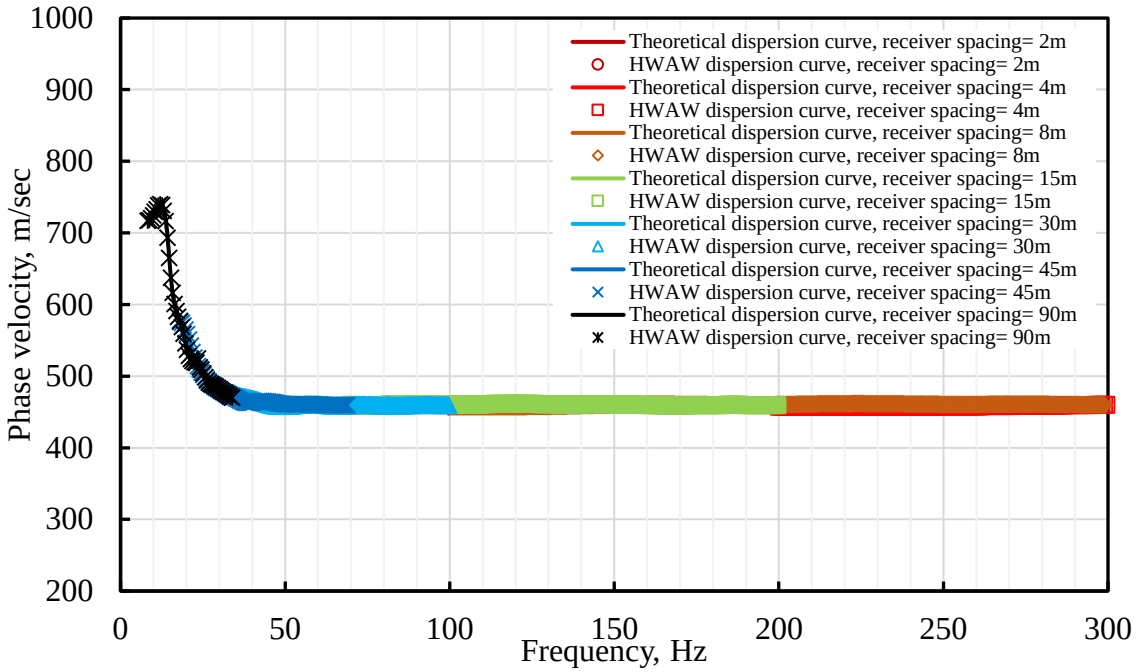

(a)

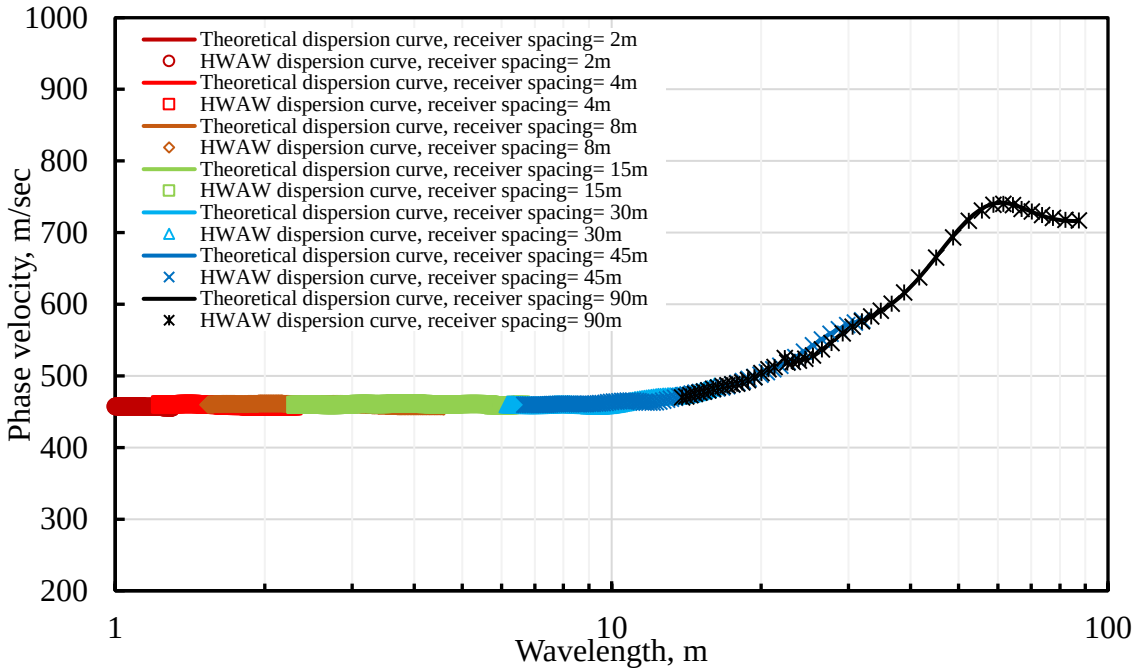

(b)

Figure 4.31 Simulated data from Profile 2 using conventional SASW source and receiver spacings but processed with the HWAW method and compared to theoretical values (a) phase velocity versus frequency and (b) phase velocity versus wavelength.

4.3.2.3 Discussions of Source and Receiver Setup for Simple Profiles

All of the results presented in published HWAW studies included very small receiver spacings (typically 2 m to 4 m) to collect the HWAW measurements. There are few studies showing the effectiveness of the HWAW method when larger receiver spacings are used. The main finding from this portion of the study is that accurate dispersion curves (i.e. matching the theoretical dispersion curve) were obtained for all combinations of source and receiver locations simulated in this study. This result was somewhat unexpected as it was anticipated that changes in the waveform over longer distances might adversely affect the HWAW processing method.

There are good reasons why short receiver spacings might be preferred in practice. First, short receiver spacings cover small areas and thus minimize errors caused by lateral variations in soil properties (Park et al., 2007 and Kim et al., 2015). Second, smaller and lower energy sources can be used since the waves do not need to travel as far. Also, the physical space required for the measurement is smaller which is advantageous in some cases.

However, there are also reasons why larger receiver spacings might be preferred. First, the SASW data collection methodology, which uses successively larger source offset and receiver spacings to collect longer wavelength, has become a standard in geotechnical practice and may be the preferred or required method of data collection. Second, the effect of mismatched phase response of geophones will be especially pronounced when short receiver spacings are used and long wavelengths are measured. This is especially important if measurements are performed near the resonant frequency of the geophones or if ground conditions (i.e. coupling) are different at the receiver locations. Third, for high Poisson's ratio sites, larger fluctuation in the dispersion curve are measured when close receiver

spacings are used, as will be discussed in the Section 4.3.3. These fluctuations can potentially cause problems in the inversion to develop the V_S profile.

Importantly, the results showing accurate recovery of the dispersion curve using the HWAW method regardless of the receiver spacings and source offsets indicates that this approach can be used to automate interpretation of SASW data collection. The manual phase unwrapping used in SASW processing is time consuming and susceptible to misinterpretation at complex sites, such as soft-over-stiff sites, (Rosenblad and Bertel, 2008) and the ability to reliably automate the interpretation of SASW measurements would be a big improvement. This issue is further studied for complex sites and real-world field data in Section 4.5 and Chapter 5, respectively.

4.3.3 Effect of Poisson's Ratio on HWAW Processing of Simple Profiles

4.3.3.1 Introduction

Poisson's ratio is an elastic constant describing the relationship between deformations of a material in orthogonal directions. Poisson's ratio also has an important influence on the partitioning of energy (i.e. body waves versus surface waves) from an impact at the surface. For low Poisson's ratio values, proportionally more of the energy goes into surface waves while at high Poisson's ratios, more of the energy goes to the body waves (Mera, 1995).

In soils, the values of Poisson's ratio can vary greatly, from 0.2 to 0.33 for dry or unsaturated conditions to nearly 0.5 under fully saturated conditions. All of the previous results presented in this thesis were performed assuming a Poisson's ratio of 0.25. In addition, all of the published studies of HWAW also assumed Poisson's ratio values that were consistent with unsaturated conditions (0.25 to 0.33). In this portion of the study, Poisson's ratios were varied from 0.25 to 0.5 to investigate if the value of Poisson's ratio affects the ability to accurately recover the theoretical dispersion curves using HWAW processing. The results of the effect of different Poisson's ratio values on the quality of fit between the HWAW and the theoretical dispersion curves are presented and discussed in this section.

4.3.3.2 Results of Effect of Poisson's Ratio Values on Simple Profiles

In this portion of the study, values of Poisson's ratio were changed over the full depth range for Profiles 1, 2 and 3. The base profile is the profile with a Poisson's ratio of 0.25 which is denoted as Profiles X-P25, while Profiles X-P33, X-P40, and X-P45 represent simulations performed using Poisson's ratios of 0.33, 0.40, and 0.45 where X is the profile

number, as illustrated in Figure 4.32. The results for these nine profiles are presented in this section. Sampling frequency, bandwidth, source offsets and receiver spacings were set to the same values as were used for base Profiles 1, 2, and 3, as shown in Table 4.7.

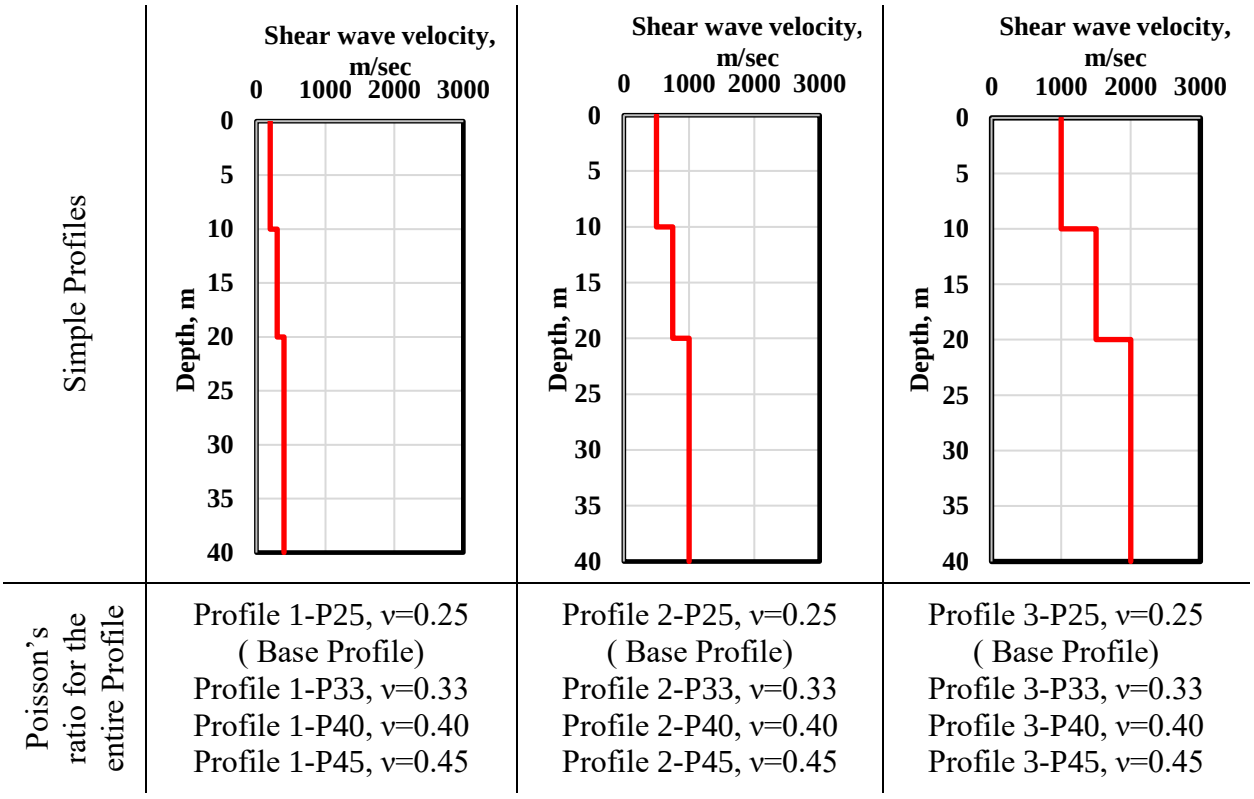

Figure 4.32 Profiles 1, 2 and 3 with different Poisson's ratio values.

Table 4.7 Data collection and processing parameters used in the simulations of Profiles 1, 2 and 3.

Sampling frequency, f_s, Hz	Bandwidth, b_w, Hz	Source offset, S-R1, m	Receiver spacing, R1-R2, m
1875	1.83	14	2
		20	4
		32	8
		32	16
		32	32

Comparisons between the theoretical and experimental dispersion curves for Profile 2 using different Poisson's ratio values for selected source offsets and receiver spacings are

presented in Figures 4.33 and 4.34 to illustrate the good agreement between the HWAW dispersion curve and the theoretical dispersion curves in all cases. Similar plots for Profiles 1 and 3 are shown in Appendix C.

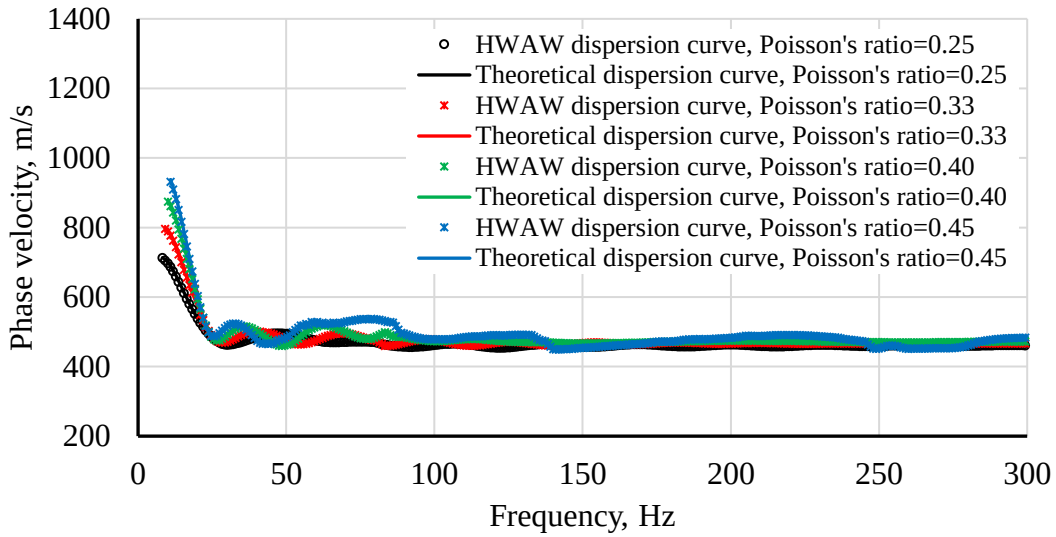

(a) receiver spacing= 2 m and source offset= 30 m

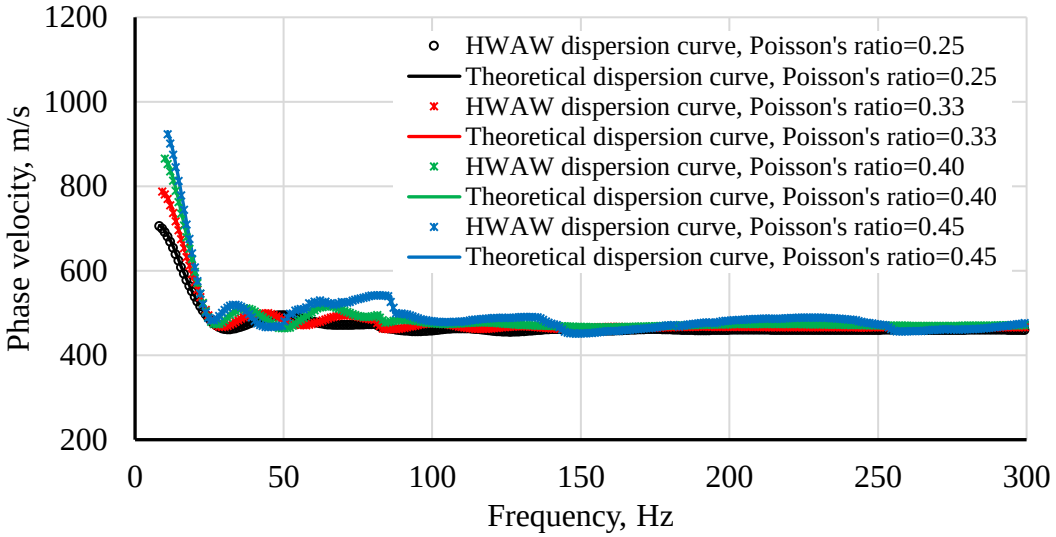

(b) receiver spacing= 4 m and source offset= 28 m

Figure 4.33 Comparison of HWAW and theoretical dispersion curves for Profiles 2-P25, 2-P33, 2-P40, and 2-P45 with: (a) receiver spacing of 2 m and source offset of 30 m, (b) receiver spacing of 4 m and source offset of 28 m.

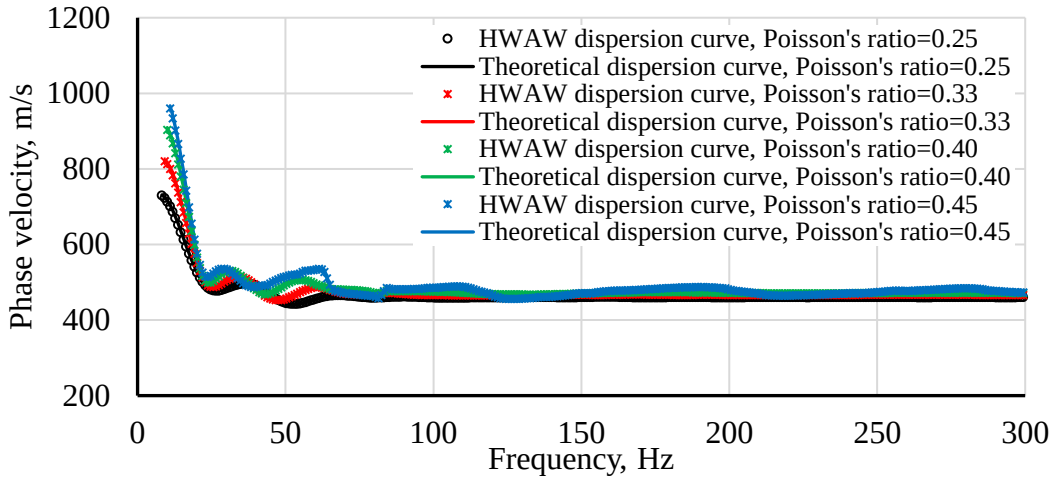

(a) receiver spacing= 8 m and source offset= 32 m

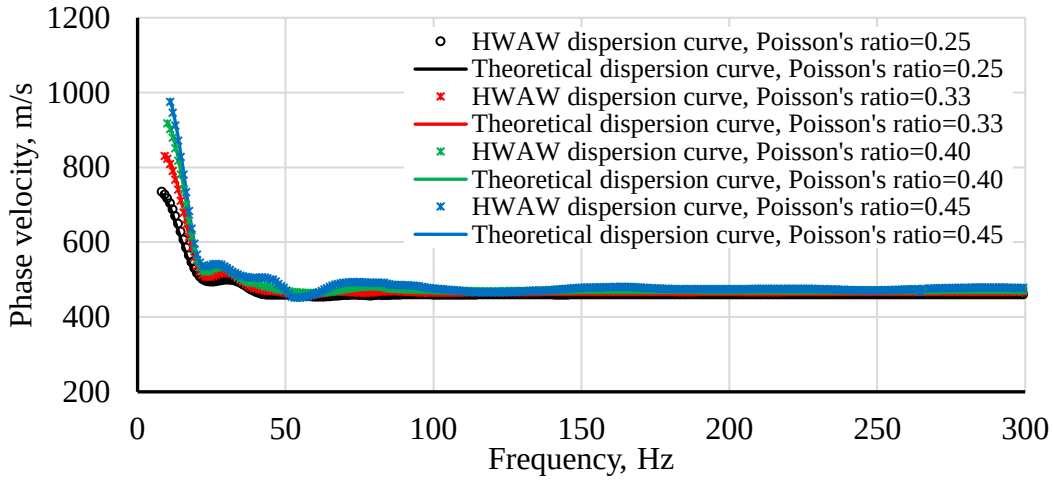

(b) receiver spacing= 16 m and source offset= 32 m

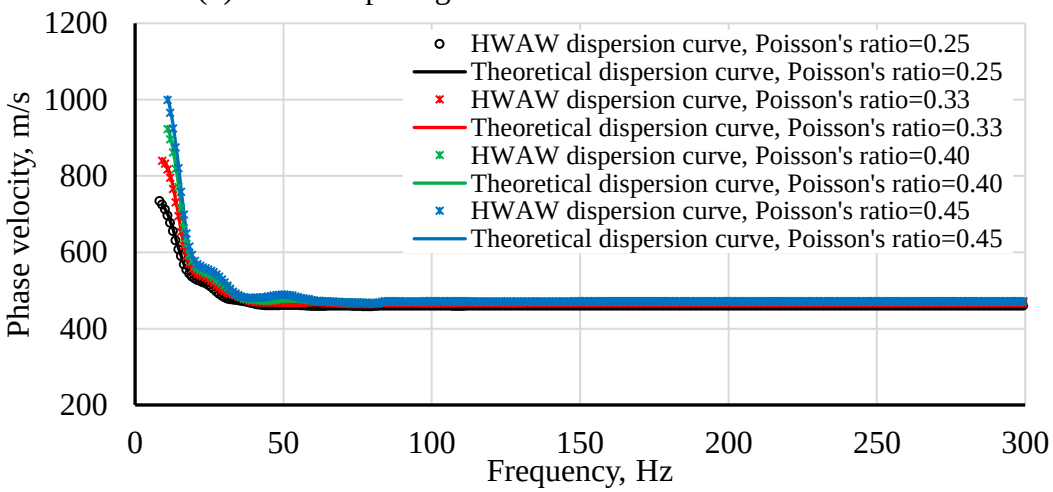

(c) receiver spacing= 32 m and source offset= 32 m

Figure 4.34 Comparison HWAW and theoretical dispersion curves for Profiles 2-P25, 2-P33, 2-P40, and 2-P45 with: (a) receiver spacing of 8 m and source offset of 32 m, (b) receiver spacing of 16 m and source offset of 32 m, and (c) receiver spacing of 32 m and source offset of 32 m.

To emphasize the effect of source offsets and receiver spacings on the shape of the dispersion curves, selected plots from different source offsets and receiver spacings are presented for Profile 1, Profile 2 and Profile 3 in Figures 4.35, 4.36 and 4.37 respectively. Results from all other source offsets and receiver spacings are shown in Appendix C.

The first observation for this portion of the study is that the value of Poisson's ratio does not affect the ability to accurately recover the dispersion curve using the HWAW method. As shown in Figure 4.34 for Profile 2, the experimental dispersion curves matches the theoretical dispersion curves within an error of 1.5% or less for all points in the dispersion curve. Similar results were found for Profiles 1 and 3, as presented in Appendix C.

The second observation is that for higher values of Poisson's ratio (0.4 and 0.45), large fluctuations in the dispersion curve were observed when close receiver spacings and large source offsets were used (as are typically used for HWAW data collection). This can be seen in Figures 4.35a and b, 4.36a and b and 4.37a and b where the receiver spacings of 2 m and 4 m were used with source offsets of 14 m and 20 m respectively. However, as the receiver spacing increases relative to the source offset, as shown in Figures 4.35c-e, 4.36 c-e, and 4.37c-e, the fluctuations for the high Poisson's ratio cases diminish. For low Poisson's ratio values of 0.25, the fluctuations were generally small for all cases of source offsets and receiver spacings. These fluctuations are accurately recovered by the HWAW method, but may present problems with the inversion of the experimental dispersion curve. The same observations were found for Profiles 1 and 3.

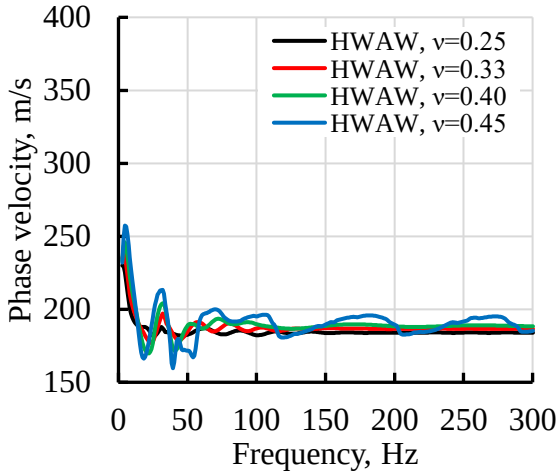

(a) Receiver spacing= 2 m, Source offset= 14 m

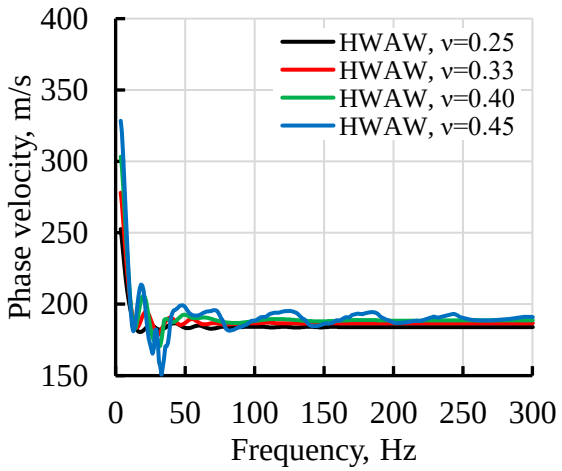

(b) Receiver spacing= 4 m, Source offset= 20 m

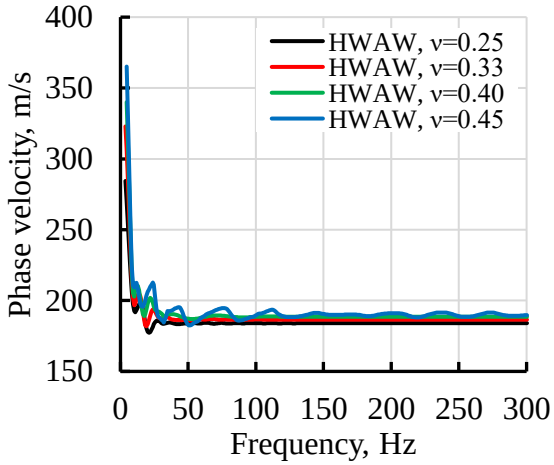

(c) Receiver spacing= 8 m, Source offset= 32 m

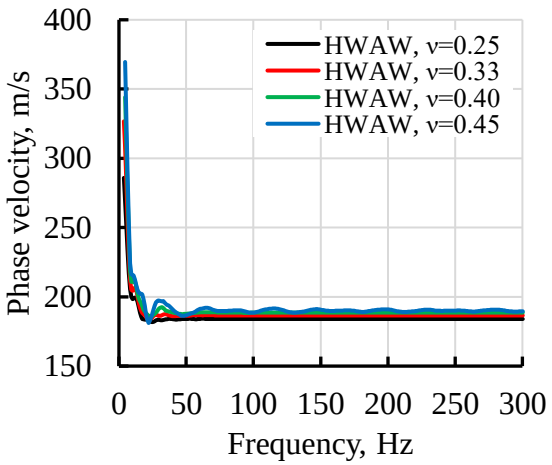

(d) Receiver spacing= 16 m, Source offset= 32m

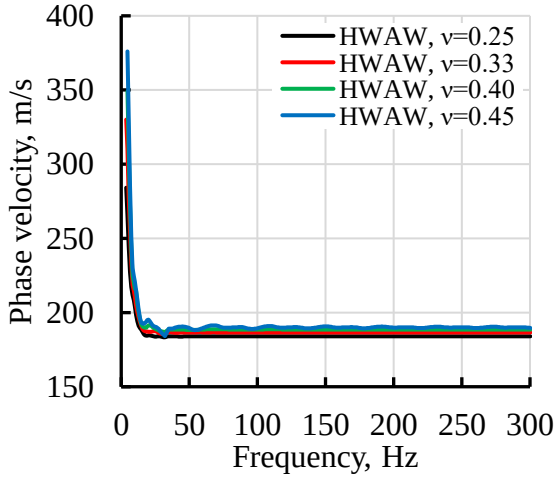

(e) Receiver spacing= 32 m, Source offset= 32 m

Figure 4.35 Effect of Poisson's ratio on the dispersion curves using different source offsets and receiver spacings for Profiles 1-P25, 1-P33, 1-P40, and 1-P45.

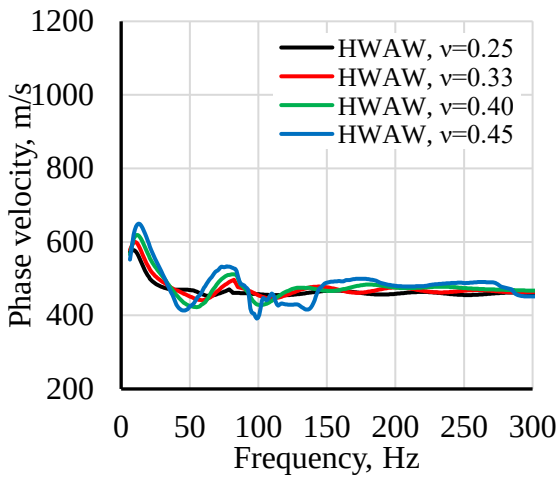

(a) Receiver spacing= 2 m, Source offset= 14 m

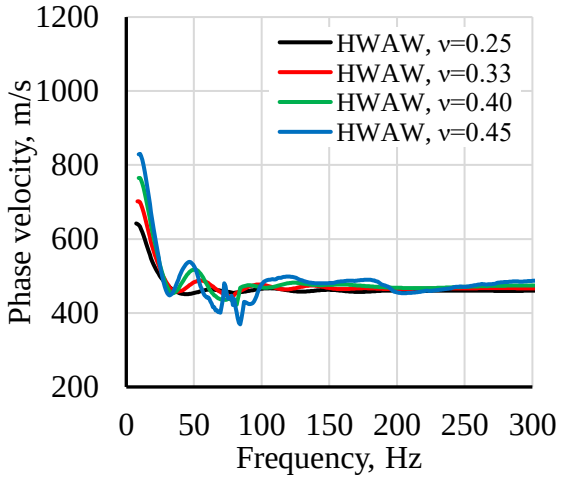

(b) Receiver spacing= 4 m, Source offset= 20 m

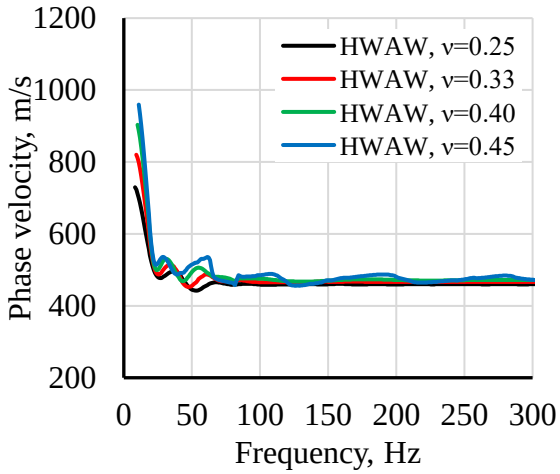

(c) Receiver spacing= 8 m, Source offset= 32 m

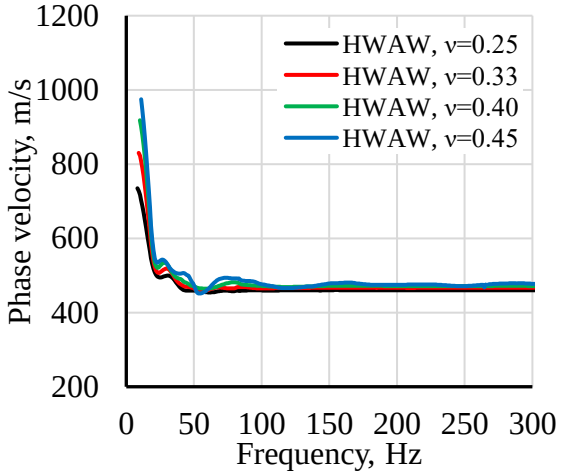

(d) Receiver spacing= 16 m, Source offset= 32m

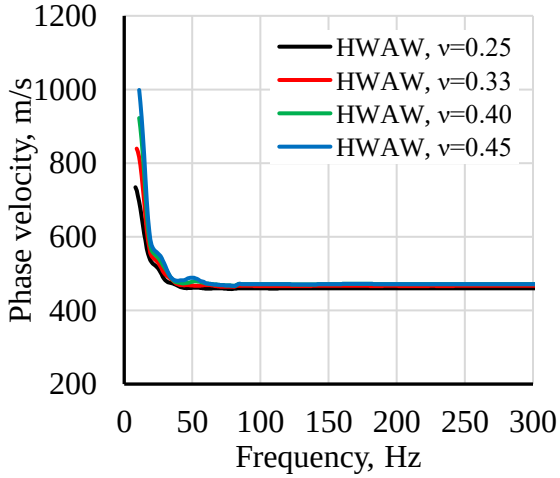

(e) Receiver spacing= 32 m, Source offset= 32 m

Figure 4.36 Effect of Poisson's ratio on the dispersion curves using different source offsets and receiver spacings for Profiles 2-P25, 2-P33, 2-P40, and 2-P45.

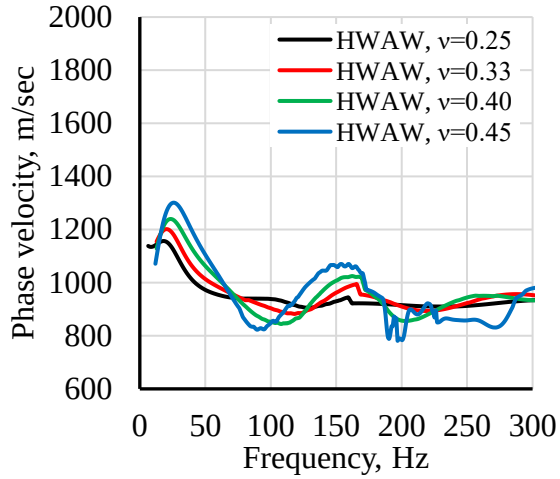

(a) Receiver spacing= 2 m, Source offset= 14 m

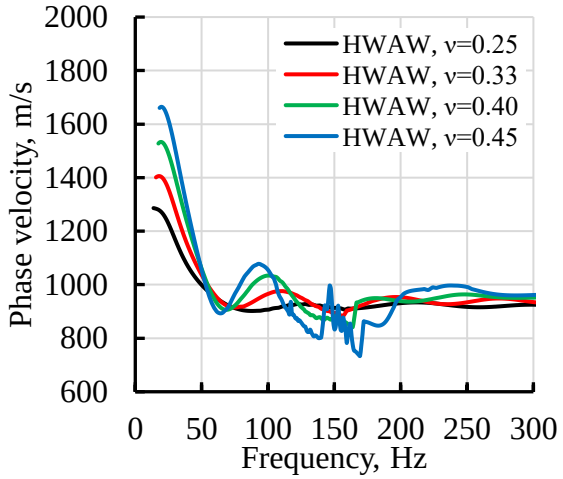

(b) Receiver spacing= 4 m, Source offset= 20 m

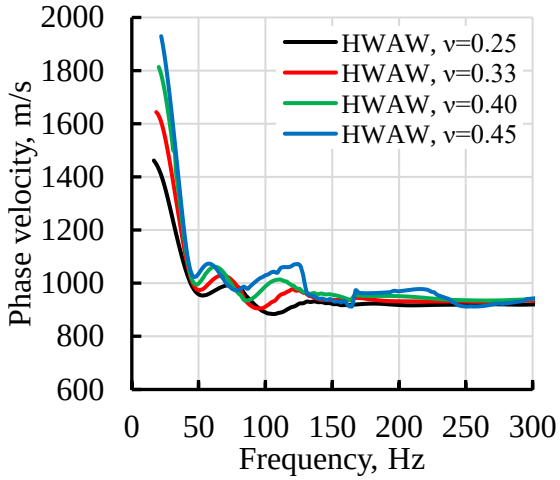

(c) Receiver spacing= 8 m, Source offset= 32 m

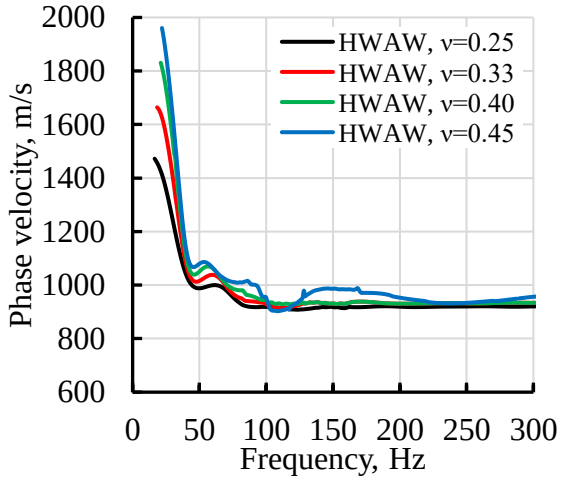

(d) Receiver spacing= 16 m, Source offset= 32m

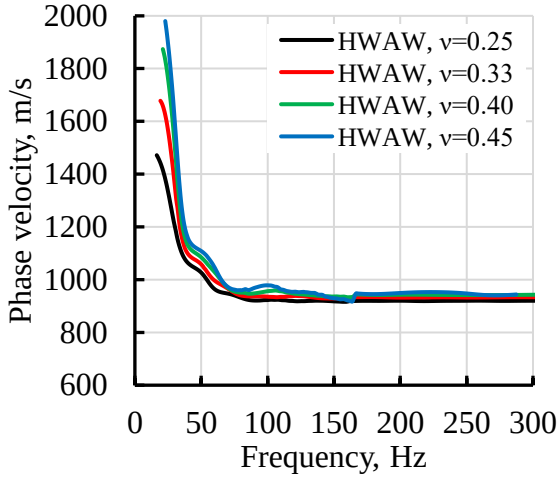

(e) Receiver spacing= 32 m, Source offset= 32 m

Figure 4.37 Effect of Poisson's ratio on the dispersion curves using different source offsets and receiver spacings for Profiles 3-P25, 3-P33, 3-P40, and 3-P45.

4.3.3.3 Discussions of Effect of Poisson's Ratio Values on Simple Profiles

The main finding from this study of the effect of Poisson's ratio on HWAW processing of simple profiles is that the experimental dispersion curves were accurately recovered for all cases of source offset, receiver spacings and Poisson's ratio used. This finding provides confidence that HWAW processing can be applied in the field regardless of saturation conditions at the site.

The second finding from this study is that for high Poisson's ratio values (i.e. saturated conditions), the selection of receiver spacing relative to the source offset has a large effect on the shape of the measured dispersion curve. The use of small receiver spacings with a large source offset for high Poisson's ratio profiles produced a dispersion curve (both theoretical and experimental) with large fluctuations as observed in Figures a and b of 4.35, 4.36, and 4.37. Therefore, the current HWAW data collection approach of using a single small receiver spacing with a single larger source offset has a distinct and strong sensitivity to changes in Poisson's ratio values when near-field effects are included in the analysis, in terms of both the velocity values and the shape of the dispersion curve.

Mera (1995), Chen et al. (2004), and McCaskill (2014) have made similar observations based on studies of the SASW two receiver test method. For example, Chen et al. (2004) performed a parametric study on source-to-first-receiver distance (r), receiver-to-receiver distance (Δx), and Poisson's ratio (ν) with an axisymmetric finite element model of a uniform elastic halfspace. The resulting dispersion curves show large fluctuations in the dispersion curves as the value of Poisson's ratio approaches saturated conditions (near ν=0.5), as shown in Figure 4.38. The effect is most notable when the receivers are closely spaced relative to the measured wavelength. Chen et al. (2004) and Chai et al. (2011) have

shown that these fluctuations are caused by body wave interference, especially P-waves, which are more easily excited at saturated sites.

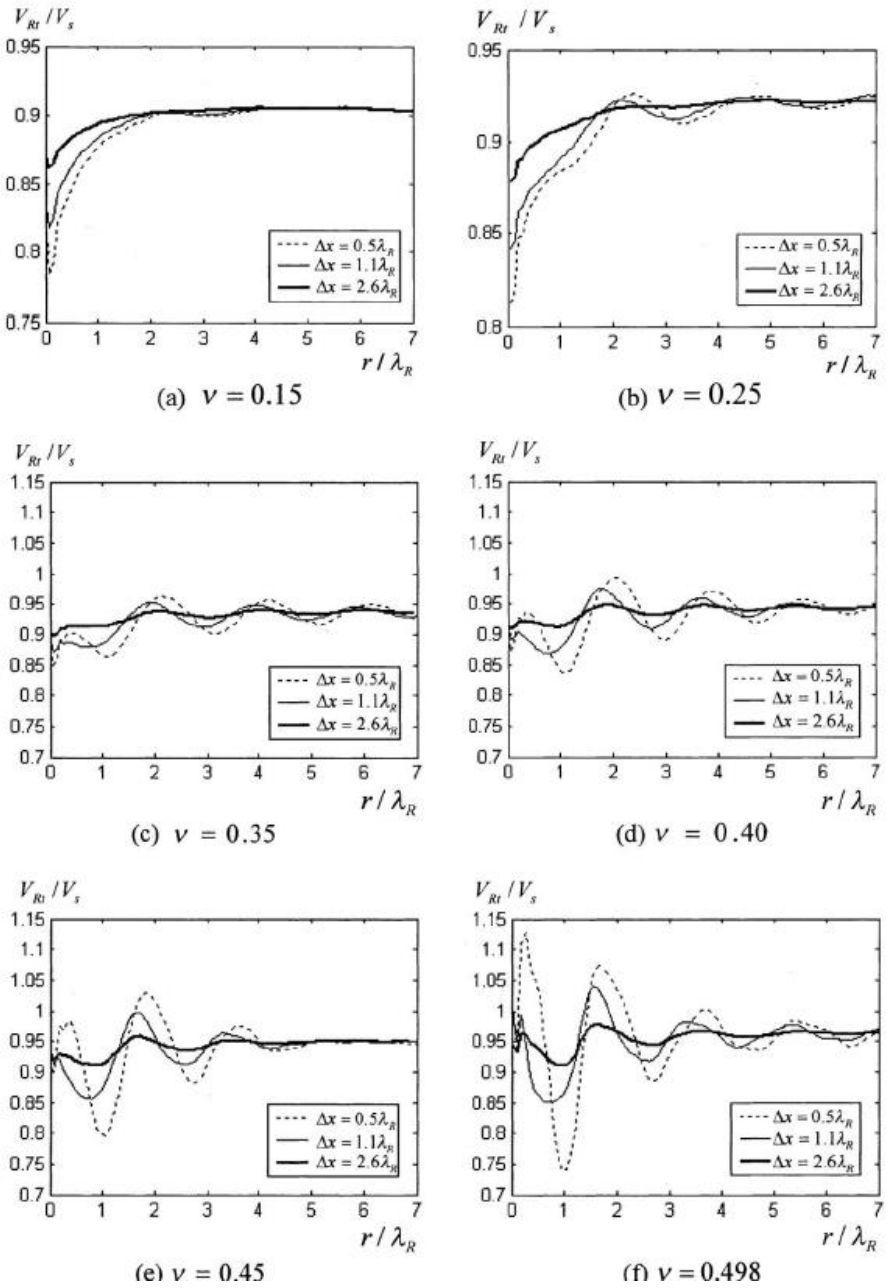

Figure 4.38 Normalized dispersion curves from a parametric study of source-to-first-receiver spacing (r), receiver-to-receiver spacing (Δx), and Poisson's ratio (ν) performed by Chen et al. (2004).

This second finding has some important implications. First, if data are recorded at a saturated site using closely spaced receivers and processed with the HWAW approach, it

is important that the theoretical model used in the inversion of the dispersion curve also accurately models the body wave contributions at the actual receiver locations. The program WinSASW does this with the 3D array inversion mode. However, the large fluctuations in the dispersion curve may still present problems with the inversion process due to the need to establish a reasonable starting model. In the case of WinSASW, the dispersion curve is used directly to create a reasonable starting model, as described by Joh (1996). As an example, two of the dispersion curves simulated from Profile 2-P45 were inverted using WinSASW using the procedure described in Joh, 1996. The dispersion curve collected with a source offset of 20 m and a receiver spacing of 4 m (typical of HWAW data collection) and the dispersion curve collected with a conventional SASW approach of equal source offset and receiver spacings (32 m in this case) were used. As shown in Figure 4.39, using the data collected with the short receiver spacings produced an erratic V_S profile that did not match well with the true profile.

However, it should also be noted that the presence of these large fluctuations in the dispersion curve clearly provide additional information about the site. Improved inversion methods, which were not a part of this study, should be investigated to better utilize this information. Potentially, both the V_S profile and Poisson's ratio could be inverted from the measurements.

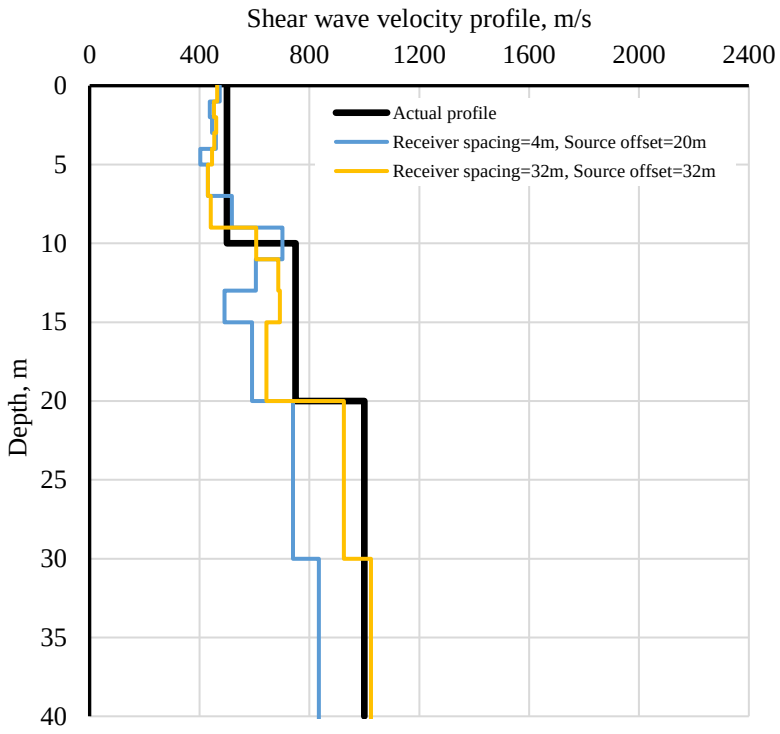

Figure 4.39 Comparison of the V_S profile for Profile 2-P45 with V_S profiles inverted by method implemented in WinSASW for different receiver spacings and source offsets.

4.4 HWAW Data Collection and Processing at Complex Profiles

4.4.1 Introduction

Based on the literature review of problematic sites for SASW and MASW testing, several complex soil V_S profiles were identified and studied, as shown in Chapter 3. These complex sites are categorized as (1) soft-over-stiff sites with large impedance contrast (2) sites with shallow and deep linear V_S gradient, (3) sites with an embedded lower velocity layer, (5) and sites with an embedded higher velocity. These V_S profiles were created to simulate common complex geotechnical profiles encountered in the field.

Data collection and processing followed the procedures developed from the study of simple soil profiles. The data collection and processing parameters used in this study of complex soil profiles are presented in Table 4.8.

Results and discussion from the simulations of complex soil profiles are presented below. Practical implications of the findings from this study are presented in Section 4.6.

Table 4.8 Data collection and processing parameters used in the study of complex soil profiles simulations

Sampling frequency, f_s, Hz	Bandwidth, b_w, Hz	Source offset, S-R1, m	Receiver spacing, R1-R2, m
1875	1.83	14	2
		18	
		22	
		26	
		30	
		12	4
		16	
		20	
		24	
		28	

4.4.2 Soft-over-Stiff Sites with Large Impedance Contrast

4.4.2.1 Introduction

The soft-over-stiff condition is commonly encountered when a soft soil layer overlies a much higher velocity layer such as a highly overconsolidated clay, dense sand or bedrock. As noted in Chapter 2, this condition is especially problematic for the SASW manual phase unwrapping procedure due to abrupt change in surface wave modes (Rosenblad and Bertel, 2008). The relevant parameter in these cases is the impedance ratio between adjacent layers. The impedance is defined as the product of the velocity and the mass density of the soil or rock. Variation in mass density between soil and rock is usually small (typically 25% or less) compared to the much larger variation in velocity between soil and rock. Therefore, the impedance ratio is dominated by the change in velocity between adjacent layers.

This section presents results and discussion of the effectiveness of the HWAW method for recovering the correct phase velocity dispersion curve at sites with high and very high impedance contrasts.

4.4.2.2 Results of HWAW at Soft-Over-Stiff Sites with High Impedance Contrast

Profile 4 (Figure 4.40a) represents a case of high contrast between soil and rock, defined here as an impedance ratio of 3. Comparisons between dispersion curves developed with the HWAW method and the theoretical dispersion curves for Profile 4 are presented in Figures 4.41 (in terms of frequency) and Figure 4.42 (in terms of wavelength). Modal dispersion curves for several modes are also presented for comparison. Receiver spacings of 2m and 4m were modeled with various source offsets. The theoretical dispersion curves

for this case follow the fundamental mode at higher frequencies, but transition to a combination of modes at lower frequencies.

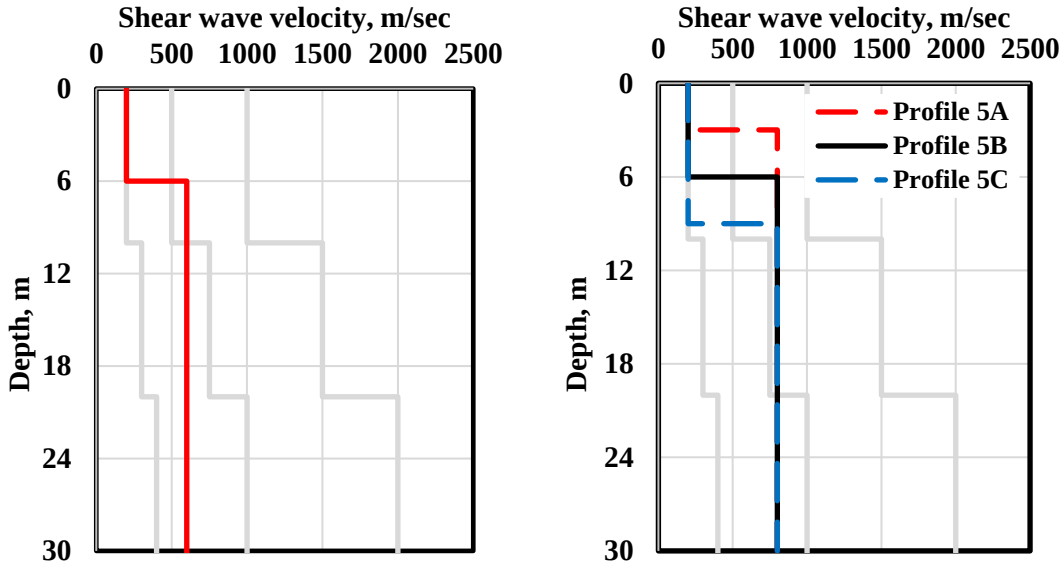

Figure 4.40 Soil profiles used for simulations of soft-over-stiff condition (a) Profile 4 (high contrast), (b) Profiles 5A, 5B, and 5C (very high contrast).

4.4.2.3 Discussions of Results from High-Contrast Profiles

The results of Profile 4 show the theoretical and HWAW dispersion curves are in generally good agreement for all of the simulated test setups. The HWAW dispersion curves correctly follow the trend of the theoretical dispersion curve for all receiver spacings and source offsets, but a small percentage of points (4%) from the HWAW dispersion curve deviated from the theoretical dispersion curve by as much as 8%. This error occurred at the frequency value around 12 Hz (red dashed circle) where the mode transformation returned back to the fundamental mode. This error was much higher than the errors observed from modeling of the simple profiles (Profile 1-3), which had errors of 1.4% or lower. The results suggest that the bandwidth-to-frequency criteria developed for the simple profiles is not

sufficient and a lower bandwidth should be used. This is investigated further in Section 4.4.5.4.

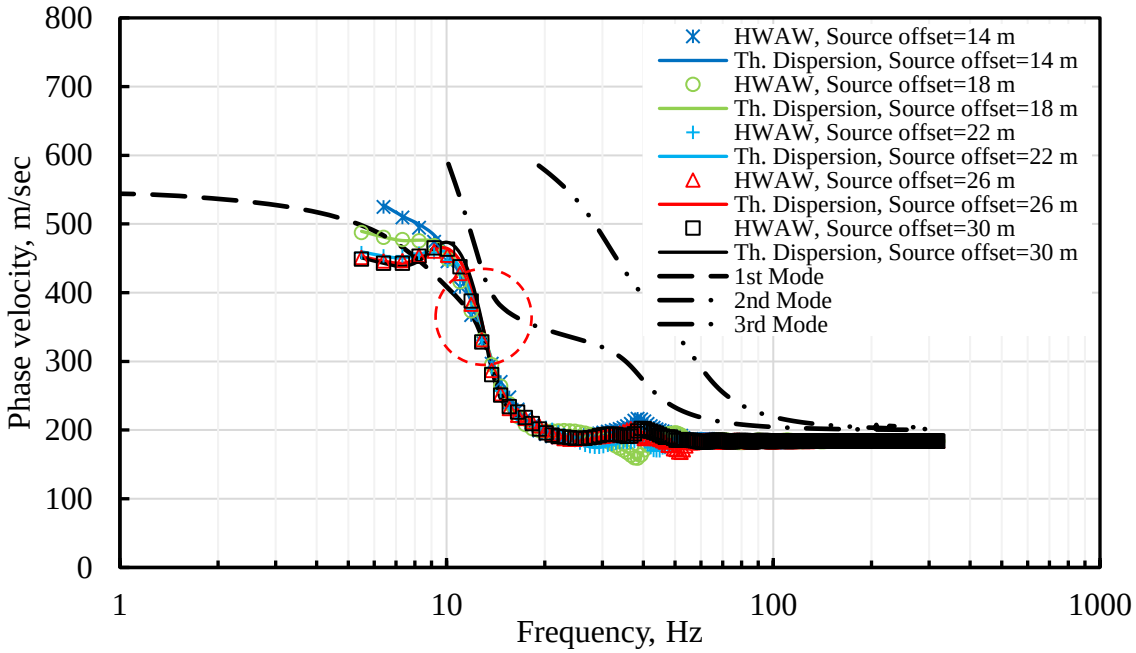

(a)

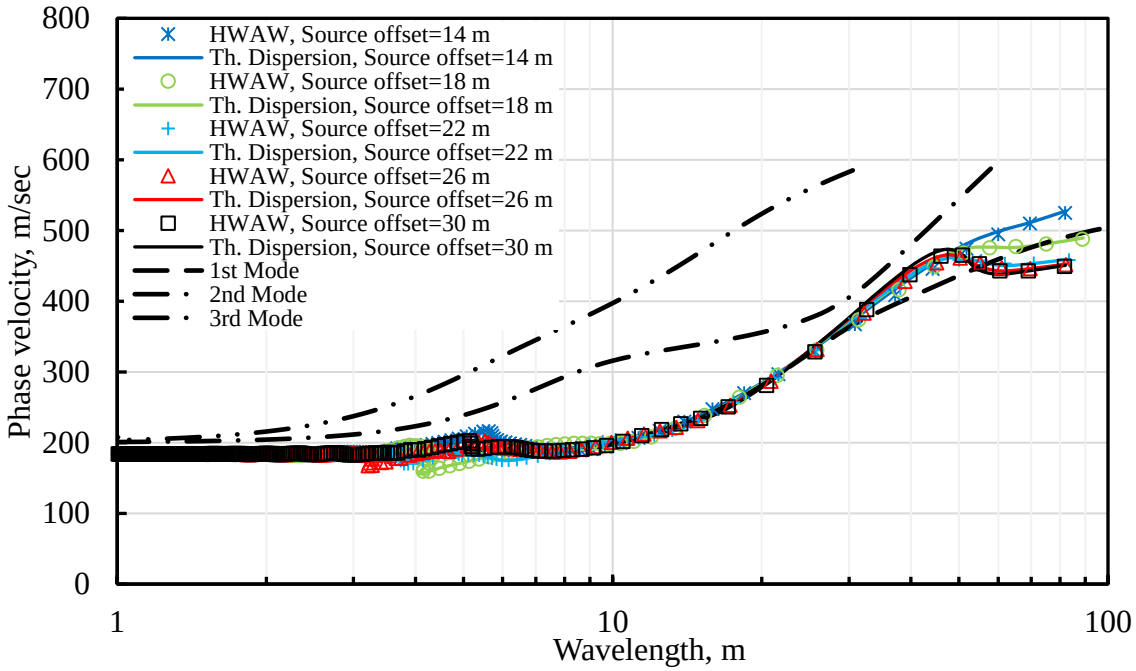

(b)

Figure 4.41 HWAW dispersion curves developed from Profile 4 using a receiver spacing of 2 m and different source offsets: (a) Phase velocity versus frequency, (b) Phase velocity versus wavelength.

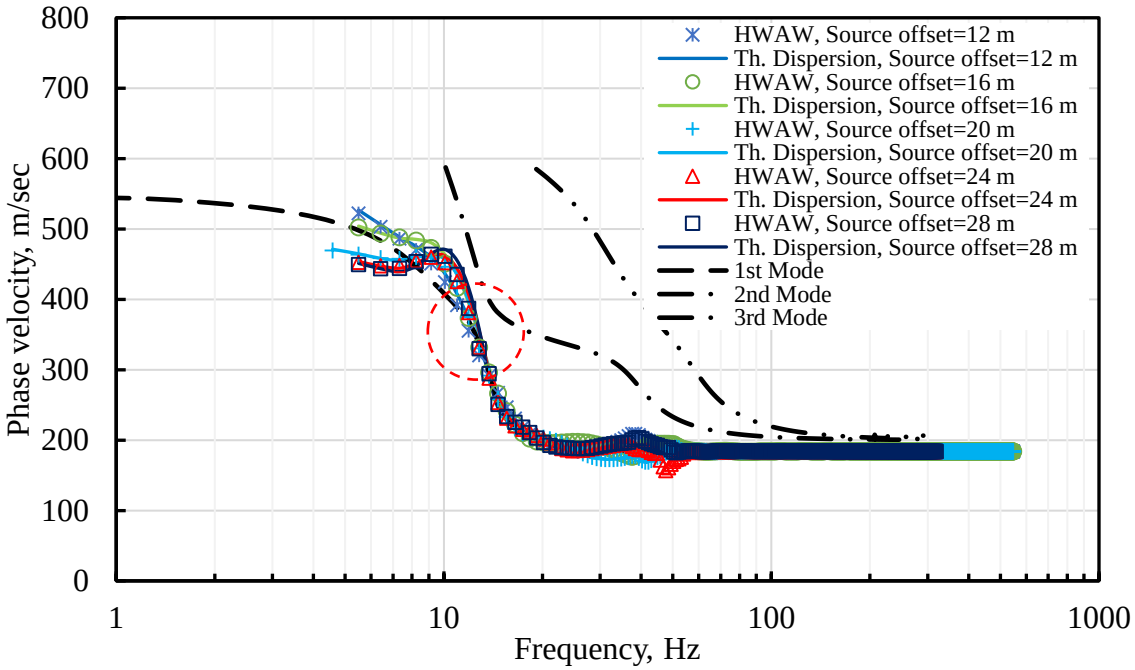

(a)

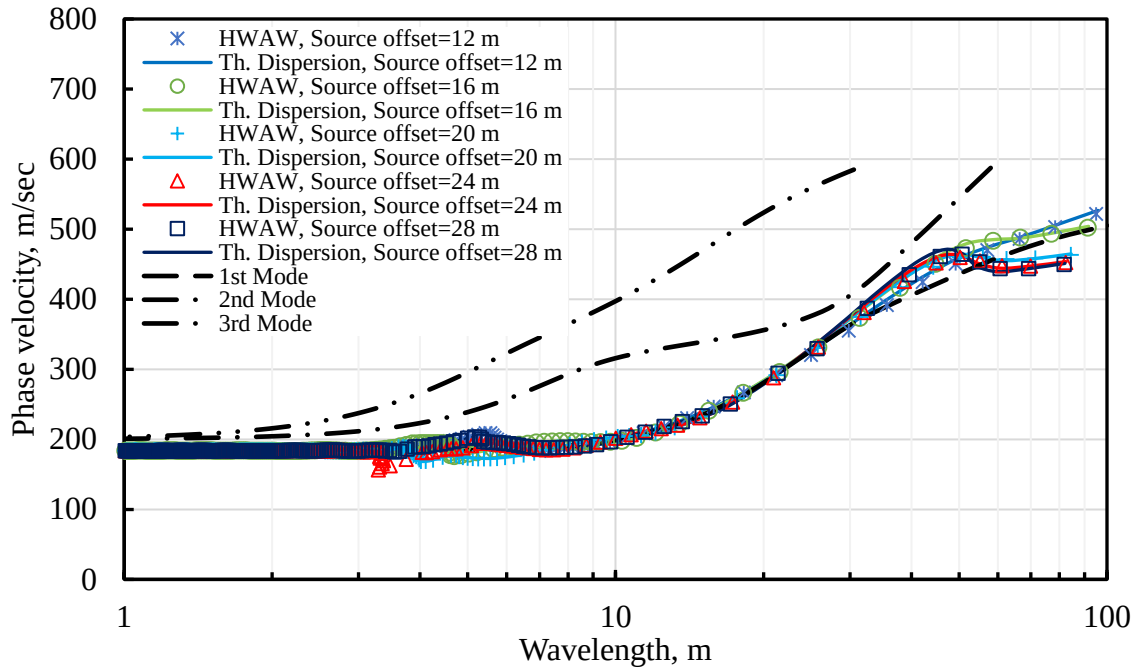

(b)

Figure 4.42 HWAW dispersion curves developed from Profile 4 using a receiver spacing of 4 m and different source offsets: (a) Phase velocity versus frequency, (b) Phase velocity versus wavelength.

4.4.2.4 Results of HWAW at Soft-Over-Stiff Sites with Very High Impedance Contrast

Profiles 5A, 5B, and 5C are shown in Figure 4.40b. These profiles are characterized as very high impedance contrast with a ratio of 4 between the soil and the rock. In this case, different depths to the high-velocity layer were also modeled, specifically, Profile 5A with 3 m rock depth, Profile 5B with 6 m rock depth, and Profile 5C with 9 m rock depth.

The HWAW and the theoretical dispersion curves are plotted in terms of frequency and wavelength for receiver spacings of 2 m and 4 m with different source offsets as listed in Table 4.8. Comparisons between the HWAW processed dispersion curves and the theoretical dispersion curves are shown for Profile 5A in Figures 4.43 and 4.44, for Profile 5B in Figures 4.45 and 4.46, and Profile 5C in Figures 4.47 and 4.48. For all of the very high contrast sites, a distinct and abrupt transformation from the fundamental mode to a higher surface wave mode was observed in the theoretical dispersion curve, regardless of rock depth or receiver spacing used. The transition is especially abrupt for the shallow rock case (Profile A) with the largest source offset. The frequencies at which this transition occurs is a function of the rock depth, with deeper rock producing a transition at lower frequencies.

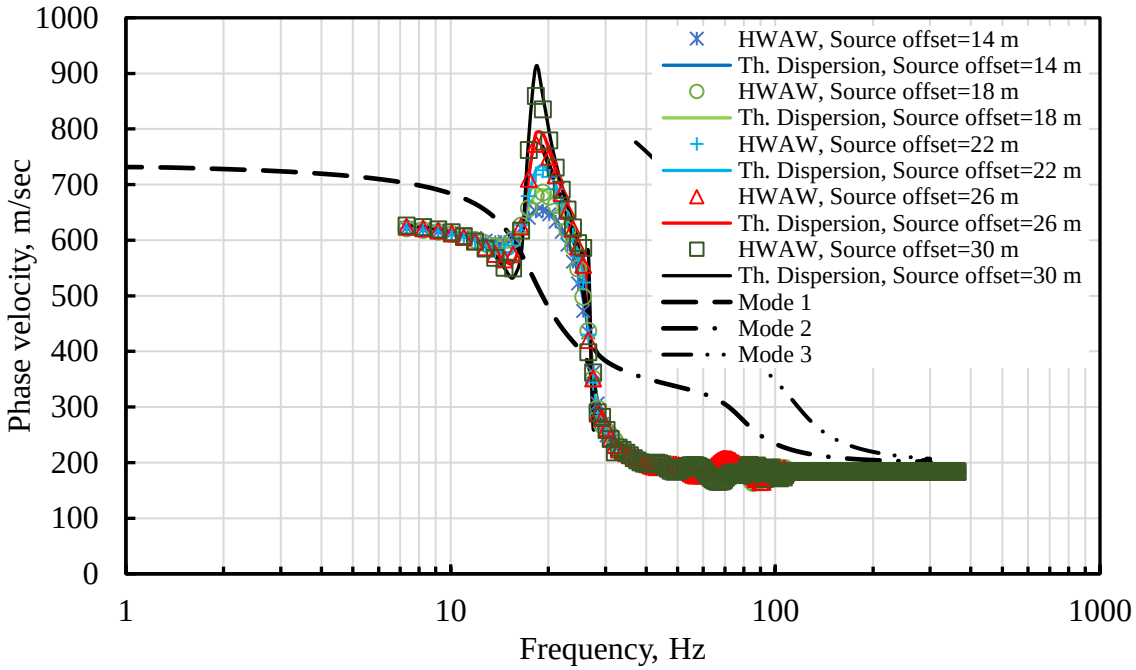

(a)

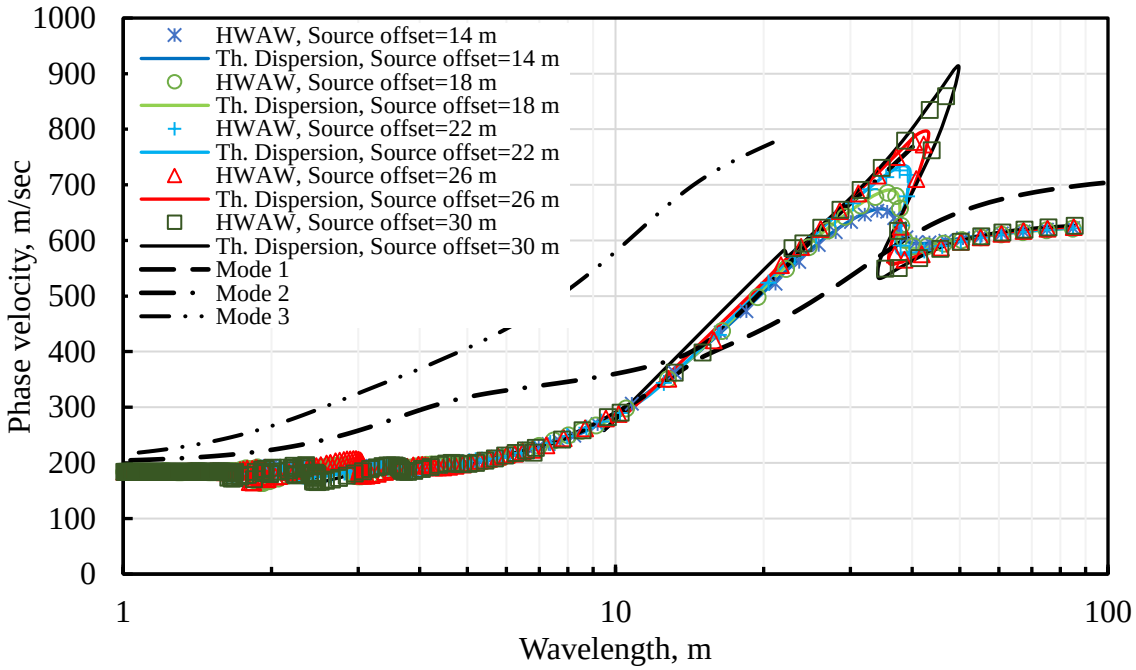

(b)

Figure 4.43 HWAW dispersion curves developed from Profile 5A (3 m depth interface) using a receiver spacing of 2 m and different source offsets: (a) Phase velocity versus frequency, (b) Phase velocity versus wavelength.

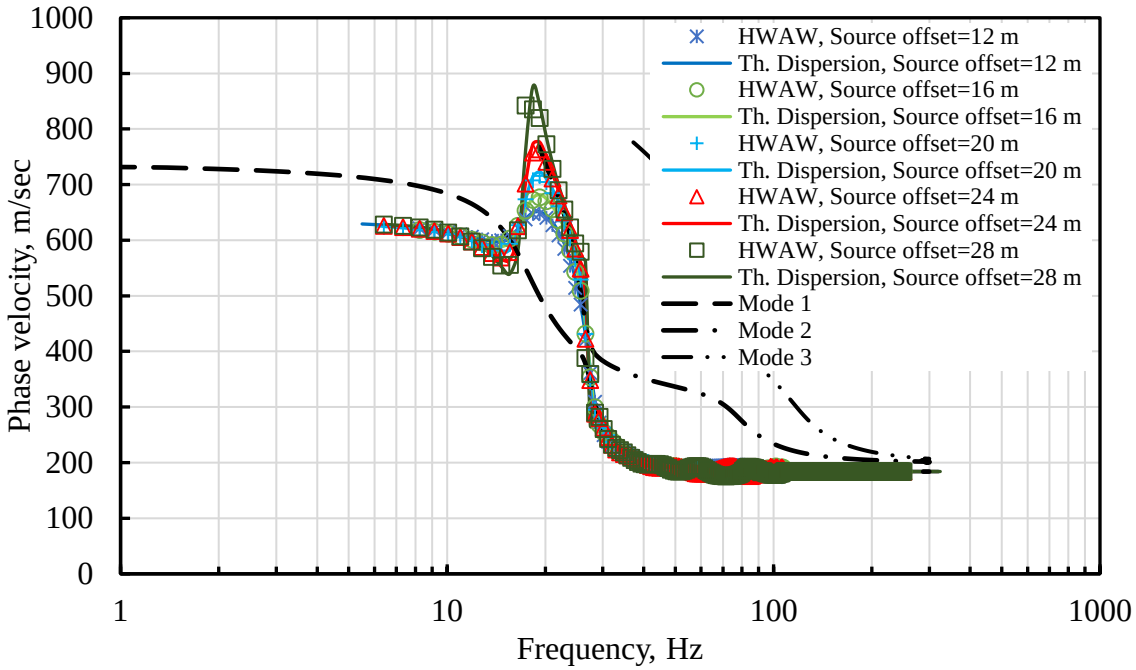

(a)

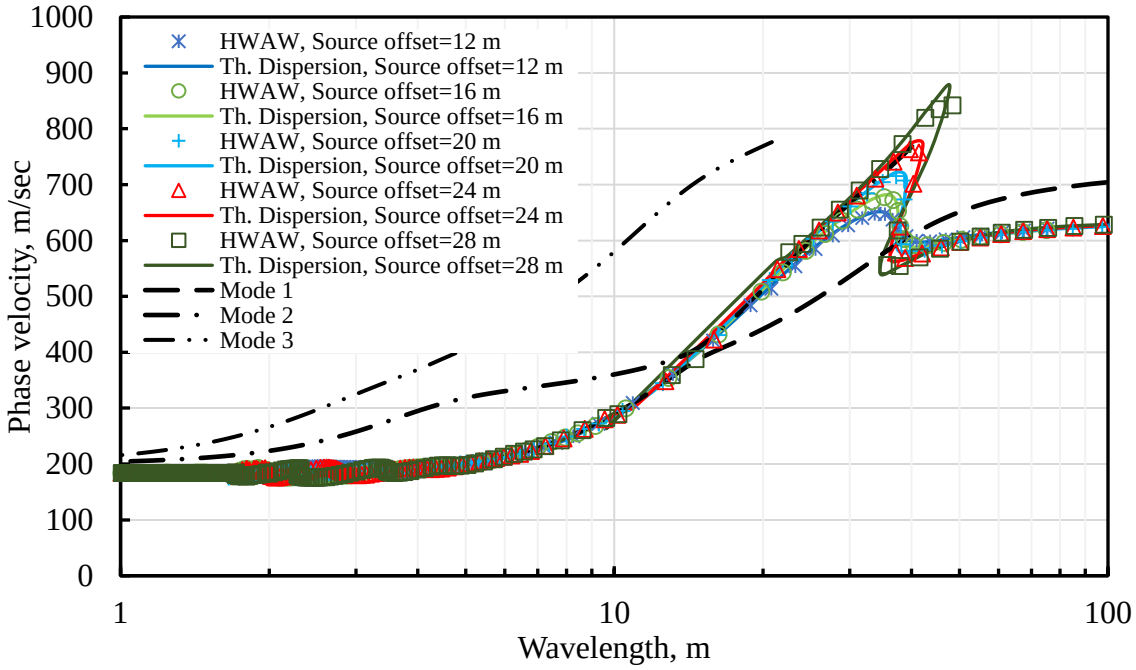

(b)

Figure 4.44 HWAW dispersion curves developed from Profile 5A (3 m depth interface) using a receiver spacing of 4 m and different source offsets: (a) Phase velocity versus frequency, (b) Phase velocity versus wavelength.

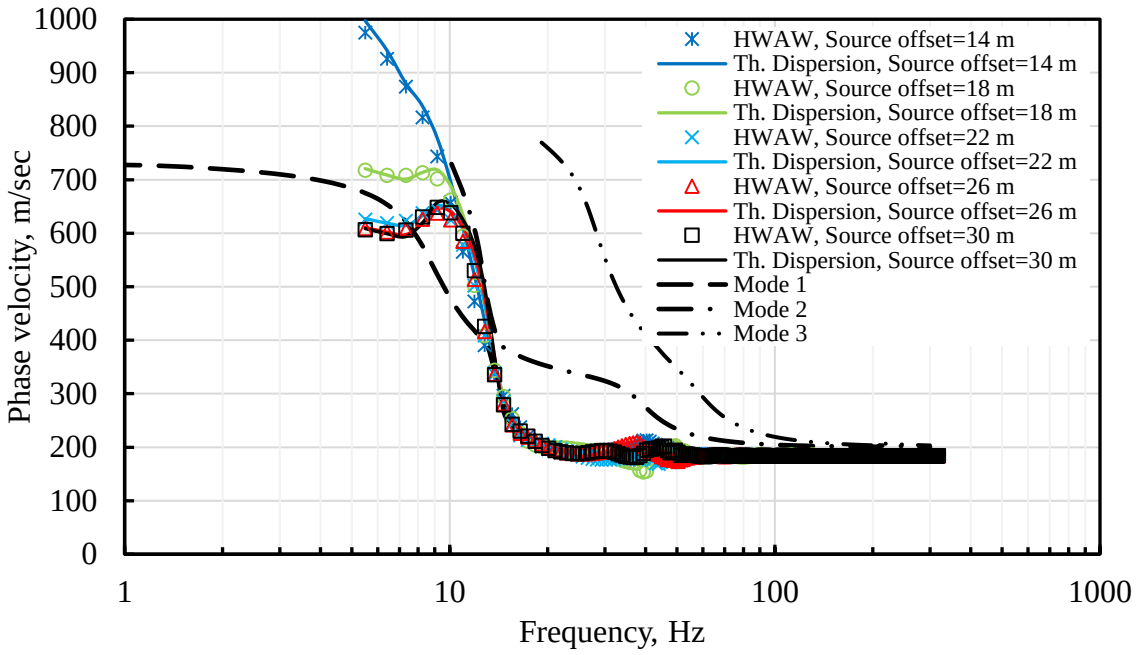

(a)

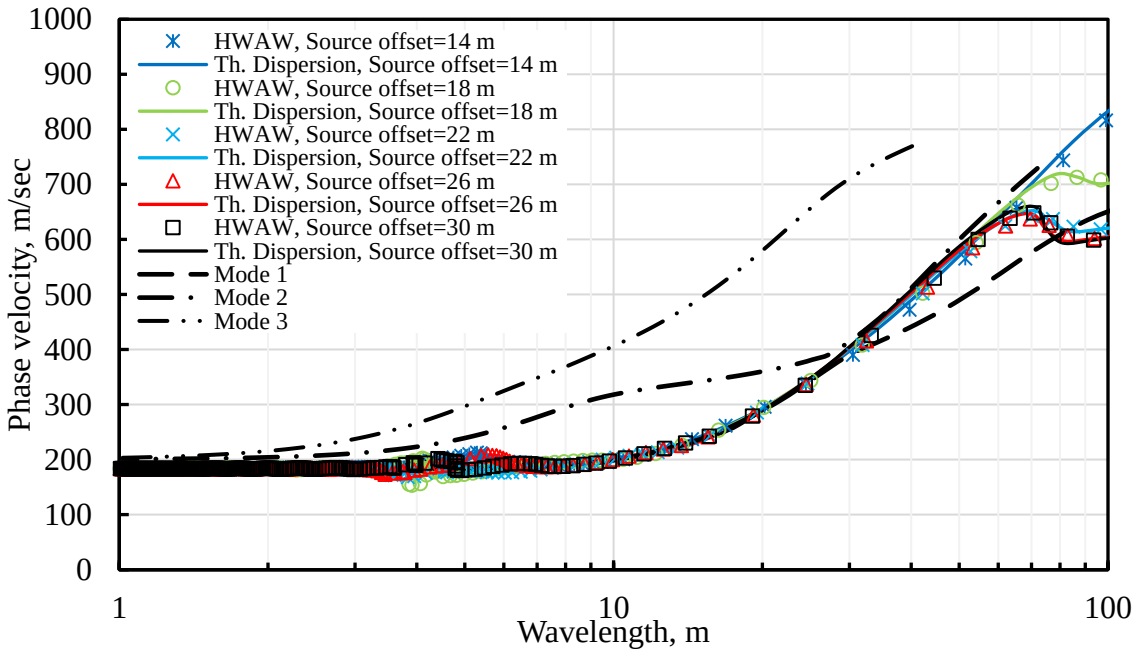

(b)

Figure 4.45 HWAW dispersion curves developed from Profile 5B (6 m depth interface) using a receiver spacing of 2 m and different source offsets: (a) Phase velocity versus frequency, (b) Phase velocity versus wavelength.

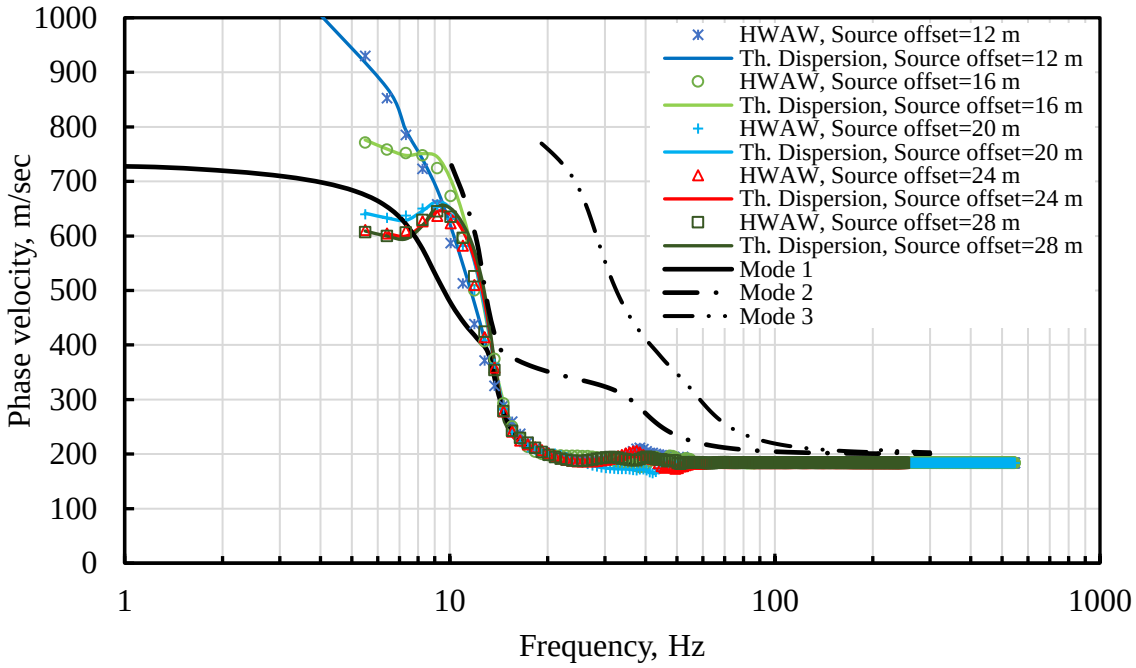

(a)

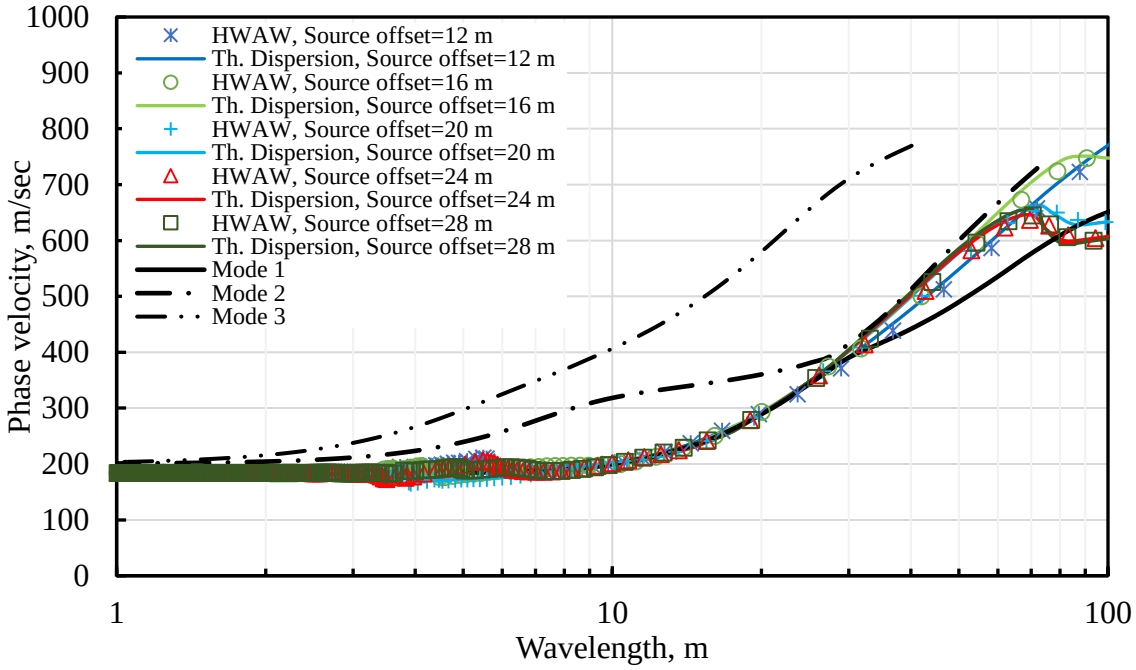

(b)

Figure 4.46 HWAW dispersion curves developed from Profile 5B (6 m depth interface) using a receiver spacing of 4 m and different source offsets: (a) Phase velocity versus frequency, (b) Phase velocity versus wavelength.

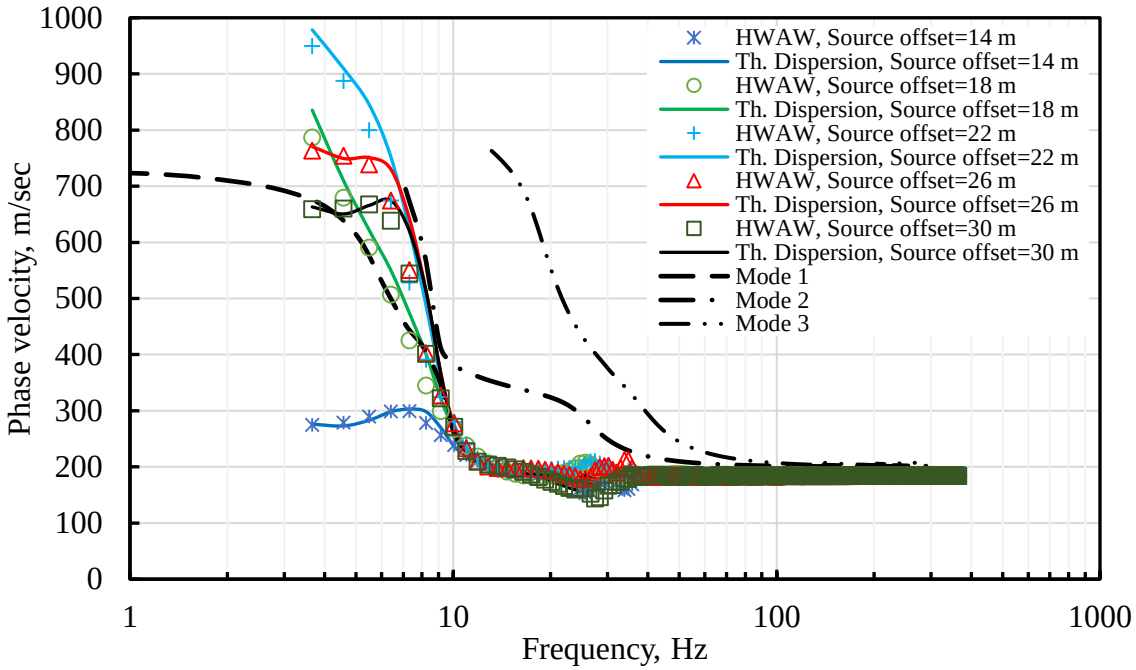

(a)

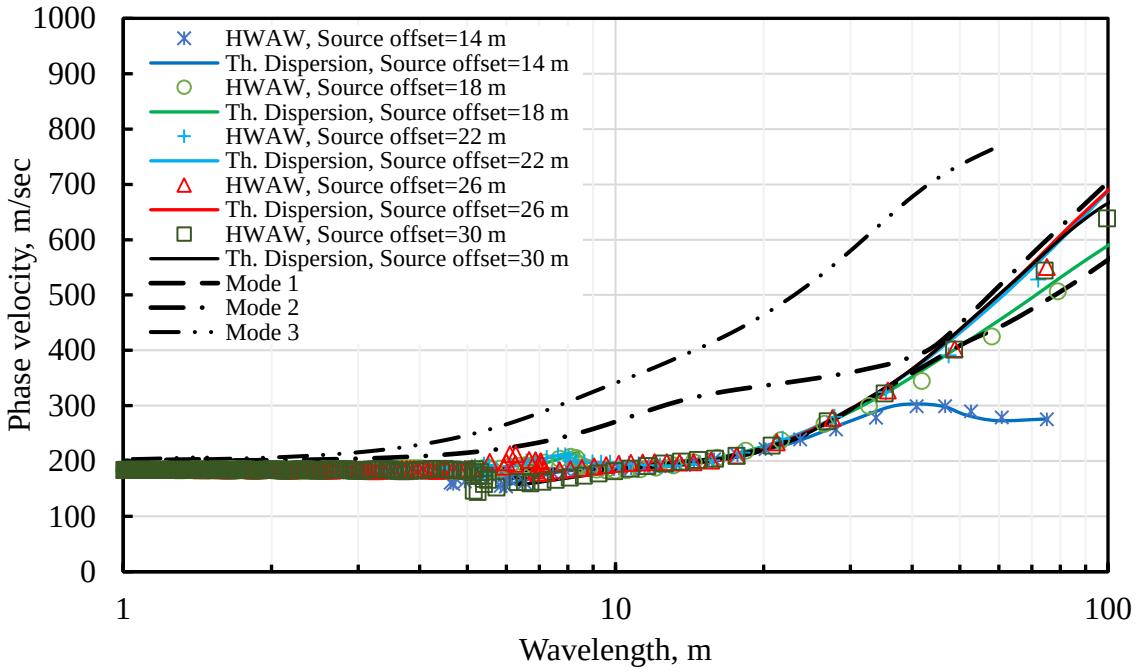

(b)

Figure 4.47 HWAW dispersion curves developed from Profile 5C (9 m depth interface) using a receiver spacing of 2 m and different source offsets: (a) Phase velocity versus frequency, (b) Phase velocity versus wavelength.

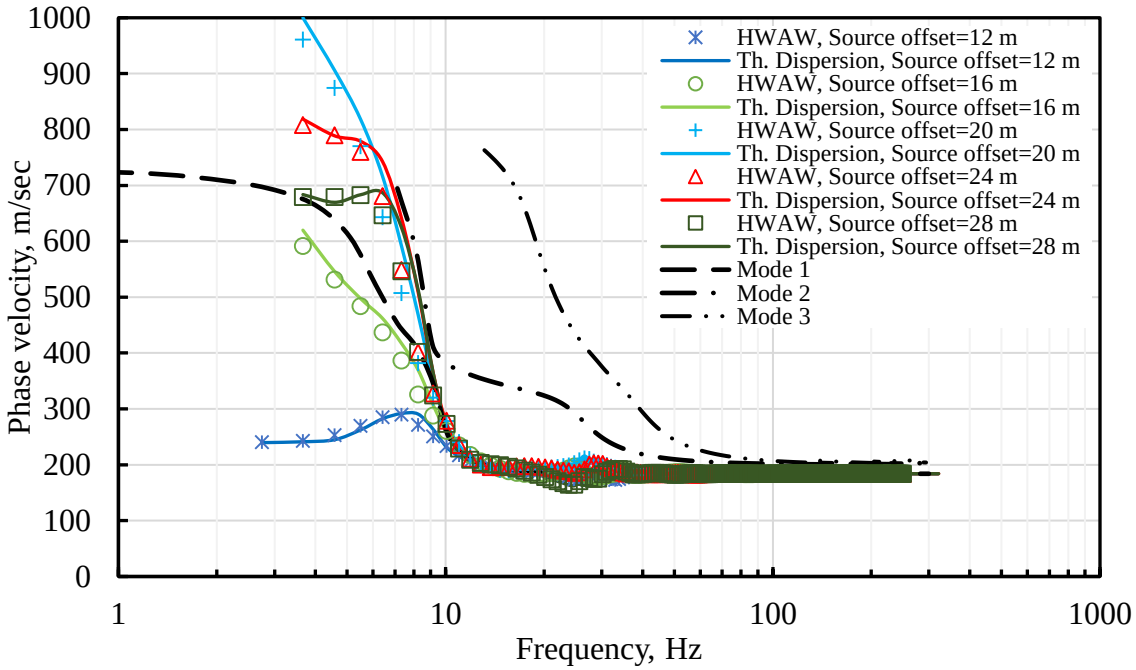

(a)

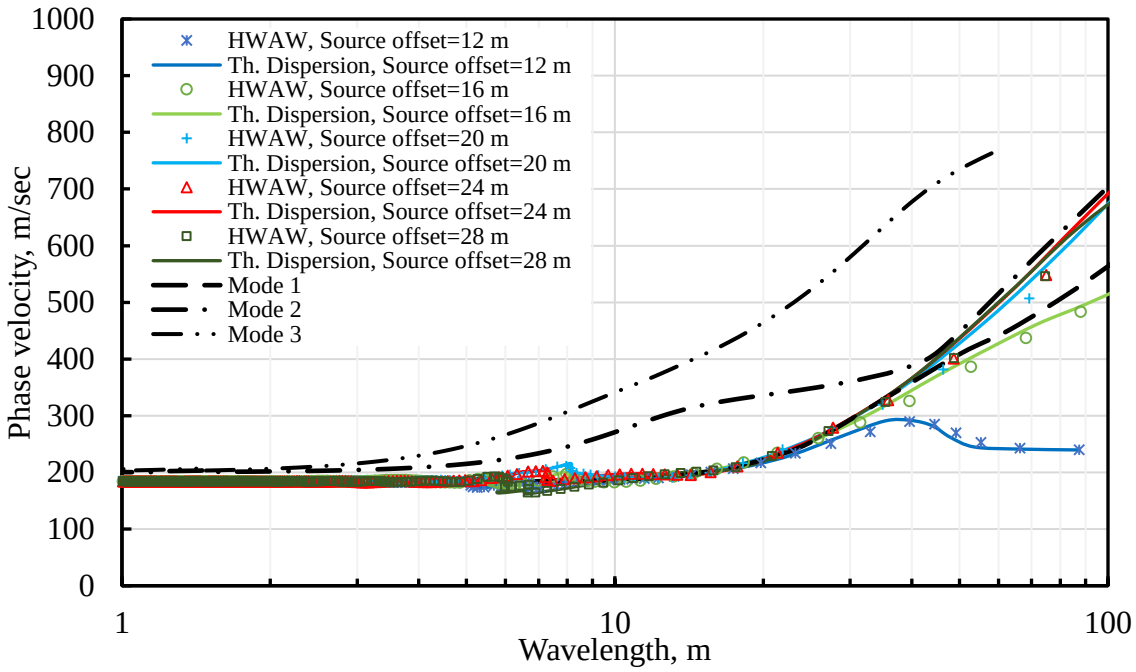

(b)

Figure 4.48 HWAW dispersion curves developed from Profile 5C (9 m depth interface) using a receiver spacing of 4 m and different source offsets: (a) Phase velocity versus frequency, (b) Phase velocity versus wavelength.

4.4.2.5 Discussions of Results from Very High-Contrast Profiles

The dispersion curves developed from HWAW processing of sites with a very high velocity contrast are in general agreement with the theoretical dispersion curves. For Profile 5A with a 3 m interface depth, the HWAW method recovers the mode jump that is observed in the frequency range of about 16 Hz to 25 Hz for all test setups. The theoretical and HWAW dispersion curves are generally consistent but in the low frequency range the phase velocity is underestimated by the HWAW method. The absolute maximum error for some points is as high as 10 %.

For Profile 5B with a 6 m interface depth, the theoretical and HWAW dispersion curves recovered the mode jump in the frequency range of about 8 Hz to 14 Hz for all test setups. The transition in this case was not as abrupt as was observed for the shallower bedrock case. The trends in the dispersion curves were generally consistent, but again the phase velocities were typically underestimated at low frequencies with some points having an absolute maximum error percentage as high as 14%.

For Profile 5C with a 9 m interface depth, the theoretical and HWAW dispersion curves again recovered the mode transition that occurs in the frequency range of about 5 Hz to 8 Hz. The transition in this case was less abrupt than the shallower bedrock cases (3m and 6 m). The trends in the dispersion curves were again generally consistent, but the phase velocities were underestimated at low frequencies with some points having an absolute maximum error percentage as high as 22%.

The larger errors observed for these cases as compared to the simple profile (Profile 1-3) cases suggests that a narrower bandwidth should be used for these complex sites where abrupt changes in phase velocity occur. This is investigated further in Section 4.4.5.

As noted above, as the depth to the halfspace increases from 3 m to 9 m, the frequency range where the mode transition occurs decreases. The transition frequencies are generally consistent with the compression wave resonance and shear wave resonance of the soil layer, where the compression wave velocity is expressed as the so called Lysmer velocity when Poisson's ratio values above 0.45. The Lysmer velocity, V_L is:

$$V_L = \frac{3.4}{\pi(1-\nu)}.V_S \qquad (4.5)$$

where v is Poisson's ratio.

Table 4.9 shows the compression and shear wave resonant frequencies for Profiles 5A, 5B and 5C calculated using:

$$f = \frac{V}{4H} \qquad (4.6)$$

Where V is the compression wave velocity (V_P) for compression waves and shear wave velocity V_S for shear waves, and H is the thickness of the layer. However, the value of V_P increases without bound as Poisson's ratio approaches 0.5. It was found that for larger values of Poisson's ratio (above 0.45), V_L which had been proposed as an estimate of the threshold vertical frequency, (Mera, 1995, and Roesset, 1998).

Table 4.9 Compression and shear wave resonant frequencies for Profiles 5A, 5B and 5C

Profile No.	H, m	V_S, m/s	Frequency, Hz	V_P, m/s	Frequency, Hz
5A	3	200	16.6	346	28.8
5B	6	200	8.3	346	14.4
5C	9	200	5.5	346	9.6

These values are approximately equal to the transition frequencies observed in the dispersion curves.

Another observation from the dispersion data is that deeper bedrock and shorter source offsets produce theoretical dispersion curves that do not transition back to the fundamental

mode at low frequencies, as seen, for example, by comparing the source offsets of 22 m and 26 m with 30 m (for receiver spacing of 2 m) and source offsets of 20 m and 24 m (for receiver spacing of 4 m) as shown in Figures 4.47 and 4.48 respectively.

Although points at certain frequencies were shown to have significant errors, the most important observation from this simulation is that the HWAW processing effectively follows the abrupt higher mode transition. This case is especially problematic for the manual phase unwrapping procedures used in conventional SASW measurements and can easily produce erroneous dispersion curves (Al-Hunaidi 1992; Al-Hunaidi 1993; Joh et al. 1997; Rosenblad and Bertel 2006). The results suggest that HWAW processing may be effective for automating the manual phase unwrapping procedure used in the SASW method, as will be investigated with simulated data in Section 4.5 and with experimental data in Chapter 5.

4.4.3 High Gradient Profiles

4.4.3.1 Introduction

In this section profiles are studied where V_S increases rapidly with depth. Linear velocity gradients from 200 m/s to 600 m/s over a depth of 6 m (Profile 6) and 12 m (Profile 7) were modeled, as shown in Figure 4.49 for Profiles 6 and 7, respectively. The effectiveness of the HWAW method at recovering the theoretical phase velocity dispersion curve are presented and discussed below.

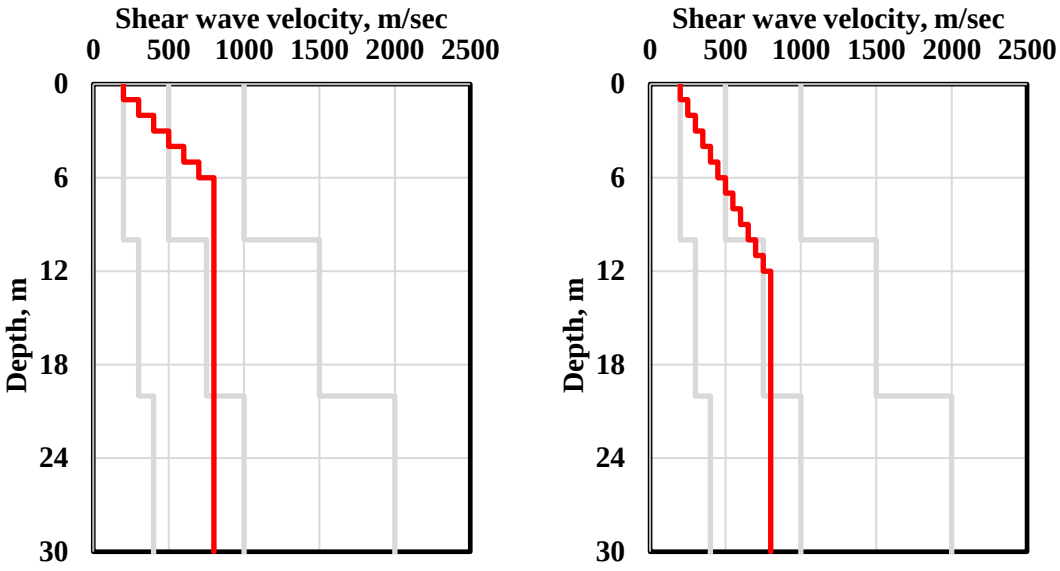

Figure 4.49 Soil profiles with a linear velocity gradient over half-space (a) Profile 6 (shallow velocity gradient) (b) Profile 7 (deeper velocity gradient).

4.4.3.2 Results from HWAW at Shallow Gradient Profile

Profiles 6 is presented in Figure 4.49(a) and Table 3.2. Figures 4.50 and 4.51 show the results of the simulated HWAW experimental and theoretical dispersion curves for Profile 6 in terms of frequency and wavelength for receiver spacings of 2 m and 4 m with a range of source offsets.

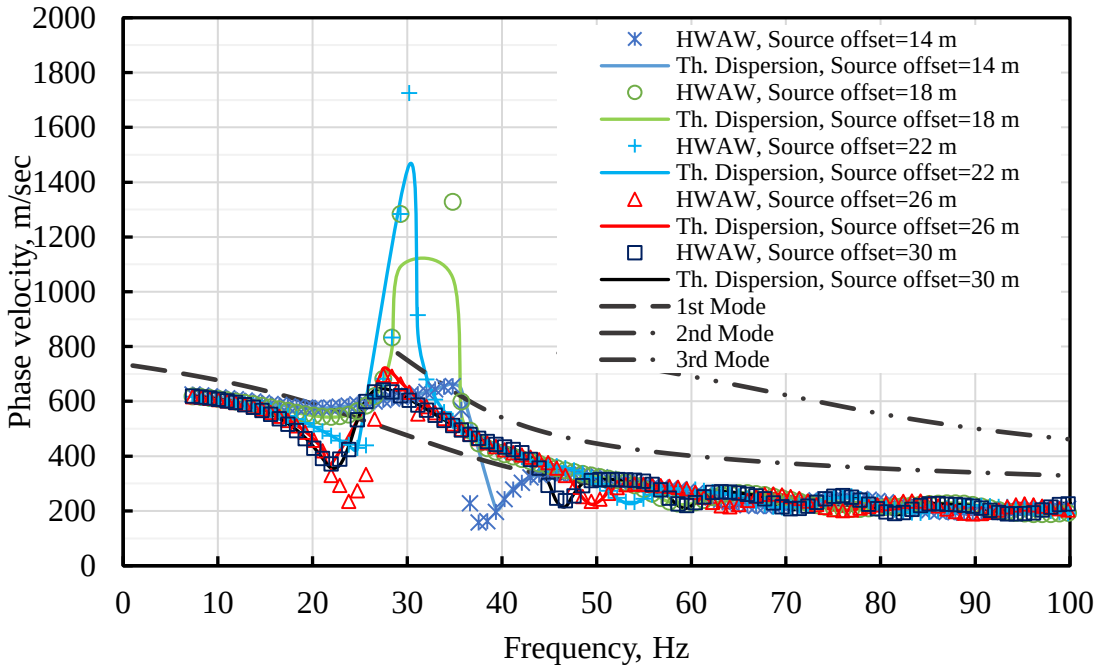

(a)

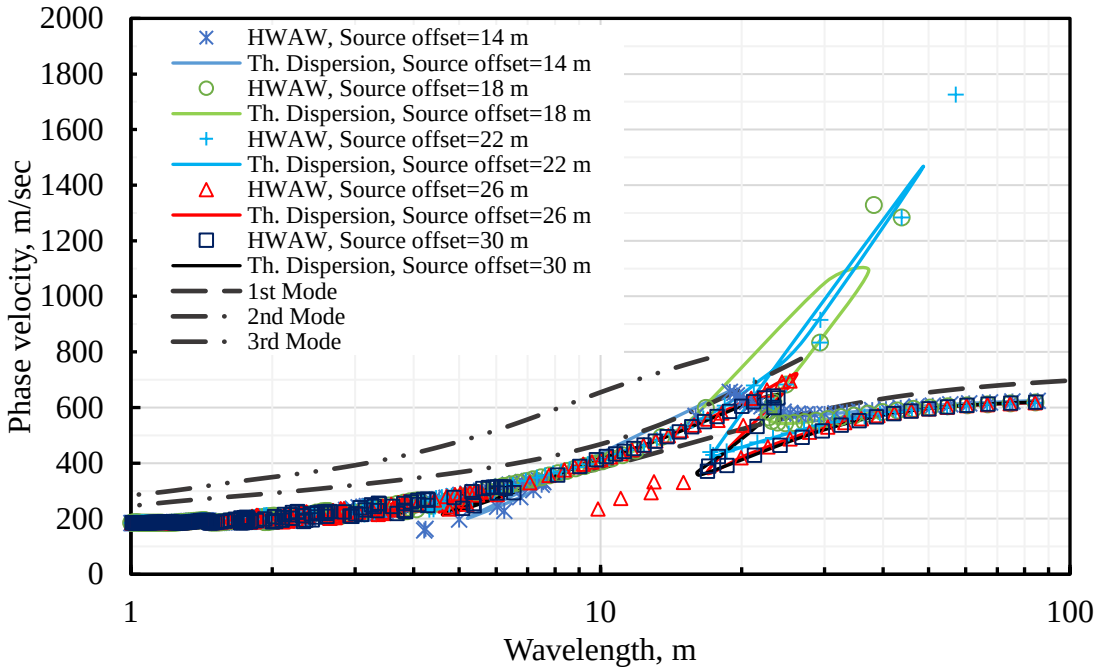

(b)

Figure 4.50 HWAW dispersion curves developed from Profile 6 using a receiver spacing of 2 m and different source offsets: (a) Phase velocity versus frequency, (b) Phase velocity versus wavelength.

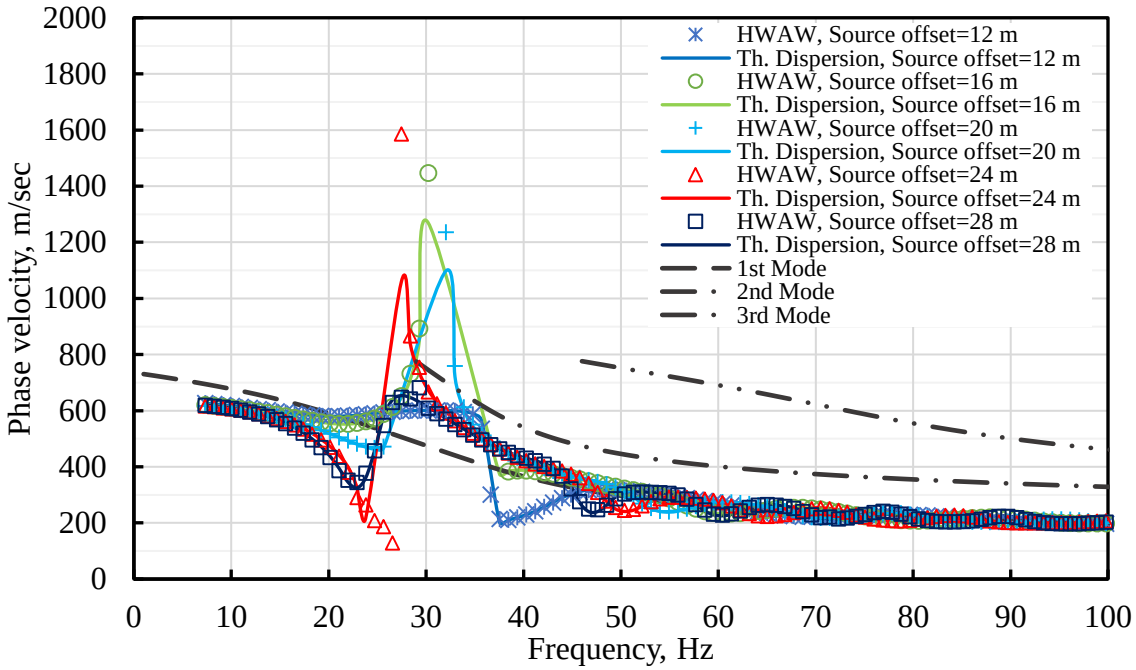

(a)

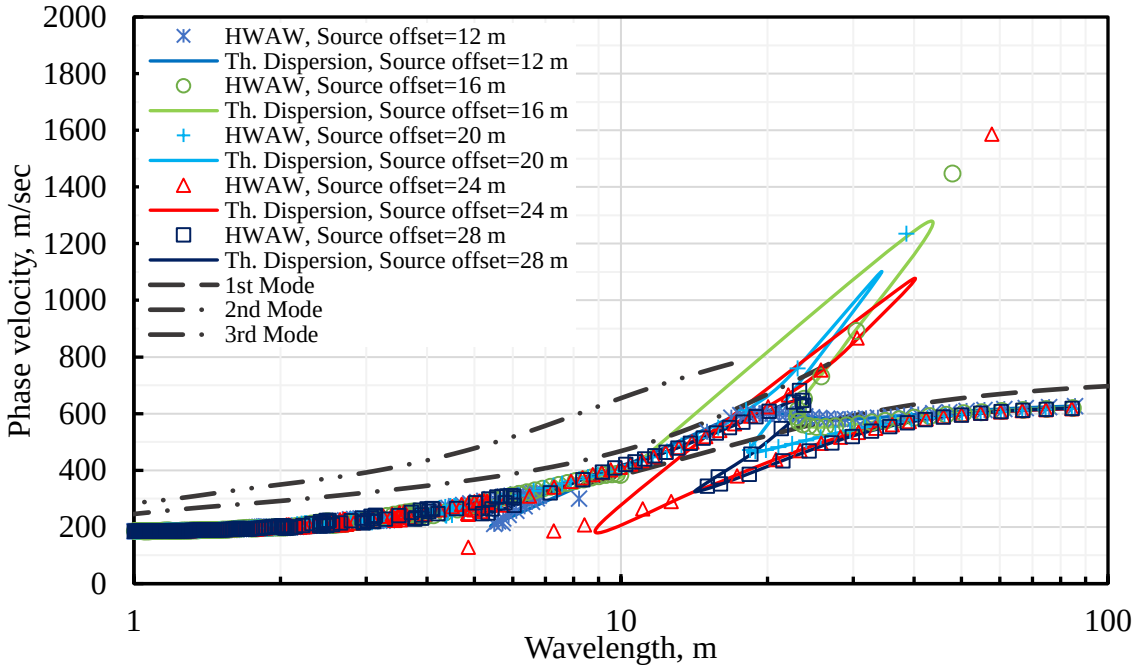

(b)

Figure 4.51 HWAW dispersion curves developed from Profile 6 using a receiver spacing of 4 m and different source offsets: (a) Phase velocity versus frequency (b) Phase velocity versus wavelength.

4.4.3.3 Discussions of Shallow Gradient Profile

The shallow gradient profile proved to be very challenging for the HWAW method. The theoretical dispersion curves for this site are highly erratic with a large and abrupt fluctuation in the frequency range of about 22 to 38 Hz. The theoretical and HWAW dispersion curves do not agree well in most cases over the frequency range where the abrupt transition from the fundamental mode occurs. The error in this range is as high as 26%. Also, the theoretical dispersion curves and the agreement between dispersion curves change with the location of the source and receivers. Generally, as the source offset increases the match between the theoretical and HWAW dispersion curves improves, with the large 28 m offset providing the best result (maximum error of 10%). The smallest source offsets provided the worst results. This behavior was observed for both receiver spacings of 2 m and 4 m. The poor performance of the HWAW is likely associated with the large change in phase velocity with frequency and use of a bandwidth that was not narrow enough to capture the rapid change in velocity. This is investigated in greater depth in Section 4.4.5.4.

4.4.3.4 Results of Deeper Gradient Profile

Profile 7 is presented in Figure 4.49(b) and Table 3.2. Figures 4.52 and 4.53 show the results of the simulated HWAW experimental and theoretical dispersion curves for Profile 7 in terms of frequency and wavelength for receiver spacings of 2 m and 4 m with a range of source offsets.

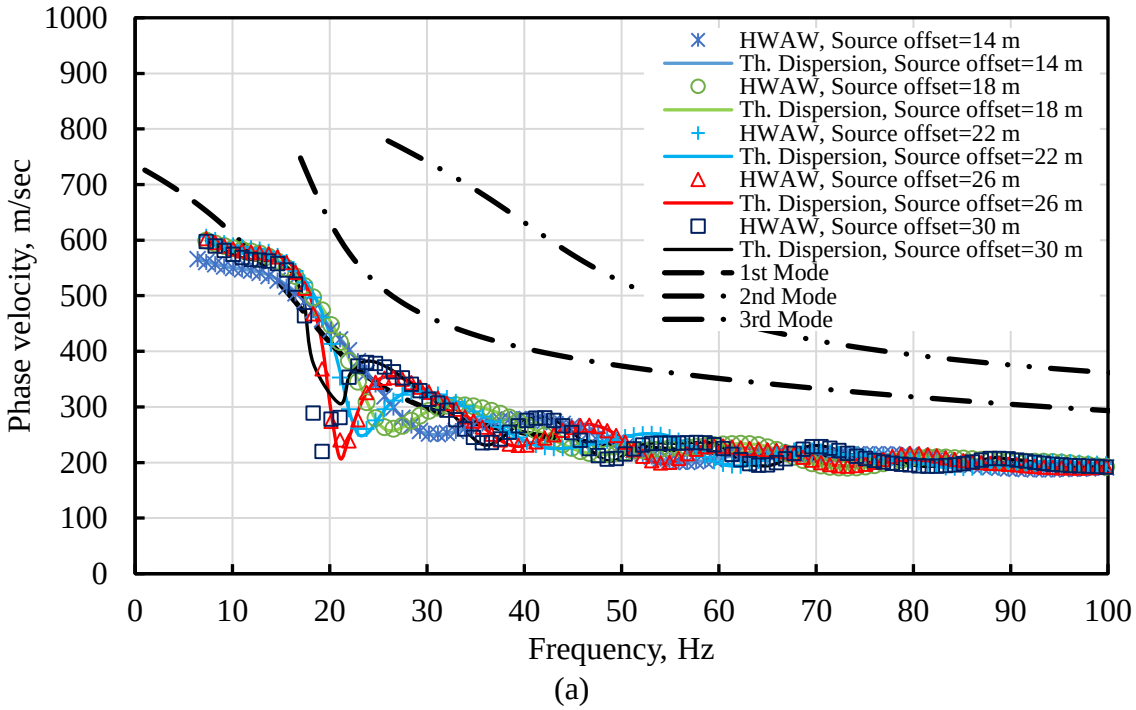

(a)

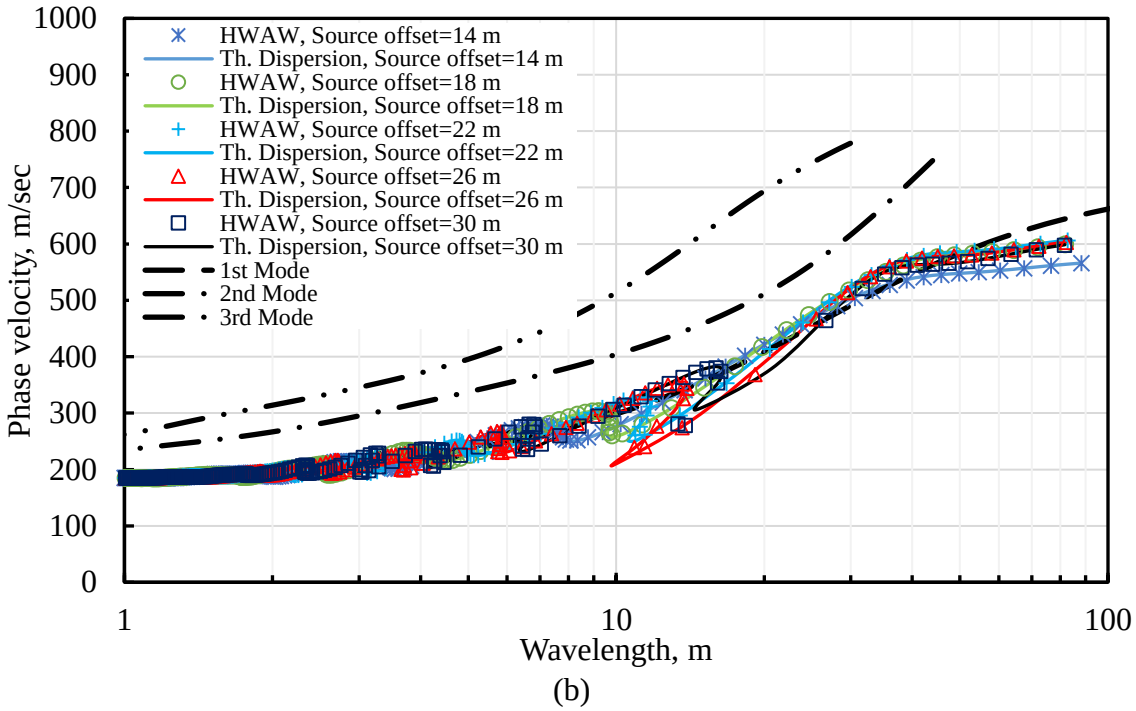

(b)

Figure 4.52 HWAW dispersion curves developed from Profile 7 using a receiver spacing of 2 m and different source offsets: (a) Phase velocity versus frequency, (b) Phase velocity versus wavelength.

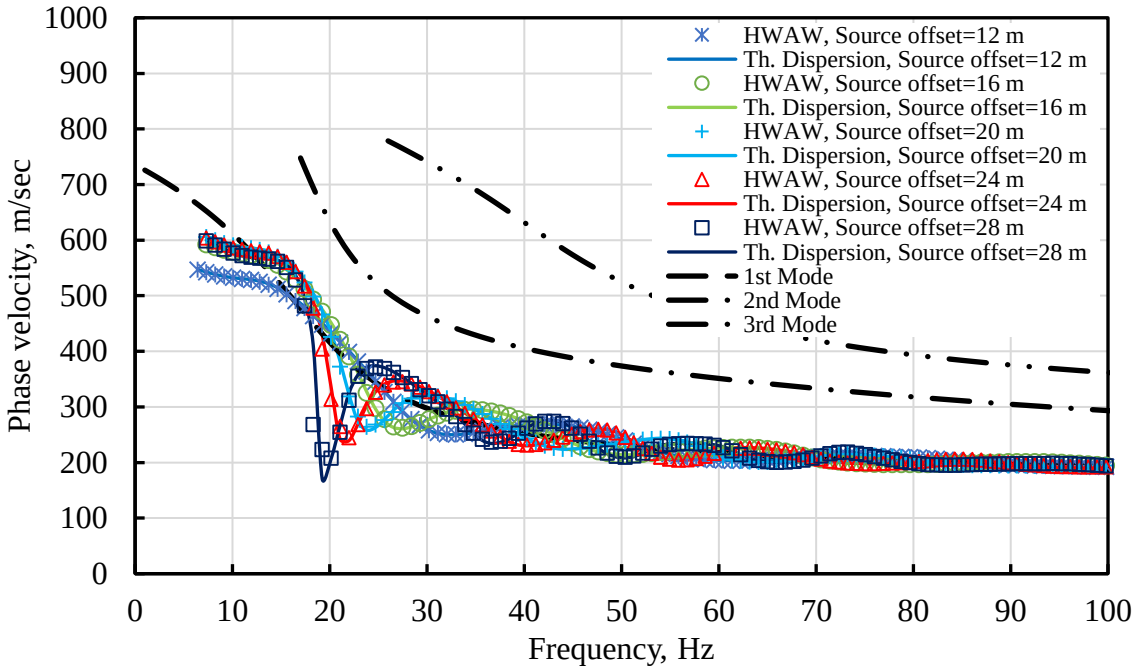

(a)

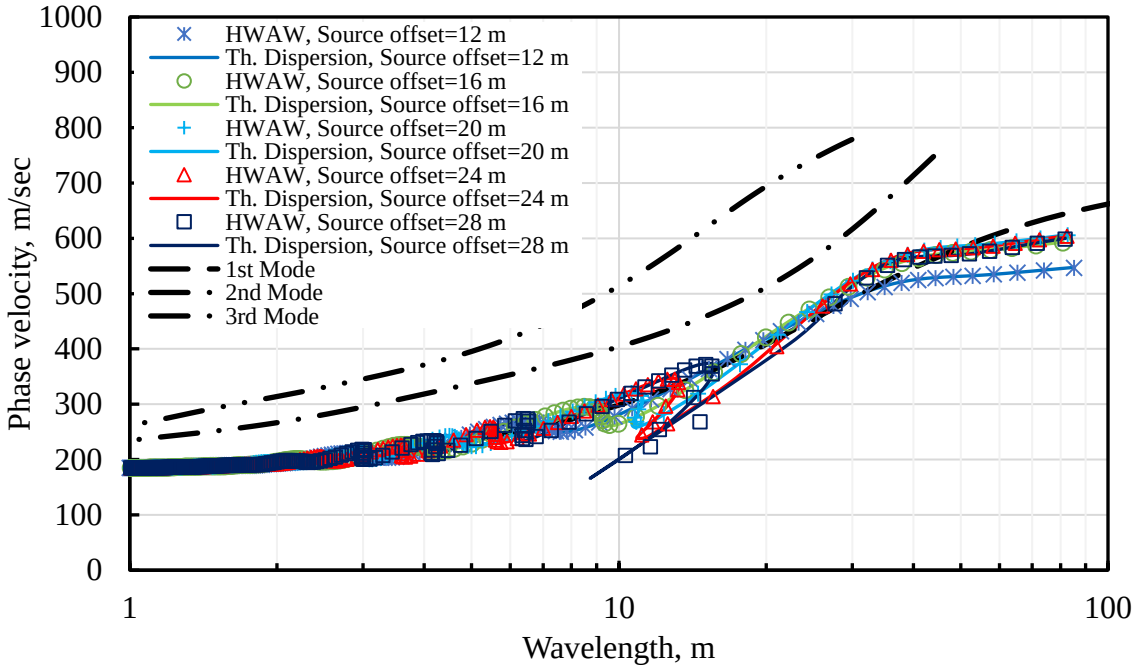

(b)

Figure 4.53 HWAW dispersion curves developed from Profile 7 using a receiver spacing of 4 m and different source offsets: (a) Phase velocity versus frequency, (b) Phase velocity versus wavelength.

4.4.3.5 Discussions of Deep Gradient Profile

For the deeper linear gradient case, the dispersion curve again shows a region of abrupt change in velocity over a narrow frequency range. However, in this case the frequency range is much smaller (18 to 25 Hz) and the agreement between dispersion curves is much better than the shallow velocity gradient case. With the exception of the 30 m source offset and 2 m receiver spacing, the agreement between the dispersion curves are very consistent with only a few points having errors as high as 9%. This performance may be improved with use of a narrower bandwidth.

4.4.4 HWAW at Sites with Velocity Inversion due to Embedded Soft Layer

4.4.4.1 Introduction

Shear wave velocity profiles with a soft layer sandwiched between two stiffer layers are often encountered in geotechnical engineering, for example where a desiccated crust exists over softer soil. The complex soil profiles modeled in this section have thin and thick embedded lower velocity layers, as shown in Figure 4.54 for Profiles 8 and 9, respectively.

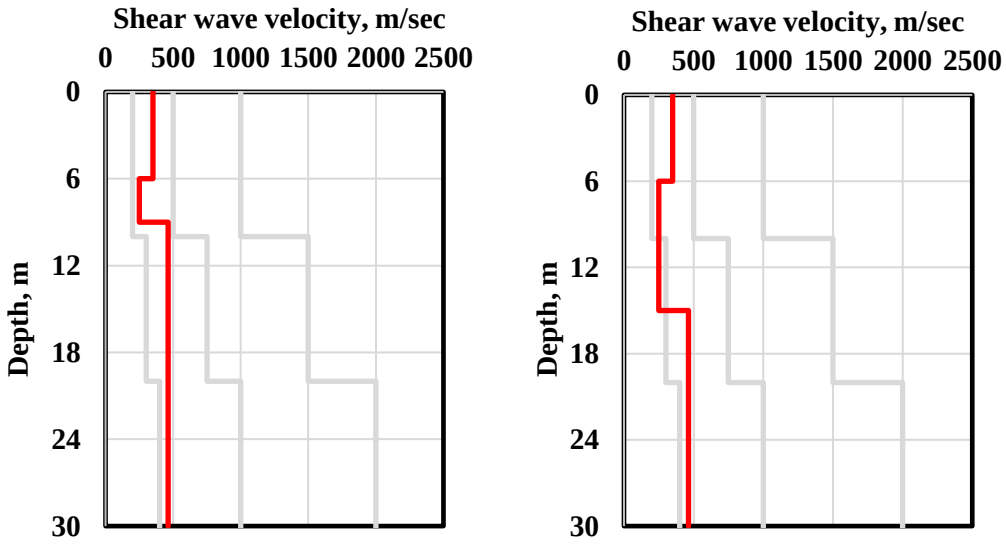

Figure 4.54 Complex soil profiles used for simulations (a) Profile 8 (velocity inversion, low-velocity thin layer) (b) Profile 9 (velocity inversion, low-velocity thick layer).

The results of the effectiveness of the HWAW method to recover the phase velocity dispersion curve for these profiles are presented and discussed below.

4.4.4.2 Results of Thin and Thick Embedded Lower Velocity Layer Profile

Profiles 8 and 9 are presented in Figure 4.54 and in tabular form in Table 3.3. The results of the simulated HWAW experimental and theoretical dispersion curves for Profiles 8 and 9 are presented in Figures 4.55 to 4.58 and plotted in terms of frequency and wavelength for receiver spacings of 2 m and 4 m with different source offsets.

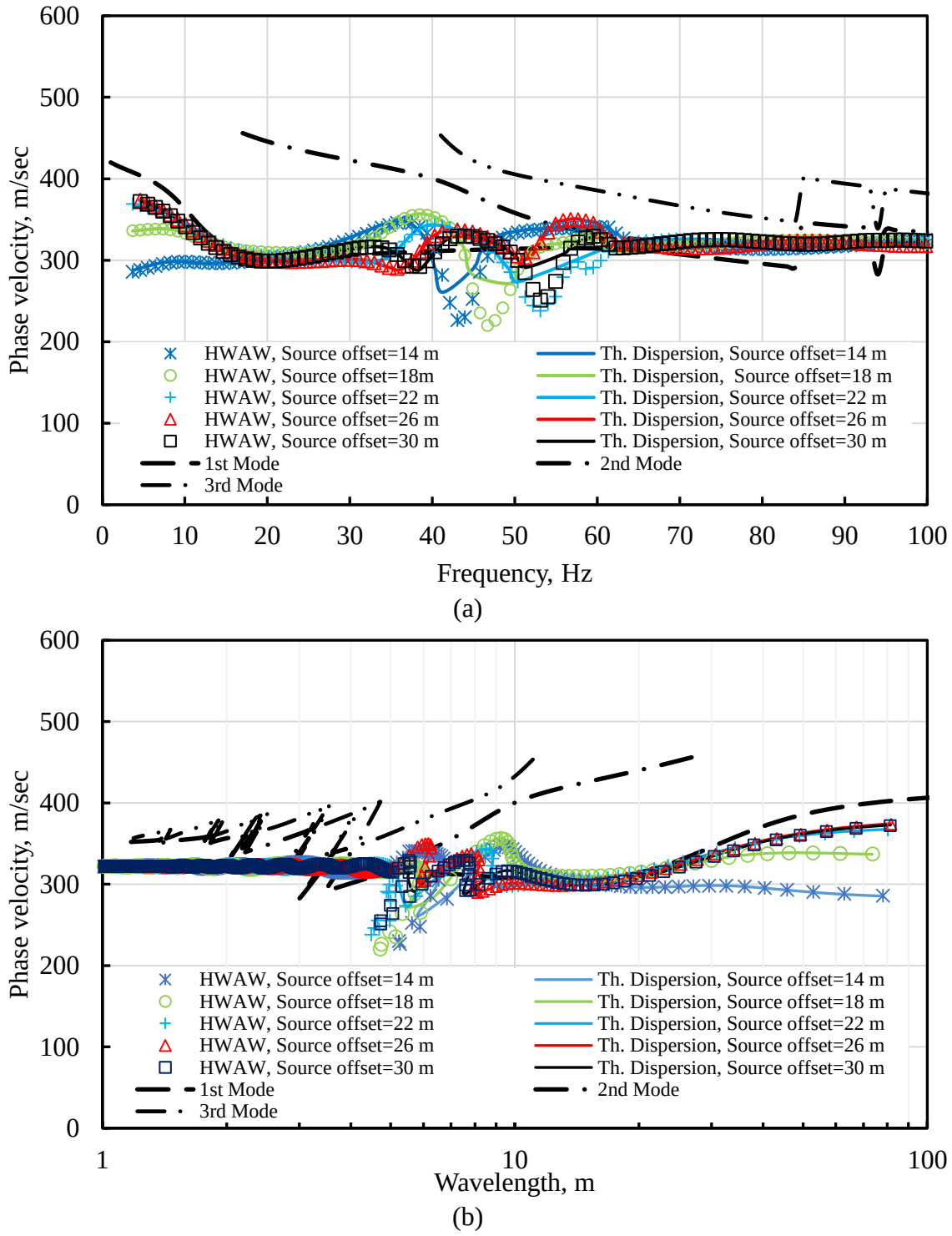

Figure 4.55 HWAW dispersion curves developed from Profile 8 using a receiver spacing of 2 m and different source offsets: (a) Phase velocity versus frequency, (b) Phase velocity versus wavelength.

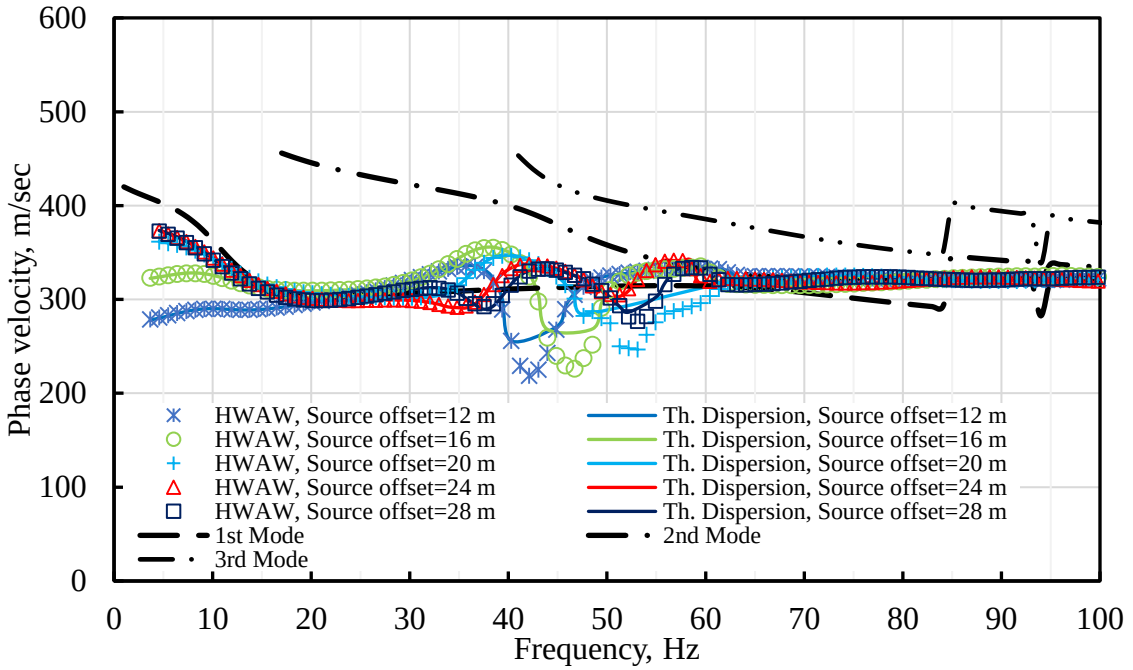

(a)

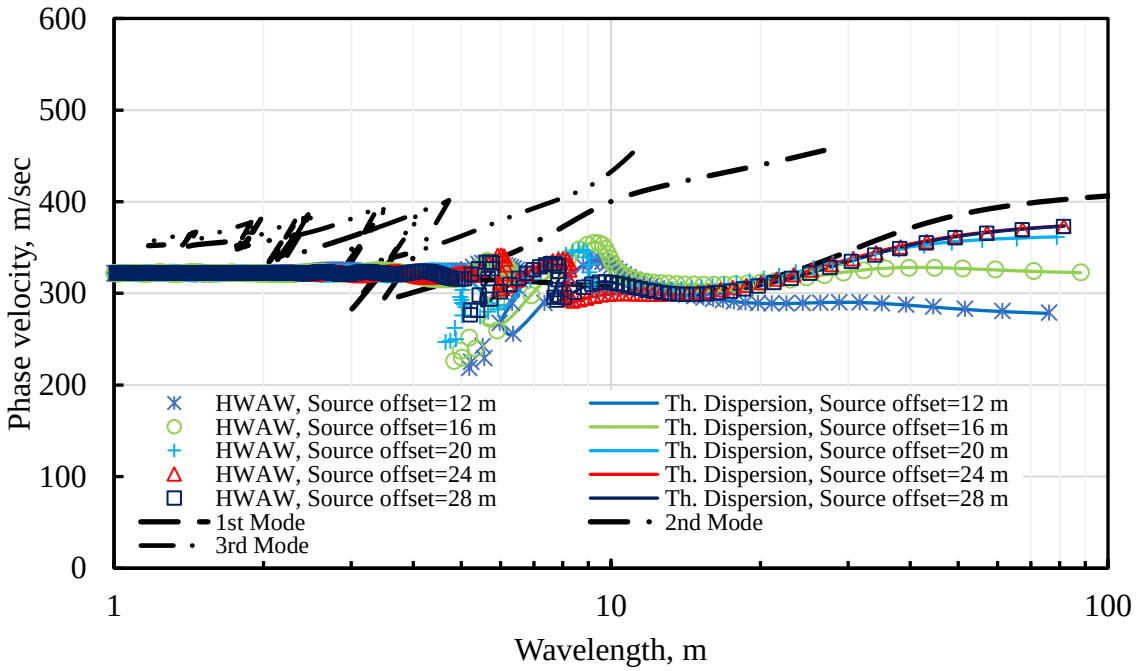

(b)

Figure 4.56 HWAW dispersion curves developed from Profile 8 using a receiver spacing of 4 m and different source offsets: (a) Phase velocity versus frequency, (b) Phase velocity versus wavelength.

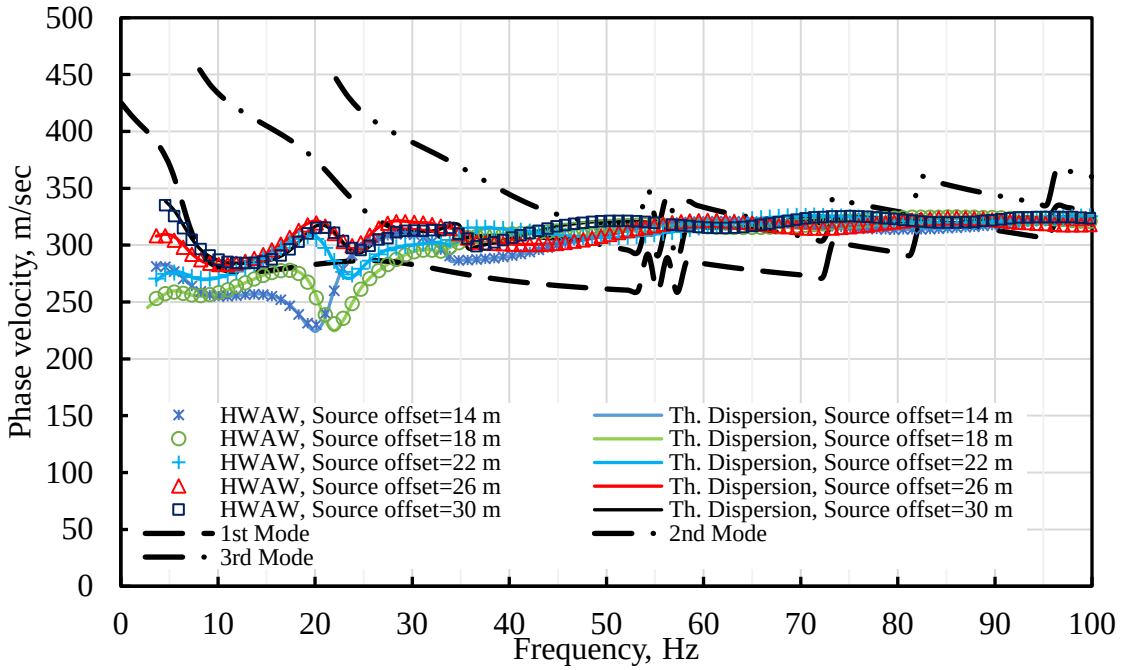

(a)

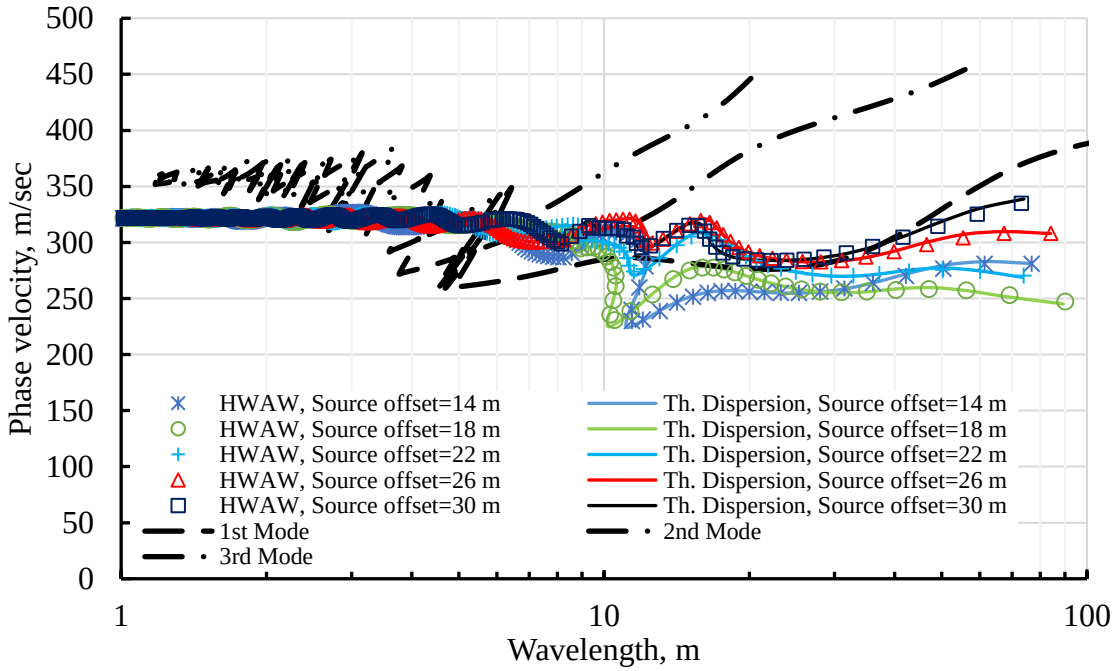

(b)

Figure 4.57 HWAW dispersion curves developed from Profile 9 using a receiver spacing of 2 m and different source offsets: (a) Phase velocity versus frequency, (b) Phase velocity versus wavelength.

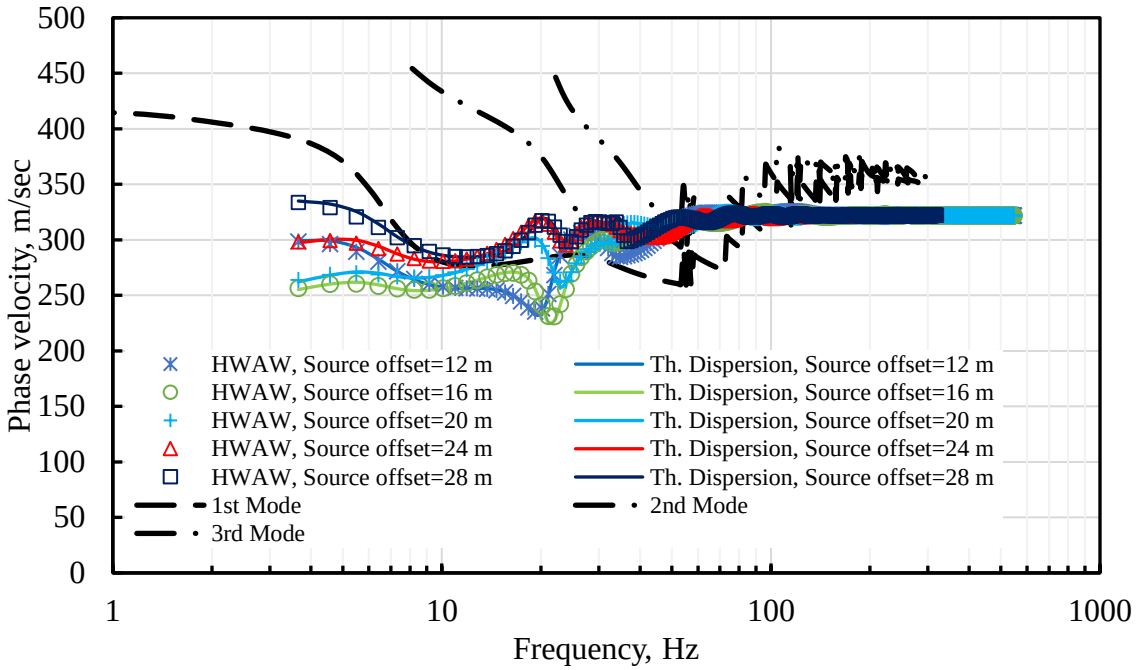

(a)

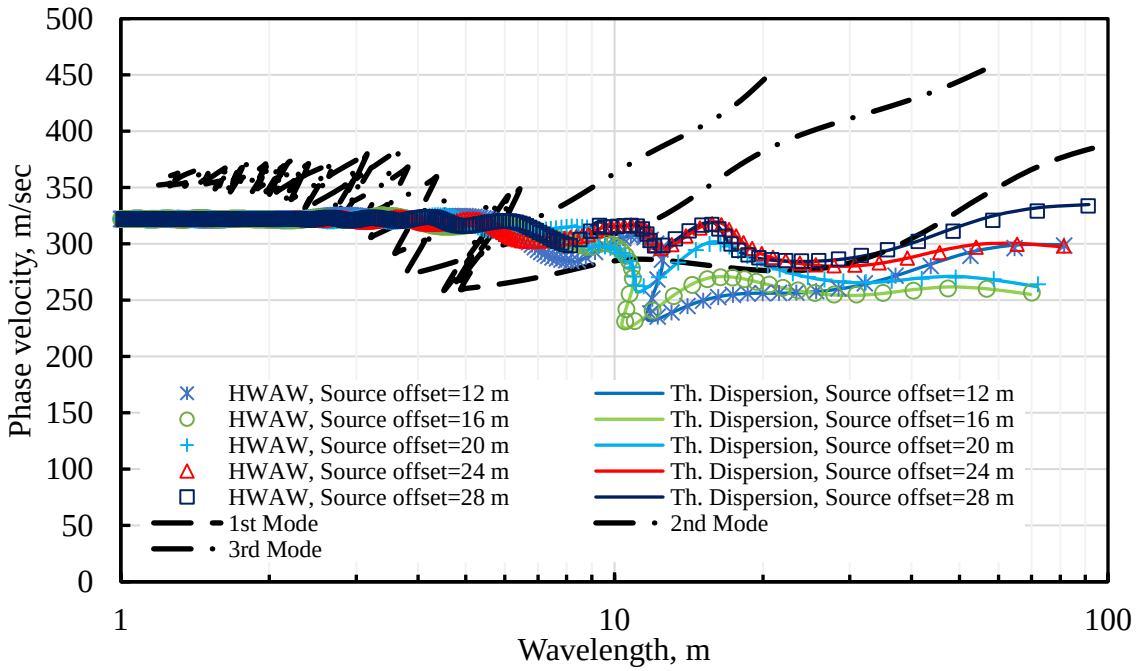

(b)

Figure 4.58 HWAW dispersion curves developed from Profile 9 using a receiver spacing of 4 m and different source offsets: (a) Phase velocity versus frequency, (b) Phase velocity versus wavelength.

4.4.4.3 Discussions of Thin and Thick Embedded Lower Velocity Layer Profile

For Profile 8, the HWAW and theoretical dispersion curves do not match over a segment of the measured frequency range between 40 Hz and 60 Hz with an error of 20% or less, as shown in Figures 4.55 and 4.56. This disagreement becomes less pronounced as the source offset increases.

However, the HWAW and theoretical dispersion curves showed good agreement for the frequency range below 40 Hz and above 60 Hz with an error of 4% or less. The mismatch in the dispersion curves occurs over the portion of the dispersion curve where the phase velocity abruptly deviates from the fundamental mode.

Several of the larger errors were observed in frequency ranges where no corresponding theoretical V_{ph} values were calculated and an interpolation was made to estimate V_{ph} in the theoretical dispersion. This may be due to an issue with the FitSASW program.

On the other hand, for Profile 9, with the thicker soft layer, although the phase velocity dispersion curves again do not follow a single mode, Figures 4.57 and 4.58 show good agreement between the HWAW and theoretical dispersion curves with an error of 3% or less for all receiver spacings and source offsets.

Based on these simulations, the main observation is that short source offsets do not perform well for Profile 8 but all offsets worked well when the soft layer was thicker.

4.4.5 Results of Thin and Thick Embedded High Velocity Layer Profile

4.4.5.1 Introduction

Shear wave velocity profiles with a stiff layer between two softer layers may be encountered in geotechnical practice. For example, when a cemented layer is encountered.

The complex soil profiles modeled in this section include thin and thick embedded higher velocity layers, as shown in Figure 4.60a and b for Profiles 10 and 11 respectively.

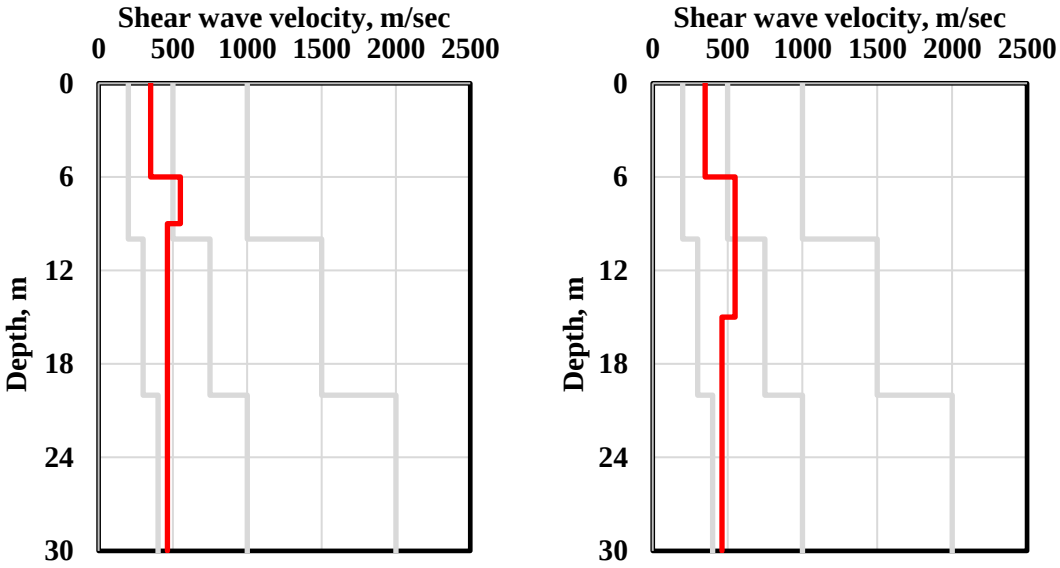

Figure 4.59 Complex soil profiles with embedded stiff layer (a) Profile 10 (thin layer) (b) Profile 11 (thick layer).

The effectiveness of the HWAW method at recovering the theoretical dispersion curves for these profiles are presented and discussed below.

4.4.5.2 Results of Thin and Thick Embedded Higher Velocity Layers Profiles

Profiles 10 and 11 are presented in Figure 4.59 and in tabular form in Table 3.4. The results of the simulated HWAW measurements and theoretical dispersion curves for Profiles 10 and 11 are shown in terms of frequency and wavelength in Figures 4.60 and 4.63. Receiver spacings of 2 m and 4 m were modeled with various source offsets.

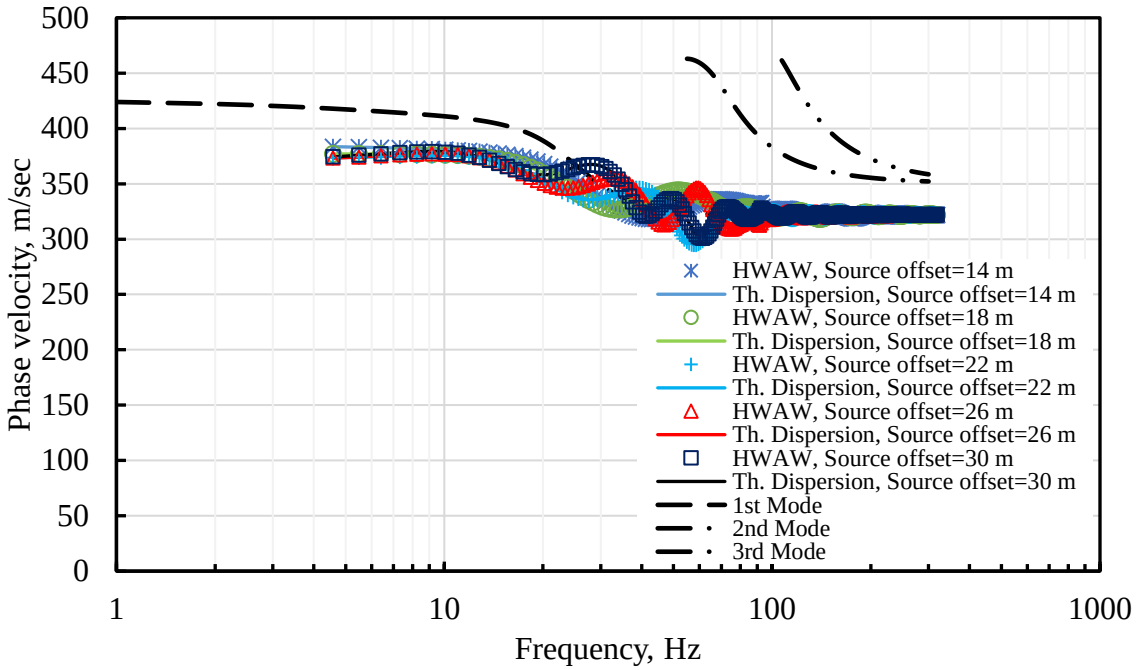

(a)

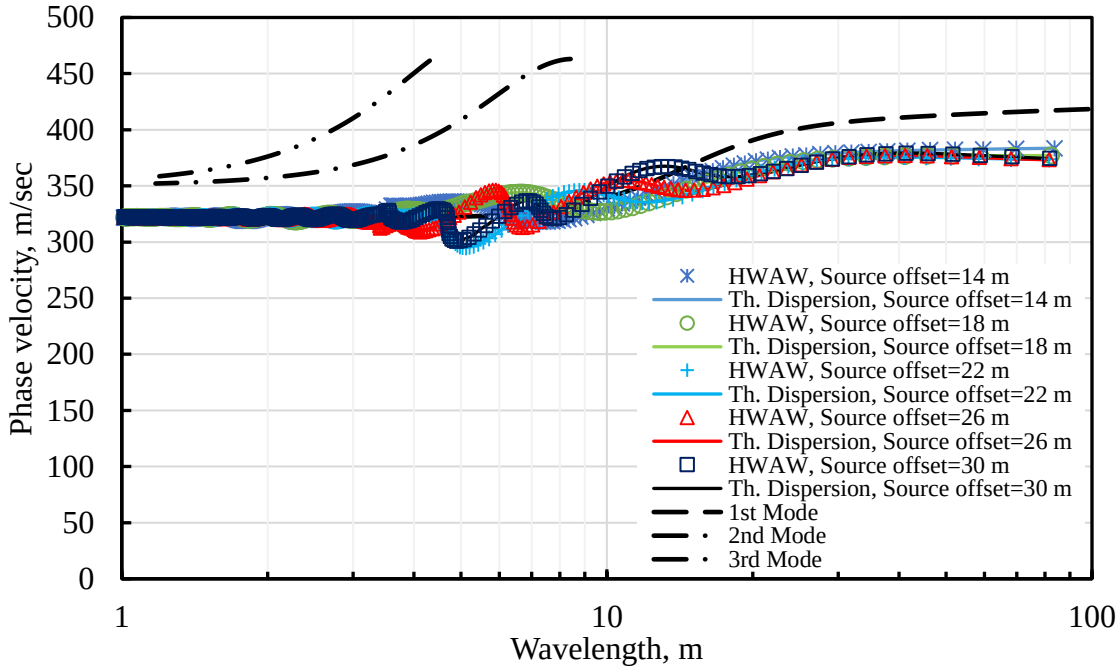

(b)

Figure 4.60 HWAW dispersion curves developed from Profile 10 using a receiver spacing of 2 m and different source offsets: (a) Phase velocity versus frequency, (b) Phase velocity versus wavelength.

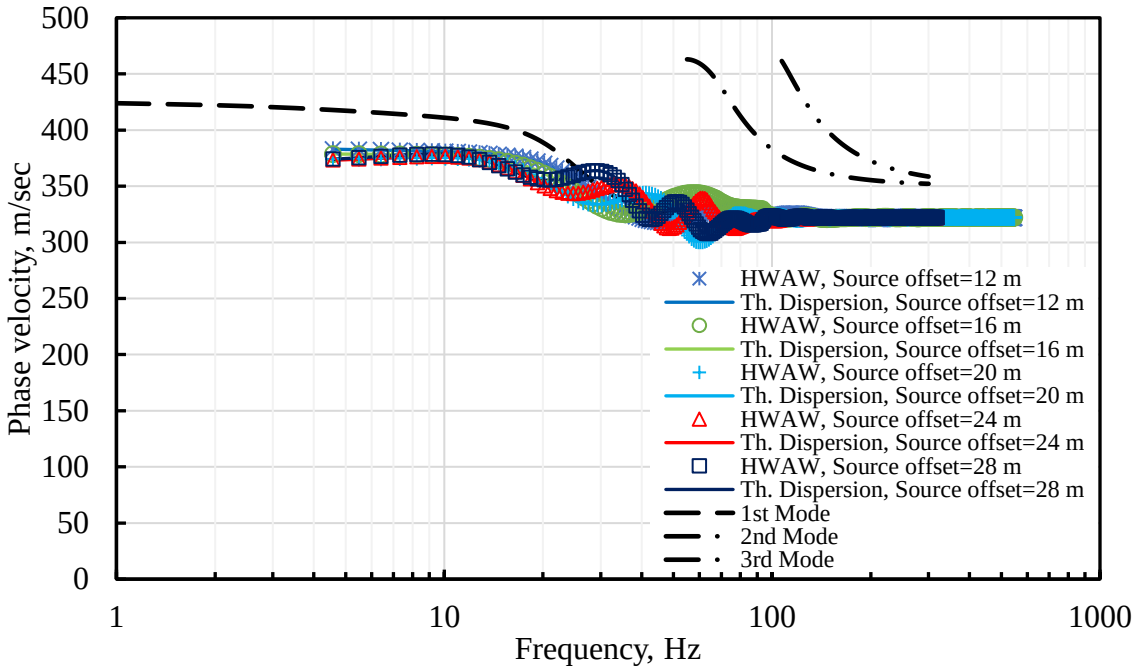

(a)

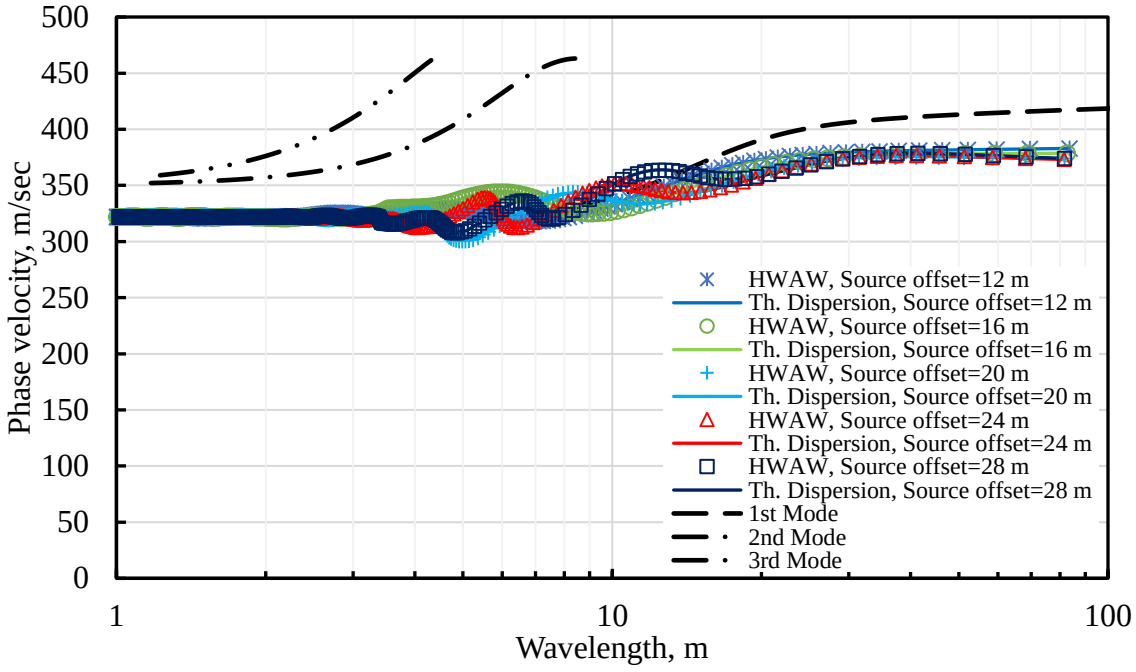

(b)

Figure 4.61 HWAW dispersion curves developed from Profile 10 using a receiver spacing of 4 m and different source offsets: (a) Phase velocity versus frequency, (b) Phase velocity versus wavelength.

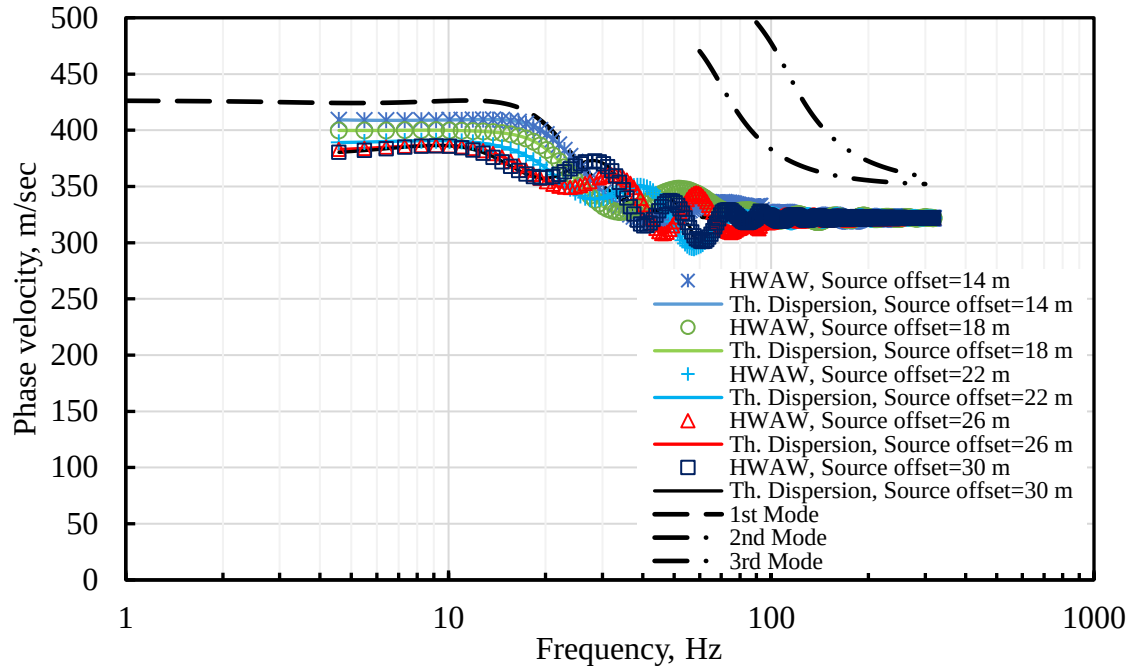

(a)

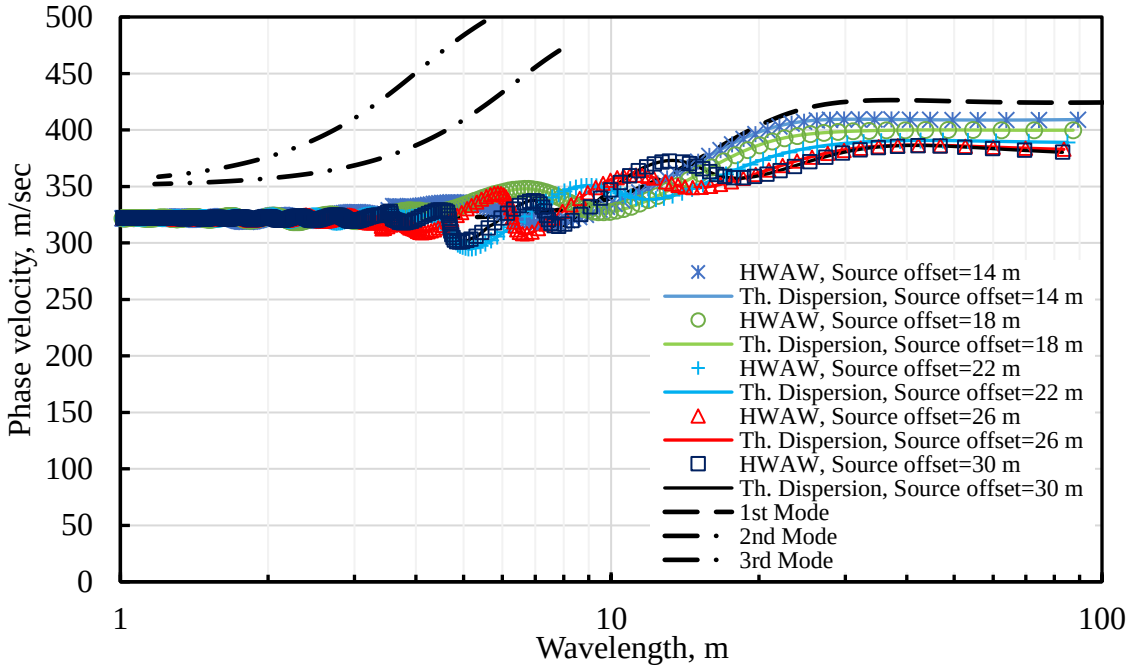

(b)

Figure 4.62 HWAW dispersion curves developed from Profile 11 using a receiver spacing of 2 m and different source offsets: (a) Phase velocity versus frequency, (b) Phase velocity versus wavelength.

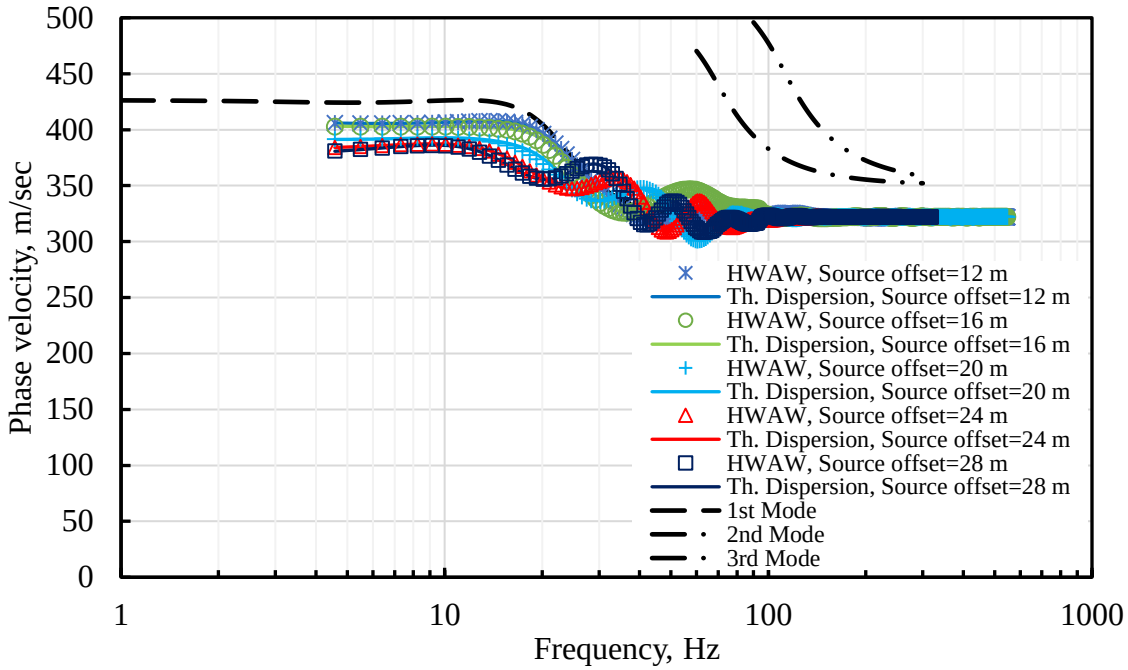

(a)

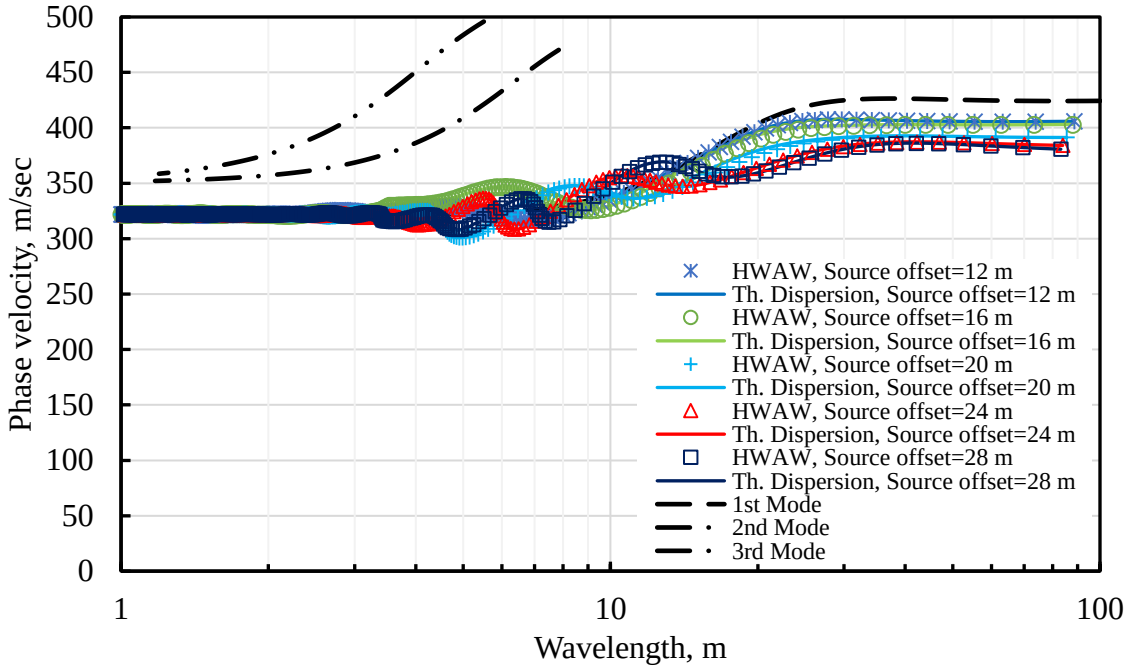

(b)

Figure 4.63 HWAW dispersion curves developed from Profile 11 using a receiver spacing of 4 m and different source offsets: (a) Phase velocity versus frequency, (b) Phase velocity versus wavelength.

4.4.5.3 Discussions of Thin and Thick Embedded Higher Velocity Layers Profiles

Based on the results of Profiles 10 and 11, it is observed that the HWAW approach works well for the case of an embedded stiff layer. The theoretical and HWAW dispersion curves are in very good agreement for both Profiles 10 and 11 with the absolute maximum error between the theoretical and HWAW dispersion curves below 1% for all cases.

Unlike the embedded soft layer case, changes in the thickness of the embedded stiff layer from 3 m to 9 m had no effect on the agreement between the experimental and theoretical dispersion curves.

4.4.5.4 Discussions of HWAW Dispersion Recovery at Complex Profiles

The main observation from the analysis of HWAW method at complex profiles is that the HWAW method was able to recover the correct trends in the dispersion curve for the simulated complex profiles when using the sampling frequency and bandwidth values developed from the study of simple profiles. However, for some of the complex profiles the disagreement between the HWAW derived dispersion curve and the theoretical dispersion curves were large for select points or regions of the dispersion curve. It was also observed, that in general very short offset distances (12 m, 15 m) performed worse than the longer offset distances. The receiver spacing of 2 m versus 4 m appeared to have little impact on the quality of agreement between the dispersion curves.

To quantify the compatibility between the HWAW and the theoretical dispersion curves for all complex profiles, as was done for simple profiles, a receiver offset of 20 m and source spacing of 4 m were chosen for presentation. The percentage error is plotted versus the ratio of bandwidth (1.83 Hz in this case) to the frequency for all investigated

simple and complex profiles analyzed in this study. As a reminder, when only the simple profiles were considered a ratio of bandwidth-to-frequency of 0.25 was found to be an acceptable ratio limit with an ADE percentage of 1 or less, as shown in Figure 4.20. The question investigated here is whether than limit holds true for complex sites.

The absolute difference error percentage plotted versus the ratio of bandwidth-to-frequency (b_w/f_r) for all simple and complex profiles are presented in Figures 4.64 and 4.65 for wavelength limits of 60 m and 90 m, respectively. In all cases the sampling frequency is 1875 Hz, the bandwidth is 1.83 Hz and the number of frequency points is 1024.

From Figures 4.64 and 4.65 it can be observed that for some of the complex profiles, select points showed very large errors (up to 18%), even in the b_w/freq. range less than 0.25. Comparing Figures 4.64 and 4.65, there is little difference between the 60 m and 90 m wavelengths ranges. In both cases, the worst performing sites were soft-over-stiff sites (Profiles 4, 5A, 5B and 5C) and the shallow gradient site (Profile 6). All other profiles showed maximum errors of 3% or less. Errors of a few percent in the experimental dispersion curve can be tolerated and are within the range of uncertainties due to other factors, such as lateral variability. However, errors as high as 18% are unacceptable. The cases with large errors are those where an abrupt change in the phase velocity occurs. It was hypothesized the analysis of these sites using a narrower bandwidth would reduce the errors.

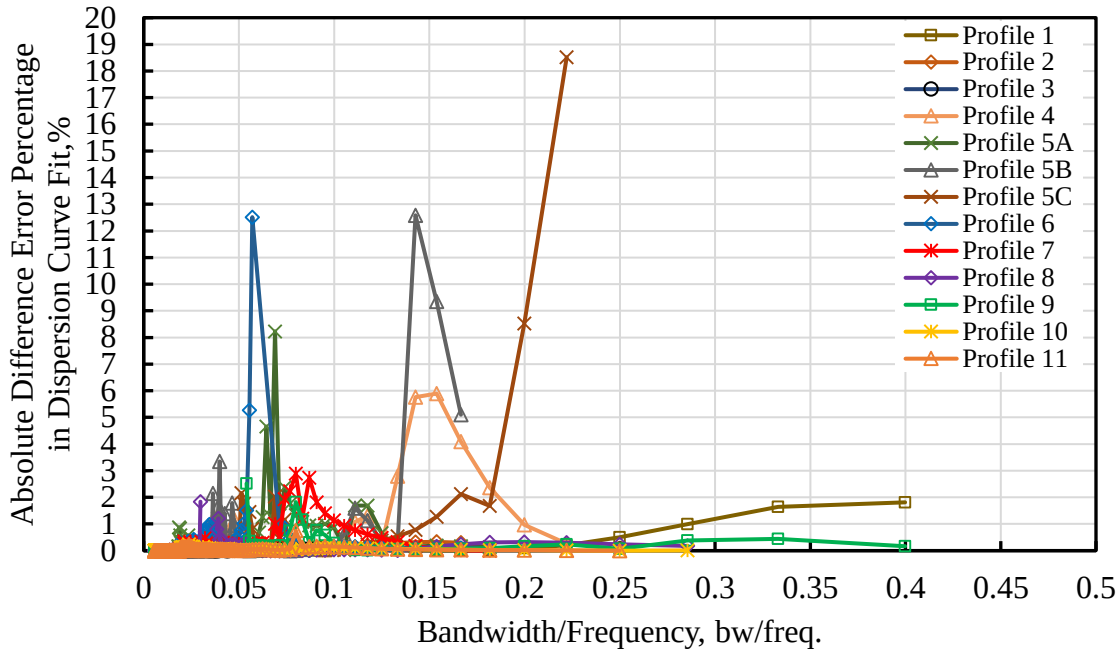

Figure 4.64 Absolute difference error percentage between theoretical and experimental dispersion curves for Profiles 1 through 11, versus ratio of bandwidth (1.83 Hz) to frequency. Data was analyzed over a frequency range corresponding to a maximum wavelength of three times the profiling depth (λ=60 m) for S-R1=20m and R1-R2=4m.

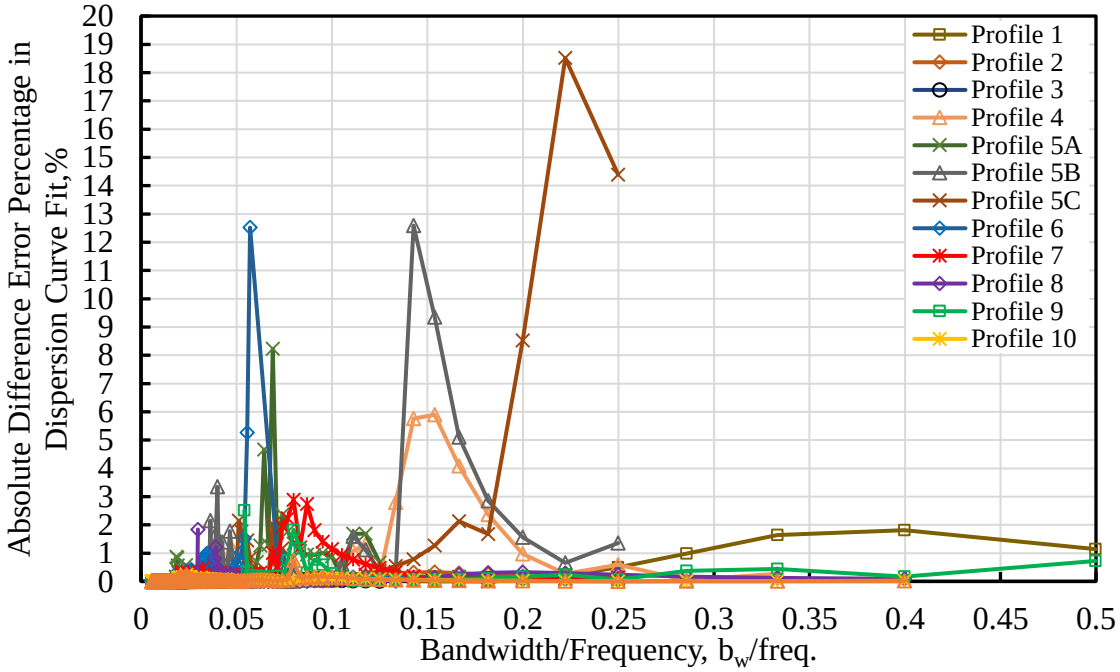

Figure 4.65 Absolute difference error percentage between theoretical and experimental dispersion curves for Profiles 1 through 11, versus ratio of bandwidth (1.83 Hz) to frequency. Data was analyzed over a frequency range corresponding to a maximum wavelength of three times the profiling depth (λ=90 m) for S-R1=20m and R1-R2=4m.

Profiles 4, 5A, 5B and 5C were reprocessed with a narrower bandwidth. A bandwidth of 0.915 Hz was used, which was half of the previous value of 1.83 Hz and used the same sampling frequency with more points. A plot of the error versus the ratio of bandwidth to frequency for Profiles 4, 5A, 5B, 5C, 6, and 7, combined with the rest of the profiles is shown in Figure 4.66.

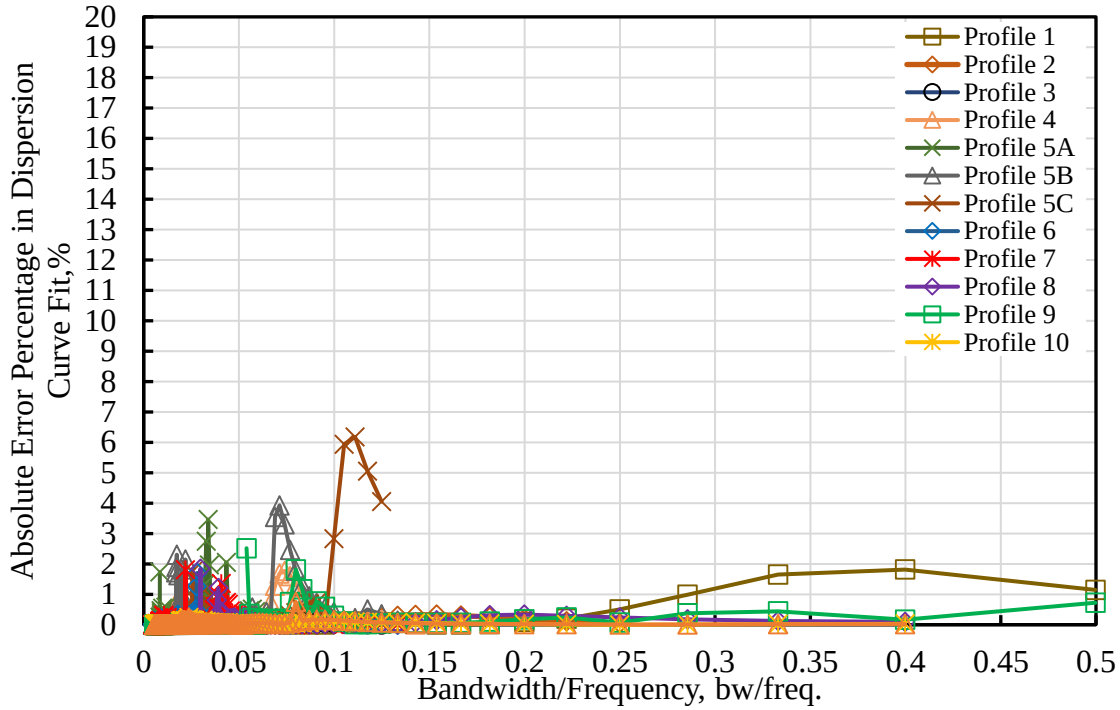

Figure 4.66 Absolute maximum error percentage between theoretical and experimental dispersion curves for Profiles 1 through 11, versus ratio of bandwidth to frequency after reducing the bandwidth for Profiles 4, 5A, 5B, 5C, 6, and 7. Data was analyzed over a frequency range corresponding to a maximum wavelength of 3 times the profiling depth (λ=90 m).

By comparing Figure 4.66 with Figure 4.65, an improvement was obtained and the percentage error was dropped from 18% to 6% for Profile 5C, while the others showed an error of 4% or less. All points with a bandwidth of one tenth or less of the frequency showed an acceptable error of 4% or less. These results demonstrate that a more stringent

bandwidth criteria is needed for complex site conditions. Based on these results, a minimum bandwidth value of 10% of the lowest frequency is recommended.

4.5 SASW Data Processed with the HWAW Method

4.5.1 Introduction

Due to the variety of near-surface soil and rock properties, surface wave methods are applied to diverse subsurface conditions, some of which can present problems in the interpretation of surface wave measurements. For some site conditions manual phase unwrapping procedures used in the SASW method can be problematic (Rosenblad and Bertel, 2008). The study of the effect of receiver spacing on HWAW processing for simple sites (Section 4.3.2) showed that HWAW processing worked well for cases where the source offset and receiver spacing are equal, as is the case with SASW data collection. This suggests that HWAW processing may be used to automate the generation of dispersion curves from data collected using the SASW methodology.

The objective of this portion of the research is to investigate the effectiveness of HWAW processing for generating an accurate dispersion curves at complex sites using data collected using the SASW methodology (i.e. multiple set ups with equal source offset and receiver spacing). If shown to be successful, this approach would eliminate the need for the time consuming and sometimes erroneous manual phase unwrapping procedure used in SASW measurements. Particular focus is placed on soft-over-stiff sites which are known to be especially problematic. Simulations of SASW measurements are presented for the seven complex profiles described in Chapter 3. Data is interpreted using the conventional phase unwrapping procedures and the automated HWAW method. The accuracy of the dispersion curves in both cases are compared and discussed.

4.5.2 Dispersion Curve Calculation from SASW Phase Unwrapping

SASW measurements were simulated for each of the seven profiles (Profiles 4-11 as described in Chapter 3). The receiver pair locations relative to the source selected for the simulation were 2 – 4m ,4– 8m, 8– 16m, 15– 30m, 30– 60m, 45– 90m, and 60– 120m. The maximum wavelength used in the traditional SASW approach is twice the source-to-near receiver spacing, and the V_S profile depth is typically reported to 0.3 to 0.5 times the maximum wavelength (Brown et al. 2002; Stokoe et al. 1994). With this testing arrangement, surface wave velocities can typically be determined from wavelengths of approximately 0.5 m to 120 m. The V_S profiles in this study are presented to a depth of 30 m, a common profiling depth of interest in geotechnical applications. Although the wavelength range is longer than necessary to profile to 30 m, it is included to illustrate issues related to SASW phase unwrapping.

Simulated time records were calculated at each of the receiver locations using the program FITSASW developed at the University of Texas at Austin as described in Chapter 3. The time records were transformed to the frequency domain and the transfer function was calculated to create the wrapped phase plots for each receiver pair. The phase plots were unwrapped manually in the program WinSASW to develop the experimental dispersion curves. Interpretation of the wrapped phase plots involved masking (i.e. omitting) portions of the phase data (shown as shaded regions in the phase plots presented below) to avoid near-field effects (typically first 180 degrees are removed for SASW data) and to exclude high-frequency data that are often not usable in real world conditions due to noise contamination. The unwrapping procedure requires interpreting the correct

number of phase “jumps”. This is easily done for simple sites, but is more difficult for some complex sites, as shown below.

4.5.3 Dispersion Curve Calculation from HWAW Processing

The same simulated time records from SASW method were also processed using the HWAW method as described in Chapter 3.

The results of the dispersion curves obtained by the HWAW method were plotted in terms of frequency and wavelength and compared with the theoretical dispersion curves calculated for each receiver pair location. Modal Rayleigh wave dispersion curves for these profiles are also shown in these results. The modal dispersion curves are independent of receiver location.

4.5.4 Soft over Stiff Sites (Profiles 4 and 5)

4.5.4.1 Results and Discussions of High-Contrast Profile (Profile 4)

Comparisons between the SASW-derived dispersion curves using phase unwrapping and the theoretical dispersion curves for Profile 4 are plotted versus frequency in Figure 4.67. Comparisons between the HWAW-processed dispersion curves and the theoretical dispersion curves for Profile 4 are plotted versus frequency in Figure 4.68. The wrapped phase plots developed for Profile 4 are presented in Figure 4.69. The number of interpreted phase jumps in the unwrapping is shown above each jump in Figure 4.69.

From the results of phase-unwrapped SASW dispersion curves (Figure 4.67), it is observed that the transition to a higher mode over a portion of the frequency range measured was not recovered accurately for the receiver spacings of 45 m and 60 m. An erroneous dispersion curve was obtained that showed low velocities where the mode transition occurred. However, the mode transition was accurately detected for the receiver

spacing of 30 m. This problem is due to an incorrect interpretation of the phase diagrams for the 45m and 60 m spacing. This issue is discussed in greater detail for Profile 5B, shown below.

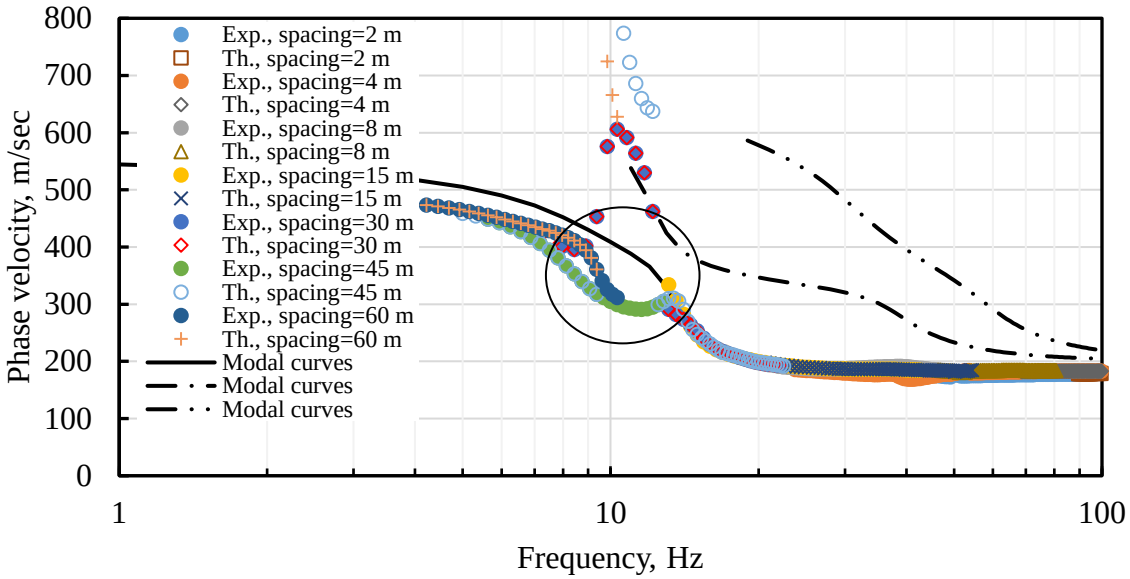

Figure 4.67 Comparison of SASW-derived experimental dispersion curve from phase unwrapping with theoretical and modal dispersion curves for Profile 4. Black circle indicates region of incorrect dispersion curve interpretation.

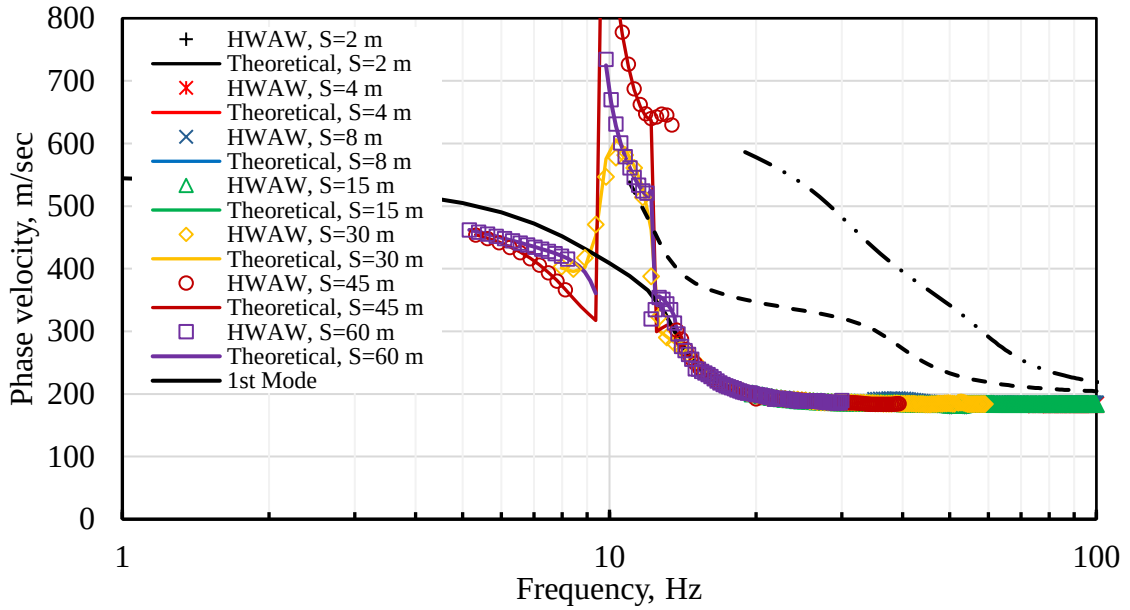

Figure 4.68 Comparison of HWAW-derived experimental dispersion curve with theoretical and modal dispersion curves for Profile 4.

On the other hand, the dispersion curve processed by the HWAW method accurately recovered the dispersion curve for all receiver pairs, as shown in Figure 4.68. For both the 45m and 60 m receiver pairs, the abrupt mode transition was accurately captured.

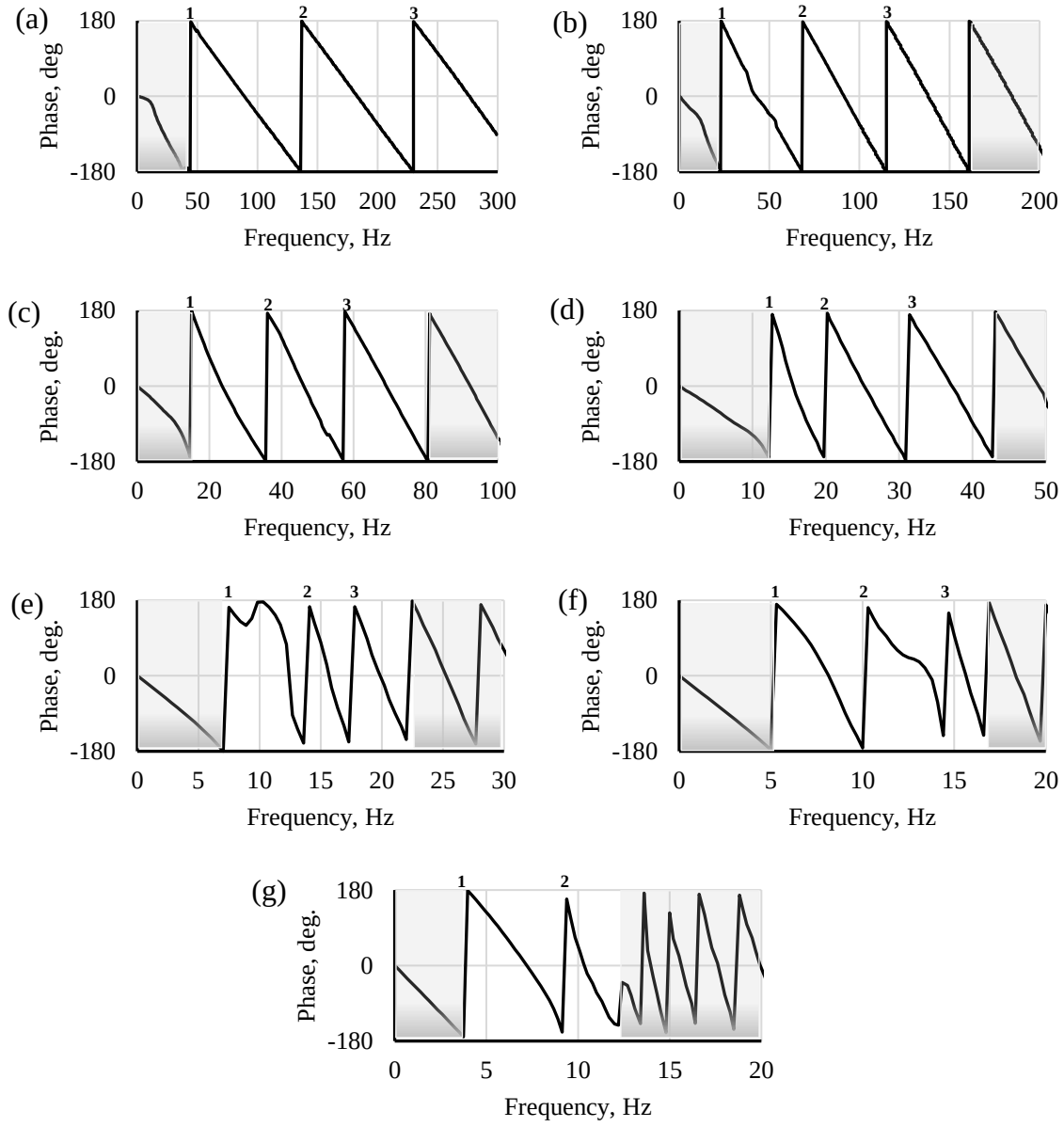

Figure 4.69 Wrapped phase plots from SASW measurements at Profile 4 with receiver spacings of (a) 2m, (b) 4m, (c) 8m, (d) 15m, (e) 30m, (f) 45m, and (g) 60m. Phase unwrapping interpretation is indicated by number of 360° "jumps." Data not used in interpretation are indicated by shaded regions.

4.5.4.2 Results and Discussions of Very High-Contrast Profiles (Profile 5)

Comparisons between the SASW derived dispersion curves using phase unwrapping and the theoretical dispersion curves for Profile 5A are plotted versus frequency in Figure 4.70. Comparisons between the HWAW-processed dispersion curves and the theoretical dispersion curves for Profile 4 are plotted versus frequency in Figure 4.71.

Similarly, dispersion curve comparisons between the SASW-derived dispersion curves and theoretical dispersion curves for Profile 5B are plotted versus frequency in Figure 4.73. Comparisons between the HWAW-derived dispersion curves and the theoretical dispersion curves for Profile 5B are plotted versus frequency in Figure 4.74.

Lastly, the dispersion curve comparisons between the SASW-derived dispersion curves and theoretical dispersion curves for Profile 5C are plotted versus frequency in Figure 4.75. Comparisons between the HWAW derived dispersion curves and the theoretical dispersion curves for Profile 5C are plotted versus frequency in Figure 4.76.

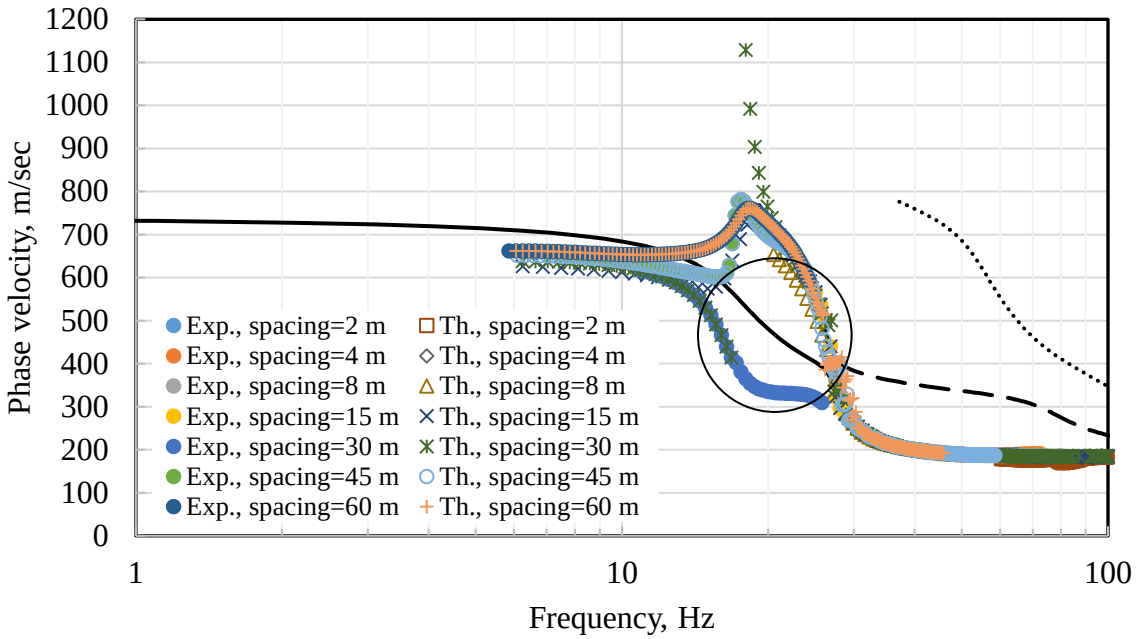

Figure 4.70 Comparison of SASW-derived experimental dispersion curve from phase unwrapping with theoretical and modal dispersion curves for Profile 5A. Black circle indicates region of incorrect dispersion curve interpretation.

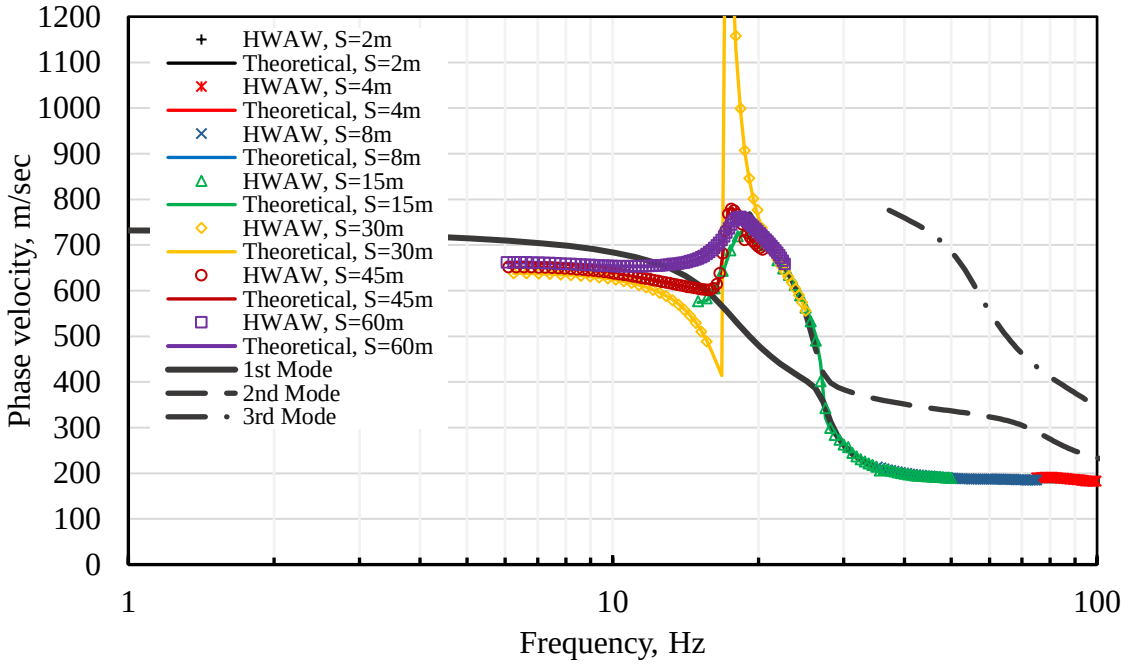

Figure 4.71 Comparison of HWAW-derived experimental dispersion curve with theoretical and modal dispersion curves for Profile 5A.

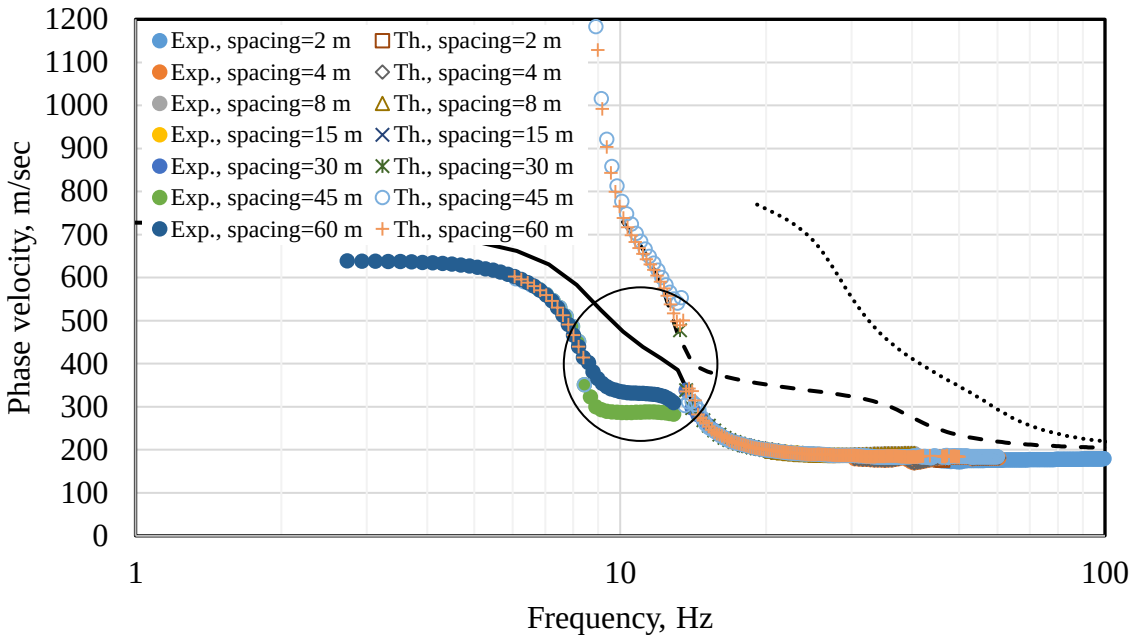

Figure 4.72 Comparison of SASW-derived experimental dispersion curve from phase unwrapping with theoretical and modal dispersion curves for Profile 5B. Black circle indicates region of incorrect dispersion curve interpretation.

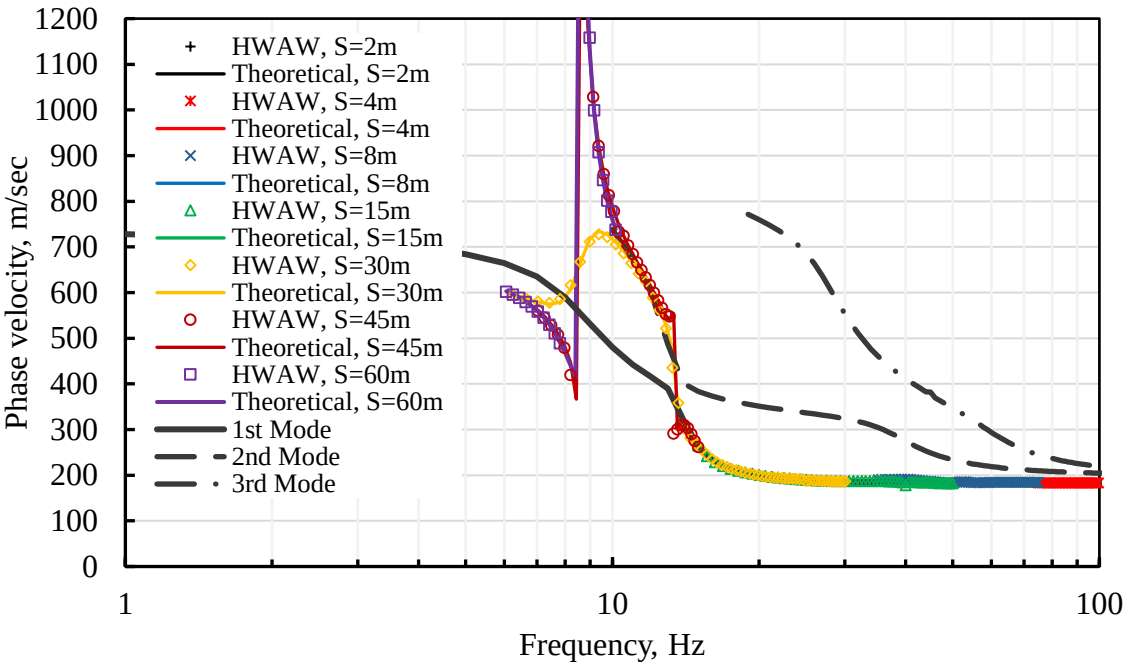

Figure 4.73 Comparison of HWAW-derived experimental dispersion curve with theoretical and modal dispersion curves for Profile 5B.

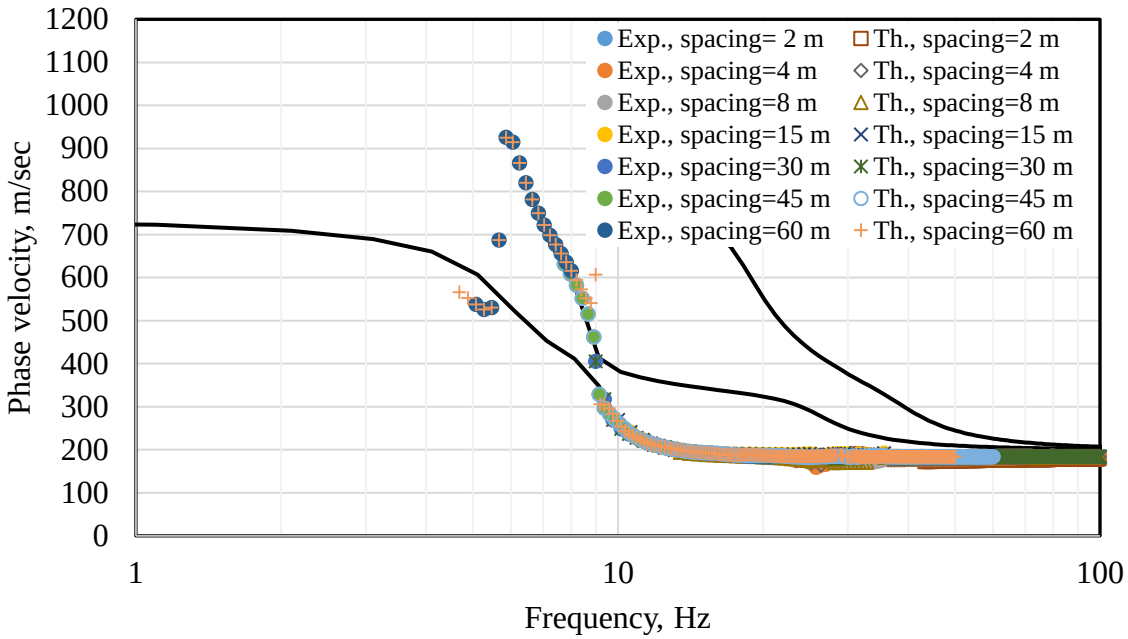

Figure 4.74 Comparison of SASW-derived experimental dispersion curve from phase unwrapping with theoretical and modal dispersion curves for Profile 5C.

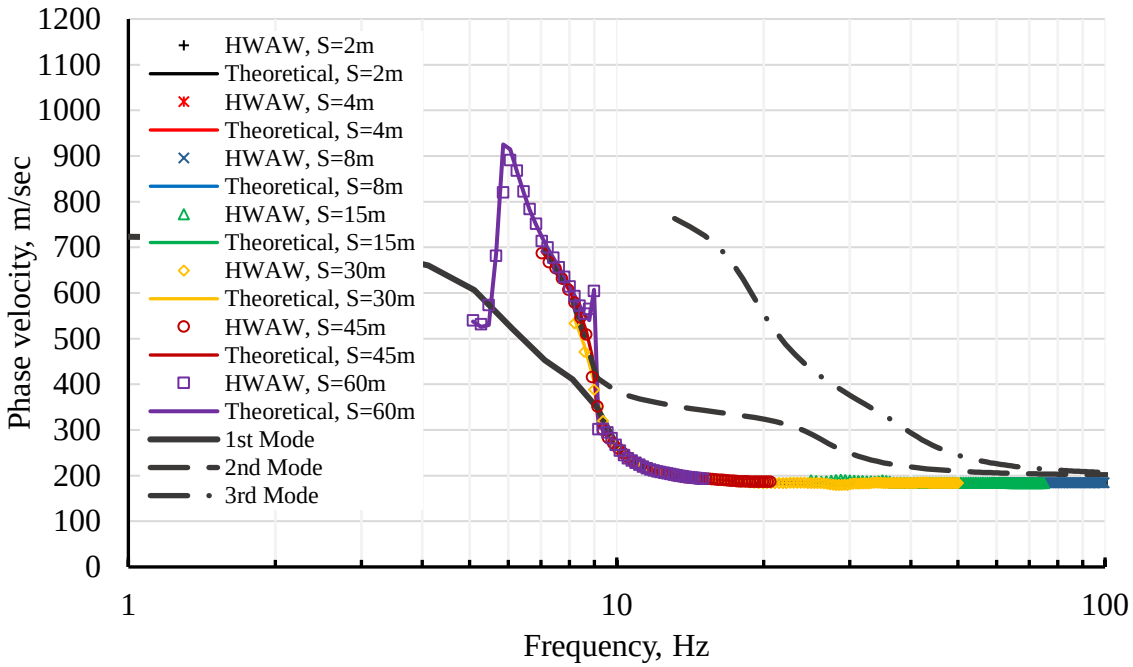

Figure 4.75 Comparison of HWAW-derived experimental dispersion curve with theoretical and modal dispersion curves for Profile 5C.

Three different types of behavior can be observed in these plots. First, for Profile 5A, the SASW phase unwrapping method correctly recovers the mode transition for the 45 m

and 60 m receiver pairs. However, the mode transition was not correctly recovered using the 30 m receiver pair.

In the second type of behavior, exhibited in Profile 5B, the transition to a higher mode was not recovered for either the 45 m or the 60 m receiver pair, as shown in Figure 4.72. An erroneous dispersion curve was obtained which showed a much lower velocity.

The third type of behavior is exhibited by Profile 5C where the SASW phase unwrapping correctly recovered the mode transition for all of the long receiver pairs, as shown in Figure 4.74.

To assist in explaining these inconsistencies, the wrapped phase plots developed for Profile 5B are presented in Figure 4.76. The phase plots for Profiles 5A and 5C are shown in Appendix D. Of the seven receiver pairs shown, the problematic interpretations are from the 45 m and 60 m receiver pairs (Figure 4.76f and 4.76g).

It can be observed in Figure 4.77 that the transition to a higher mode occurs over a frequency range of 8.2 Hz to 13.3 Hz. Because of the abrupt transition occurring at 8.2 Hz, it is not valid to interpret the unwrapped phase at frequencies above 8.2 Hz based on a single unwrapping of the phase plot. Instead, the correct interpretation requires unwrapping the two sections of the phase plot separately, as shown in Figures 4.77b and 4.77c for the 45 m pair and 4.77e, and 4.77f the 60 m receiver pair.

Unwrapping of the higher mode portion of the phase plot is ambiguous due to the unknown number of preceding phase jumps (Rosenblad and Bertel, 2006). However, when the interpretation of the phase plot shown in Figure 4.77 is applied, the simulated and theoretical dispersion curves come into good agreement, as shown in Figure 4.78. It is

important to note that this correct phase unwrapping interpretation is not apparent from observing the phase plot alone and would be difficult to detect and interpret correctly.

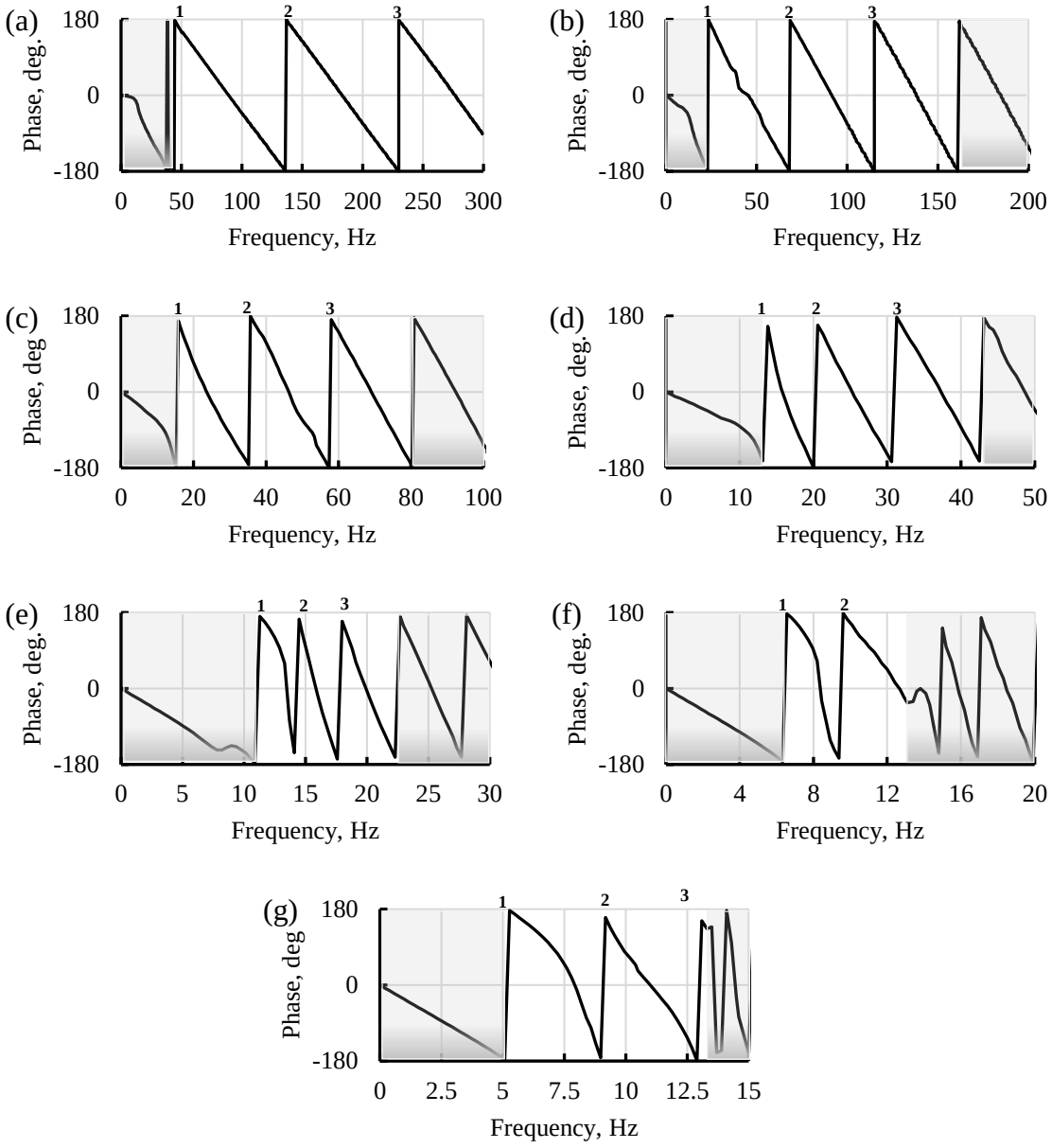

Figure 4.76 Wrapped phase plots from SASW measurements at Profile 5B with receiver spacings of (a) 2m, (b) 4m, (c) 8m, (d) 15m, (e) 30m, (f) 45m, and (g) 60m. Phase unwrapping interpretation is indicated by number of 360° "jumps." Data not used in interpretation are indicated by shaded regions.

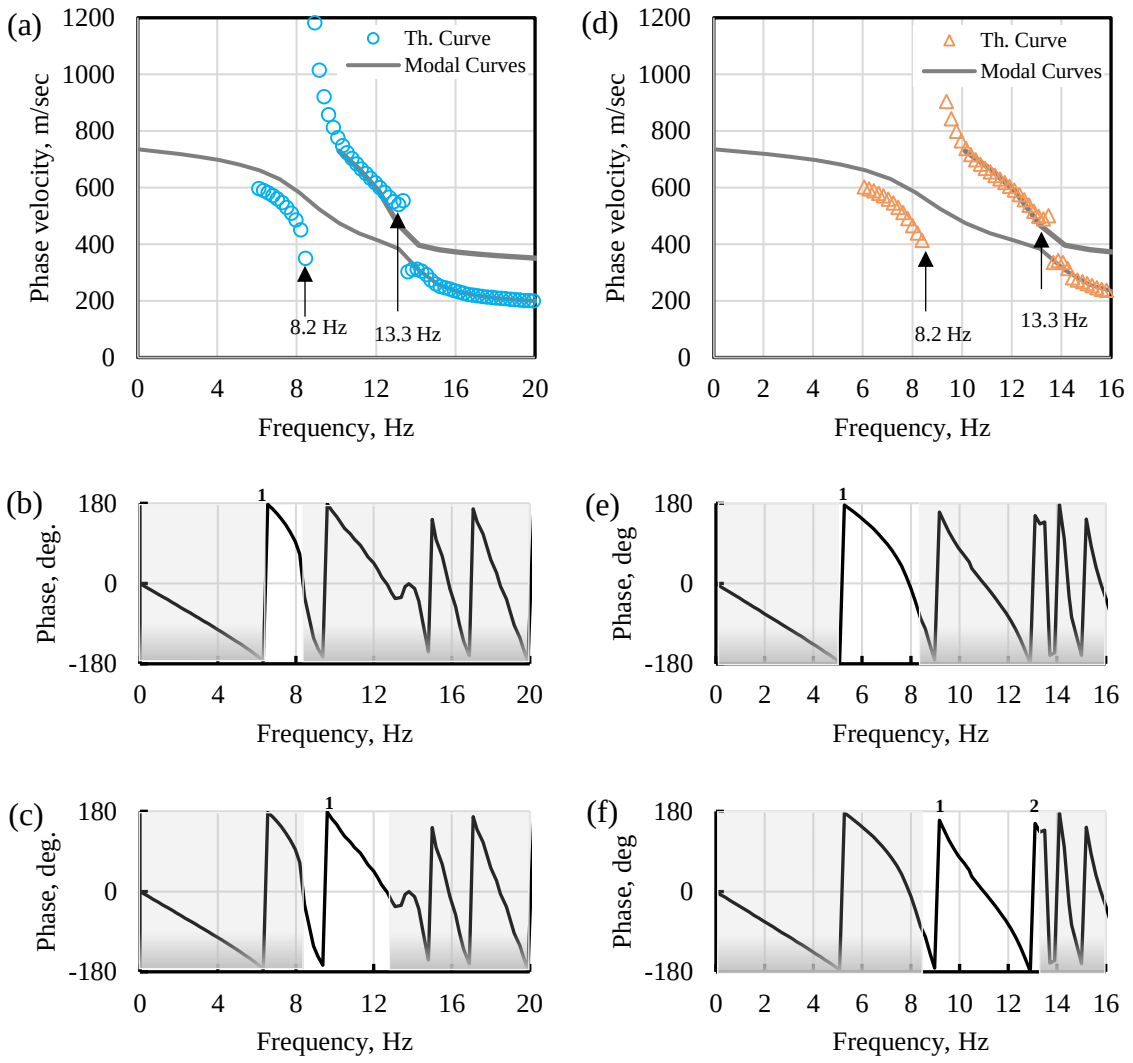

Figure 4.77 Correct interpretation of the 45 m and 60 m receiver pairs phase data for Profile 5B showing (a) the higher mode transition between 8.2 Hz and 13.3 Hz for 45 m, (b) phase unwrapping of the lower mode at frequencies less than 8.2 Hz for 45 m, (c) phase unwrapping of higher mode between 8.2 Hz and 13.3 Hz for 45 m, (d) the higher mode transition between 8.2 Hz and 13.3 Hz for 60 m, (e) phase unwrapping of the lower mode at frequencies less than 8.2 Hz for 60 m, and (f) phase unwrapping of higher mode between 8.2 Hz and 13.3 Hz for 60 m. Data not used in interpretation are indicated by shaded regions.

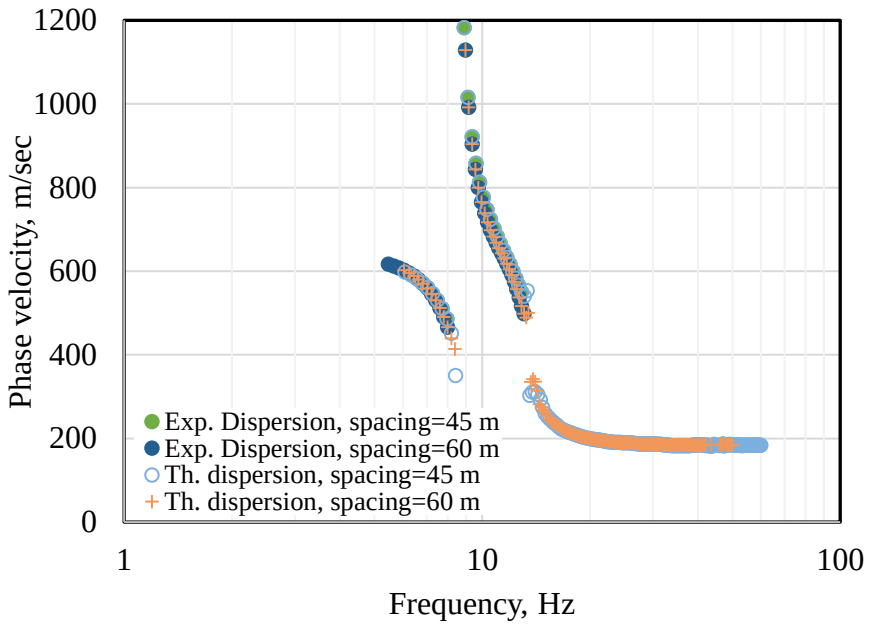

Figure 4.78 Comparison between the simulated experimental dispersion curve and theoretical dispersion curve for Profile 5B after correct phase unwrapping is applied.

The results of the comparisons between the SASW data processed with the HWAW method showed good agreement with the theoretical dispersion curves for all receiver pairs at Profiles 5A, 5B, and 5C, as shown in Figures 4.71, 4.73 and 4.75, respectively.

Soft-over-stiff profiles are among the most problematic conditions when using conventional SASW phase unwrapping procedures due to the abrupt and distinct jumps to higher modes. As shown above, the phase may be erroneously interpreted as a continuous dispersion curve resulting in a lower phase velocity and ultimately an incorrect V_S profile.

The main finding from this portion of the for study is that HWAW processing of SASW data was able to accurately recover the mode transition and overcome the issues related to manual phase unwrapping of the SASW data, as shown in Figures 4.79 and 4.80 for Profile 5B. Based on these results, the HWAW method appears to be a viable and superior approach to interpreting SASW data and could be easily implemented in an automated

procedure. The performance of HWAW processing for other complex sites is presented below.

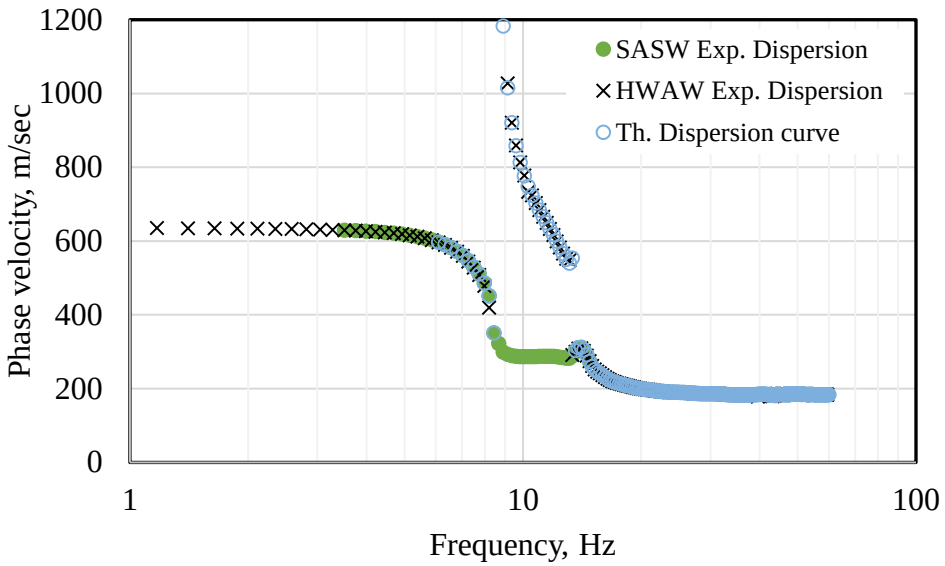

Figure 4.79 Comparison between the experimental and theoretical dispersion curves of Profile 5B for the receiver spacing of 45 m obtained by incorrect SASW phase unwrapping and automated HWAW processing.

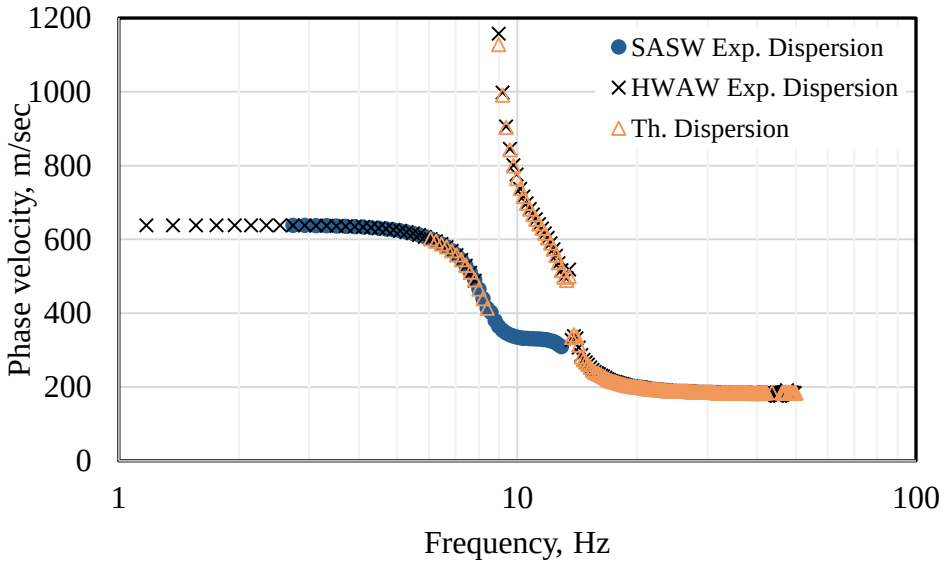

Figure 4.80 Comparison between the experimental and theoretical dispersion curves of Profile 5B for receiver spacing of 60 m obtained by incorrect SASW phase unwrapping and automated HWAW processing.

4.5.5 Shallow and Deep Linear Gradient Profiles (Profiles 6 &7)

4.5.5.1 Results and Discussions of Shallow Gradient Profile (Profile 6)

Comparisons between the SASW-derived dispersion curve using phase unwrapping and theoretical dispersion curves for Profile 6 are plotted versus frequency in Figure 4.81. The dispersion curve comparisons between the HWAW-derived dispersion curves and the theoretical dispersion curves for Profile 6 are plotted versus frequency in Figure 4.82. The SASW wrapped phase plots developed for Profile 6 are presented in Figure 4.83.

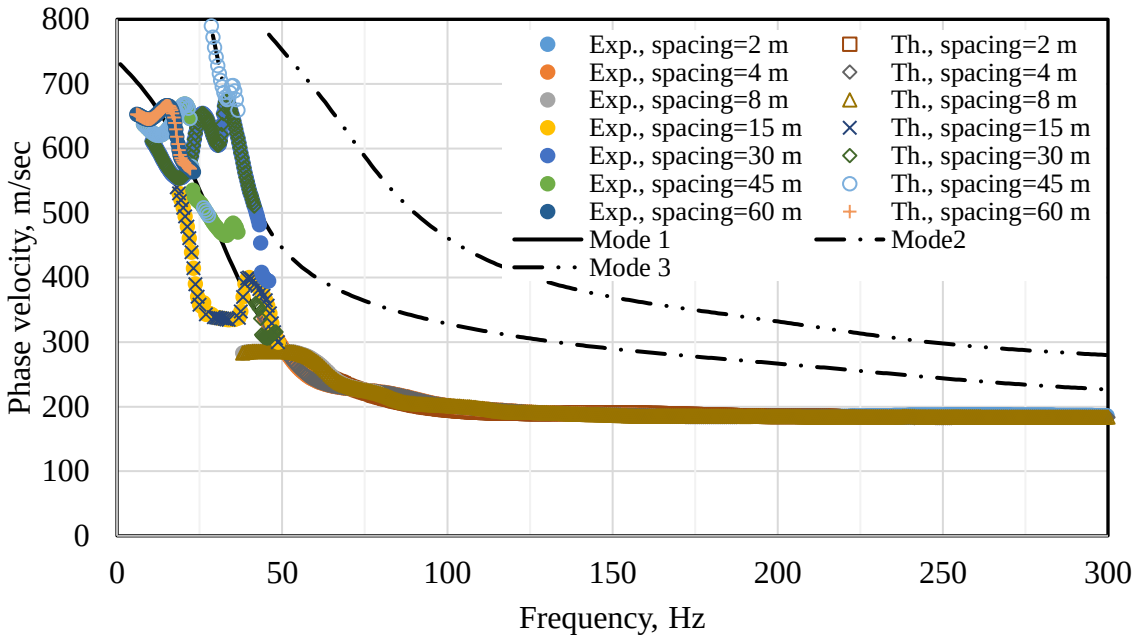

Figure 4.81 Comparison of SASW-derived experimental dispersion curve from phase unwrapping with theoretical and modal dispersion curves for Profile 6.

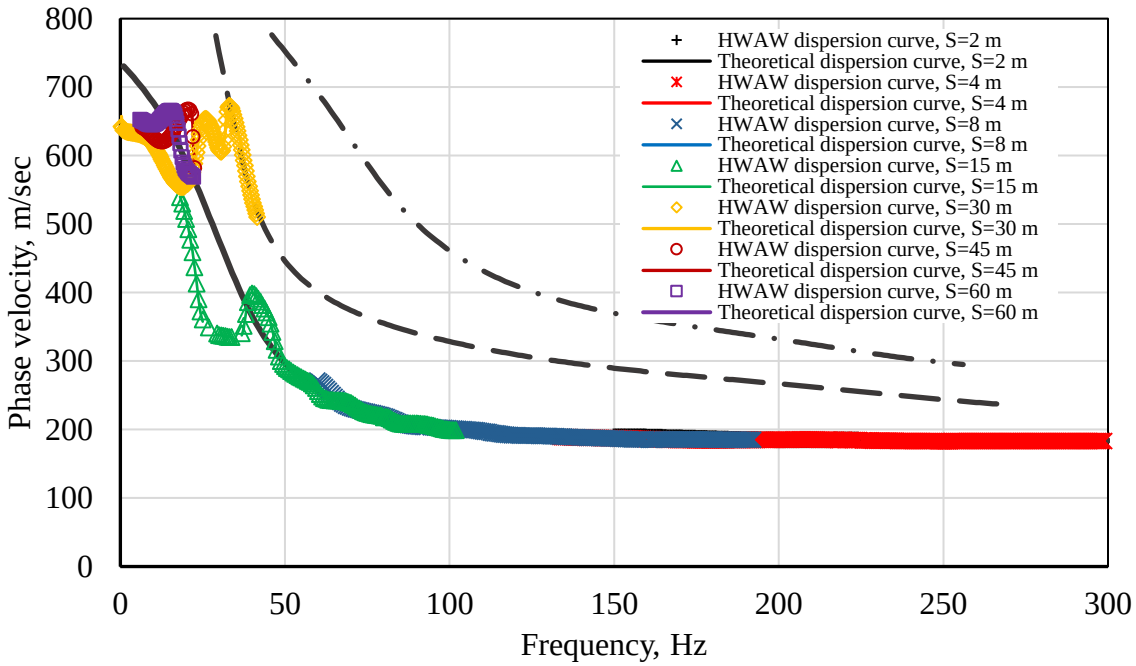

Figure 4.82 Comparison of HWAW-derived experimental dispersion curve with theoretical and modal dispersion curves for Profile 6.

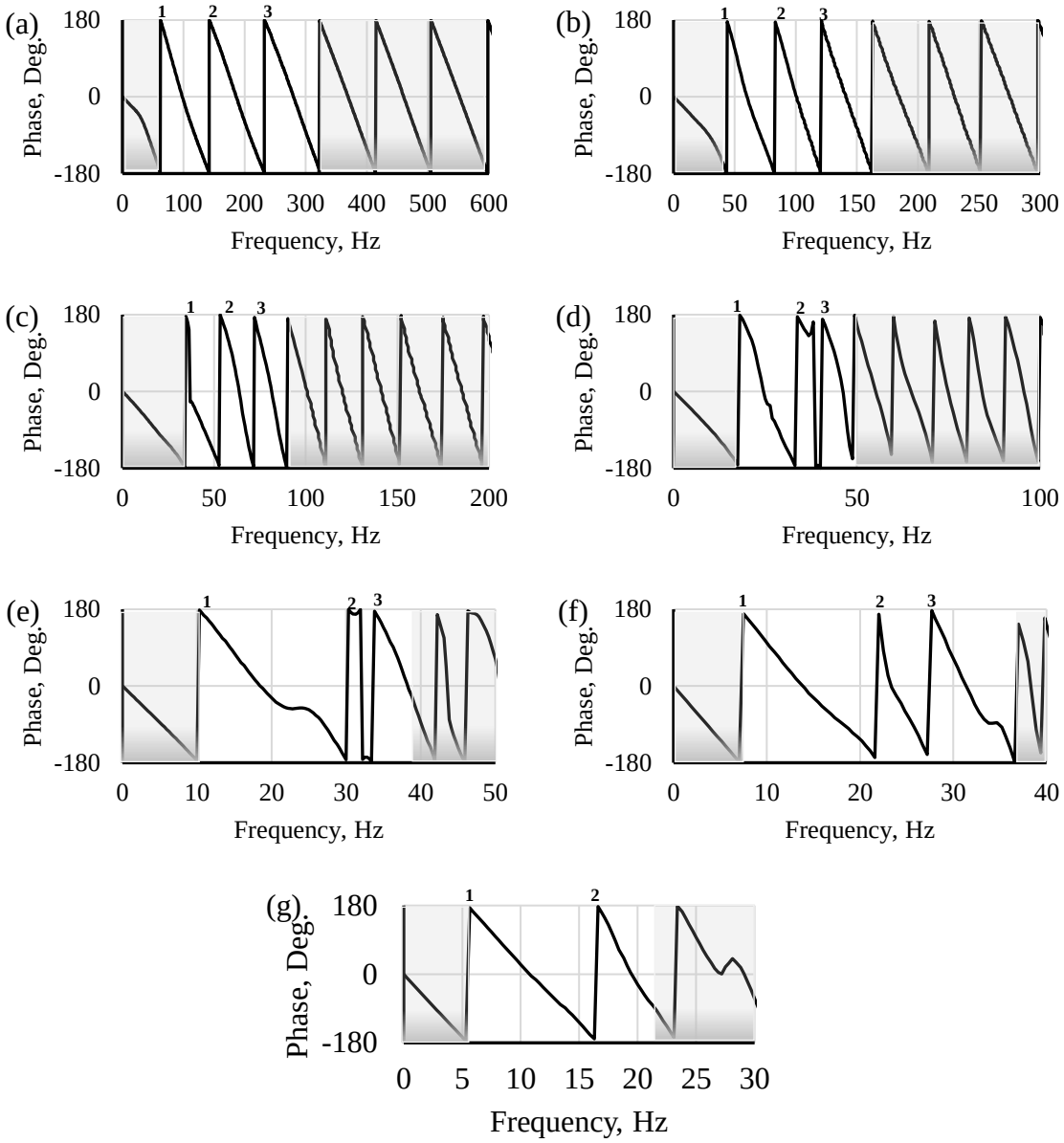

Figure 4.83 Wrapped phase plots from SASW measurements at Profile 6 with receiver spacings of (a) 2m, (b) 4m, (c) 8m, (d) 15m, (e) 30m, (f) 45m, and (g) 60m. Phase unwrapping interpretation is indicated by number of 360° "jumps." Data not used in interpretation are indicated by shaded regions.

This profile condition produces a complex dispersion curve with abrupt mode transitions at low frequencies (Figure 4.81). The SASW-derived dispersion curve shown in Figure 4.81 shows that the phase interpretation produced inconsistencies in the

dispersion curve for the 45 m receiver pair. This is again due to a misinterpretation of the phase diagram (Figure 4.83f) as a single continuous mode. The HWAW interpretation, on the other hand, produced dispersion curves that were consistent with the theoretical dispersion curves for all receiver pairs. These results also support the use of HWAW processing over manual phase unwrapping for interpreting SASW data.

4.5.5.1 Results and Discussions of Deep Gradient Profile (Profile 7)

Comparisons between the SASW-derived dispersion curves and the theoretical dispersion curves for Profile 7 are plotted versus frequency in Figure 4.84. Comparisons between the HWAW-derived dispersion curves and the theoretical dispersion curves for Profile 7 are plotted versus frequency in Figure 4.85. The wrapped phase plots developed for Profile 7 are presented in Figure 4.86.

The results of HWAW processing of the SASW time records for Profile 7 showed generally good agreement with the theoretical dispersion curves for all test setups with the exception of the 60 m spacing where the interpretation did not correctly identify the mode jump in the frequency range of 15 to 19 Hz.

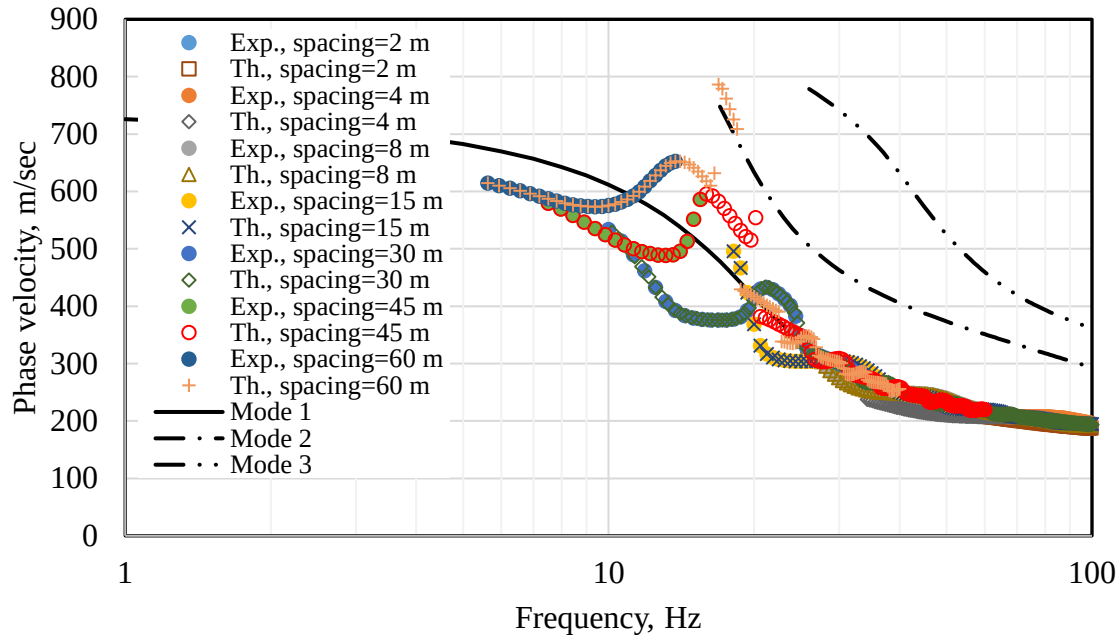

Figure 4.84 Comparison of SASW-derived experimental dispersion curve from phase unwrapping with theoretical and modal dispersion curves for Profile 7.

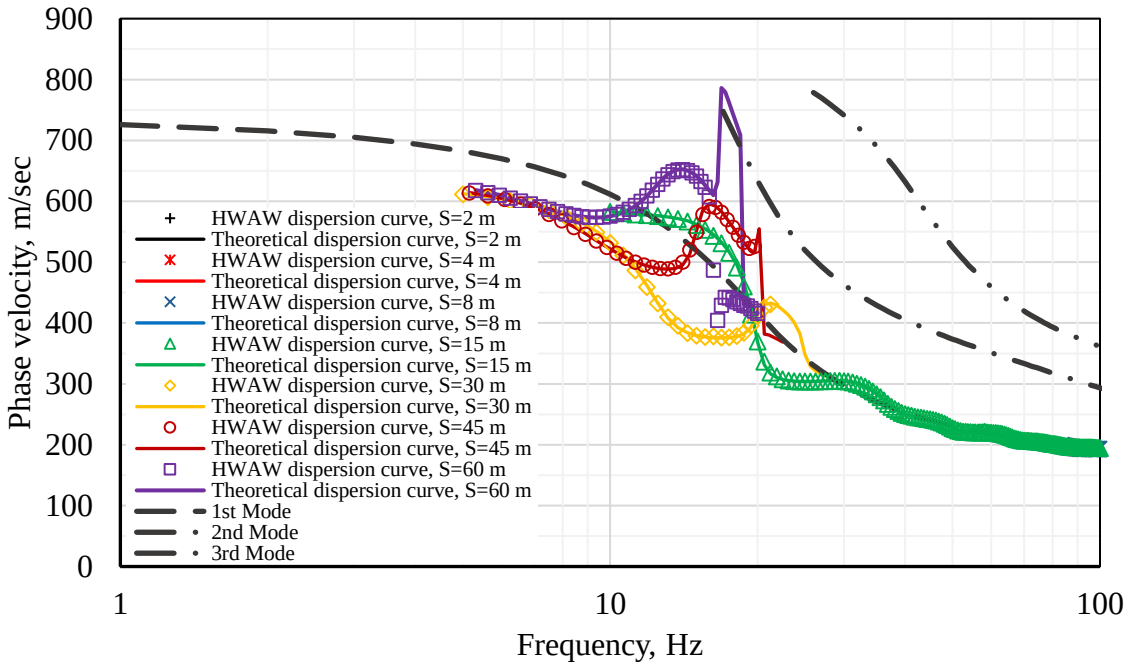

Figure 4.85 Comparison of HWAW-derived experimental dispersion curve with theoretical and modal dispersion curves for Profile 7.

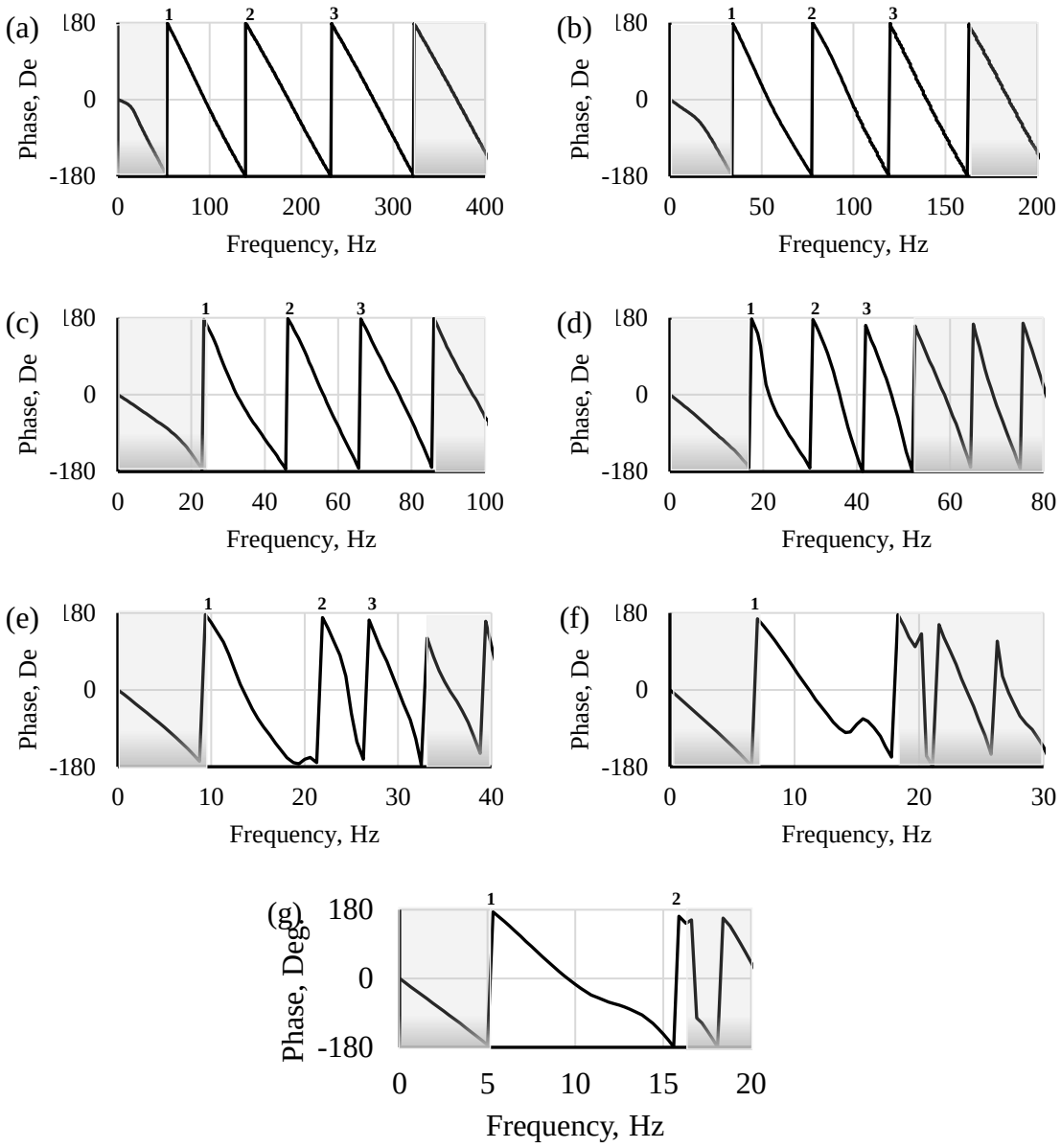

Figure 4.86 Wrapped phase plots from SASW measurements at Profile 7 with receiver spacings of (a) 2m, (b) 4m, (c) 8m, (d) 15m, (e) 30m, (f) 45m, and (g) 60m. Phase unwrapping interpretation is indicated by number of 360° "jumps." Data not used in interpretation are indicated by shaded regions.

4.5.6 Velocity Inversion-Embedded Lower Velocity Layer (Profiles 8&9)

4.5.6.1 Results and Discussions of Thin and Thick Embedded Lower Velocity Layer Profile

Comparisons between the SASW-derived dispersion curves and the theoretical dispersion curves for Profile 8 are plotted versus frequency in Figures 4.87. Comparisons between the HWAW-derived dispersion curves and the theoretical dispersion curves for Profile 8 are plotted versus frequency in Figure 4.88. The SASW wrapped phase plots developed for Profile 8 are presented in Figure 4.89. Similar figures are generated for Profile 9 which are shown in Figures 4.90, 4.91, and 4.92 respectively.

The HWAW processing of data from Profiles 8 and 9 yielded experimental dispersion curves that are in very good agreement with the theoretical dispersion curves for all receiver pairs. Dispersion curves for these profiles were also accurately resolved using the conventional SASW phase unwrapping shown in Figures 4.87 and 4.90, respectively for Profiles 8 and 9. The good performance of phase unwrapping in this case is due to the continuous dispersion curve with no abrupt mode transitions. The phase velocity dispersion curves follow the fundamental mode up to a frequency of approximately 60 Hz for Profile 8 and 30 Hz for Profile 9 and then follows a continuous curve that is a superposition of modes at higher frequencies.

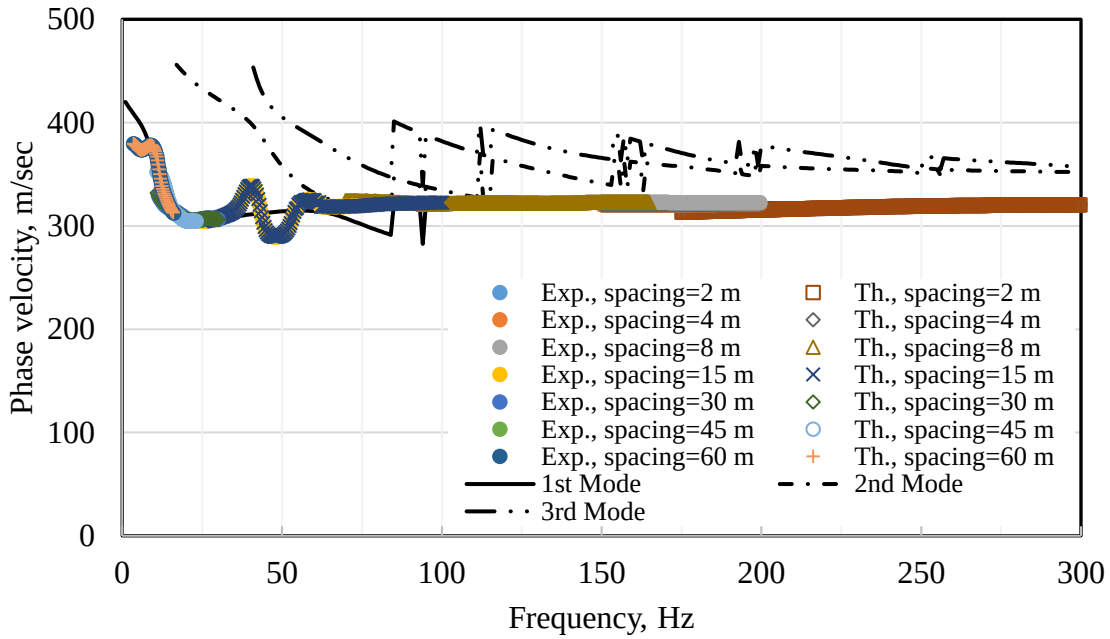

Figure 4.87 Comparison of SASW-derived experimental dispersion curve from phase unwrapping with theoretical and modal dispersion curves for Profile 8.

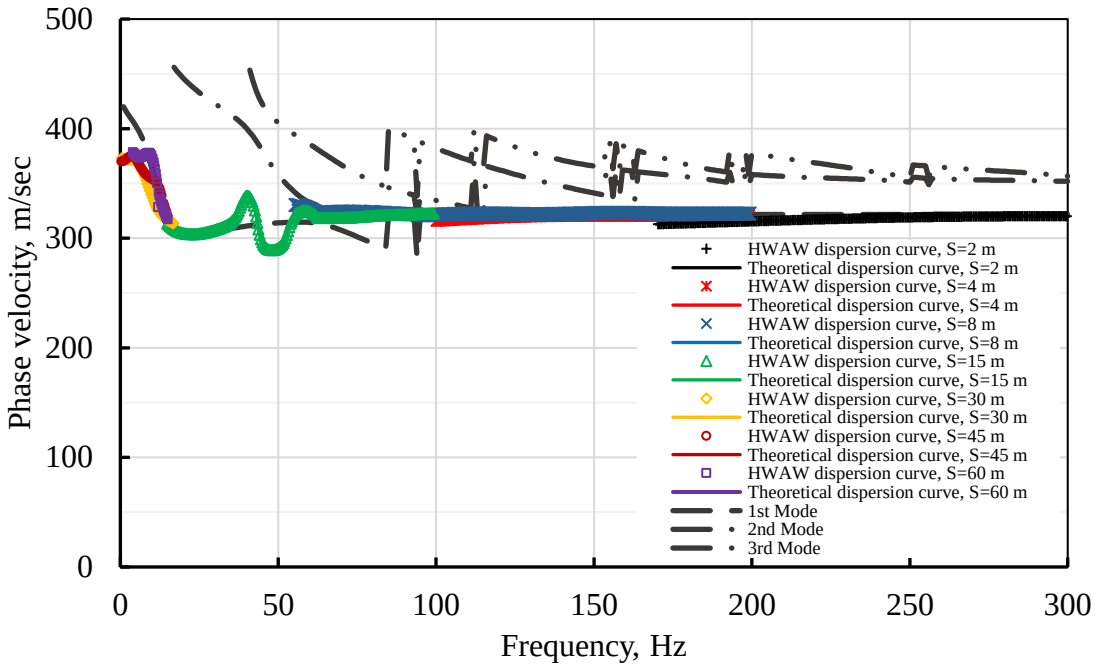

Figure 4.88 Comparison of HWAW-derived experimental dispersion curve with theoretical and modal dispersion curves for Profile 8.

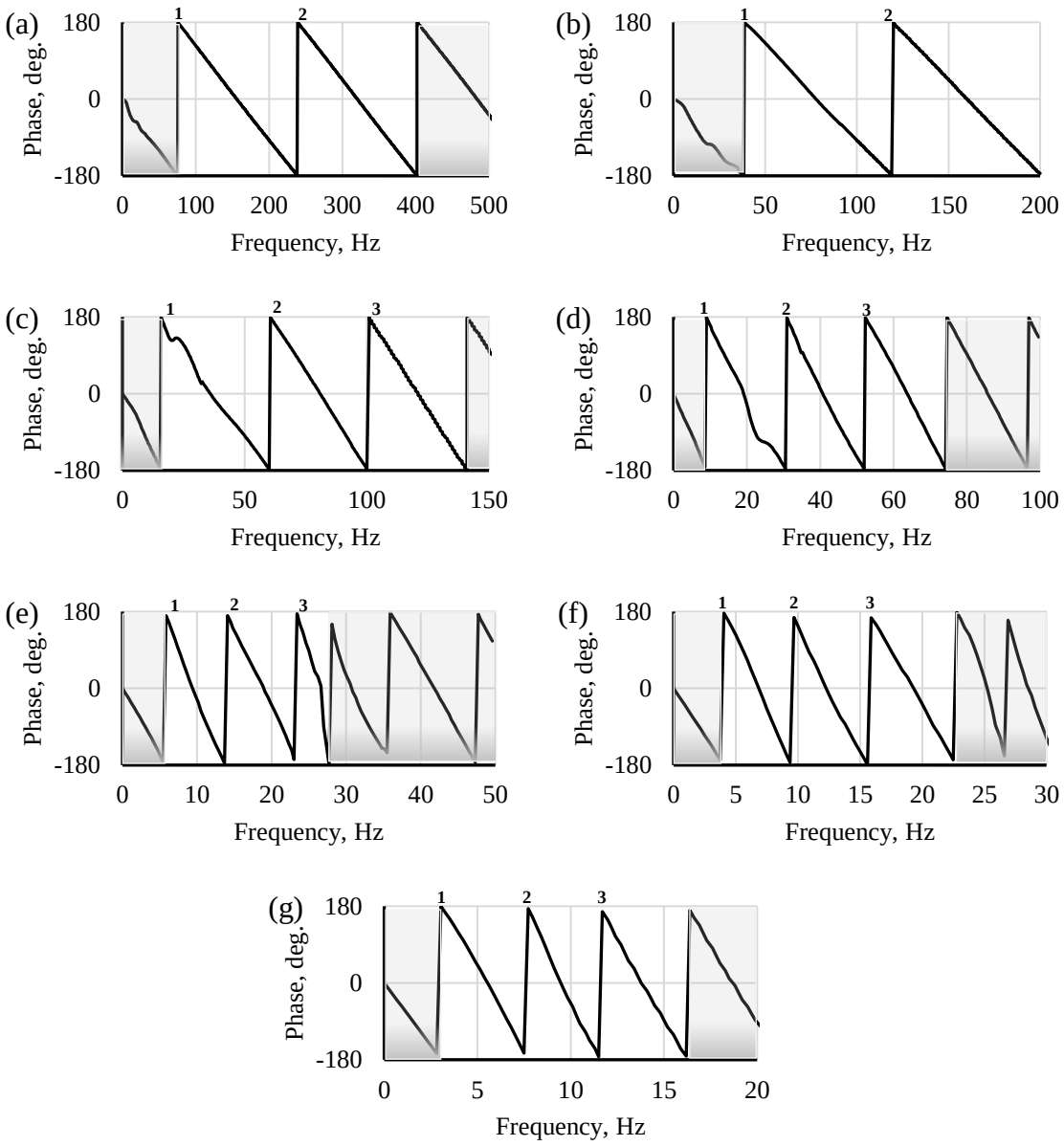

Figure 4.89 Wrapped phase plots from SASW measurements at Profile 8 with receiver spacings of (a) 2m, (b) 4m, (c) 8m, (d) 15m, (e) 30m, (f) 45m, and (g) 60m. Phase unwrapping interpretation is indicated by number of 360° "jumps." Data not used in interpretation are indicated by shaded regions.

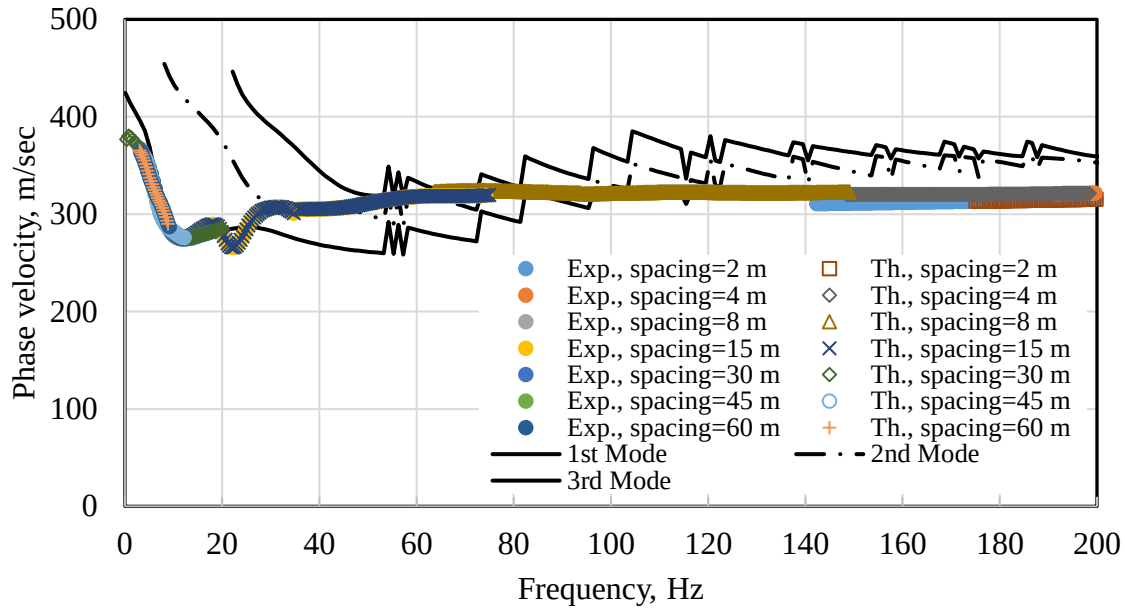

Figure 4.90 Comparison of SASW-derived experimental dispersion curve from phase unwrapping with theoretical and modal dispersion curves for Profile 9.

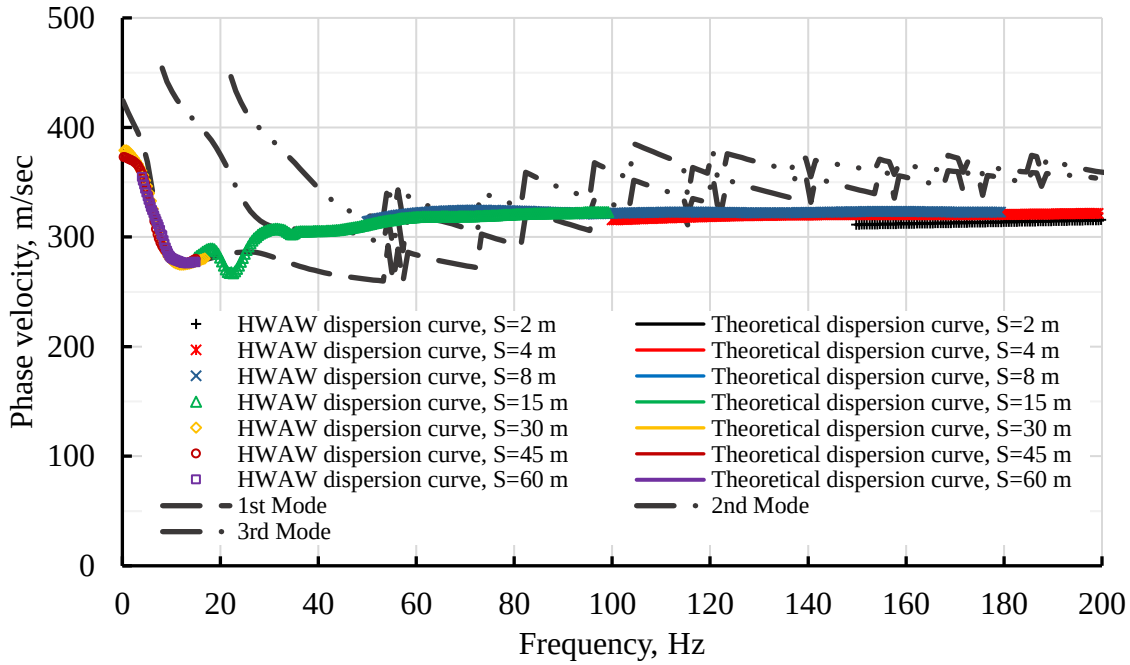

Figure 4.91 Comparison of HWAW-derived experimental dispersion curve with theoretical and modal dispersion curves for Profile 9.

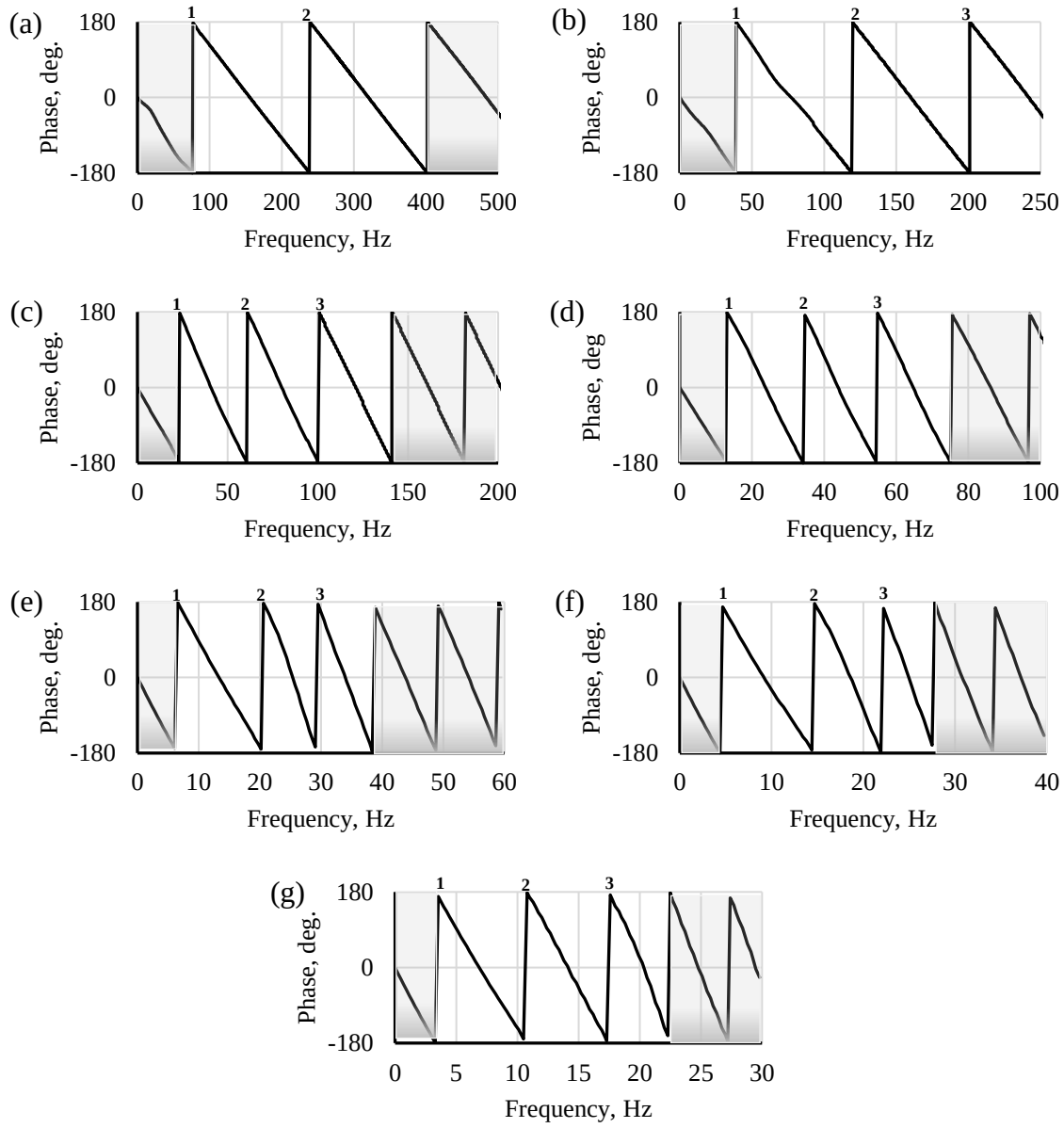

Figure 4.92 Wrapped phase plots from SASW measurements at Profile 9 with receiver spacings of (a) 2m, (b) 4m, (c) 8m, (d) 15m, (e) 30m, (f) 45m, and (g) 60m. Phase unwrapping interpretation is indicated by number of 360° "jumps." Data not used in interpretation are indicated by shaded regions.

4.5.7 Velocity Inversion-Embedded Higher Velocity Layer (Profiles 10 & 11)

4.5.7.1 Results and Discussions of Thin and Thick Embedded Higher Velocity Layers Profiles

Comparisons between the SASW-derived experimental dispersion curves and the theoretical dispersion curves for Profile 10 are plotted versus frequency in Figure 4.93. Comparisons between the HWAW-derived dispersion curves and the theoretical dispersion curves for Profiles 10 are plotted versus frequency in Figure 4.94. The SASW wrapped phase plots developed for Profiles 10 are presented in Figure 4.95. Similar plots were generated for Profile 11 which are presented in Figures 4.96, 4.97, and 4.98 respectively.

The HWAW processing of data from Profiles 10 and 11 with embedded stiff layers (thin and thick) yielded experimental dispersion curves that are in very good agreement with the theoretical dispersion curves. The dispersion curves are also accurately resolved using conventional SASW phase unwrapping. The wrapped phase plots for each receiver spacing of Profiles 10 and 11 show the characteristic “sawtooth” pattern of SASW data with unambiguous phase jumps, as shown in Figures 4.96 and 4.99. The single continuous dispersion curve in these cases allows for accurate recovery of the dispersion curve using manual phase unwrapping.

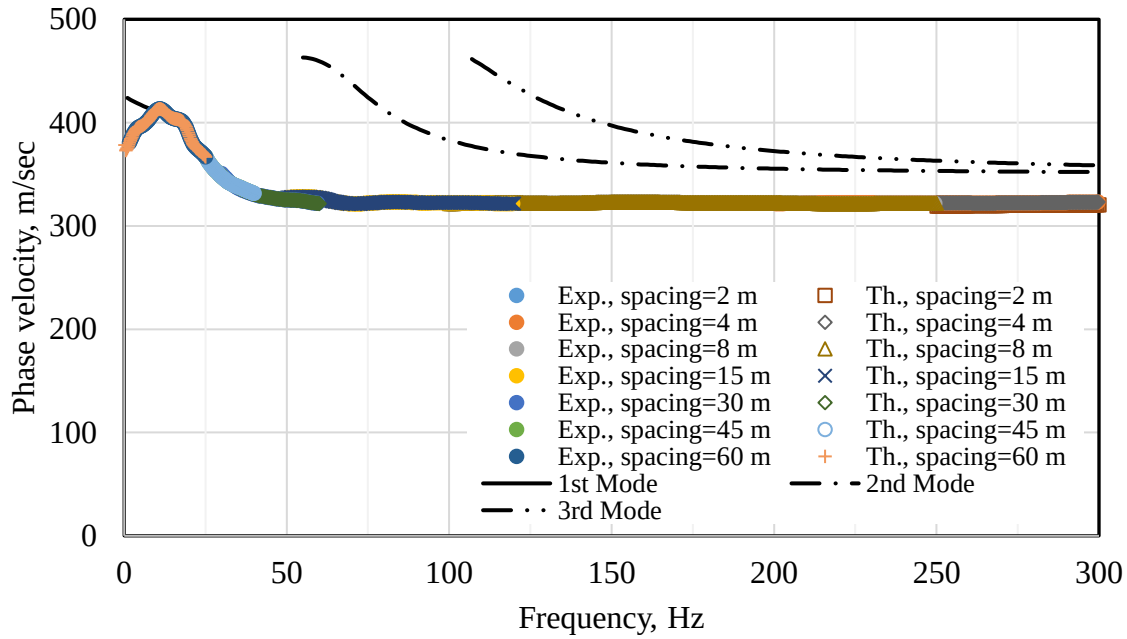

Figure 4.93 Comparison of SASW-derived experimental dispersion curve from phase unwrapping with theoretical and modal dispersion curves for Profile 10.

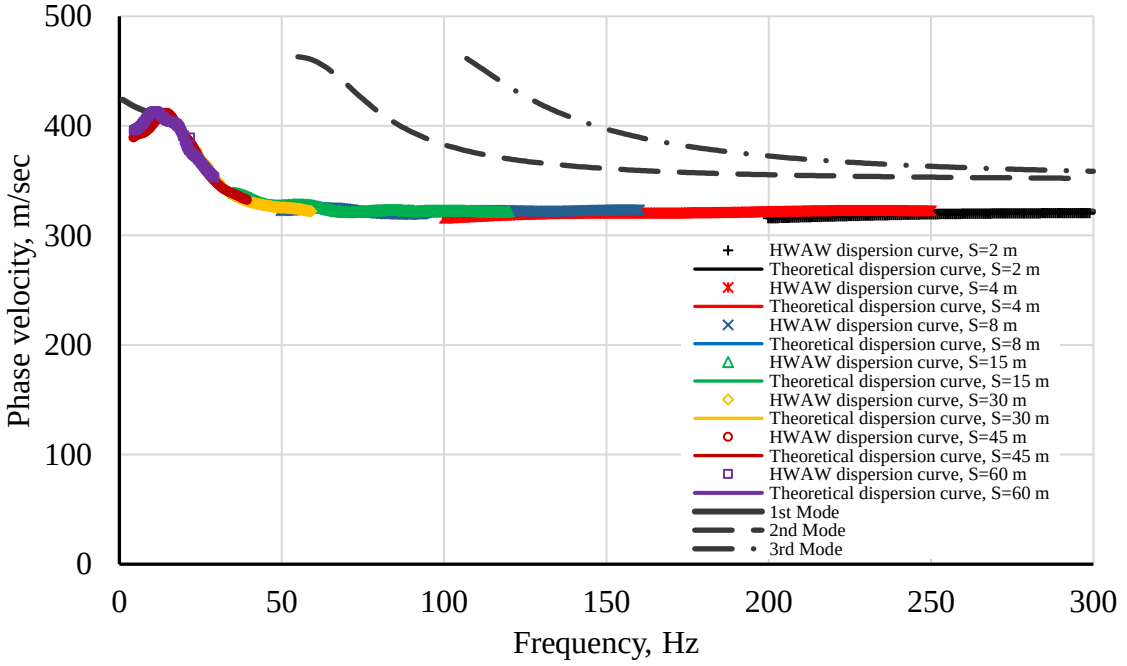

Figure 4.94 Comparison of HWAW-derived experimental dispersion curve with theoretical and modal dispersion curves for Profile 10.

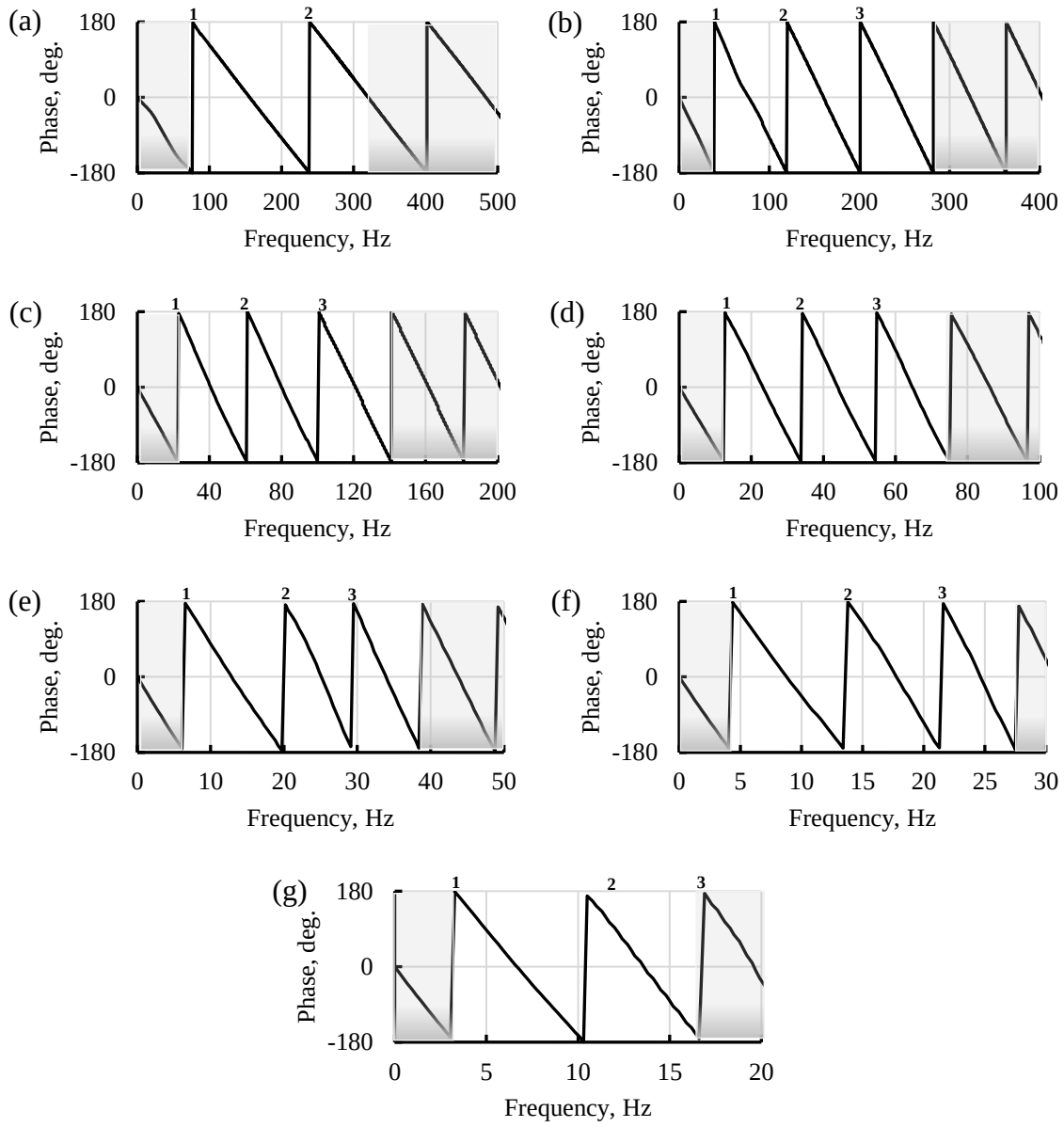

Figure 4.95 Wrapped phase plots from SASW measurements at Profile 10 with receiver spacings of (a) 2m, (b) 4m, (c) 8m, (d) 15m, (e) 30m, (f) 45m, and (g) 60m. Phase unwrapping interpretation is indicated by number of 360° "jumps." Data not used in interpretation are indicated by shaded regions.

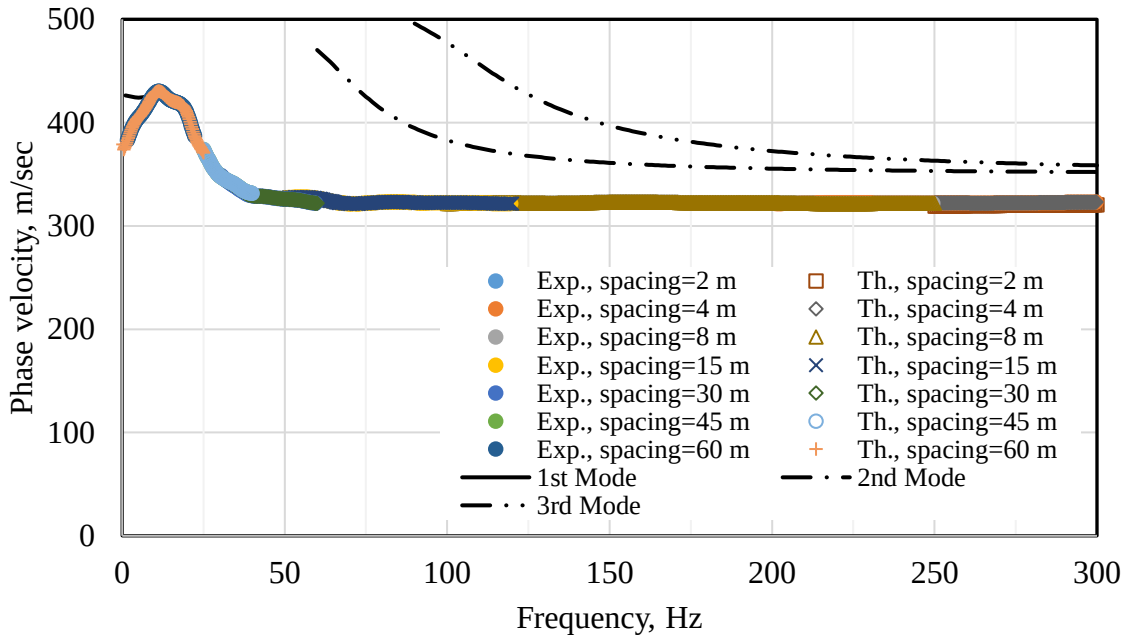

Figure 4.96 Comparison of SASW-derived experimental dispersion curve from phase unwrapping with theoretical and modal dispersion curves for Profile 11.

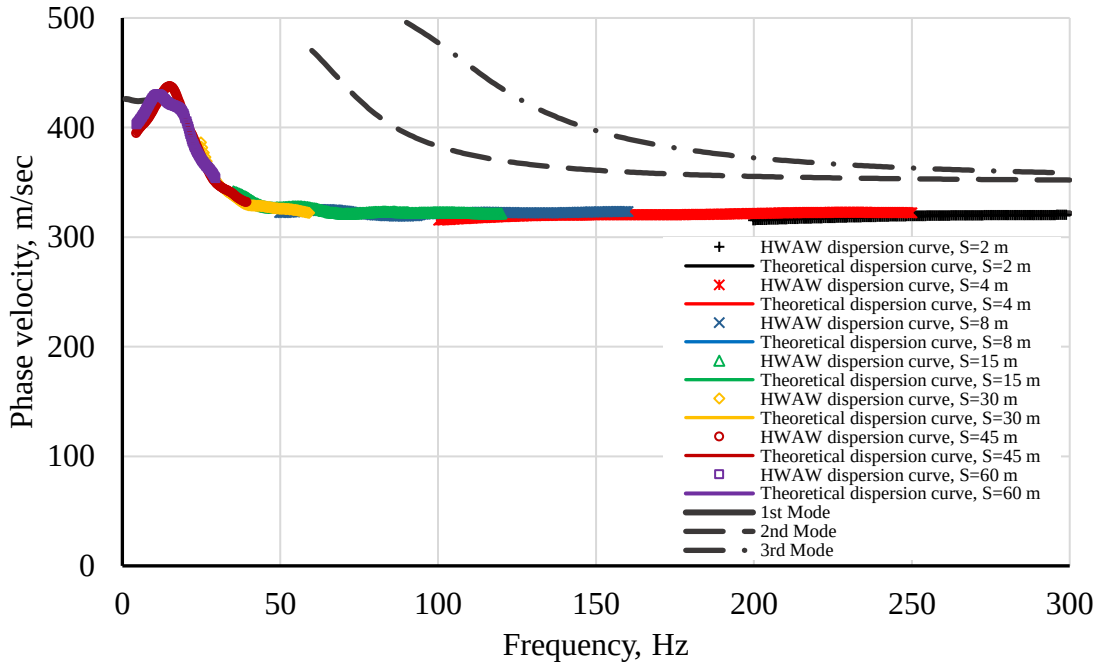

Figure 4.97 Comparison of HWAW-derived experimental dispersion curve with theoretical and modal dispersion curves for Profile 11.

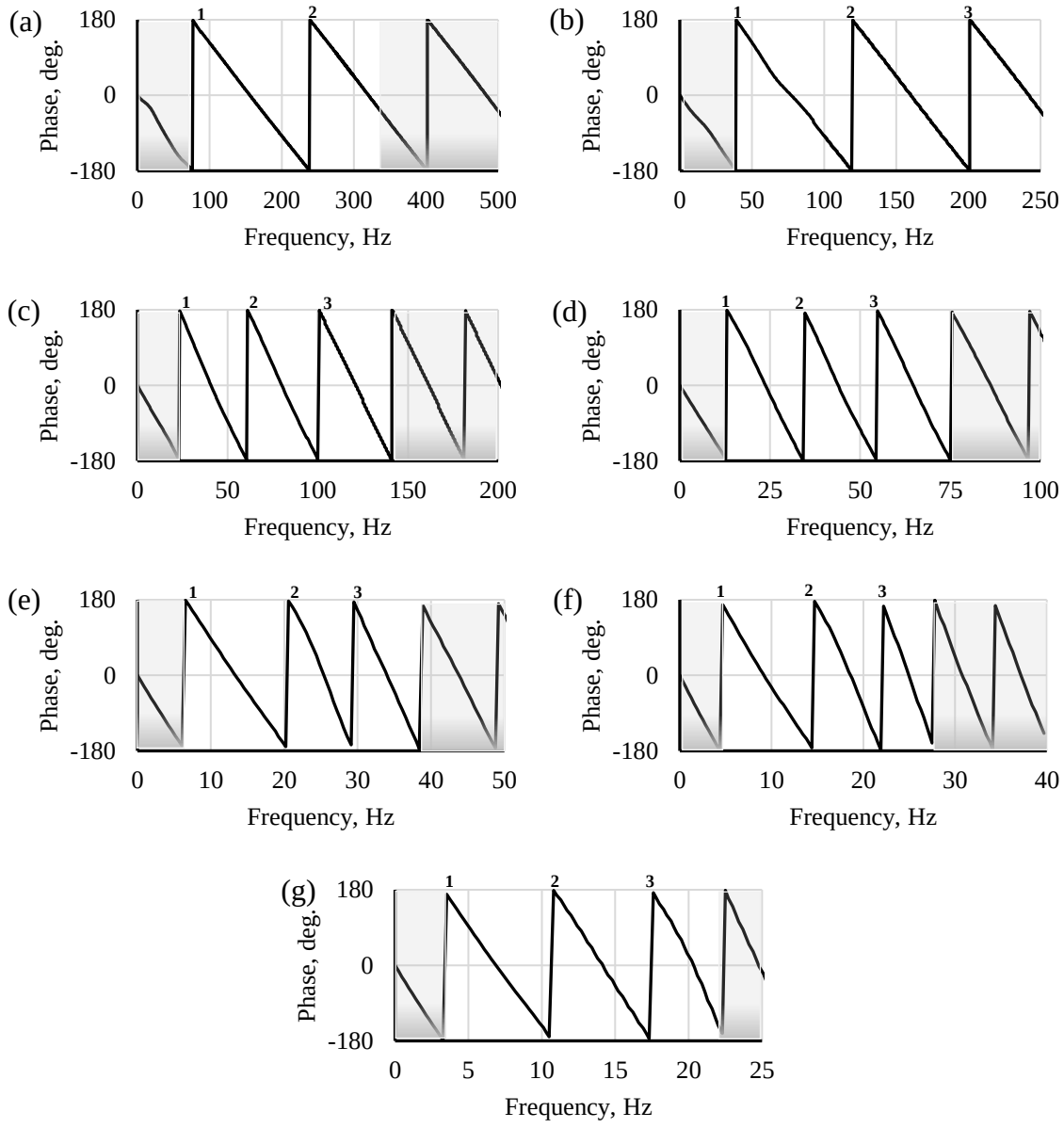

Figure 4.98 Wrapped phase plots from SASW measurements at Profile 11 with receiver spacings of (a) 2m, (b) 4m, (c) 8m, (d) 15m, (e) 30m, (f) 45m, and (g) 60m. Phase unwrapping interpretation is indicated by number of 360° "jumps." Data not used in interpretation are indicated by shaded regions.

4.5.8 Summary

Surface wave data were simulated using the conventional SASW source and receiver arrangements and processed using: (1) the SASW manual phase unwrapping approach and (2) the automated HWAW approach. Based on comparisons of the dispersion curve to the theoretical dispersion curves, the HWAW outperformed the SASW phase unwrapping method. For some of the profiles (Profiles 8, 9, 10, and 11) both methods produced reliable dispersion curves. However, for the stiff-over-soft sites (Profiles 4 and 5) and shallow gradient site (Profile 6) SASW phase unwrapping produced an erroneous dispersion curve for many of the receiver pairs. The HWAW processing produced an erroneous dispersion curve in only one case (Profile 7 – 60 m Receiver Pair). Importantly, the HWAW technique demonstrated the ability to overcome the issue of phase unwrapping difficulty due to abrupt mode transitions, especially at soft-over-stiff sites.

These results using simulated data demonstrate the effectiveness of HWAW processing when applied to data collected using the SASW methodology. Given the time consuming nature of SASW phase unwrapping and the demonstrated ineffectiveness for many profiles, the HWAW method appears to be a better alternative that could be used to develop an automated and instant interpretation of SASW data. Field verifications of the HWAW method for three experimental sites are presented in Chapter 5.

4.6 General Guidelines and Procedures for HWAW Implementation

4.6.1 Introduction

This section presents proposed recommendations and guidelines for implementing the HWAW method based on the results from the study performed using simulated data. An example of HWAW data collection and processing parameter selection for a soil site is provided.

4.6.2 Summary of Findings

The present guidelines provide recommendations on data collection and processing parameters to be used with the HWAW method. These guidelines are based on the findings from the study performed using simulated data, as presented in the previous sections. The parameters discussed below are: bandwidth, sampling frequency, source offset and receiver spacing.

Bandwidth: The results of simulated study showed that the bandwidth was the most critical parameter for recovering an accurate dispersion curve. It was found that for simple sites the ratio of bandwidth to frequency should be 0.25 or less. For these cases an error of 1% or less was observed. However, for complex profiles it was found that a lower bandwidth to frequency ratio of 0.10 or less was needed to maintain errors below 4%. Based on this study, it is recommended that the bandwidth to frequency ratio should be no larger than 0.10 for all frequencies.

The bandwidth value is controlled by the frequency resolution which is controlled by the length of the time record, as described in Section 4.3.1. Therefore, the length of the time record should be set to an appropriate value, as shown in the example below.

Sampling frequency: As described in Section 4.3.1.4, the sampling frequency did not significantly affect the accuracy of low frequency velocity measurements. However, for high frequency velocity measurements, higher sampling frequency is preferred to better define the phase plot. In order to have a sufficient characterization of the high frequency phase values, it is suggested that the sampling frequency should be at least ten times the highest frequency recorded.

Source Offset: Based on the results of the simulated data, the source offset did not affect the ability of the HWAW to recover the dispersion curve for any source offset investigated in this study. However, it should be understood that using a short source offset with long wavelengths produces significant near-field effects which may not work well in the inversion process. This issue was not studied here and should be considered in future research. Therefore, the recommendation here is to continue to use the offset criteria established for the SASW testing method which is that the source offset should be at least equal to the desired investigation depth.

Receiver Spacing: The receiver spacing also did not affect the ability of the HWAW method to recover the dispersion curve. However, practical issues with the receiver spacing include (1) mismatch of phase response between the receivers will produce larger errors when the receiver spacing is close and (2) for saturated sites, the dispersion curve can exhibit large fluctuation that can affect the inversion procedure. Therefore, the selection of the receiver spacing is up to users' decision but they should be aware of these issues.

4.6.3 Data Collection Steps for Implementing the HWAW Method

A general idea of the site condition is required to set up reasonable data collection and processing parameters. After the dispersion curve is generated, those default parameters

can be adjusted based on the measured dispersion curve. The following procedure is proposed for the HWAW method implementation in the field.

1. Determine the desired depth of the V_S profile, D.
2. Estimate V_S at the longest and shortest wavelengths, $V_{S,\,long}$ and $V_{S,\,short}$. for the expected site conditions (e.g. soil versus rock)
3. Estimate the shortest wavelength, λ_{short} based on the desired near surface resolution (λ_{short} equals about two times the shallowest depth).
4. Calculate the longest wavelength, λ_{long} needed to profile to the desired depth. Typically, this is two or three times the profile depth, D.
5. Calculate the lowest required frequency $f_{r,low}$, using the estimated $V_{S,\,long}$ and calculated λ_{long}:

$$V = f_r . \lambda$$

$$f_{r,low} = {V_{long}}/{\lambda_{long}}$$

6. Calculate the highest frequency, $f_{r,high}$, using the estimated $V_{S,\,short}$ and the shallowest depth requirement, λ_{short}:

$$f_{r,high} = {V_{short}}/{\lambda_{short}}$$

7. Calculate the required bandwidth, b_w, at a minimum:

$$b_w = 0.1 \times f_{r,low}$$

8. Calculate the required frequency resolution, Δf based on a three-point b_w:

$$\Delta f = {b_w}/{2}$$

9. Based on the calculated frequency resolution, Δf , determine the required time record, t_{length}:

$$t_{length} = \frac{1}{\Delta f}$$

10. Determine the sampling frequency, f_s based on the highest frequency,

$$f_s = 10 \times f_{r,high}$$

11. Determine the receiver spacing, *S*, and source offset based on the criteria described in Section 4.6.2.

4.6.4 Illustrated Example of a Soil Profile

The following example is provided to illustrate the implementation of the guidelines of the HWAW method in the field at a typical soil site.

Example:

Consider a site with a desired profile depth of 30 m (step 1) and the shallowest required depth of 0.5m. The user estimates that V_S ranges between 200 m/s near the surface and 350m/s at the desired depth (step 2). This is an estimate to establish the data collection parameters.

Based on the desired depths of investigation and the shallowest depth of 0.5 m, the shortest wavelength, λ_{short} is 1 m (step 3) and the anticipated longest wavelength is 60 m (step 4). Therefore, the calculated low frequency using the estimated $V_{S,\,long}$ of 350 m/s and the expected λ_{long} of 60 m (step 5) will be:

$$f_{r,low} = \frac{V_{long}}{\lambda_{long}} = \frac{350}{60} = 5.8\ Hz$$

The highest sampling frequency based on the short wavelength of 1m (step 6):

$$f_{high} = \frac{V_{short}}{\lambda_{min}} = \frac{200}{1} = 200Hz$$

The calculated bandwidth based on the $f_{r,low}$ (step 7):

$$b_w = 0.1 \times f_{r,low} = 0.1 \times 5.8 = 0.58\ Hz$$

Based on a 3-point bandwidth, the frequency resolution (step 8),

$$\Delta f = \frac{0.58}{2} = 0.29\ Hz$$

Based on the calculated frequency resolution, Δf , the time length (step 9),

$$\therefore t_{length} = \frac{1}{\Delta f} = \frac{1}{0.29} \approx 3.5\ sec$$

The sampling frequency, f_s is set at 10 times the highest frequency (step 10),

$$\Delta t_s = 10 \times 200 = 2000\ samples/sec$$

Based on the criteria described in Section 4.6.2, the source offset should be equal to the desired profiling depth which is 30 m. Regarding the receiver spacing, a range of 4 m to 30 m can be used based on other considerations (step 11).

After running the test using the automated HWAW processing and generating the dispersion curve, the dispersion curve should be checked to see if the estimated velocities are consistent with the measurements. If large differences are observed the parameters should be adjusted and the test repeated.

4.7 Summary

This chapter presents the results and discussion from the processing of simulated surface wave data using the HWAW method at simple and complex geotechnical profiles. A validation study of the HWAW algorithm developed for this research was presented and corrections to the dispersion curve were described. Data collection and data processing parameters were investigated by applying the HWAW algorithm to simple sites. The effect of these parameters on the accuracy of the dispersion curve was discussed and acceptable values for the parameters were identified. The effect of Poisson's ratio on the effectiveness of the HWAW was examined and the consistency between the HWAW and the theoretical dispersion curves were evaluated quantitatively. The results of applying the HWAW method at complex sites were presented and comparisons of HWAW and theoretical dispersion curves were presented. The use of HWAW processing on data collected using the conventional SASW data collection procedures was investigated and the consistency between the HWAW-derived and the SASW-derived dispersions curves was evaluated. It was found that the HWAW processing method can be effectively applied to SASW data. Finally, guidelines based on the results of the simulated surface wave data processing using the HWAW method were developed and presented, along with an example.

CHAPTER 5 Field Validation of the HWAW Method

5.1 Introduction

The final stage of this research used field data to validate the findings from some of the numerical simulations presented in Chapter 4. The field study used data collected at a local field site (Site 1) as well as existing shared-use data collected by other researchers (Site 2 and Site 3). The results from the three field sites are presented below.

5.2 Site 1: Very High Impedance Contrast Site – University of Missouri

Site 1 was chosen because the boring log at this location (Boring B7) indicated shallow soil underlain by hard limestone rock, as shown in the boring log in Figure 3.12. The thickness of the soil at this location is 2.68 m. The estimated V_S of the soil based on measurements in this area is approximately 150 m/s and the estimated V_S of the rock based on laboratory measurements of cores is at least 1500 m/s. Therefore, this site has an impedance ratio of at least 10 and classifies as a soft-over-stiff site with a very high impedance contrast. The primary objective of this field study was to verify that HWAW processing could accurately recover the mode transition expected at this site.

5.2.1 SASW Data Collection and Interpretation

Measurements were performed using typically SASW data collection pairs, as shown in Table 3.11. The data were processed using both the conventional SASW phase unwrapping method as well as the automated HWAW processing approach. The phase plots for each of the receiver pairs used to generate the dispersion curve are presented in Figure 5.1. A walk through of the phase unwrapping issues at this site are presented and explained in this section.

Typically, the interpretation of these phase plots involves masking out near field conditions (typically the first 180 degrees of phase) at low frequencies and excluding high-frequency data that are noisy or do not follow a clear “saw-tooth” trend. These masked regions are shaded in Figure 5.1, indicating they were not used in the interpretation. This process relies on the judgement and experience of the analyst and is subject to errors. The unwrapping interpretation applied to these data is indicated in Figure 5.1 with the number above each phase jump indicating the interpreted number of cycles. In this case insufficient energy was available to generate usable phase data at low frequencies for the longest receiver spacing (Figure 5.1f), so these data was not used.

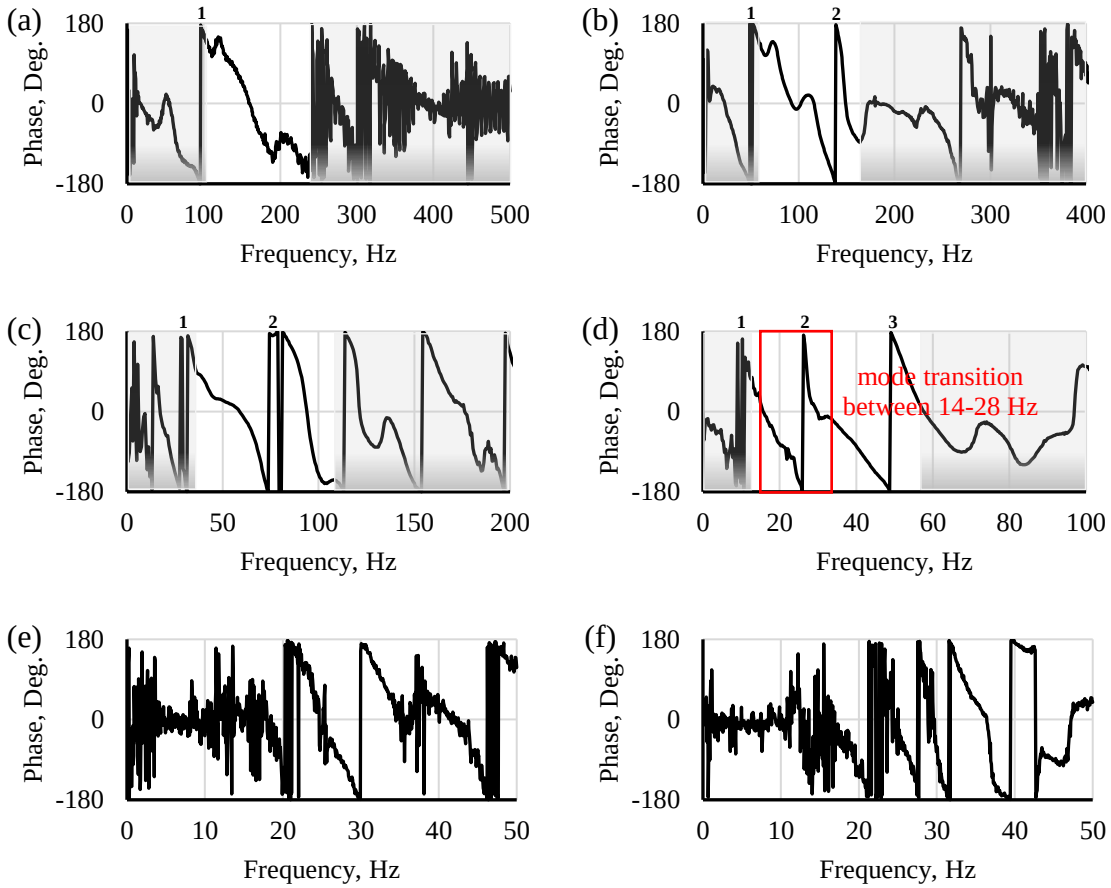

Figure 5.1 Incorrect interpretation for the wrapped phase plots calculated from the six receiver pairs of SASW measurements at Site 1 with receiver spacings pairs of (a) 0.61-1.22 m, (b) 1.22-2.44 m, (c) 2.44-4.88 m, (d) 4.57-9.14 m, (e) 9.14-18.28 m, and (f) 12.20-24.40 m. Phase unwrapping interpretation is indicated by number of 360° "jumps." Data not used in interpretation are indicated by shaded regions.

Note that the phase plot for the receiver pair at 4.57 m and 9.14 m presents a clear sawtooth pattern that is reasonably interpreted as the 1st, 2nd cycle, and 3rd cycles of phase (Figure 5.1d). The unwrapped phase using the interpretation shown in Figures 5.1 was used to develop the dispersion curve presented in Figure 5.2

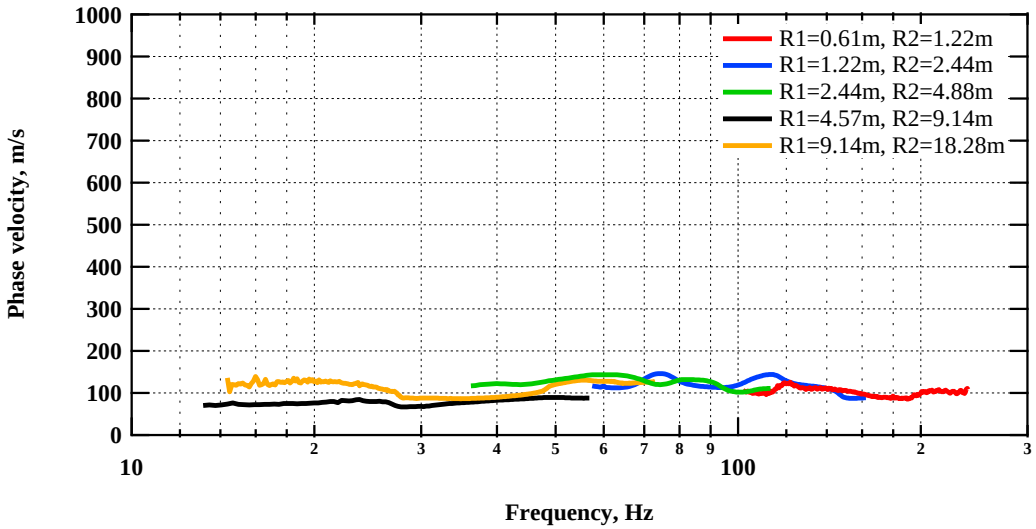

Figure 5.2 Phase velocity dispersion curve developed from the unwrapping of phase plots shown in Figure 5.1 for Site1.

The resulting dispersion curve for Site 1 erroneously indicates a uniform, low velocity material with no indication of the shallow stiff rock. It is easy to see how SASW phase data could be reasonably interpreted and create an erroneous dispersion curve.

The same data were processed using the HWAW approach (much like what was done in Chapter 4 using synthetic data) which produced the dispersion curve shown in Figure 5.3.

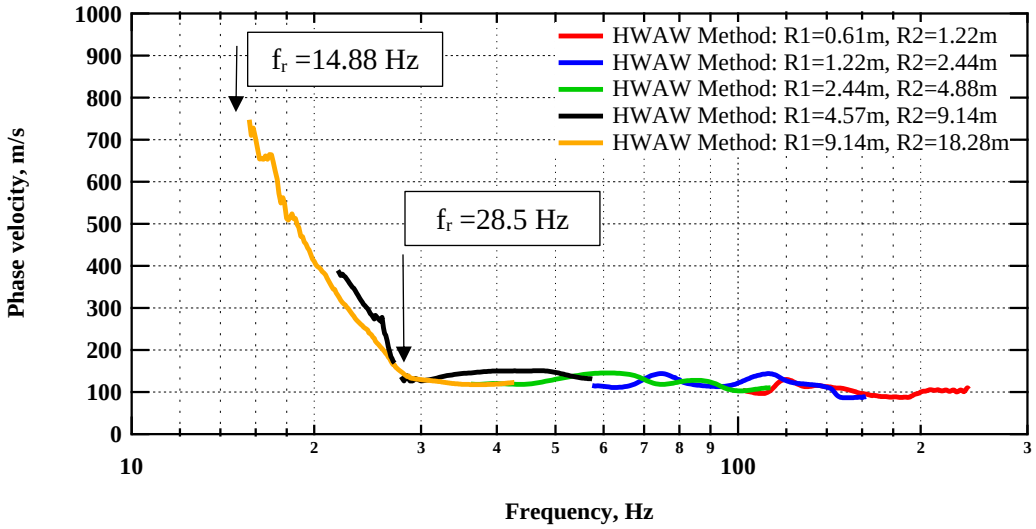

Figure 5.3 Phase velocity dispersion curves using the HWAW method to process the SASW data for Site1.

The HWAW dispersion curve is the same as the phase unwrapped dispersion curve for the three smallest receiver spacings. However, the dispersion curve from the HWAW processing clearly and correctly recovers the transition to a higher mode at frequencies below 28.0 Hz.

As noted in Chapter 4, the transition frequencies for stiff-over-soft sites can be estimated from the resonant frequencies of compression and shear waves. The V_S is approximately 150 m/s (based on the shallow dispersion data) and the thickness of the soil from the borehole log is 2.68 m. Assuming a Poisson's ratio of 0.33 for the soil, the calculated V_P is 297.78 m/s and using Equation 4.6 in Section 4.4.2.5, the transition is expected to be in the range of 14.0 Hz to 27.78 Hz which is consistent with what is observed in the experimental results.

The HWAW method is able to provide the correct result where phase unwrapping fails because the HWAW processing operates on each frequency independent of the others, whereas the SASW phase unwrapping requires knowledge of the number of cycles (i.e. phase jumps) at lower frequencies. When there is an abrupt transition to a higher mode the phase unwrapping method cannot be easily applied. The phase interpretation for receiver spacings of 0.61m-1.22 m, 1.22m-2.44m, and 2.44m-4.88m were correct because these dispersion curves are continuous. However, the phase plots from the receiver pairs at 4.57m-9.14m, and 9.14m-18.28m included a section containing the abrupt mode jump. The red rectangle in Figure 5.1d shows the transition to a higher mode that occurs over the frequency range of 14.0 Hz to 28.0 Hz. Because of the abrupt transition occurring at 14.0 Hz, it is invalid to interpret the unwrapped phase at frequencies above 14.0 Hz based on a single unwrapping of the phase plot. Instead, the correct interpretation requires unwrapping

the two sections of the phase plot separately, as shown in Figures 5.4 and 5.5 for the receiver pairs 4.57m-9.14m, and 9.14m-18.28m, respectively. When these phase plots are unwrapped as two modes the dispersion curve comes into agreement with the dispersion curve generated from the HWAW processing.

The full, correctly interpreted phase unwrapping is shown in Figure 5.6. It is important to note that this phase unwrapping interpretation is only possible in hindsight knowing the presence and depth of the limestone layer. Without this prior knowledge this site would likely be misinterpreted.

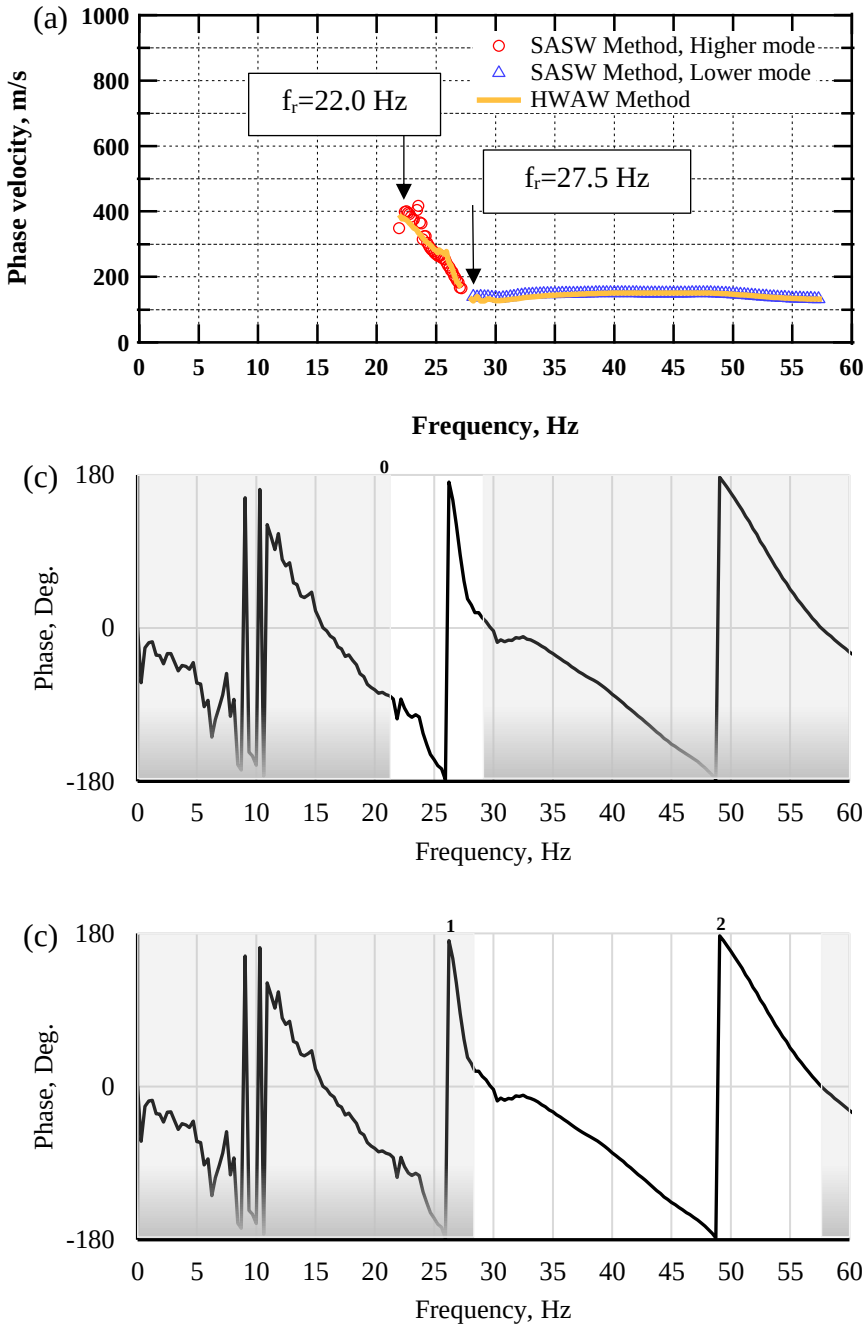

Figure 5.4 Correct interpretation of the 4.57-9.14 m receiver pairs phase data at Site 1 showing (a) the higher mode transition between 21.88 Hz and 27.8 Hz, (b) phase unwrapping of the higher mode between 21.88 and 27.1 Hz, and (c) phase unwrapping of the lower mode between 27.8 and 57.5 Hz. Data not used in interpretation are indicated by shaded regions.

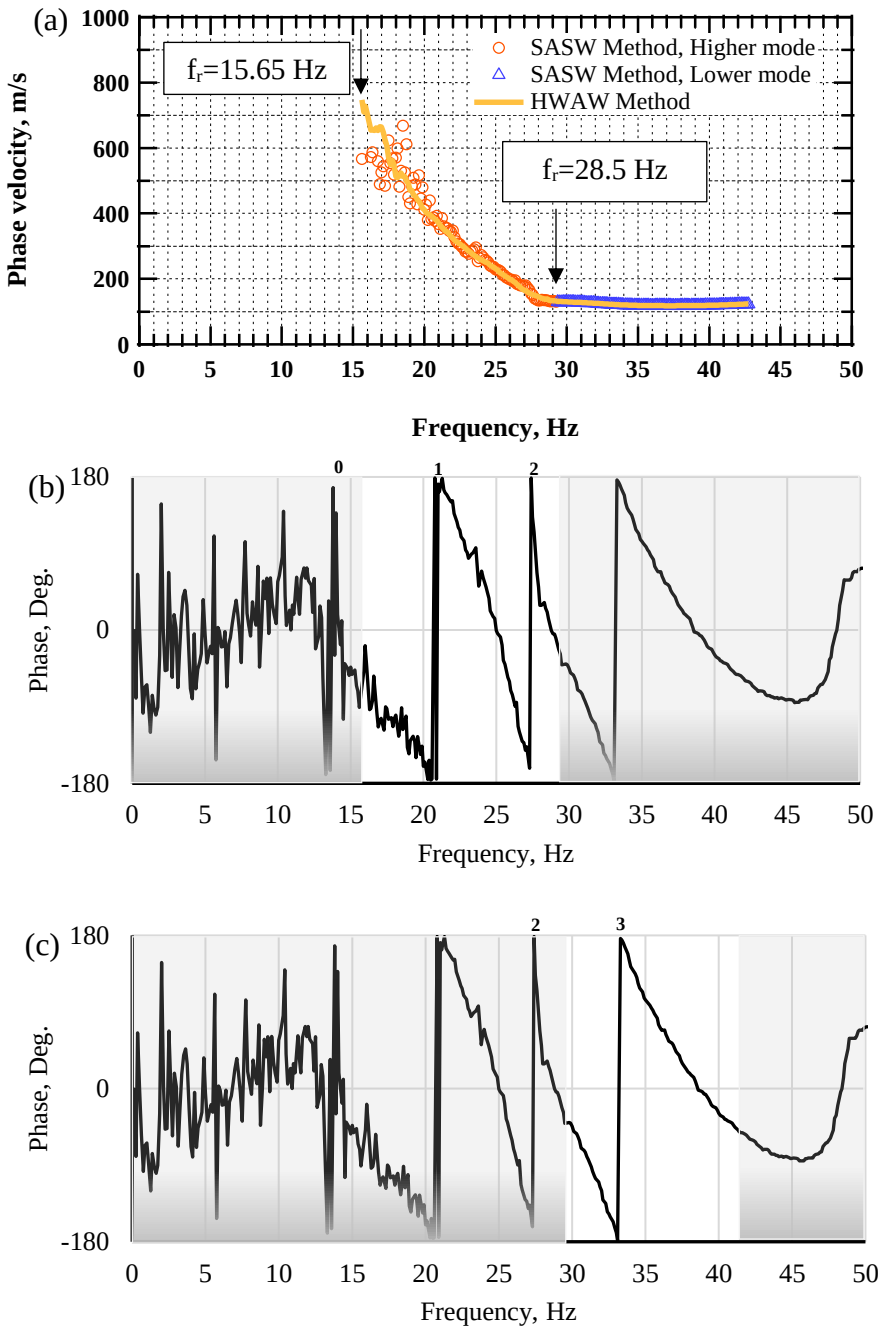

Figure 5.5 Correct interpretation of the 9.14 m-18.28 m receiver pairs phase data for Site1 showing (a) the higher mode transition between 14.88 Hz and 28.25 Hz, (b) phase unwrapping of the higher mode between 14.88 and 28.25 Hz, and (c) phase unwrapping of the lower mode between 28.25 and 42.88 Hz. Data not used in interpretation are indicated by shaded regions.

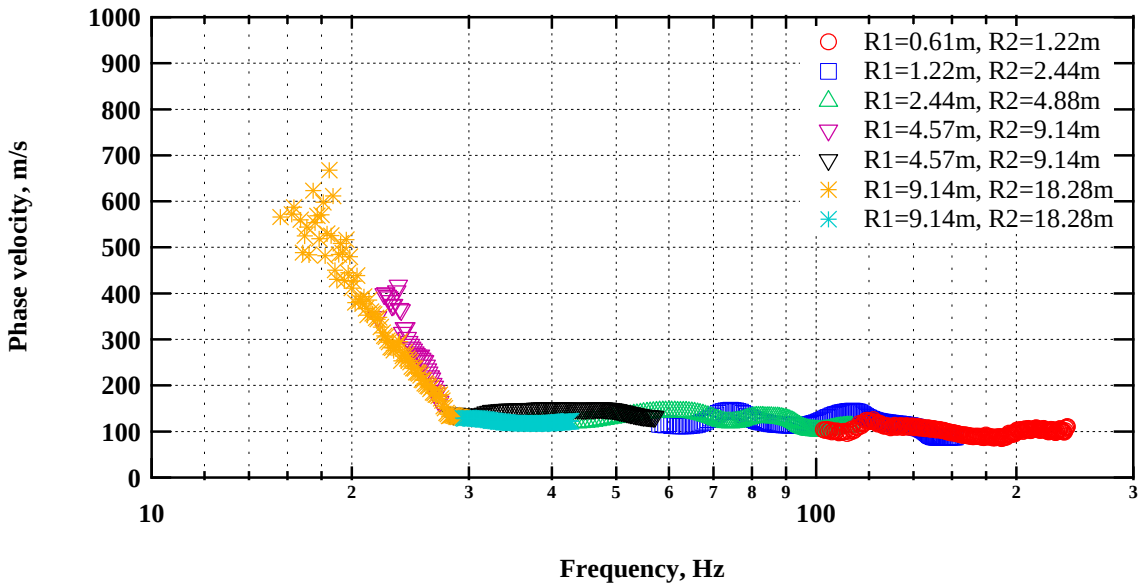

Figure 5.6 Phase velocity dispersion curves using the SASW method for Site 1 based on the correct interpretation of phase plots.

The dispersion curve comparisons between the correct SASW dispersion curve and the dispersion curve obtained by processing the SASW data with the HWAW method over the same frequency ranges are presented individually for each receiver pair in Figure 5.7. In all cases, the HWAW produces a dispersion curve that is consistent with the correctly interpreted phase unwrapped dispersion curve. It is also notable that the dispersion curve from HWAW is much less noisy than the phase unwrapped dispersion curve at the longest receiver spacings where energy levels are lowest (Figure 5.7f). This indicates that HWAW processing is better able to handle noisy data as compared to conventional SASW phase unwrapping.

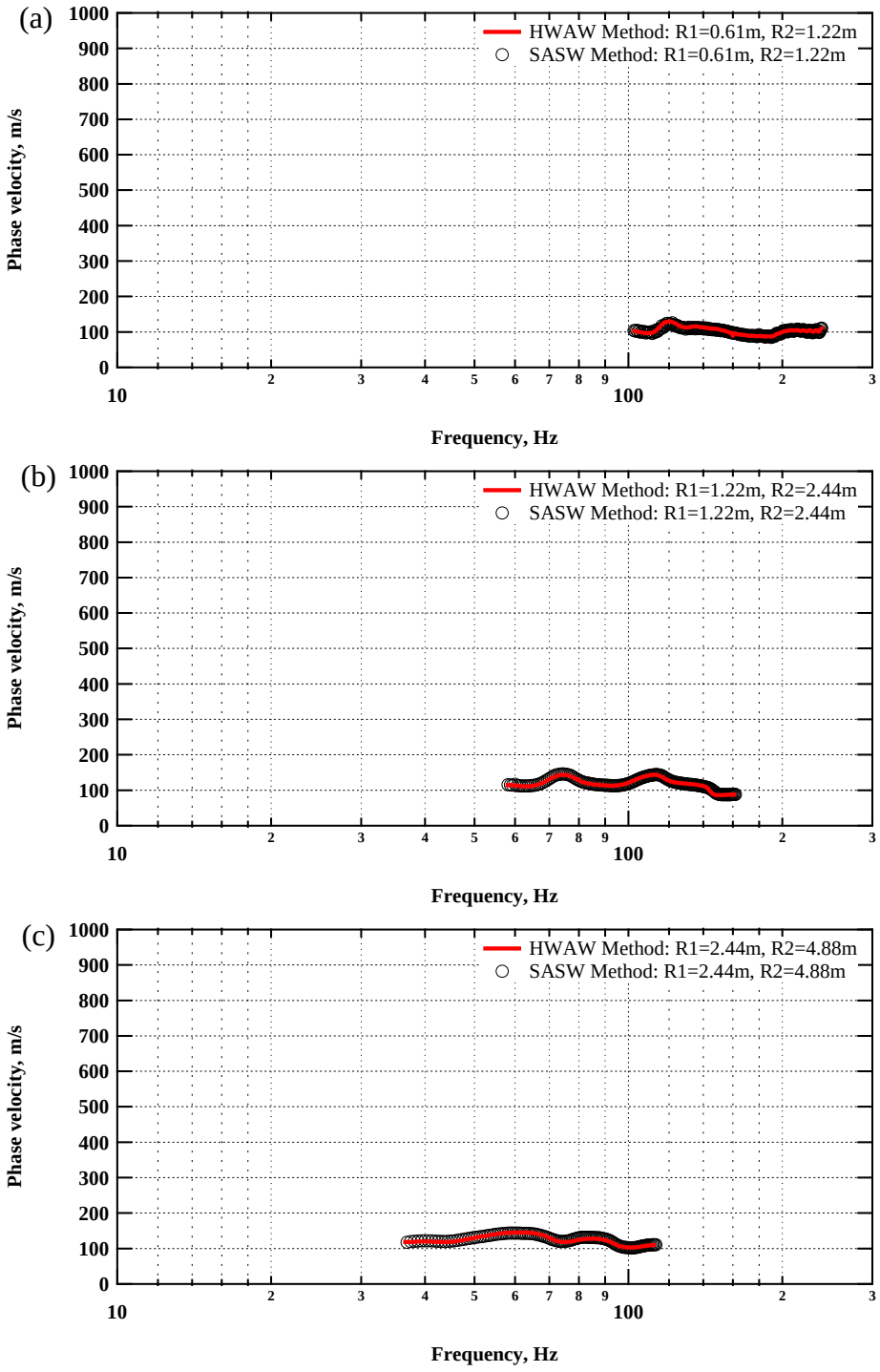
(a)
HWAW Method: R1=0.61m, R2=1.22m
SASW Method: R1=0.61m, R2=1.22m
Phase velocity, m/s
Frequency, Hz
(b)
HWAW Method: R1=1.22m, R2=2.44m
SASW Method: R1=1.22m, R2=2.44m
Phase velocity, m/s
Frequency, Hz
(c)
HWAW Method: R1=2.44m, R2=4.88m
SASW Method: R1=2.44m, R2=4.88m
Phase velocity, m/s
Frequency, Hz

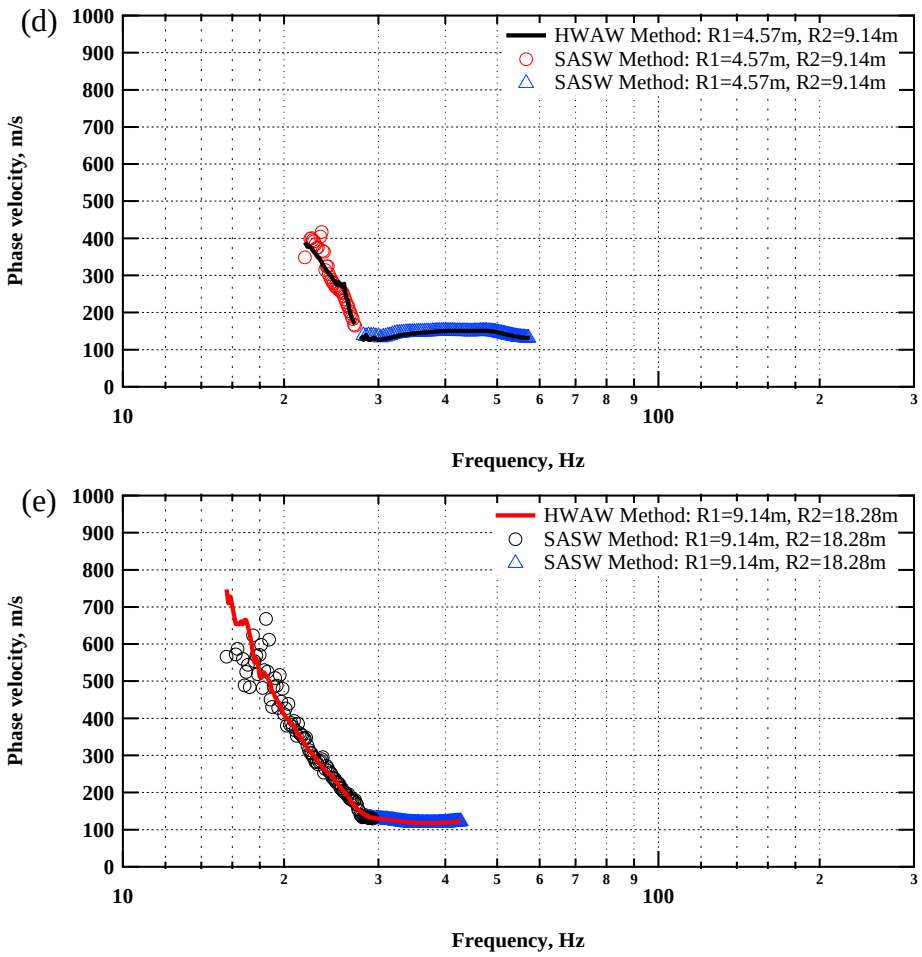

Figure 5.7 Comparison of the dispersion curves from Site 1 obtained by the SASW method and by processing the time records of SASW data by the HWAW method for receiver pairs: (a) 0.61-1.22 m, (b) 1.22-2.44 m, (c) 2.44-4.88 m, (d) 4.57-9.14 m, (e) 9.14-18.28 m.

The main finding from the analysis of Site 1 is that the HWAW method is able to deal with the mode transition where the SASW phase unwrapping fails. This result is consistent with the findings from the simulated data for soft-over-stiff sites presented in Section 4.5 and supports the use of HWAW to process SASW data. Secondly, the use of real field data demonstrated that the HWAW method is better able to handle noisy data than SASW phase unwrapping.

5.2.2 HWAW Data Collection and Interpretation

Time records were also recorded at Site 1 using an HWAW-type arrangement consisting of a single array with a short receiver spacing of 4 m and source offsets of 8, 12 and 16 m. Phase velocity dispersion curves developed by HWAW processing of this data are presented in Figure 5.8. The correctly interpreted dispersion curves from the SASW testing arrangement are also shown in these figures for comparison. It is expected that these dispersion curves would not be in perfect agreement with the SASW curves since they were collected at different locations relative to the source and contributions from body waves and near field effects are different.

However, these results show that reasonable dispersion curve were obtained in all cases and the mode transition at low frequencies was correctly identified. The only significant deviation was at frequencies about 100 Hz, which corresponds to short wavelengths (less than 1 m) which are not of interest in most cases. It should be noted that much of this low-frequency data is in the near field and the utility for inverting deep V_S profiles needs to be investigated as part of a future study.

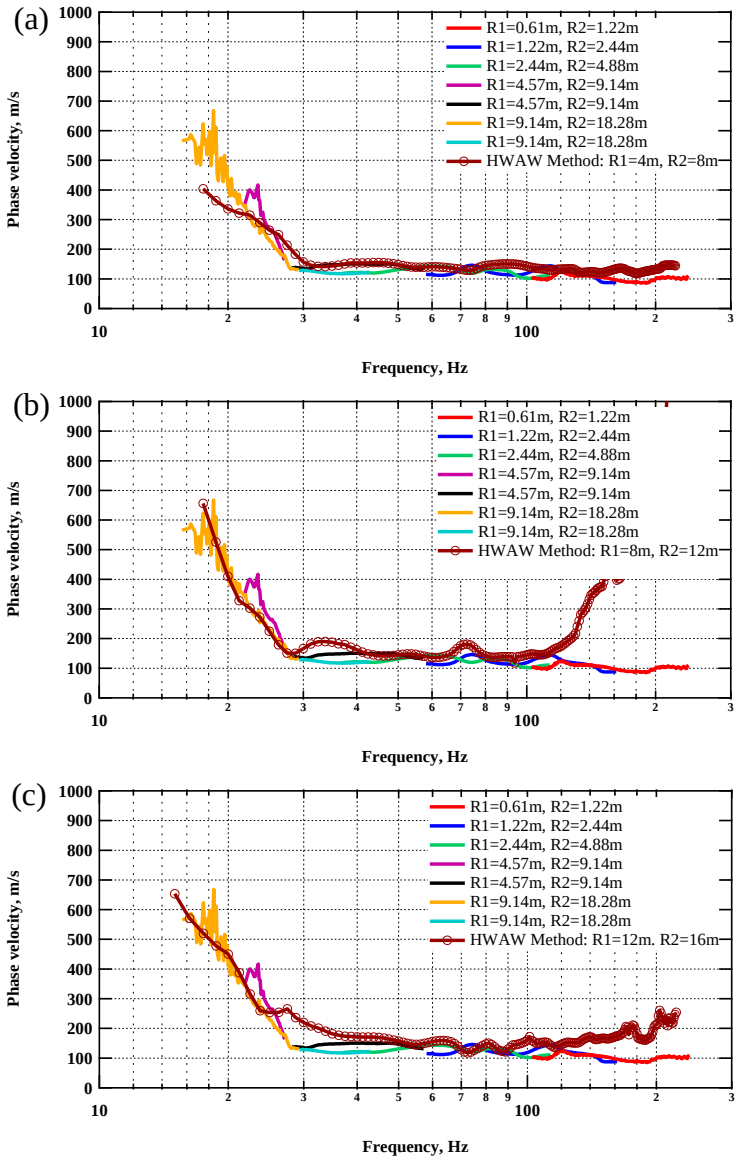

Figure 5.8 Comparison of dispersion curves obtained by the SASW and the HWAW method with short test setup for Site 1.

5.3 Site 2: Low Velocity Saturated Soil– Christchurch, New Zealand

Site 2 was chosen because it is a site consisting of soft, saturated soils with no large near-surface impedance interfaces. Therefore, it is a simple site in terms of the V_S profiles but saturated, meaning the Poisson's ratio is high. The two objectives of this portion of the study were to: (1) validate that the HWAW processing could be applied successfully to the SASW data and (2) validate the observations from the study with simulated data showing large fluctuations in the dispersion curve when using close receivers spacings at saturated sites.

5.3.1 SASW Data Collection and Interpretation

Data were analyzed from this site using source offsets and receiver pair spacings consistent with SASW data collection procedures, as shown in Table 3.13. The wrapped phase plots calculated from each of the receiver pairs used in the analysis are presented in Figure 5.9. The dispersion curves developed from phase unwrapping of the SASW data test using the sledge hammer and Vibroseis sources are presented in Figure 5.10.

In Figure 5.9, the 180° filtering criteria was again used to mask near field effects. However, in some cases the masking extends beyond 180 degrees due to poor quality signals, as shown in Figures 5.9b, 5.9c. Data from the 40 m and 66 m receiver pairs did not produce interpretable phase plots with the sledgehammer source so they were not used.

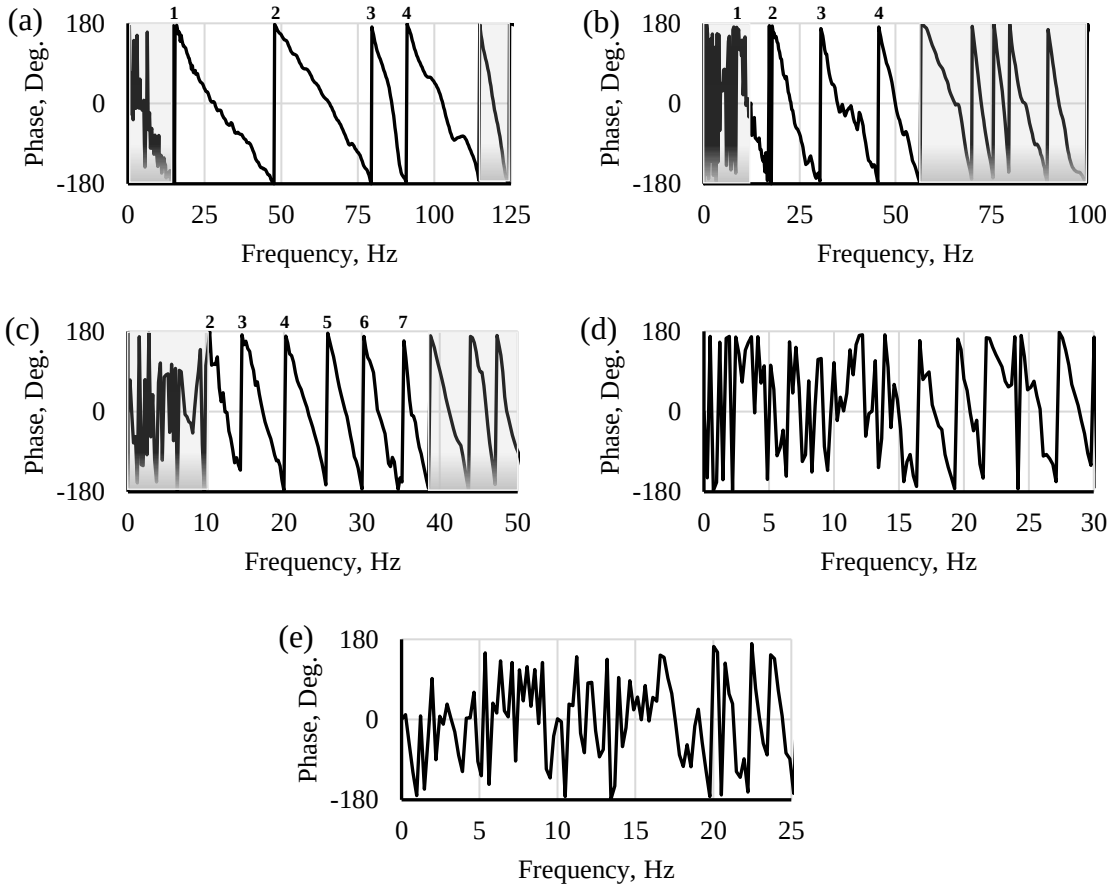

Figure 5.9 Wrapped phase plots calculated from the five receiver pairs of SASW measurements at Site 2 with receiver spacing pairs of (a) 5m-9m, (b) 10m-20m, (c) 20m-40m, (d) 40m-80m, and (e) 66m-132m. Phase unwrapping interpretation is indicated by number of 360° "jumps." Data not used in interpretation are indicated by shaded regions.

Therefore, the receiver spacings of 5m-9m, 10m-20m, and 20m-40m with the sledgehammer source were used to generate the experimental dispersion curve, as shown in Figure 5.10. To provide data at lower frequencies, data generated from the Vibroseis source using a 40 m receiver pair was analyzed which extended the dispersion curve to frequencies below 10 Hz. The phase unwrapping shown in Figure 5.9 produced dispersion curves that are consistent with the expected site conditions. Conventional SASW phase unwrapping worked correctly at this site because this simple site condition produces a continuous dispersion curve with no abrupt mode transitions. However, the 20m-40m pair

recorded from the sledgehammer source produced noisy phase data and a somewhat scattered dispersion curve due to the noise contributions.

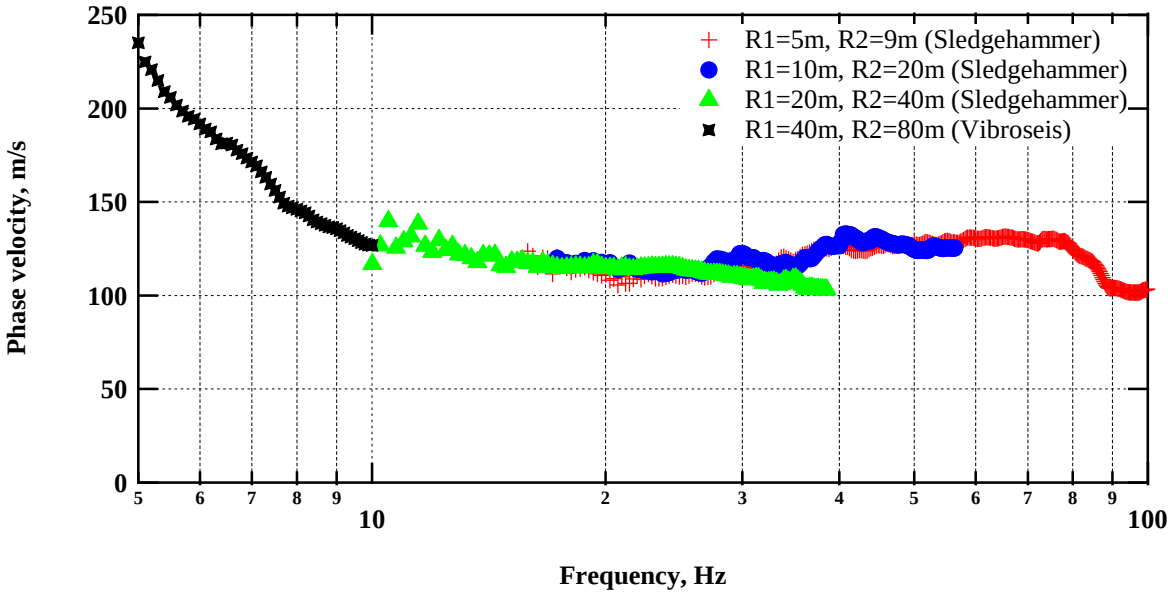

Figure 5.10 Experimental dispersion curves developed from SASW phase unwrapping using active source measurements data performed by sledgehammer and Vibroseis for Site 2.

Comparisons of HWAW-processed dispersion curves to the SASW phase unwrapped dispersion curves are shown over the same frequency ranges for receiver pairs of 4m-9m, 10m-20m, and 20-40m in Figure 5.11. In each case the HWAW automated phase unwrapping produced the same dispersion curve as the manual SASW phase unwrapping. In addition, as was observed at Site 1, the HWAW processing performed better with noisy data, as is apparent from the 20m-40m receiver pair data in Figure 5.11c.

These results confirm that the HWAW method provides an automated means to develop dispersion curves from SASW data. The results also show that HWAW processing performs better than phase unwrapping for noisy data (i.e. low energy) conditions.

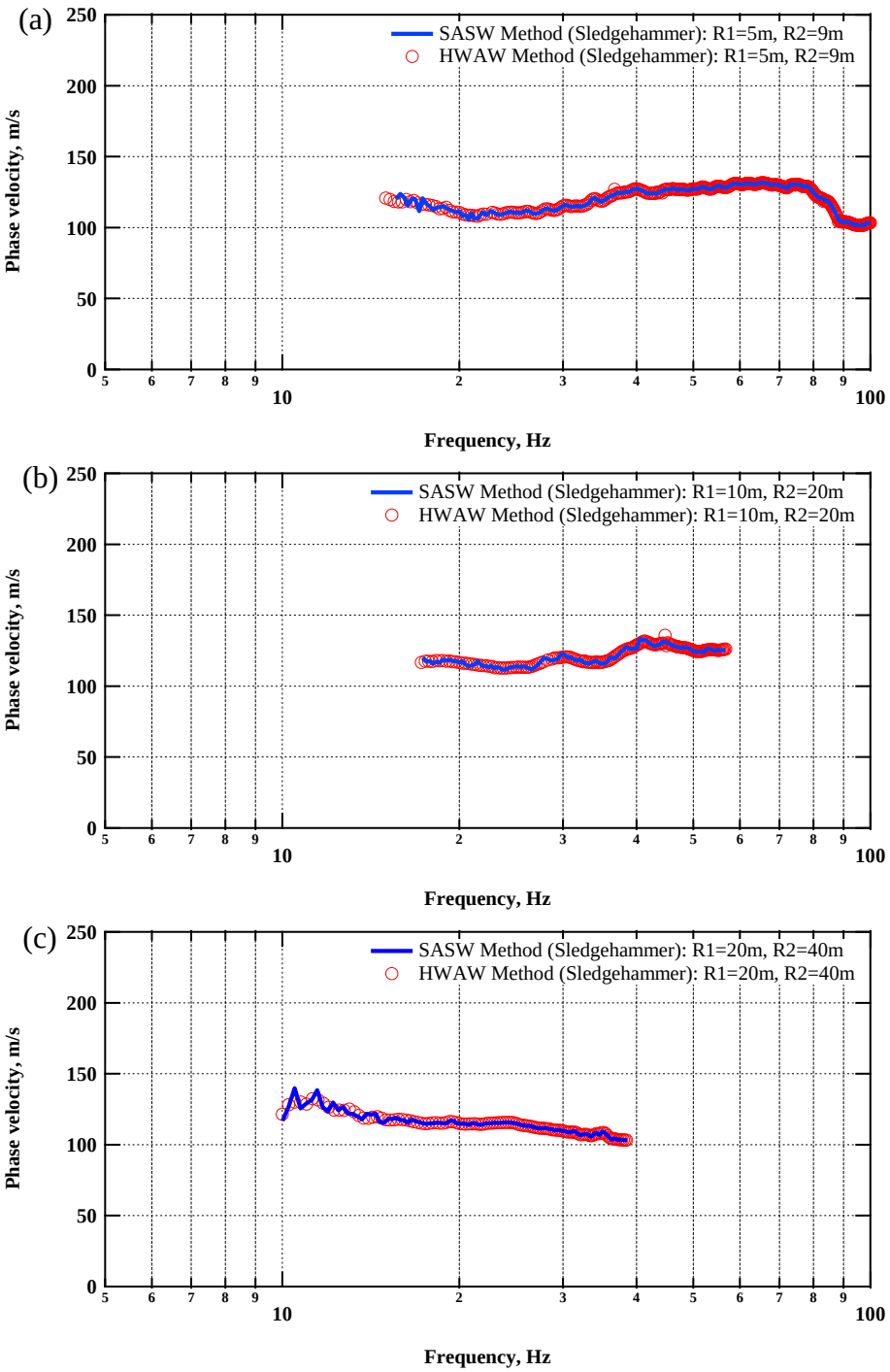

Figure 5.11 Comparison of the dispersion curves obtained using SASW phase unwrapping and HWAW processing of the SASW data for Site 2 with receiver pairs of: (a) 4m-9m, (b) 10m-20m, and (c) 20m-40m.

To further investigate the ability of HWAW processing to handle noisy data, phase unwrapping was extended into more of the low-frequency range where the SASW phase

showed significant scatter due to noise. Figures 5.12, 5.13, and 5.14 show the extended phase range considered and the resulting dispersion curve comparisons for the 5m-9m, 10m-20m, and 20m-40m receiver pairs, respectively. For the 5m-9m and 10m-20m pairs the HWAW processing extended the range of the dispersion curve significantly and was in general agreement with the dispersion data from the high-energy Vibroseis source. However, dispersion curves for the 20m-40m pair did not improve, suggesting that energy levels were too low for either method.

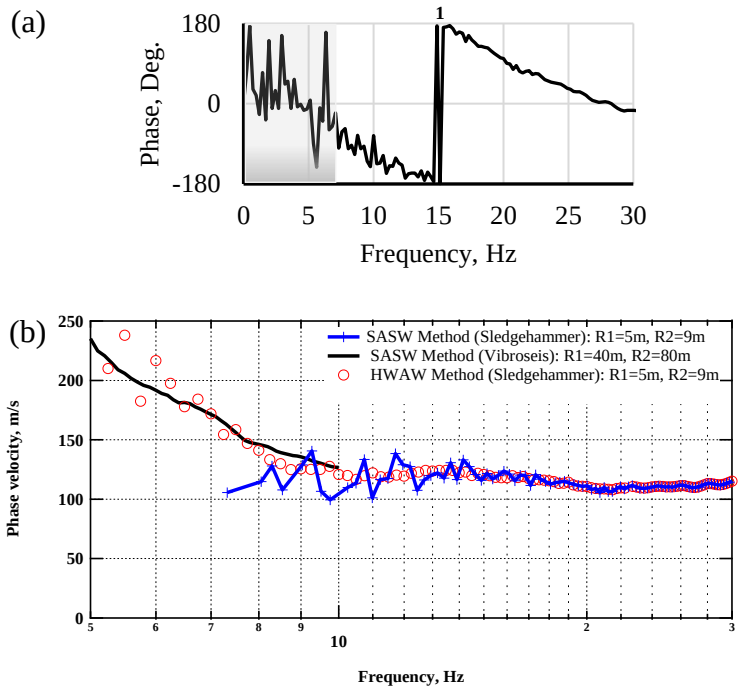

Figure 5.12 Phase velocity dispersion curves using SASW and HWAW methods by extending the low frequency range for receiver pairs of 5m-9m.

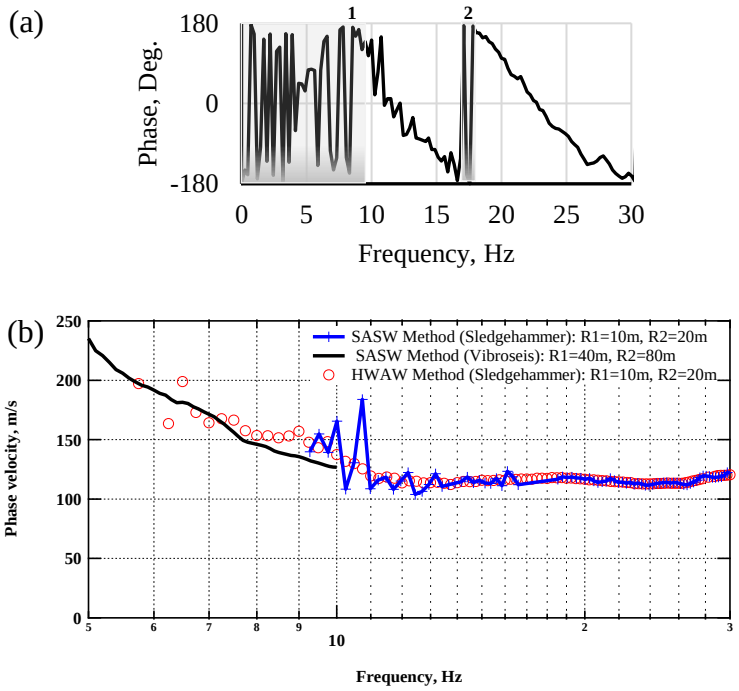

Figure 5.13 Phase velocity dispersion curves using SASW and HWAW methods by extending the low frequency range for receiver pairs of 10m-20m.

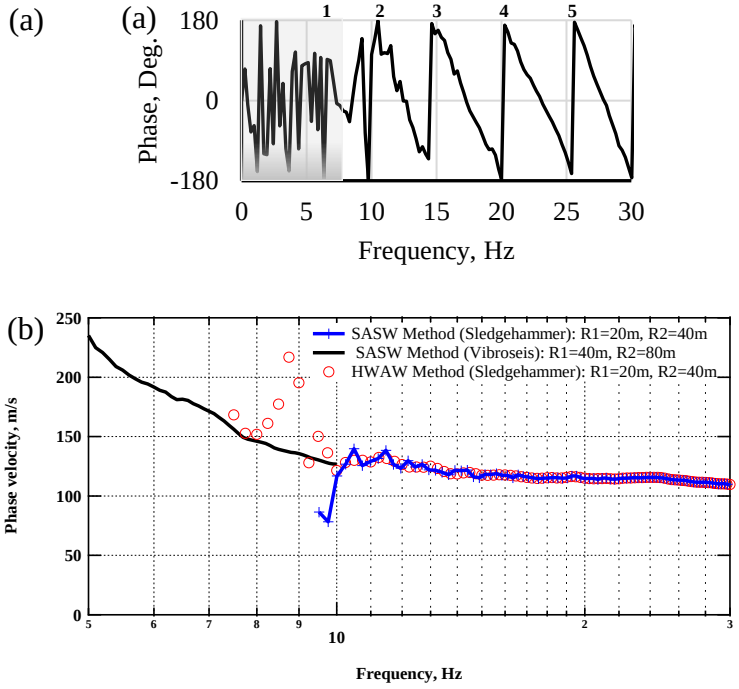

Figure 5.14 Phase velocity dispersion curves using SASW and HWAW methods by extending the low frequency range for receiver pairs of 20m-40m.

5.3.2 HWAW Data Collection and Interpretation

The typical HWAW data collection procedure is to use a single pair of receivers that are closely spaced (typically only a few meters). The study using simulated data showed that at saturated sites this testing configuration produced dispersion curves with large fluctuations, apparently due to body wave contributions. The second objective of this field study was to validate the observation from the simulated data study by analyzing data collected with a range of source offset and receiver pair spacings.

The various HWAW test setups used at this site are presented in Table 3.13. The dispersion curves obtained from these test setups are shown in Figures 5.15 to 5.19. Dispersion curves obtained from various investigators using different surface wave methods are shown in for comparison (Cox et al., 2014).

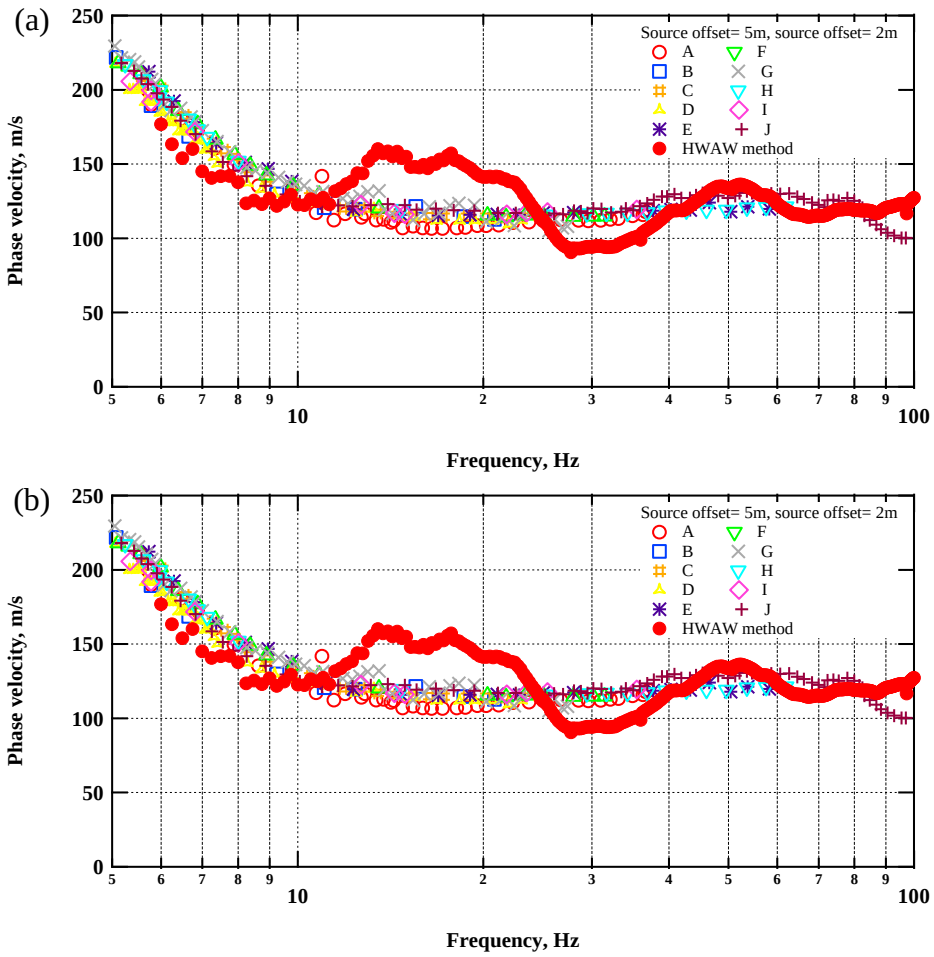

Figure 5.15 Comparison of surface wave dispersion curves from several analysts using various methods with the HWAW method for: (a) receiver spacing of 2m and source offset of 5m, and (b) receiver spacing of 4m and source offset of 5m. The letters A through J indicate different analysts as presented in Cox et al. (2014).

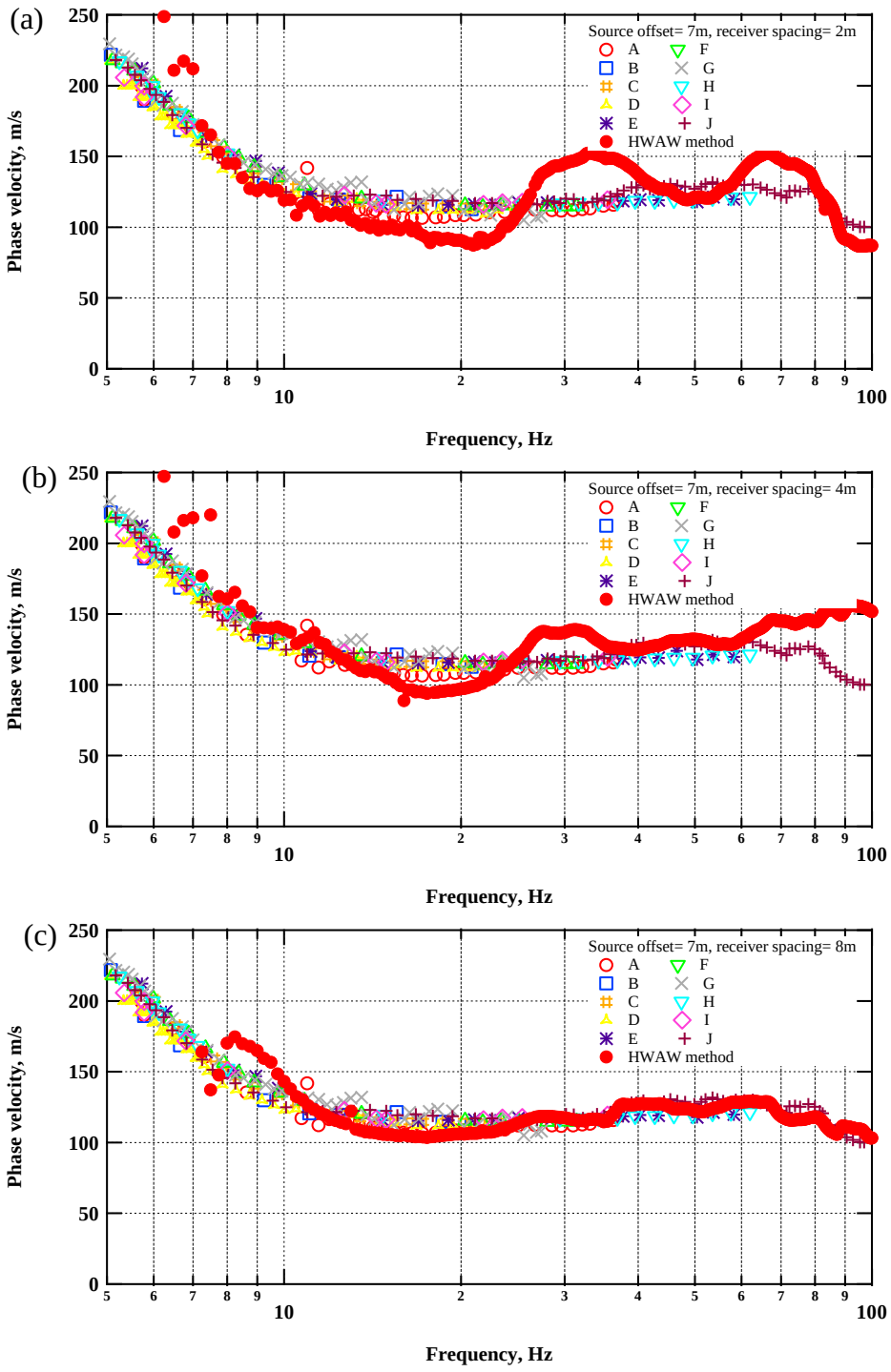

Figure 5.16 Comparison of surface wave dispersion curves from several analysts using various methods with the HWAW method for: (a) receiver spacing of 2m and source offset of 7m, (b) receiver spacing of 4m and source offset of 7m, and (c) receiver spacing of 8m and source offset of 7m. The letters A through J indicate different analysts as presented in Cox et al. (2014).

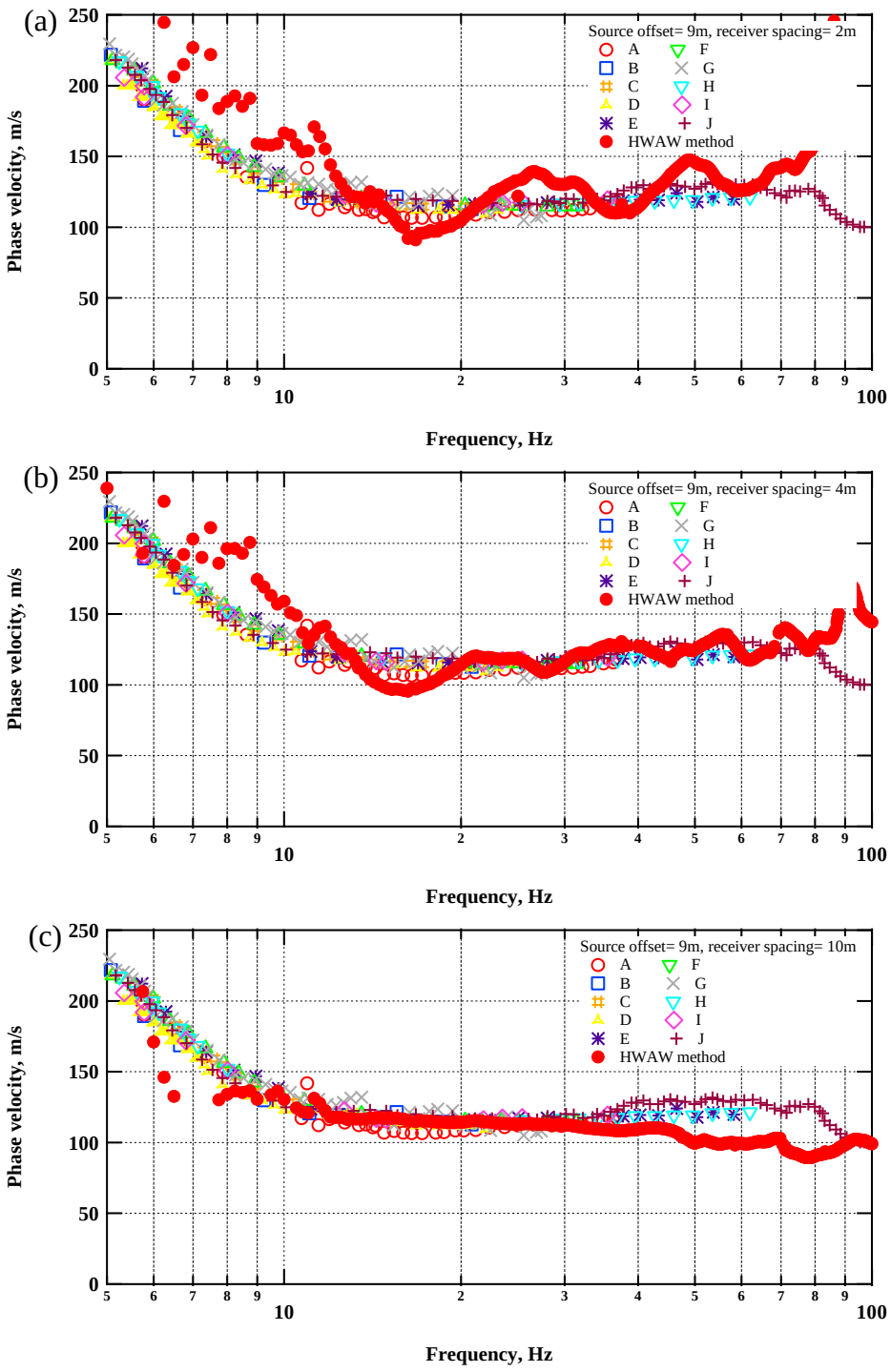

Figure 5.17 Comparison of surface wave dispersion curves from several analysts using various methods with the HWAW method for: (a) receiver spacing of 2m and source offset of 9m, (b) receiver spacing of 4m and source offset of 9m, and (c) receiver spacing of 10m and source offset of 9m. The letters A through J indicate different analysts as presented in Cox et al. (2014).

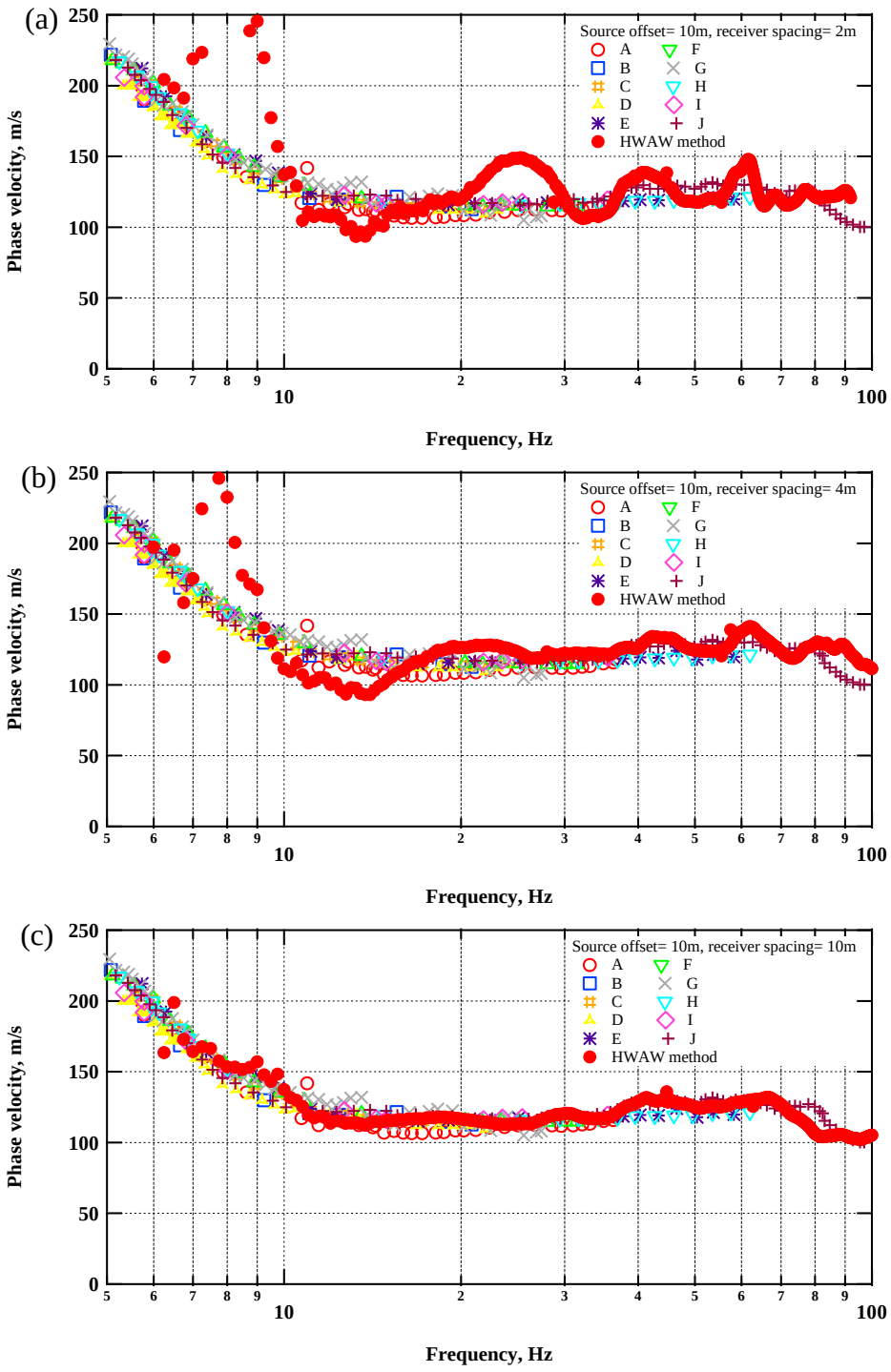

Figure 5.18 Comparison of surface wave dispersion curves from several analysts using various methods with the HWAW method for: (a) receiver spacing of 2m and source offset of 10m, (b) receiver spacing of 4m and source offset of 10m, and (c) receiver spacing of 10m and source offset of 10m. The letters A through J indicate different analysts as presented in Cox et al. (2014).

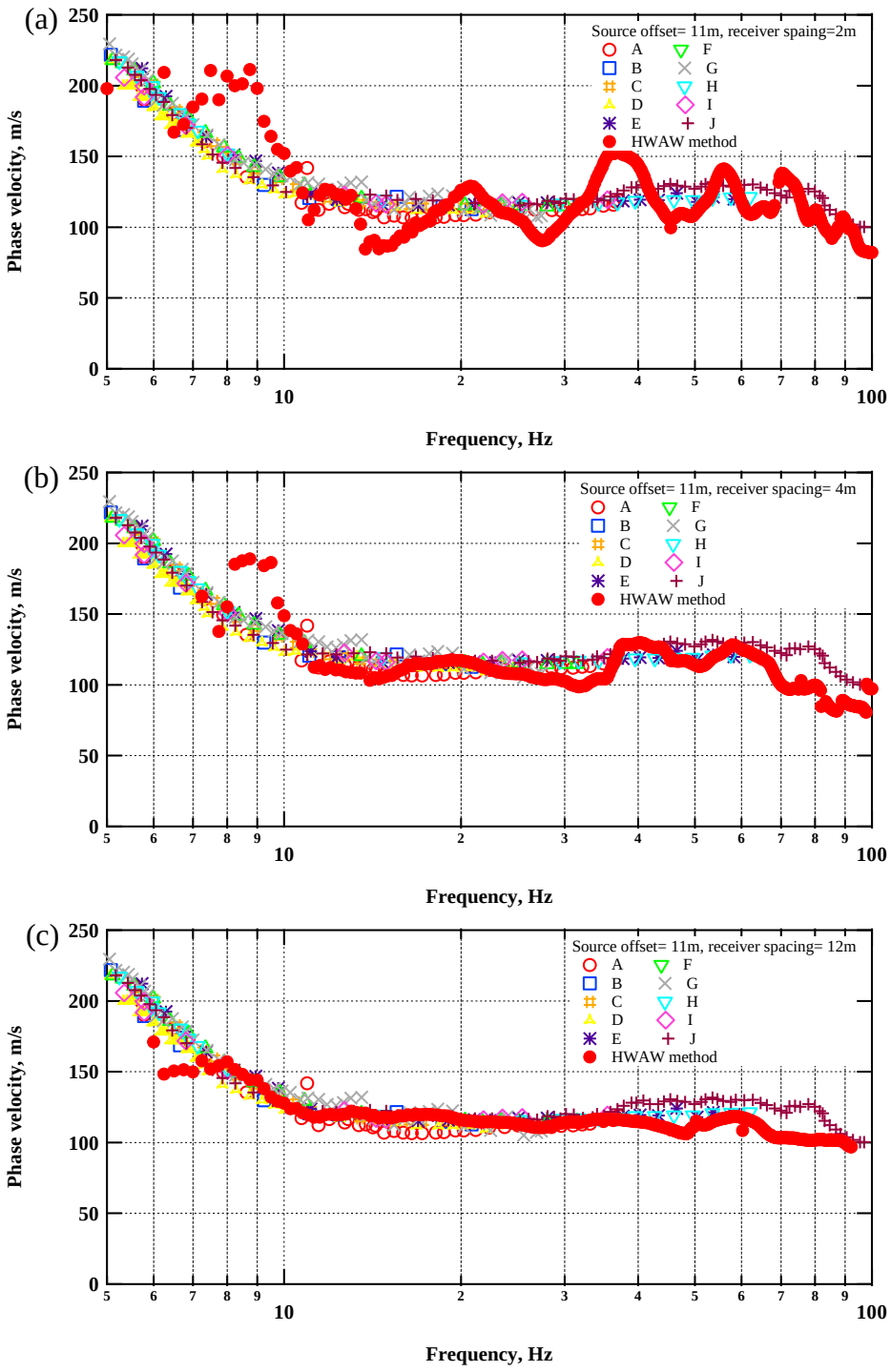

Figure 5.19 Comparison of surface wave dispersion curves from several analysts using various methods with the HWAW method for: (a) receiver spacing of 2m and source offset of 11m, (b) receiver spacing of 4m and source offset of 11m, and (c) for receiver spacing of 12m and source offset of 11m. The letters A through J indicate different analysts as presented in Cox et al. (2014).

The dispersion curves in Figures 5.14 to 5.18 show that when the source offset and receiver spacing were kept about equal, a smooth dispersion curve was obtained that was generally consistent with the dispersion curves obtained by the other analysts, as presented in Cox et al. (2014). However, when a smaller receiver spacing relative to the source offset was used, large fluctuations in the dispersion curve were observed. This supports the observation from the study using simulated data that the receiver spacing has an impact on the shape of the dispersion curve when measurements are performed at saturated sites.

This information can be useful, as it can be used to identify that the site is saturated (which is often not known beforehand). However, it can also be detrimental in that inverting these highly fluctuating dispersion curves may be more difficult. Therefore, for known saturated site conditions, the use of short receiver spacing is discouraged due to fluctuations in the dispersion curves caused by strong contributions of body waves. The results from this site support the SASW data collection approach of using equal source offset and receiver pair spacings to minimize fluctuations in the dispersion curve. It is interesting to note that in this case, the single setup using 10m-10m spacing with a sledge hammer source and HWAW processing produced a dispersion curve over a broad frequency range from about 7 Hz to 100 Hz (wavelengths from 1 m to 23.5 m) that was consistent with both the sledgehammer data and Vibroseis data. This suggests that in many cases, fewer test setups may be required to cover the necessary wavelength range than are currently used in the conventional SASW testing methodology.

5.4 Site 3: Moderate Impedance Contrast-Boise, Idaho

This site was chosen because it was thought to represent a profile condition with a moderate impedance contrast (~2) such that no mode transition was anticipated. This was based on nearby ground truth information obtained from downhole measurements. The main objectives of this portion of the study were to validate that HWAW processing could be successfully applied to SASW data and that the HWAW data collection approach produced dispersion curves that are consistent with the known site conditions.

5.4.1 SASW Data Collection and Interpretation

Data were analyzed from this site using source offsets and receiver pair spacings consistent with SASW data collection procedures, as shown in Table 3.14. The wrapped phase plots calculated from the six receiver pairs: 5 m-11 m, 7 m-15 m, 11 m-23 m, 13 m-27 m, 15 m-31 m, and 17 m-35 m are presented in Figure 5.19. As described above, portions of the phase plot that were not used in the interpretation (i.e. masked) are shown as shaded in Figure 5.20.

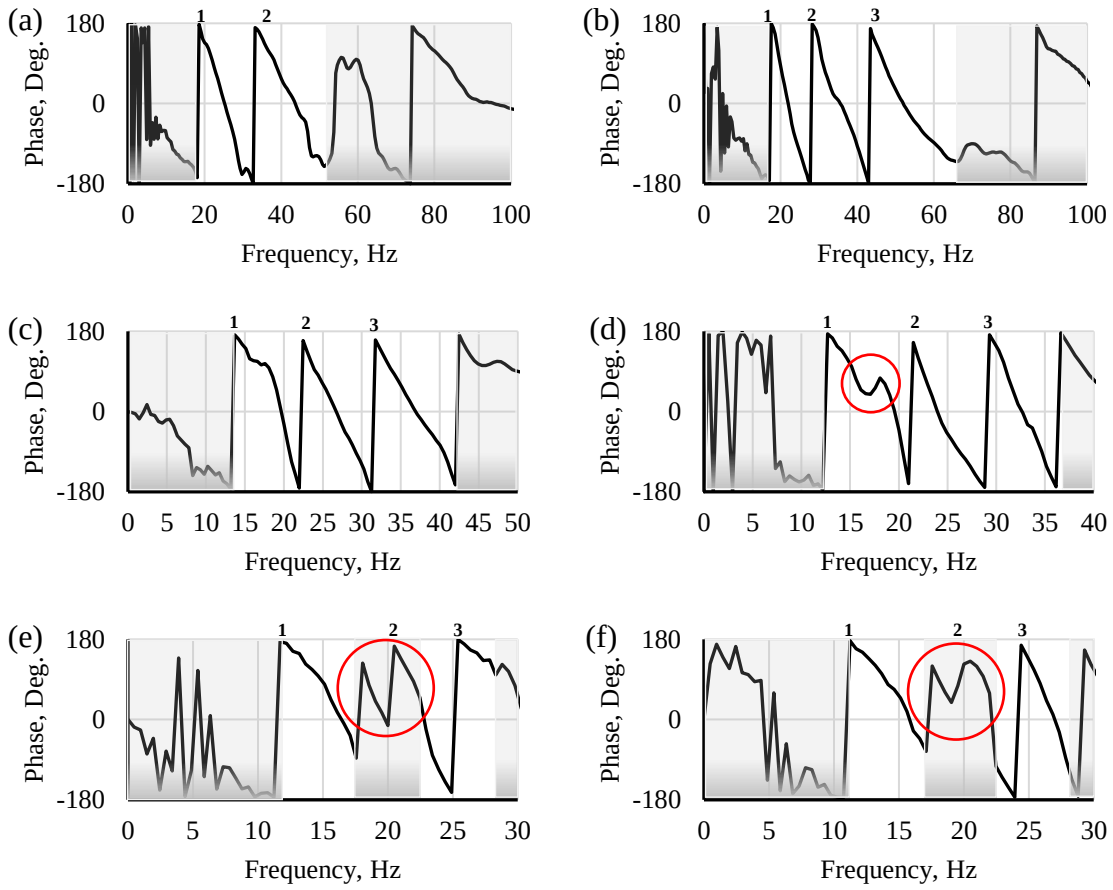

Figure 5.20 Wrapped phase plots from simulated SASW measurements at Site 3 with receiver spacing's pairs of (a) 5 m-11 m, (b) 7 m-15 m, (c) 11 m-23 m, (d) 13 m-27 m, (e) 15 m-31 m, and (f) 17 m-35 m. Phase unwrapping interpretation is indicated by number of 360° "jumps." Data not used in interpretation are indicated by shaded regions.

In this case, the phase plots for the four shortest spacing follow the conventional "sawtooth" pattern and two or three cycles of phase are interpreted in each case. A small deviation in the phase trend is observed in the frequency range of 16 to 22 Hz for receiver pairs 11 m-23 m and 13 m-27 m. At the bigger receiver spacings, this deviation becomes much larger and disrupts the phase trend (Figures 5.20e and f). Therefore, this portion of the phase diagram was masked from the interpretation. The SASW dispersion curves interpreted from phase unwrapping are shown in Figure 5.21.

Dispersion curves were then developed using the same SASW data but processed with the HWAW approach over the same frequency ranges, as shown in Figure 5.22. Comparisons between the SASW phase-unwrapped dispersion curve and the HWAW-processed curve for the individual receiver pairs are shown in Figure 5.23 and 5.24. The HWAW dispersion curves for the shorter receiver pairs (5 m-11 m, 7 m-15 m, 11 m-23 m, and 13 m-27 m) were continuous over the full frequency range and in excellent agreement with the dispersion curves from SASW phase unwrapping (Figure 5.23a-d and Figure 5.24a-d). Dispersion curves from the two longest receiver pairs (15m-31 m and 17m-35 m) were also in excellent agreement with the SASW results but produced an erratic phase response over the frequency range of 16 Hz to 22 Hz, where the SASW data could not be interpreted.

Typically, this abrupt change in phase could indicate the presence of a high impedance contrast at the site, as previously demonstrated for soft-over-stiff profiles. However, as noted above this site has a relatively small impedance contrast and the transition frequencies (16 Hz to 22 Hz) are not consistent with the expected values based on Equation 4.6.

Using the V_S velocity obtained from the downhole measurements of 185 m/s and V_P of 925 m/s (Poisson's ratio of 0.48), calculating the V_L velocity, using Equation 4.5, and the layer thickness of 7.5 m, the expected transition frequency range should be about 6.2 Hz to 12.8 Hz based on Equation 4.6. It should also be noted that the surface wave velocities measured at this site at high and low frequencies are in good agreement with the expected values based on the downhole measurements.

Although this site was more complex than expected, the results still confirmed that the HWAW processing performed as well as the SASW phase unwrapping without the need for manual interpretation.

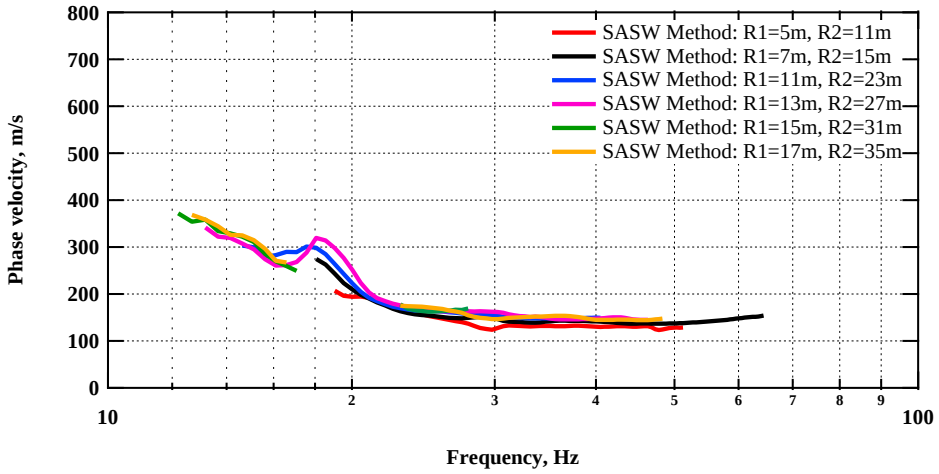

Figure 5.21 SASW dispersion curves produced from the phase plots interpretation in Figure 5.19 for Site 3.

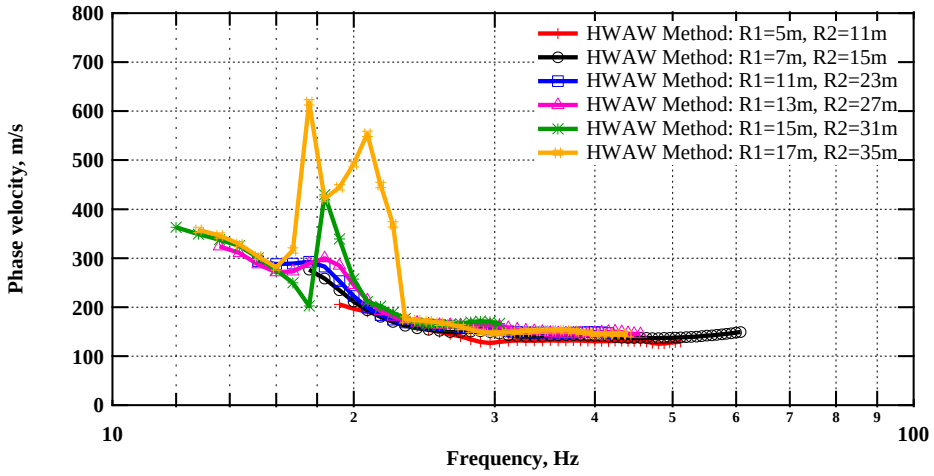

Figure 5.22 Phase velocity dispersion curves using the HWAW method to process the SASW data for Site 3.

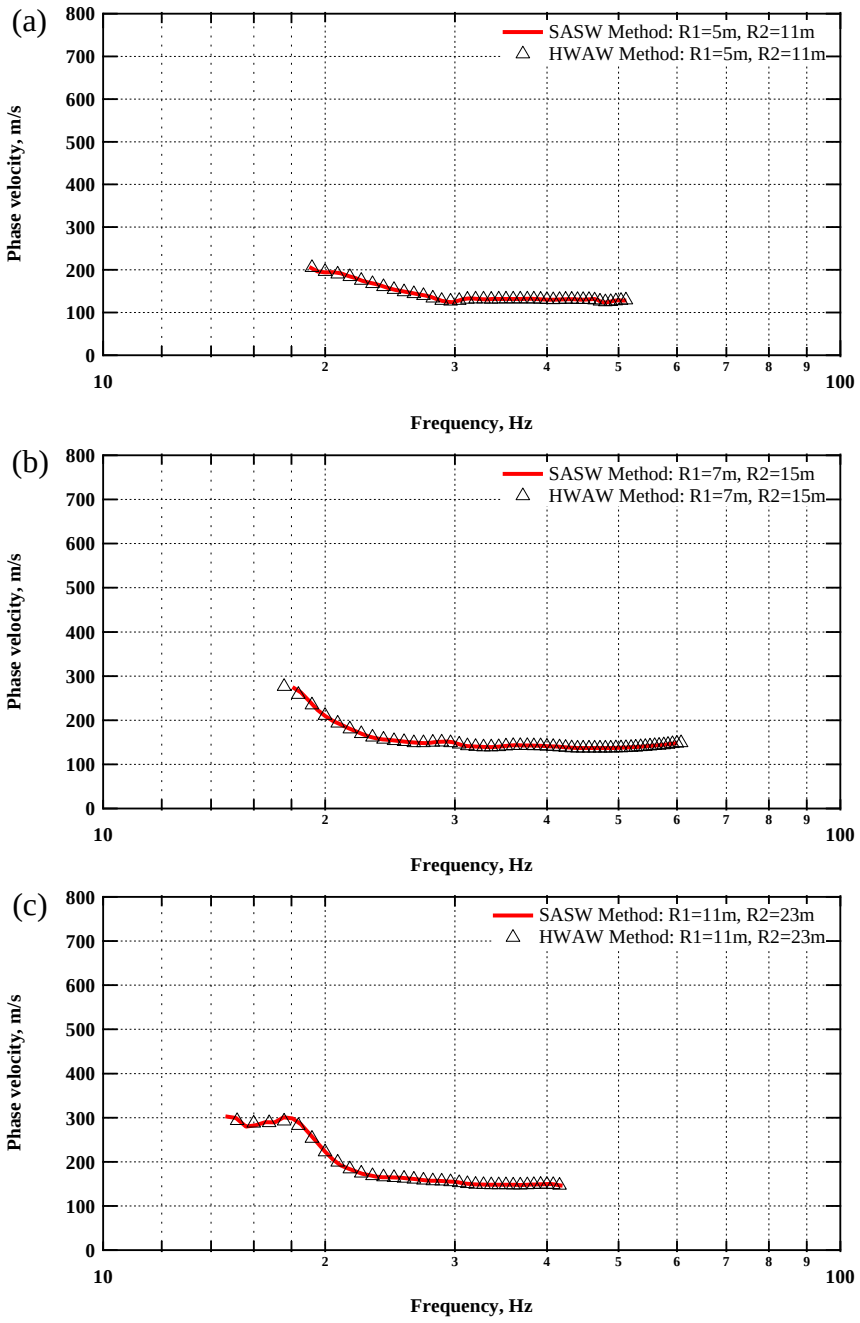

Figure 5.23 Comparison between the phase velocity dispersion curves obtained by SASW and HWAW methods for receiver pairs: (a) 5 m-11 m, (b) 7 m-15 m, and (c) 11 m-23 m.

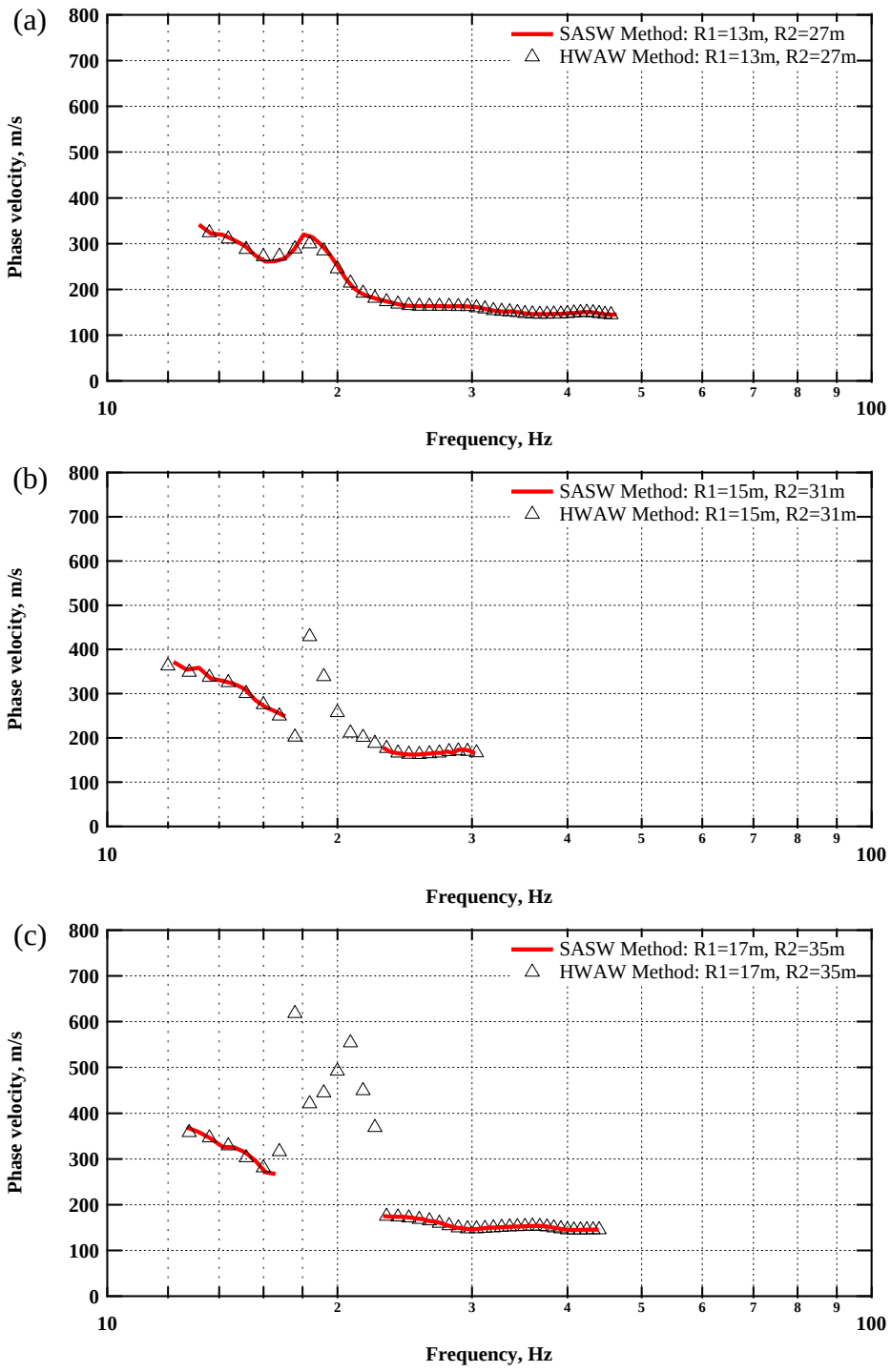

Figure 5.24 Comparison between the phase velocity dispersion curves obtained by SASW and HWAW methods for receiver pairs: (a) 13 m-27 m, (b) 15 m-31 m, and (c) 17 m-35 m.

5.4.2 HWAW Data Collection and Interpretation

The typical HWAW data collection procedure documented in the literature uses a single, closely-spaced receiver pair (typically only a few meters). The various HWAW test setups used at this site are presented in Table 3.14. The dispersion curves obtained from these test setups are in general agreement with dispersion curves from the SASW measurements, as shown in Figures 5.25, 5.26, 5.27. It is not expected that these dispersion curves would be in perfect agreement with the SASW dispersion curves since measurements were collected at very different locations relative to the source and the contributions from body waves and near field effects are different.

However, these results show that high-quality dispersion curves can be measured over a broad frequency range (12 Hz to 45 Hz) using a single receiver pair arrangement. In this case, use of the closely-spaced receiver pair allowed for interpretation of the phase velocity in the problematic frequency range of 16 Hz to 22 Hz in all cases. The use of small source offsets produced lower phase velocity values at low frequencies due to the contributions of near-field effects (e.g. Figure 5.25a, b and c and Figure 5.26 a, b, and c). Although this research established that reliable dispersion curves can be measured with the HWAW method, the question of whether these near-field measurements can be reliably inverted to obtain an accurate V_S profile was not investigated as part of this research and should be considered as part of future research.

Downhole data from this site showed high V_P values indicating nearly saturated conditions. Based on the V_P and V_S values Poisson's ratio is calculated to be 0.48. Therefore, based on the observations from the simulation studies and the results from Site 2, it is expected that these close receiver pairs would produce dispersion curves with large

fluctuations. This was not generally observed at this site, with the exception of the data collected with the longest source offset (Figure 5.27b).

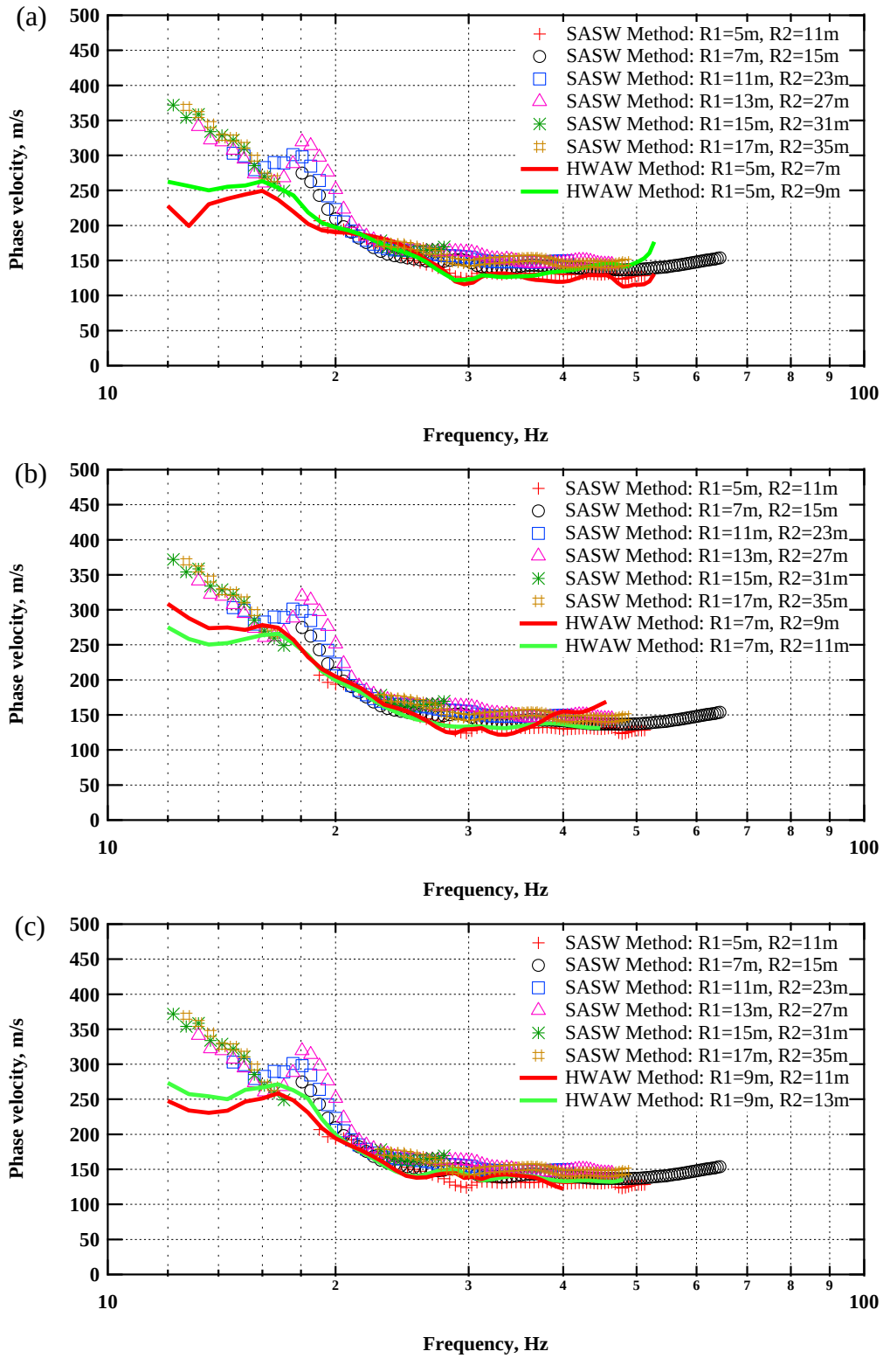

Figure 5.25 Comparison of SASW dispersion curve with the HWAW method for the receiver pairs of: (a) 5 m-7 m, and 5 m-9 m, (b) 7 m-9 m, and 7 m-11 m, and (c) 9 m-11 m, and 9 m-13 m.

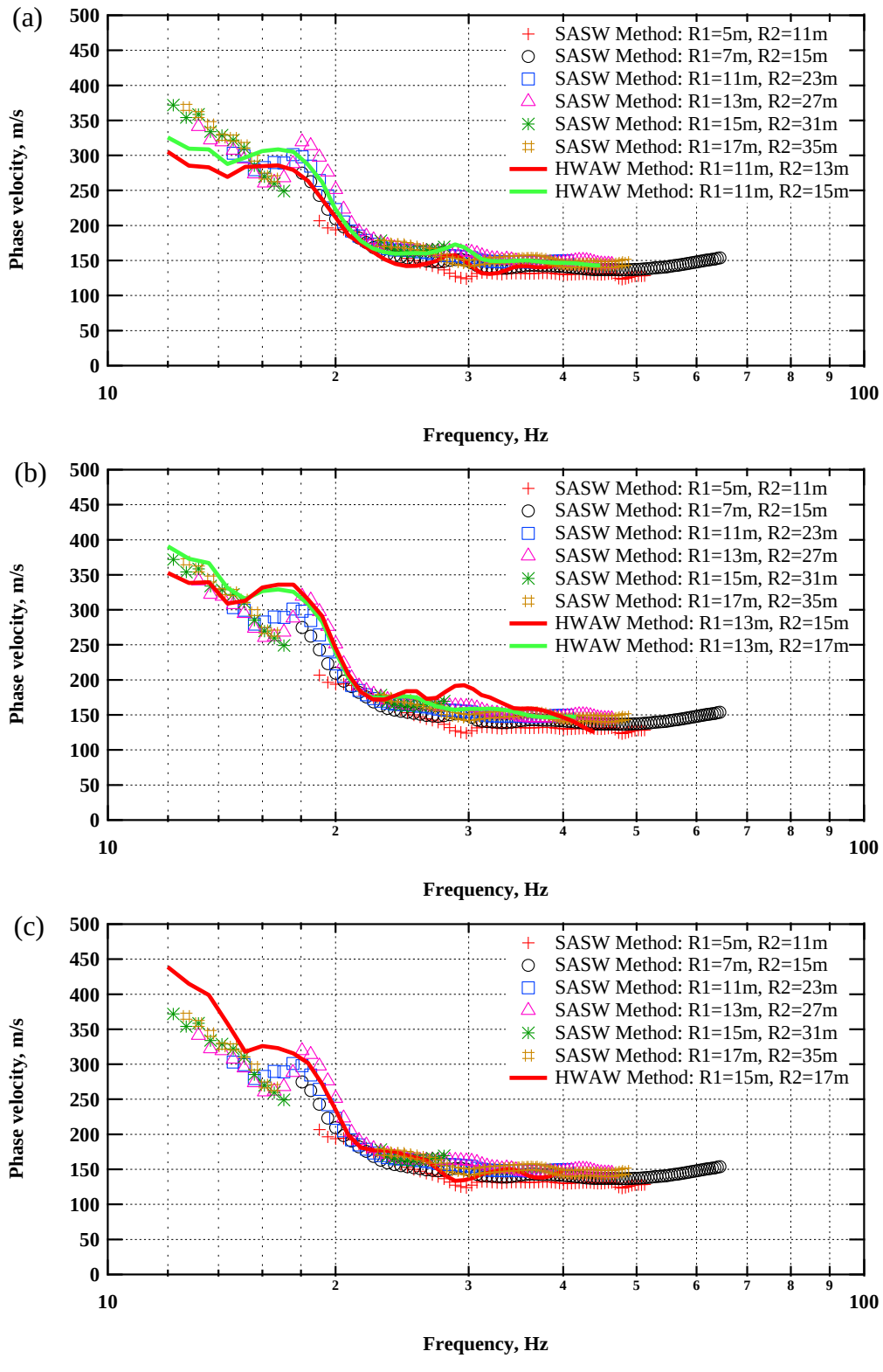

Figure 5.26 Comparison of SASW dispersion curve with the HWAW method for the receiver pairs of: (a) 11 m-13 m, and 11 m-15 m, (b) 13 m-15 m, and 13 m-17 m, and (c) 15 m-17 m.

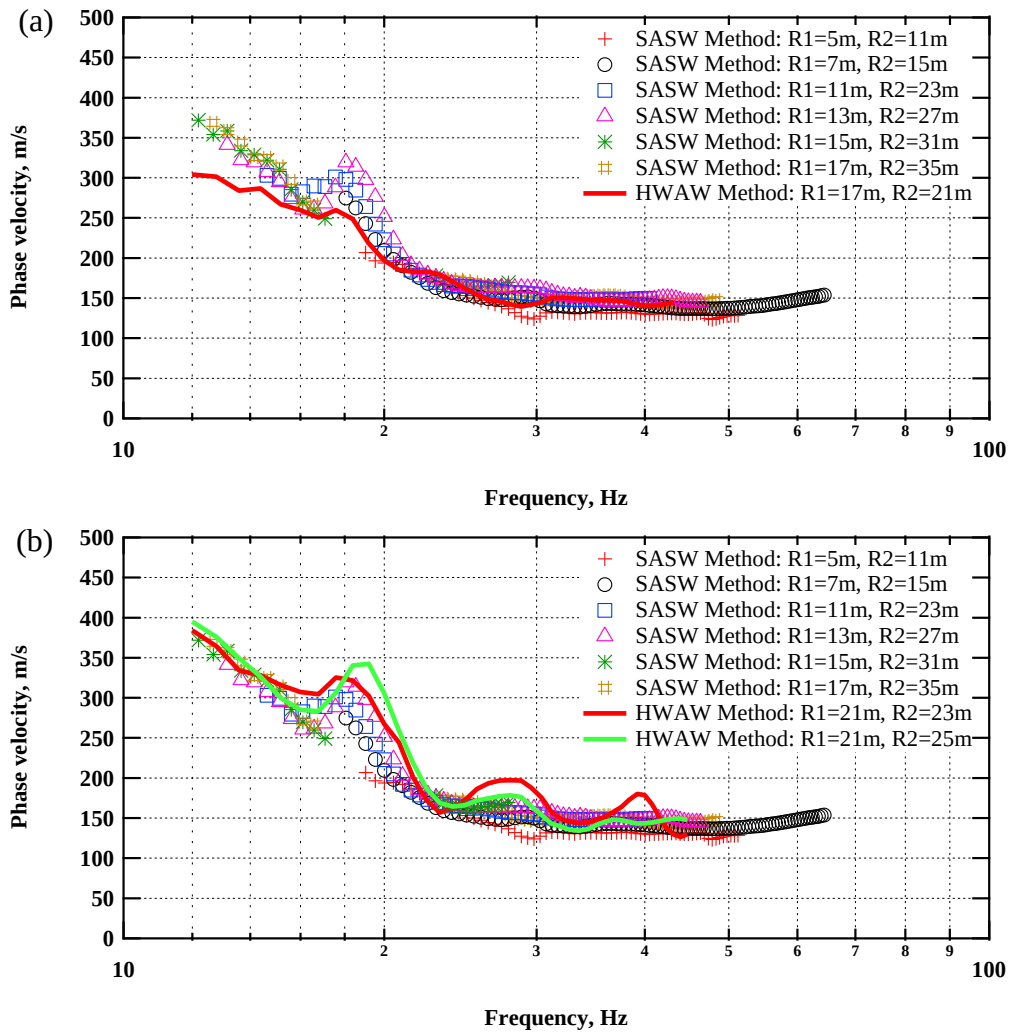

Figure 5.27 Comparison of SASW dispersion curve with the HWAW method for the receiver pairs of: (a) of 17 m-21 m, and (b) 21 m-23 m, and 21 m-25 m.

5.5 Comparison of Data Collection Parameters from the Field Studies of Three Sites to the Guidelines Developed from the Simulated Surface Data

The comparison of the processing parameters that were used at each site investigated in this study and how they compared to the suggested guidelines are presented in the following Tables 5.1, 5.2, and 5.3 for Site 1, Site 2 , and Site 3 respectively.

Table 5.1 Processing parameters used for Site 1.

Sampling frequency, f_s, Hz	Time length, sec	Δf, Hz	b_w, Hz	b_w/fr.
1280	1.6	0.625	1.25	0.083
1280	1.6	0.625	1.25	0.083
1280	1.6	0.625	1.25	0.083
256 and 640	8 and 3.2	0.125-0.3125	0.25-0.625	0.017-0.042
256	8	0.125	0.25	0.017
2560	0.8	1.25	2.5	0.17

Table 5. 2 Processing parameters used for Site 2.

Sampling frequency, f_s, Hz	Total time, seconds	Number of samples	sampling period, milliseconds	b_w, Hz	b_w/fr.
250	4	1000	4	0.25	0.025

Table 5.3 Processing parameters used for Site 3.

Sampling frequency, f_s, Hz	Total time, seconds	Number of samples	sampling period, milliseconds	b_w, Hz	b_w/fr.
2000	1.25	2500	0.5	1.6	0.13

For site 1 and 2, the ratios of bandwidth-to-the frequency were in the range of 0.017 to 0.17. The suggested guidelines developed from the simulated study, were 0.1 as a minimum and the values of bandwidth-to-the frequency obtained from the field studies were able to resolve the dispersion curve accurately.

For site 3, it was found that the bandwidth ratio-to-the frequency was 0.13 which was close to what have established for simple sites. These comparisons for the three sites

validate what has suggested for the processing parameter of the bandwidth-to-frequency ratio of 0.1 as a minimum.

5.6 Summary

This chapter presents experimental results from three field sites. The results from Site 1 validate the ability of the HWAW to handle the abrupt mode transition and recover the dispersion curve correctly. The main findings from Site 2 results showed the consistency of the dispersion curves between the HWAW-processed data and SASW phase unwrapped data for high Poisson's ratio sites. The results also showed large fluctuations in the dispersion curves when short receiver pair spacings were used with long source offsets. This results confirmed the observations from the numerical study. Results from Site 1 and Site 2 also demonstrated the ability of HWAW processing to better handle noise and extend the low frequency range of measurements, as compared to SASW phase unwrapping. For Site 3, the results show a consistency between the SASW and HWAW dispersion curves but a mode transition could not be explained for this site.

CHAPTER 6
SUMMARY, CONCLUSIONS, AND RECOMMENDATIONS

6.1 Summary

The goal of this research was to improve the application of surface wave methods in geotechnical practice by evaluating the effectiveness of the HWAW method at complex geotechnical sites and developing guidelines for implementing this method generally. It was hypothesized that the HWAW method can overcome issues associated with applying the SASW method at complex geotechnical sites. Simulated surface wave measurements and field studies were performed to meet this goal.

A literature review was performed by looking at relevant literature of SASW, MASW, and HWAW methods. Simple V_S profiles and complex V_S profiles that have proven problematic for conventional surface wave methods were identified. A MATLAB algorithm was developed to perform the HWAW processing and a method to correct erroneous points in the dispersion curve was developed and implemented.

A parametric study of data collection and data processing parameters of the HWAW method was performed for simple sites using simulated surface wave data. Also, the effect of Poisson's ratio on the effectiveness of the HWAW was investigated.

The performance of the HWAW method at complex sites using simulated data was evaluated and comparison between the SASW-derived and HWAW-derived dispersion curves were presented.

Based on the study of simulated data, guidelines for implementing the HWAW method were developed and presented. Verification of major findings from the simulated studies

were performed using experimental data from three field sites. The conclusions and recommendations derived from this study are presented in this chapter.

6.2 Conclusions

Major findings from this study are summarized below.

1. A sufficiently narrow bandwidth is the most important data processing parameter for determining an accurate dispersion curve from HWAW processing. Based on simulations of simple and complex sites it is recommended that the bandwidth/frequency ratio should be 0.1 as a minimum for all points. Sampling frequency has a minor effect, but higher rates are preferred. A sampling rate of ten times the highest frequency of interest is recommended to provide good resolution at high frequencies.
2. Source location and receiver spacing had no effect on the reliability of the HWAW dispersion curves. This finding indicates that the short receiver spacings used in published HWAW studies are not required for applying the HWAW processing but may be used.
3. The value of Poisson's ratio did not affect the ability to accurately recover the dispersion curve using the HWAW method. This conclusion provides confidence that HWAW processing can be applied in the field regardless of saturation conditions at the site. However, when short receiver spacings were used with a much longer source offset at saturated sites, the dispersion curve showed large fluctuations, which could prove problematic for some inversion programs
4. The HWAW method performed well for each of the complex sites studied over a range of source offsets and receiver spacings. Most importantly, the HWAW

method was able to effectively capture the higher mode transition which is characteristic of soft-over-stiff sites. This case is especially problematic for the manual phase unwrapping procedures used in conventional SASW measurements, and can easily produce erroneous dispersion curves.

5. HWAW processing can be used effectively with data collected using the conventional SASW field procedures. This was observed for all profiles using both simulated as well as experimental data. As noted above, the mode transition issue was better handled with HWAW processing than phase unwrapping. This finding suggests that the time consuming and problematic phase unwrapping procedures used in SASW data processing should be abandoned and replaced with an automated HWAW-based approach.
6. The short receiver offsets used in published HWAW studies produce lower phase velocities at low frequencies due to near-field effects. This was expected and may prove problematic for inversion methods, but was not investigated in this research.
7. Analysis of experimental field data from Site 1 and Site 2 demonstrated that the HWAW method is better able to handle noisy data than conventional SASW phase unwrapping and may extend the low frequency range.

6.3 Significance, Recommendations and Future Research

This study has demonstrated the effectiveness of the HWAW method when applied at complex geotechnical sites. It has been shown that when applied correctly, the HWAW method accurately recovers the dispersion curve, captures higher mode transitions, and overcomes the issue of phase unwrapping difficulty due to abrupt mode transitions, especially at soft-over-stiff sites. As shown, the soft-over-stiff case is especially

problematic for the manual phase unwrapping procedure used in conventional SASW measurements, and can easily produce erroneous dispersion curves. Moreover, it has also been shown that the HWAW method deals with noisy data better than that SASW method and can extend the dispersion curve to lower frequencies, thus providing deeper V_S profiles. These findings support the hypothesis that the HWAW method can overcome the issues associated with applying SASW at complex geotechnical sites.

Future work should focus on implementing an automated HWAW program with data collection software so that the dispersion curve can be generated on site, essentially automating the phase unwrapping process using the HWAW technique.

The results also demonstrate that a variety of source offset and receiver configurations can be effectively used with the HWAW processing. It did not, however, address the question of whether data collected in the near field using short source offsets can be effectively inverted. Future research should focus on this question and establish new criteria for near-field measurements. Until this work is performed it is recommended that the current SASW approach for collecting data should be used, but the phase unwrapping procedure should be replaced with automated HWAW processing.

Furthermore, there is currently no quantitative means to evaluate quality thresholds for acceptance of data using the HWAW method. Therefore, it is recommended that future research should focus on field measurements to develop a method to evaluate data quality and limits of interpretation, such as coherence values between an instrumented source and receivers.

REFERENCES

Al-Hunaidi, M. O. (1993): "Insights on SASW nondestructive testing method." Canadian Journal of Civil Engineering, 20(6), 940-950.

Andrus, R.D. and Stokoe, K.H., II (1999): "SASW Testing to Delineate Potentially Liquefiable Zones and Evaluate Remediation Measures." 7th United States-Japan Workshop on Earthquake Resistance Design of Lifeline Facilities and Countermeasures against Liquefaction, Seattle, WA. August 15-17, 1999, Biennial Conference on Vibration and Noise, Sacramento, California.

Antonini, M., Barlaud, M., Mathieu, P., and Daubechies, I. (1992): "Image coding using Wavelet Transform." IEEE Transactions on Image Processing. Vol.1, No.2, April 1992.

Boore, D.M. and L.T. Brown (1998): "Comparing shear-wave velocity profiles from inversion of surface-wave phase velocities with downhole measurements." Systematic differences between the CXW method and downhole measurements at six USC strong-motion sites, Seismology Research Letters 69, 222-229.

Chai, Hua-You, Phoon, Kok-Kwang Wei, Chang-Fu, and Lu, Ying-Fa, (2011): "Analysis of effects of active sources on observed phase velocity based on the thin layer method." Journal of Applied Geophysics, Volume 73, Issue 1, 2011, Pages 49-58, ISSN 0926-9851.

Chen, L., Zhu, J., Yan, X., and Song, C. (2004). "On arrangement of source and receivers in SASW testing." Soil Dynamics and Earthquake Engineering, 24(5), 389-396.

Cox, B.R, Wood, C., Teague, D. (2014): "Synthesis of the UTexas1 Surface Wave Dataset Blind-Analysis Study: Inter-Analyst Dispersion and Shear Wave Velocity Uncertainty." Geo-Congress 2014, 850-859.

Foti, S., Hollender, F., Garofalo, F. et al. (2017): "Guidelines for the good practice of surface wave analysis: a product of the InterPACIFIC project." Bulletin of Earthquake Engineering, Vol. pp 1–54. Springer Netherlands. https://doi.org/10.1007/s10518-017-0206-7.

Foti, S., Lai, C.G., Rix, G.R., and Strobbia, C. (2015): "Surface Wave Methods for Near-Surface Site Characterization." CRC Press, Taylor and Francis Group, LLC, London, UK.

Foti, Sebastiano, Cesare Comina, Daniele Boiero, and L. V. Socco. (2009): "Non-uniqueness in surface-wave inversion and consequences on seismic site response analyses." Soil Dynamics and Earthquake Engineering 29, No. 6 (2009): 982-993.

Gazetas, G., (1991). "Foundation Vibrations," in Foundation Engineering Handbook, 2nd Ed., H.Y. Fang, Ed., Van Nostrand Reinhold.

Gucunski and Shokouhi (2004): "SASW Dispersion Curve Generation by Wavelet Transform." Proceedings of the Symposium on the Application of Geophysics to Engineering and Environmental Problems, SAGEEP 2004, Colorado Springs, Colorado, February 24-28.

Gucunski, N. and Shokouhi, P. (2005): "Wavelet Transforms in Surface Wave Analysis." Soil Dynamics Symposium in Honor of Professor Richard D. Woods Geo-Frontiers Congress 2005, January 24-26, 2005 | Austin, Texas, United States.

Gucunski, N., and Woods, R. D. (1992). "Numerical simulation of the SASW test." Soil Dynamics & Earthquake Engineering, 11(4), 213-227.

Hou, Z., Noori, M., and Amand, R.St. (2000): "Wavelet-based approach for structural damage detection." American Society for Civil Engineering. Journal of Engineering Mechanics. Volume 126 Issue 7 - July 2000.

Hwang, H.-J., and Park, H.-C. (2014): "Evaluation of condition of gravel ballast layer on high-speed railway using surface wave method based on harmonic wavelet analysis of waves." NDT&E International 68, pp.78–87.

Joh, S.-H. (1996): "Advances in the Data Interpretation Technique for Spectral-Analysis-of-Surface-Waves (SASW) Measurement." Doctor of Philosophy, University of Texas at Austin, Austin, TX.

Kafadar, O. (2020): "A geophone-based and low-cost data acquisition and analysis system designed for microtremor measurements." Geoscientific Instrumentation, Methods

and Data Systems, Vol.9, 365–373, 2020.

Kausel, E., and Roesset, J., (1981): “Stiffness Matrices for Layered Soils.” Bulletin of the Seismological Society of America, Vol. 70, pp. 1743-1761.

Kim, D.-S. & Park, H.-C. (2001): “Evaluation of dispersive phase and group velocities using harmonic wavelet transform.” NDT E Inter; Volume 34, No.7, pp.457–67.

Kim, D.-S. & Park, H.-C. (2002): “Determination of Dispersion Phase Velocities for SASW method Using Harmonic Wavelet Transform.” Soil Dynamics and Earthquake Engineering, Volume 22, No.8, pp.675-684.

Kim, D.-S., Kim, J.-T., Park, H.-J., Bang, E. S., and Park, H.-C (2015): “Verification study for a surface wave method based on harmonic wavelet analysis waves using a large-scale model testing site.” Journal of Applied Geophysics 113, pp.74–85.

Li, J., and Rosenblad, B. (2011): “Experimental study of near-field effects in multichannel array-based surface wave velocity measurements.” Near Surface Geophysics, 9(4), 357-366.

Lo Presti, D.C.F., Pallara, O. and Puci, I. (1995): “A modified commercial triaxial testing system for small strain measurements.” Preliminary results on Pisa clay. Geotechnical Testing Journal, 18, 15–31.

Mayne, P. (2000): “Enhanced geotechnical site characterization by seismic piezocone penetration tests.” [Keynote lecture] In Proceedings of the Fourth International Geotechnical Engineering Conference: Applications of seismic penetration testing in geotechnical explorations, Cairo University, Cairo, Egypt. pp. 95–120.

McCaskill, A. (2014): “A Study on the Benefits of including Near-Field Effects in Active-Source Surface Wave Data Collection and Interpretation.” Master's Thesis, University of Missouri - Columbia, Columbia, MO.

Mera, R. F. (1995). “Dynamic Nondestructive Testing of Pavements.” Doctor of Philosophy, University of Texas at Austin, Austin, TX.

Nazarian, S., and Stokoe, K. H., II (1984): “In situ shear wave velocities from Spectral

Analysis of Surface Waves." Proceedings of the 8th World Conference on Earthquake Engineering, Prentice-Hall, Inc., Englewood Cliffs, New Jersey, Vol. III, 31-38.

Newland, D. E., (1998): "Time-frequency and time-scale signal analysis by harmonic wavelets." Chapter 1 of the book Signal Analysis and Prediction, A. Procházka, J. Uhlír, P.J.W. Rayner and N.G. Kingsbury (eds.), Birkhäuser, Boston.

Newland, D.E. (1993): "Harmonic wavelet analysis", Proceedings of Royal Society, Mathematical, Physical, and Engineering Sciences. Vol. 443, Issue 1917, pp 203-225. London, SW1Y 5AG, UK.

Newland, D.E. (1994a): "Wavelet analysis of vibration, part I: Theory, Journal of Vibrations and Acoustics." Volume116, pp.409-416.

Newland, D.E. (1994b): "Wavelet analysis of vibration, part II: Wavelet maps, Journal of Vibrations and Acoustics." Volume 116, pp.417-425.

Newland, D.E. (1997): "Practical signal analysis: do wavelets make any difference?" Proceedings of the 1997 ASME Design Engineering Technical Conferences, 16th

Newland, D.E. (1999): "Ridge and phase identification in the frequency analysis of transient signals by harmonic wavelets." Journal of Vibrations and Acoustics, Volume 121, pp.149-155.

Park, C. B., Ivanov, J., Miller, R. D., Xia, J., and Ryden, N. (2001). "Seismic investigation of pavements by MASW method; geophone approach." Proceedings - Symposium on the Application of Geophysics to Engineering and Environmental Problems (SAGEEP), 2001. Park, C.B., Miller, R.D., and Xia. , J. (1999): "Multi-channel analysis of surface waves," Geophysics, 64(3), pp.800-808.

Park, C., Miller, R., and Xia, J., (1999b): "Multimodal analysis of high frequency surface-waves." Symposium on the Application of Geophysics to Engineering and Environmental Problems 1999, p. 115-121.

Park, H.-C., and Joh, S.-E. (2009): "Determination of phase spectrum using harmonic wavelet transform." NDT&E International 42, pp.534–542.

Park, H.-C., Kim, D.-S. , Bang, E.-S., and Kim, J.-T. (2007): “Seismic Site Characterization using HWAW (Harmonic Wavelet Analysis of Waves) Method.” 4th International Conference on Earthquake Geotechnical Engineering, Thessaloniki, Greece, June 25-28, 2007.

Rioul, O., and Vetterli, M. (1991): “Wavelets and Signal Processing.” IEEE Signal Processing Magazine, October 1991.

Rix, Glenn J., and Stokoe II, Kenneth H. (1990): “Stiffness Profiling of Pavement Subgrades.” Transportation Research Record 1235 Transportation Research Board, ISSN: 0361-1981.

Roesset, J. M. (1998): “Nondestructive Dynamic Testing of Soils and Pavements.” Tamkang Journal of Science and Engineering, vol.1, No. 2, pp. 61-81 (1998).

Roesset, J. M., and Foinquinos, R. (1991): “User's guide to SASWFI, a program for forward modeling and inversion analysis for the surface waves.” The University of Texas at Austin, Austin, TX.

Rosenblad, B. L. and Bertel, J. D. (2008): “Potential Phase Unwrapping Errors Associated with SASW Measurements at Soft-Over-Stiff Sites.” Geotechnical Testing Journal, Volume 31, No. 5, 2008, pp. 433-441.

Rosenblad, B. L., and Li, C.-H. (2011): “Influence of Poisson's ratio on surface wave near-field effects.” Proceeding of Geo-Frontiers 2011: Advances in Geotechnical Engineering, March 13, 2011 - March 16, 2011, American Society of Civil Engineers (ASCE), 2554-2563.

Rosenblad, B.L. (2014): “Shear Wave Velocity Profile Determined from the UTexas1 Surface Wave Dataset.” Geo-Congress 2014, 791-799.

Rosenblad, B.L. and Boeckmann, A.Z. (2020): “NCHRP Synthesis 547, Advancements in Use of Geophysical Methods for Transportation Projects.” Transportation Research Board, National Academies, Washington, D.C.

Sanchez-Salinero, I., Roesset, J., Shao, K.-Y., Stokoe, K., and Rix, G. (1987). “Analytical evaluation of variables affecting surface wave testing of pavements.”

Transportation Research Record (1136), 86-95.

Spanos, Pol D., Giuseppe, F., Adolfo, S., and Massimiliano, P. (2006): "Damage detection in Euler–Bernoulli beams via spatial wavelet analysis." Structural Control and Health Monitoring. Wiley InterScience DOI: 10.1002/stc.118.

Stokoe, K. H., Wright, S. G., Bay, J. A., and Roesset, J. M. (1994). "Characterization of geotechnical sites by SASW method." Proceedings of 13th International Conference on Soil Mechanics and Foundation Engineering, Oxford & IBH Publishing Company, New Delhi, India, 15-25.

Stokoe, K.H., Kacar, O., and Van Pelt, J. (2013): "Predicting settlements of shallow footings on granular soil using nonlinear dynamic soil properties." Proceedings of the 18th International Conference on Soil Mechanics and Geotechnical Engineering, Paris 2013.

Tran K. T., M. Mirzanejad, M. McVay, and D. Horhota. (2019): "3D Time-Domain Gauss–Newton Full Waveform Inversion for Near-Surface Site Characterization." Geophysical Journal International, Vol. 217, 2019, pp. 206–218.

Xu, Y., Xia, J., and Miller, R. D. (2006): "Quantitative estimation of minimum offset for multichannel surface-wave survey with actively exciting source." Journal of Applied Geophysics, 59(2), 117-125.

Yoon, S., and Rix, G. J. (2009): "Near-Field Effects on Array-Based Surface Wave Methods with Active Sources." Journal of Geotechnical and Geo-environmental Engineering, 135(3), 399-406.

Zywicki, D.J. (1999). "Advanced signal processing methods applied to engineering analysis of seismic surface waves." Ph.D. dissertation, Georgia Institute of Technology.

Appendix A

This appendix documents the supplementary figures regarding sampling frequency and bandwidth for Profile 1 and Profile 3.

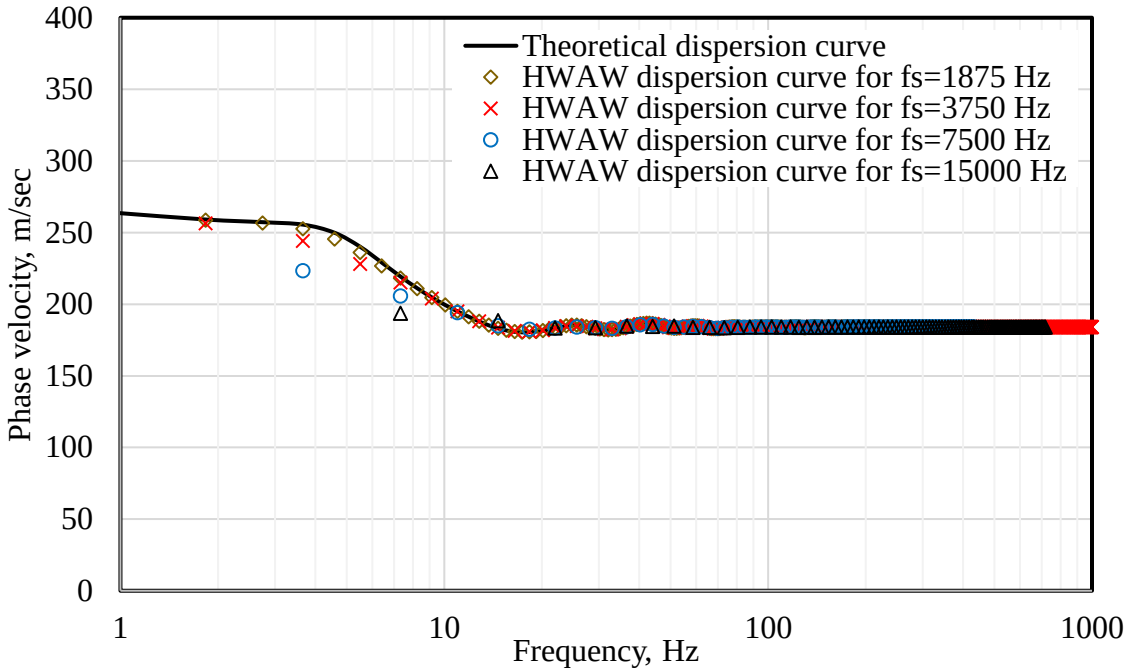

Figure A.1 Comparison of phase velocity dispersion curves generated for Profile 1 (plotted in terms of frequency) using different sampling frequencies and a three-point bandwidth. Receiver spacing is 4 m and Source offset is 20 m.

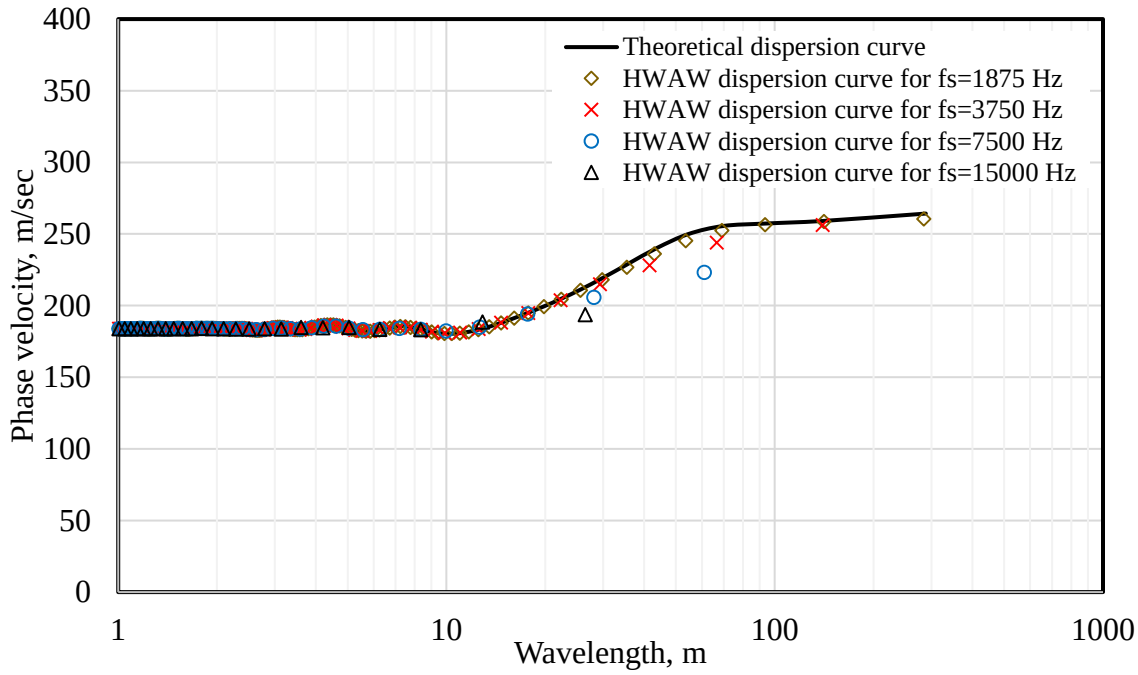

Figure A.2 Comparison of phase velocity dispersion curves generated for Profile 1 (plotted in terms of wavelength) using different sampling frequencies and a three-point bandwidth. Receiver spacing is 4 m and Source offset is 20 m.

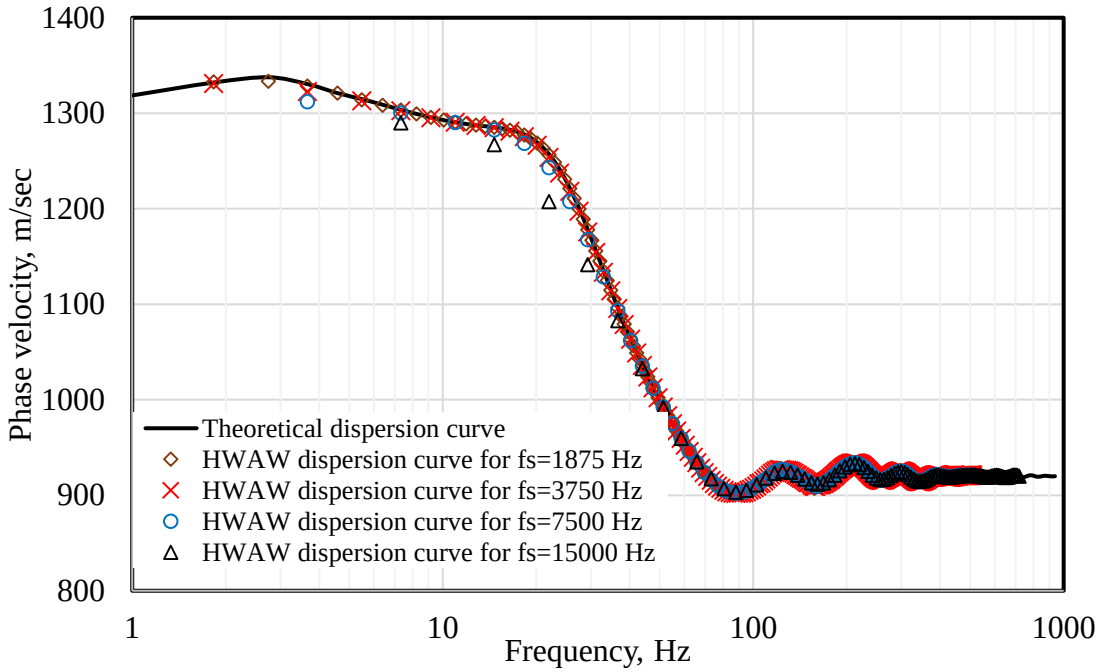

Figure A.3 Comparison of phase velocity dispersion curves generated for Profile 3 (plotted in terms of frequency) using different sampling frequencies and a three-point bandwidth.

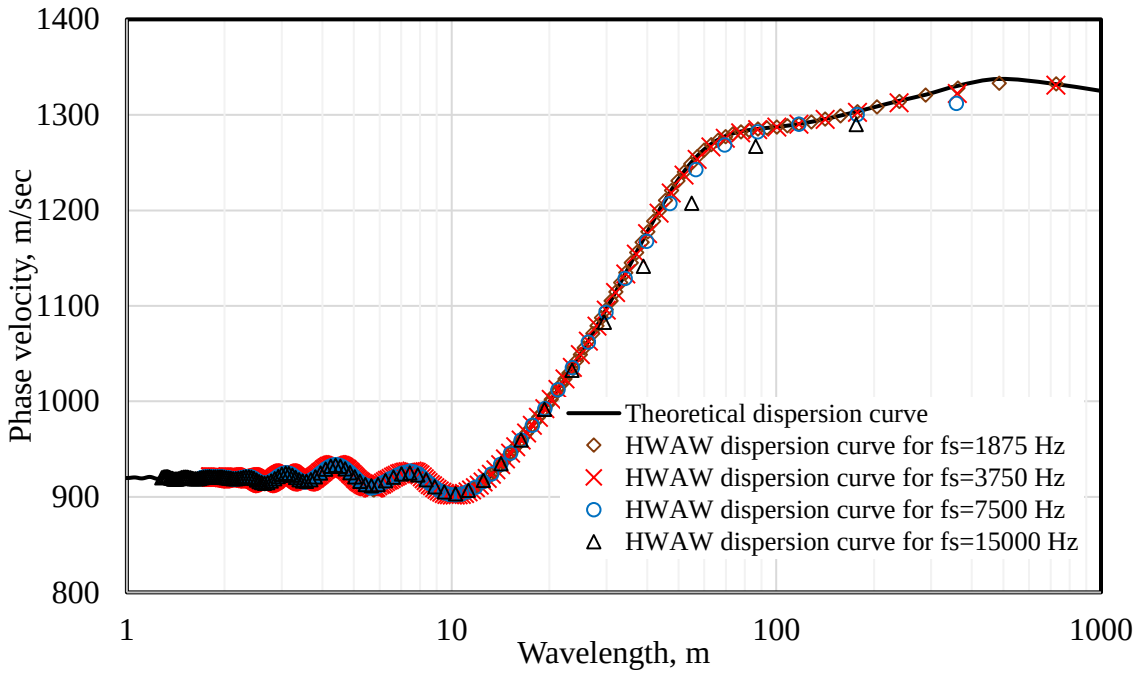

Figure A.5 Comparison of phase velocity dispersion curves generated for Profile 3 (plotted in terms of wavelength) using different sampling frequencies and a three-point bandwidth. Receiver spacing is 4 m and Source offset is 20 m.

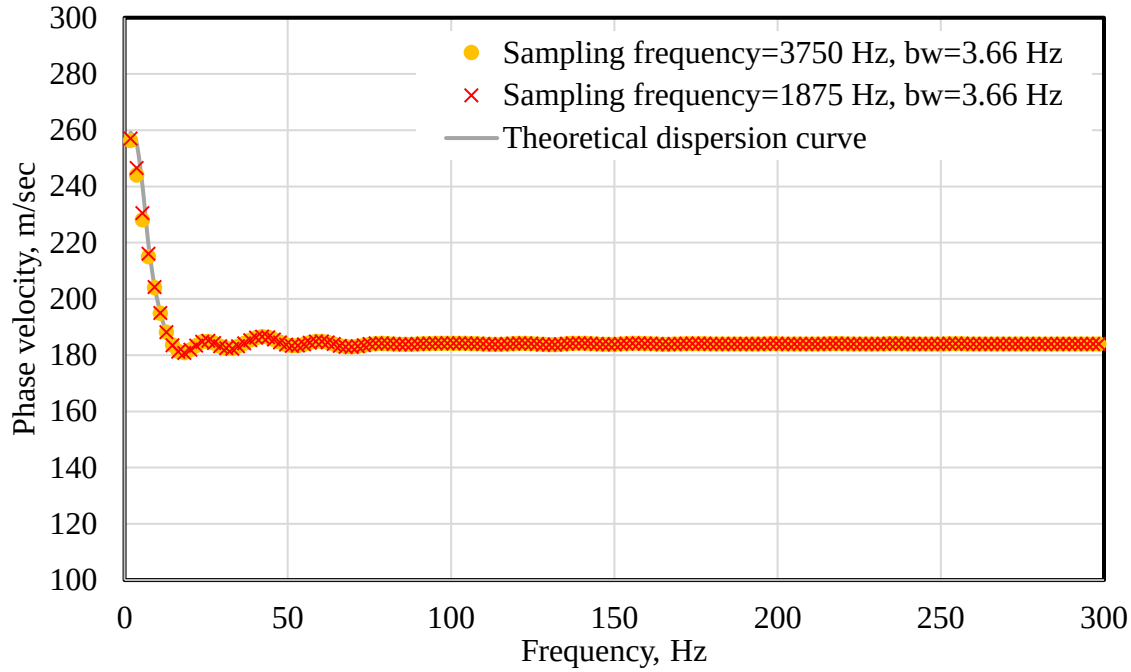

(a)

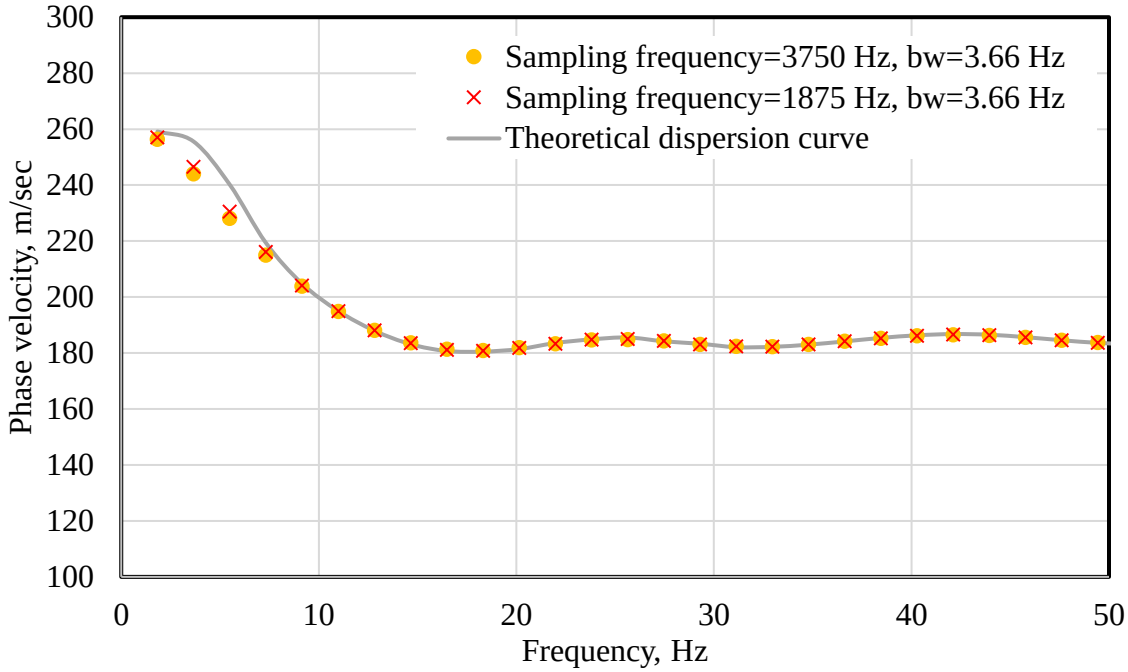

(b)

Figure A.6 V_s versus frequency dispersion curves for Profile 1 obtained from HWAW method for receiver spacing=4 m and source offset=20 m using same bandwidth frequency of 3.66 Hz for sampling frequencies 1875 Hz and 3750 Hz.(a) full frequency range (b) Zoom in frequency range from 0 to 50 Hz.

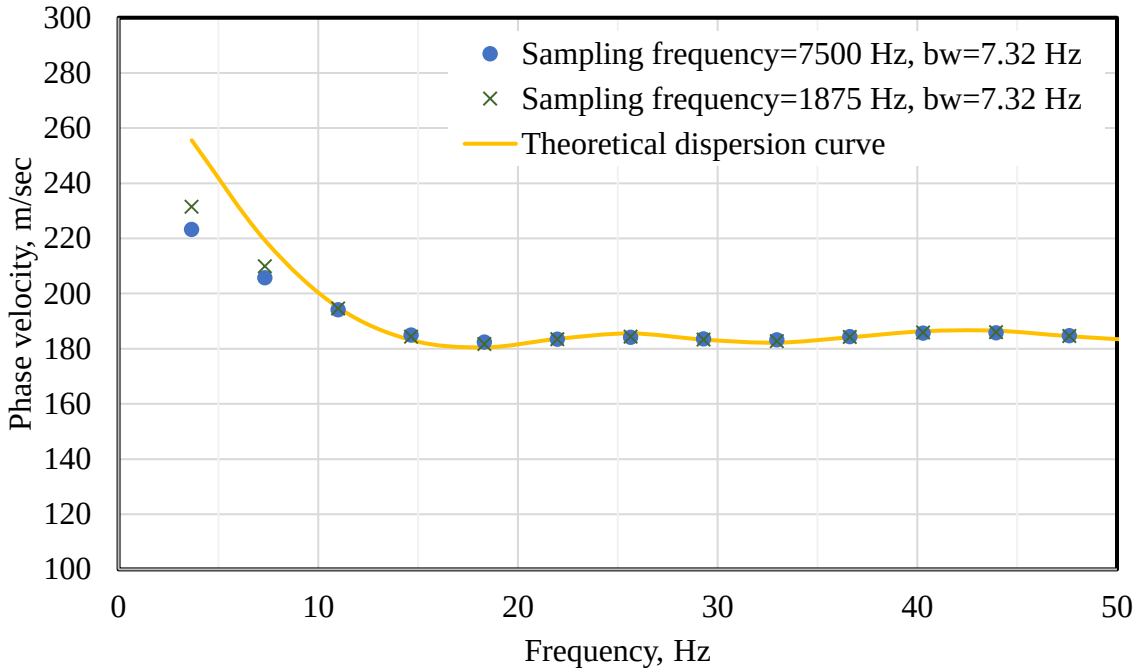

Figure A.7 Zoom in V_s versus frequency dispersion curves for Profile 1 obtained from HWAW method for receiver spacing=4 m and source offset=20 m using same bandwidth frequency of 7.32 Hz for sampling frequencies 1875 Hz and 7500 Hz.

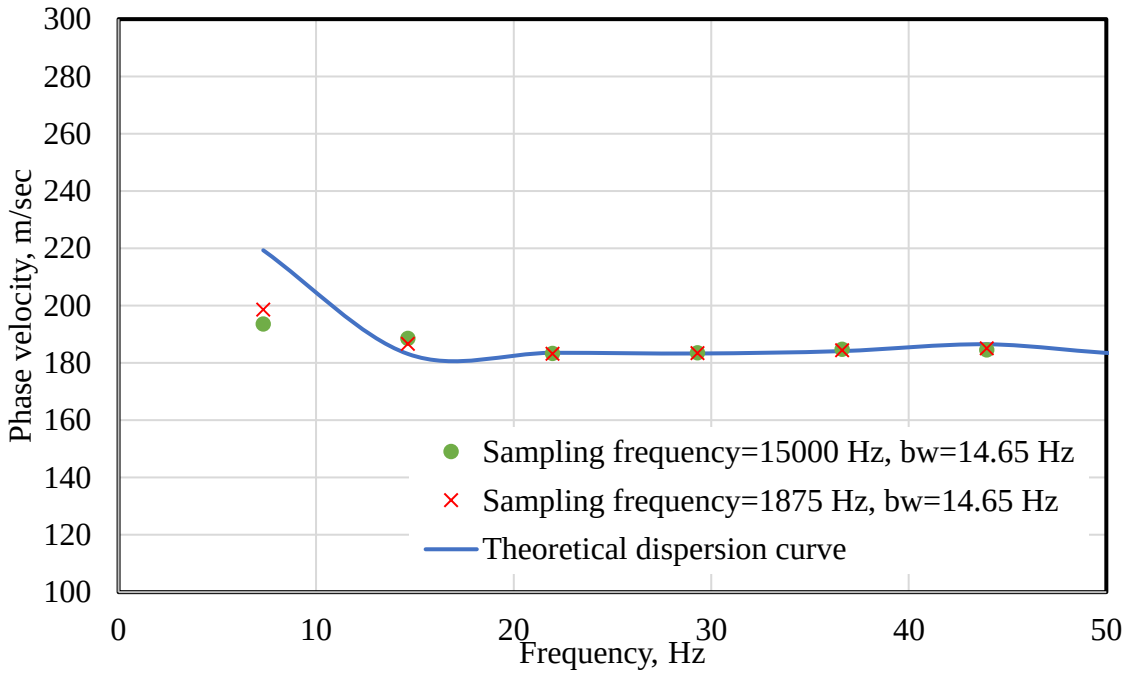

Figure A.8 Zoom in V_s versus frequency dispersion curves for Profile 1 obtained from HWAW method for receiver spacing=4 m and source offset=20 m using same bandwidth frequency of 14.65 Hz for sampling frequencies 1875 Hz and 15000 Hz.

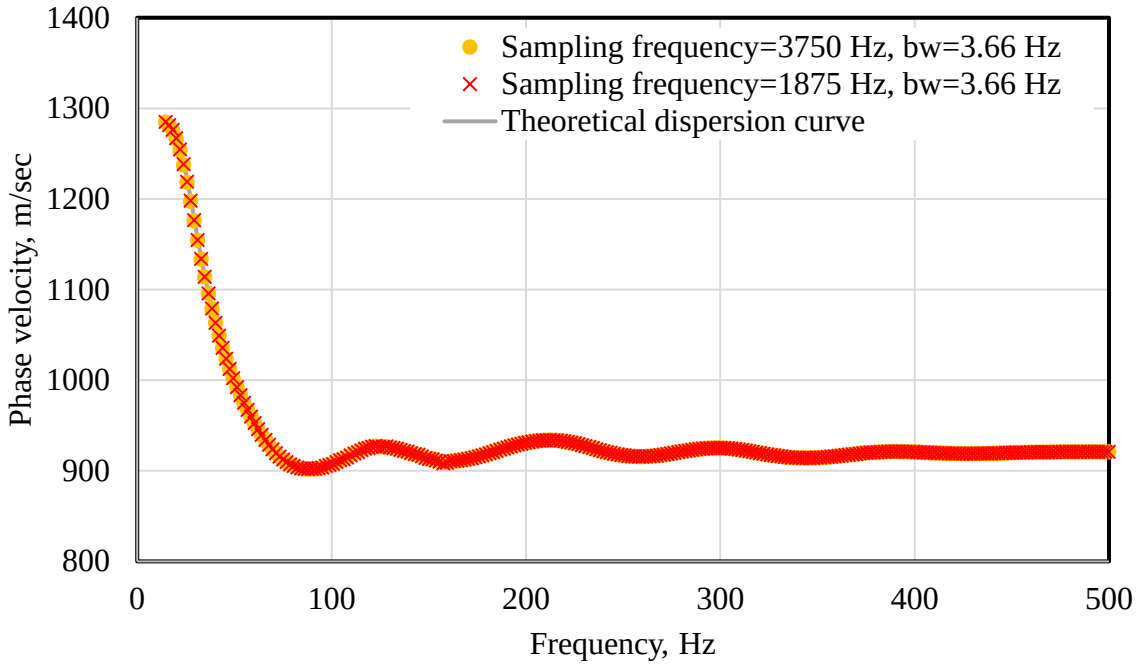

(a)

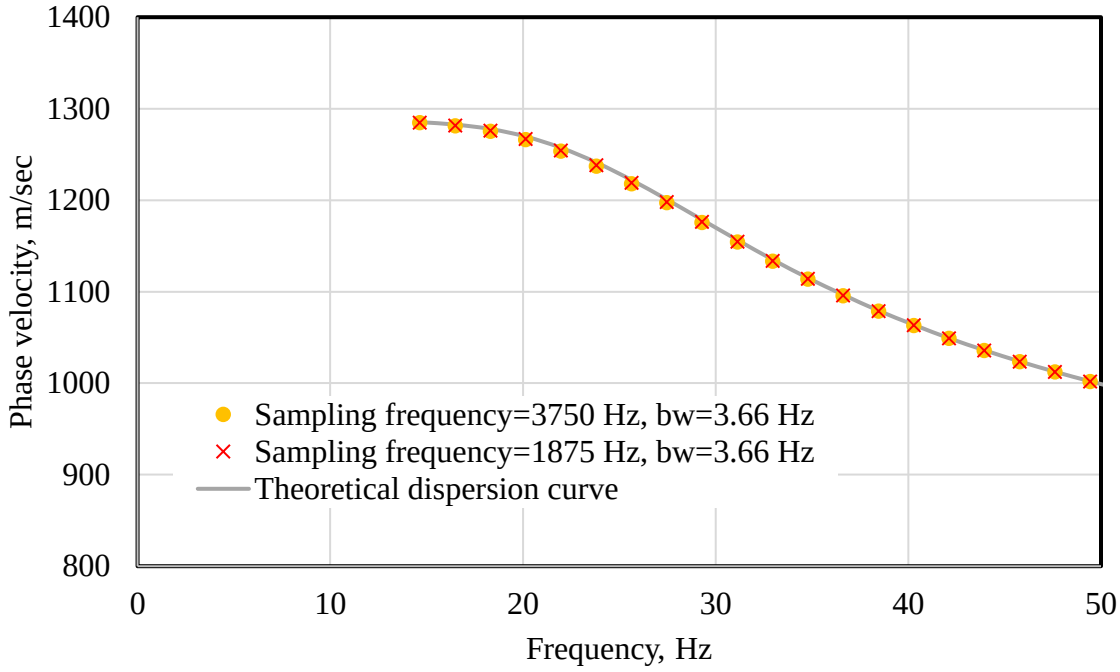

(b)

Figure A.9 V_s versus frequency dispersion curves for Profile 3 obtained from HWAW method for receiver spacing=4 m and source offset=20 m using same bandwidth frequency of 3.66 Hz for sampling frequencies 1875 Hz and 3750 Hz.(a) full frequency range (b) Zoom in frequency range from 0 to 50 Hz.

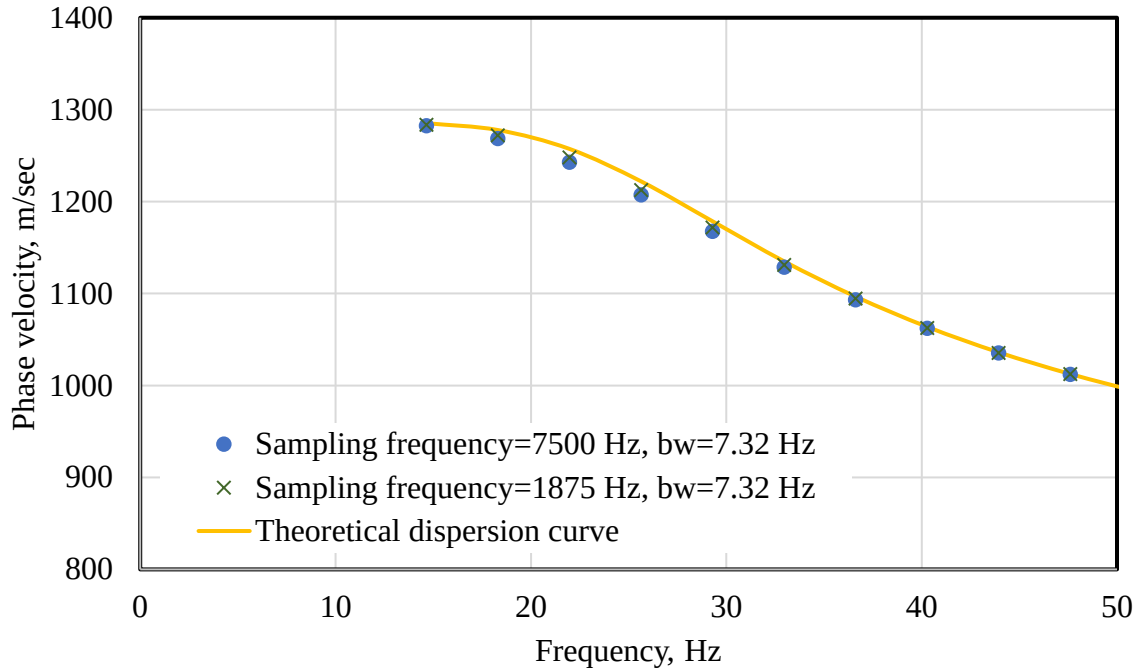

Figure A.10 Zoom in V_s versus frequency dispersion curves for Profile 3 obtained from HWAW method for receiver spacing=4 m and source offset=20 m using same bandwidth frequency of 7.32 Hz for sampling frequencies 1875 Hz and 7500 Hz.

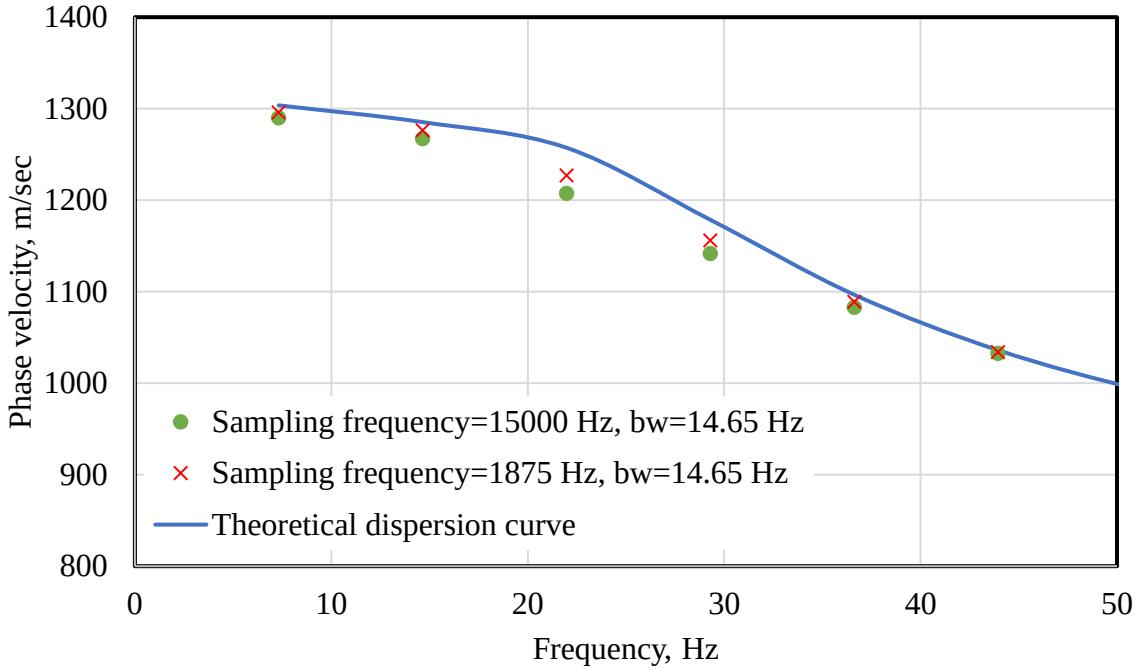

Figure A.11 Zoom in V_s versus frequency dispersion curves for Profile 3 obtained from HWAW method for receiver spacing=4 m and source offset=20 m using same bandwidth frequency of 14.65 Hz for sampling frequencies 1875 Hz and 15000 Hz.

Appendix B

This appendix documents figures of source offset and receiver spacing arrangements for Profile 1 and Profile 3. Also, it documents the phase velocity dispersion curves obtained from SASW data processed by HWAW method for Profile 1 and Profile 3.

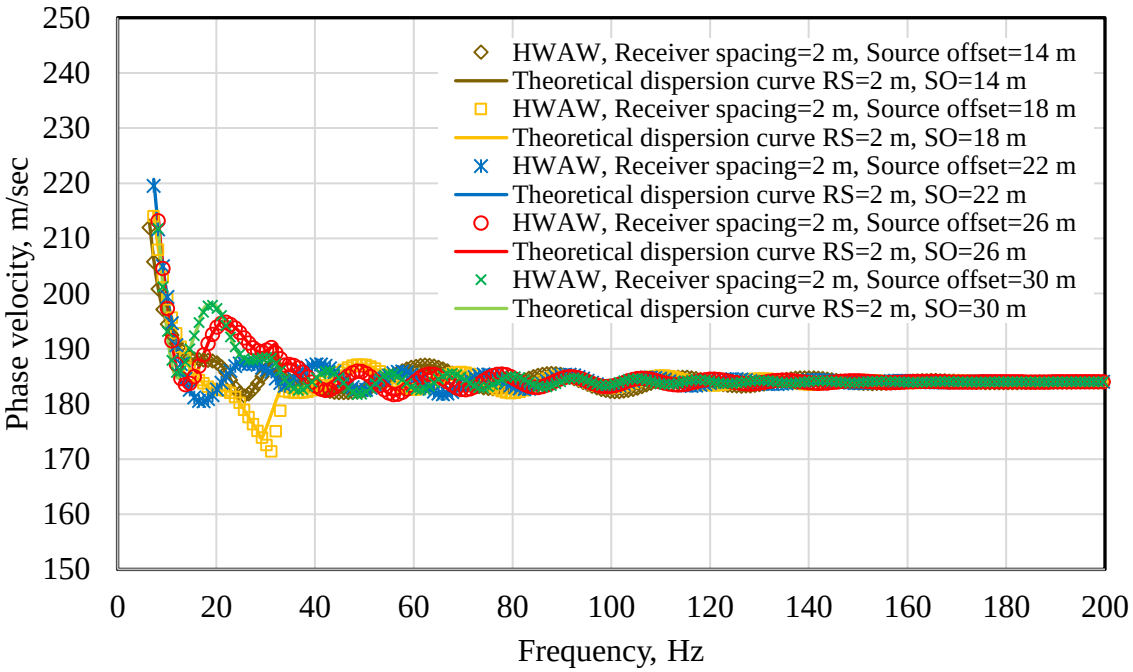

(a)

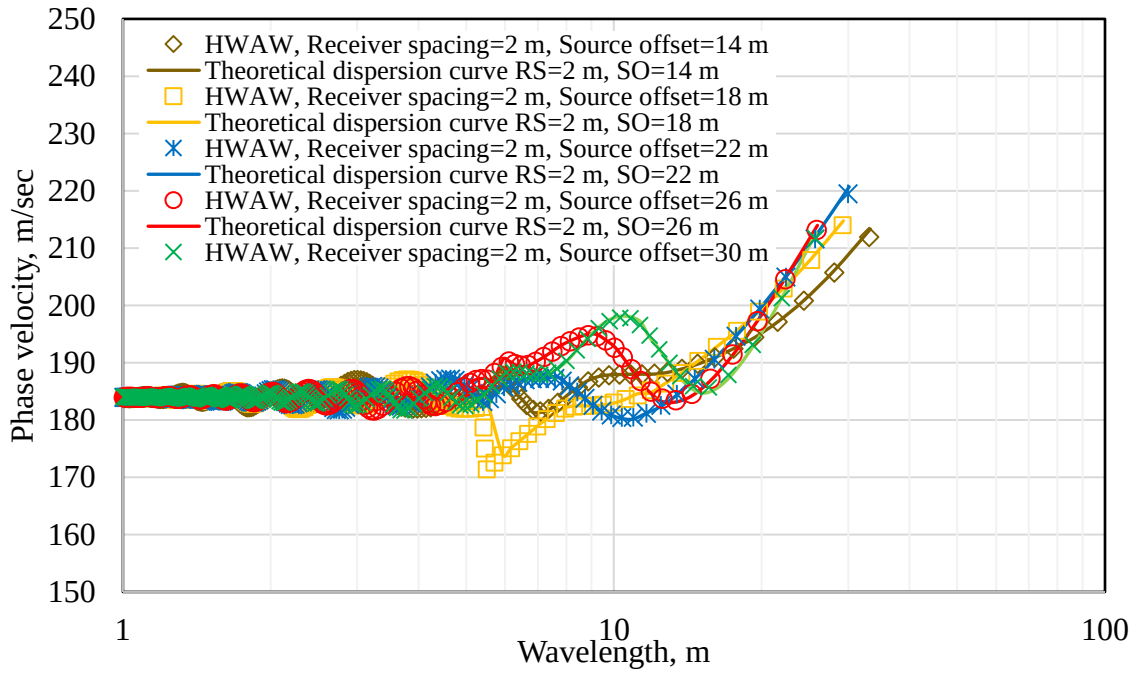

(b)

Figure B.1 Comparison of theoretical and HWAW processed phase velocity dispersion curves from Profile 1 with receiver spacing of 2 m and different source offsets using f_s=1875 Hz (a) Velocity versus frequency (b) Velocity versus wavelength.

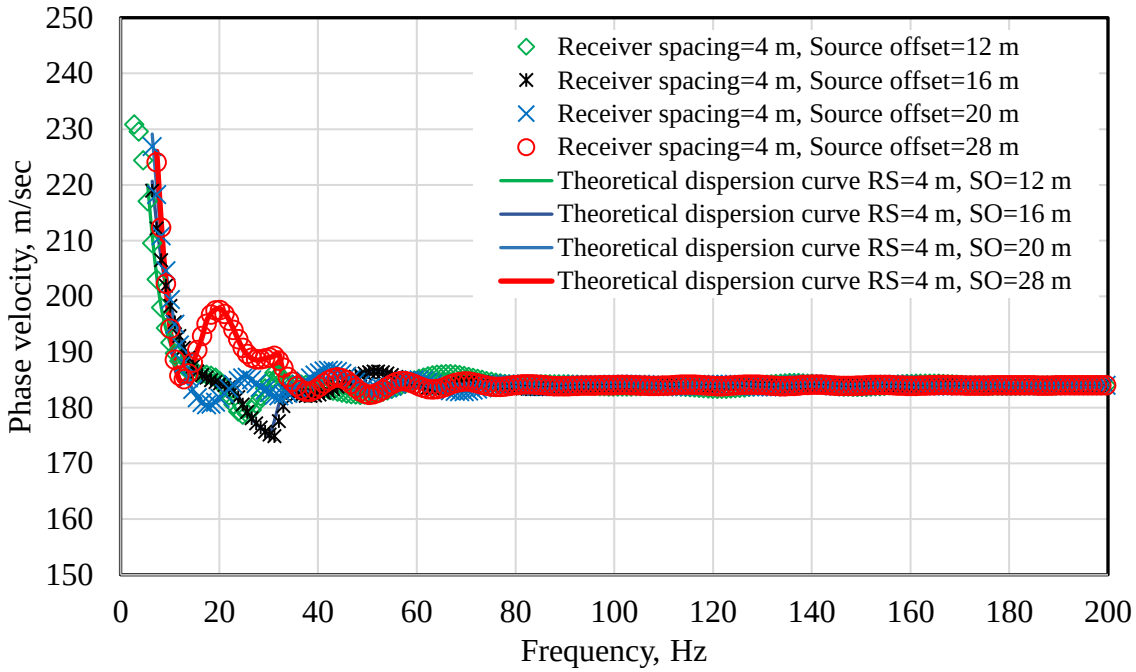

(a)

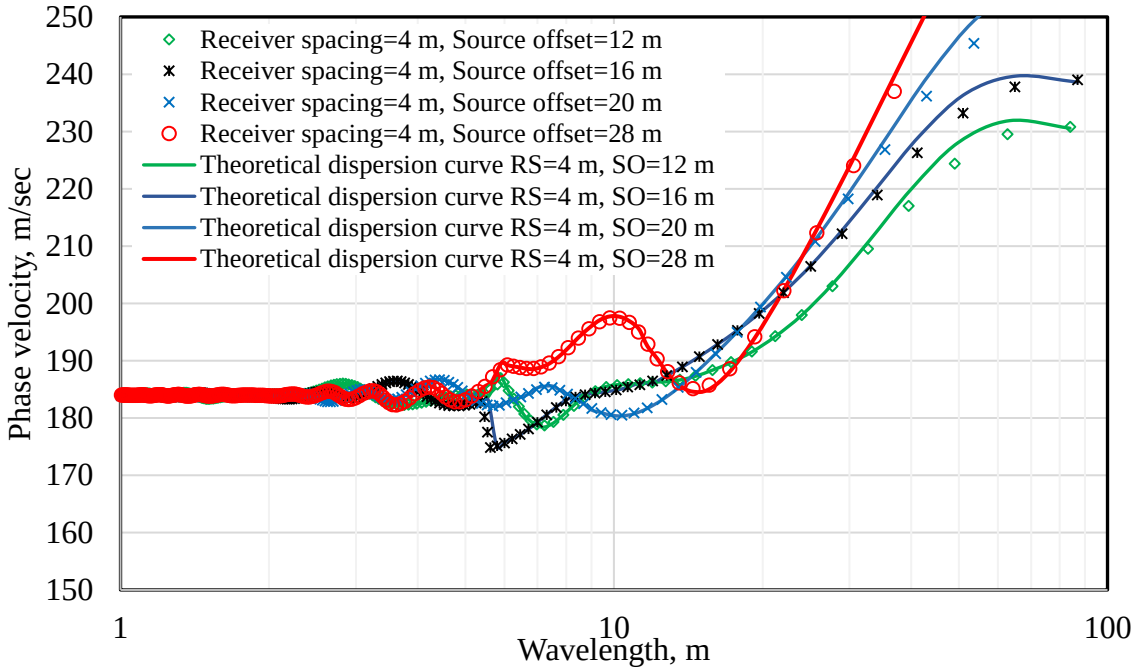

(b)

Figure B.2 Comparison of theoretical and HWAW processed phase velocity dispersion curves from Profile 1 with receiver spacing of 4 m and different source offsets using f_s=1875 Hz (a) Velocity versus frequency (b) Velocity versus wavelength.

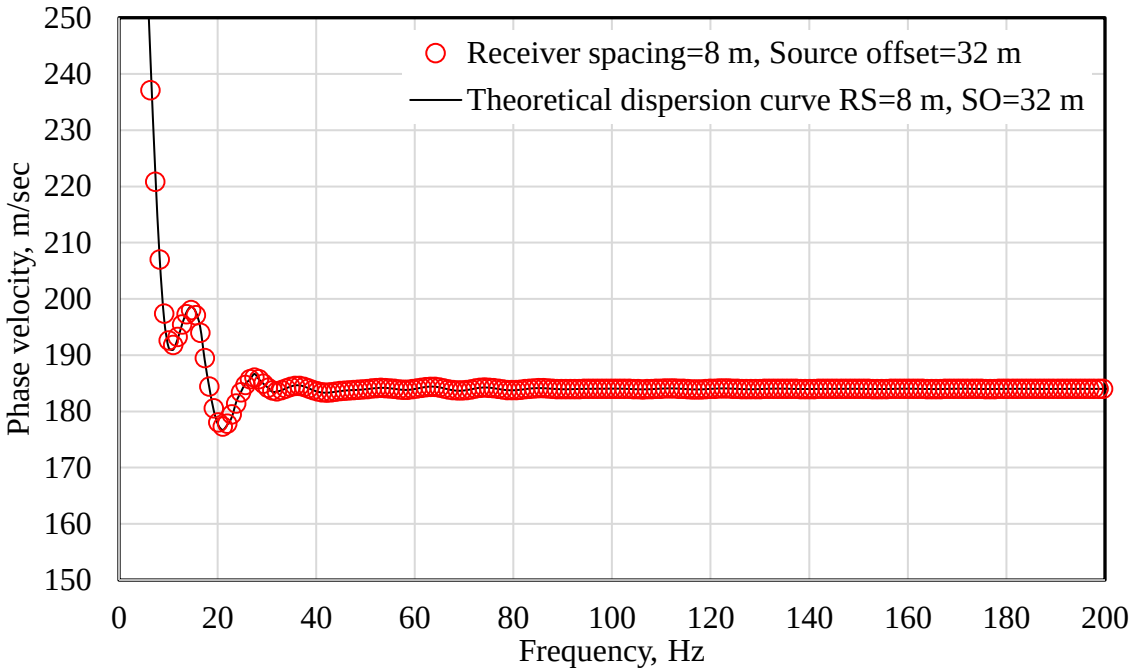

(a)

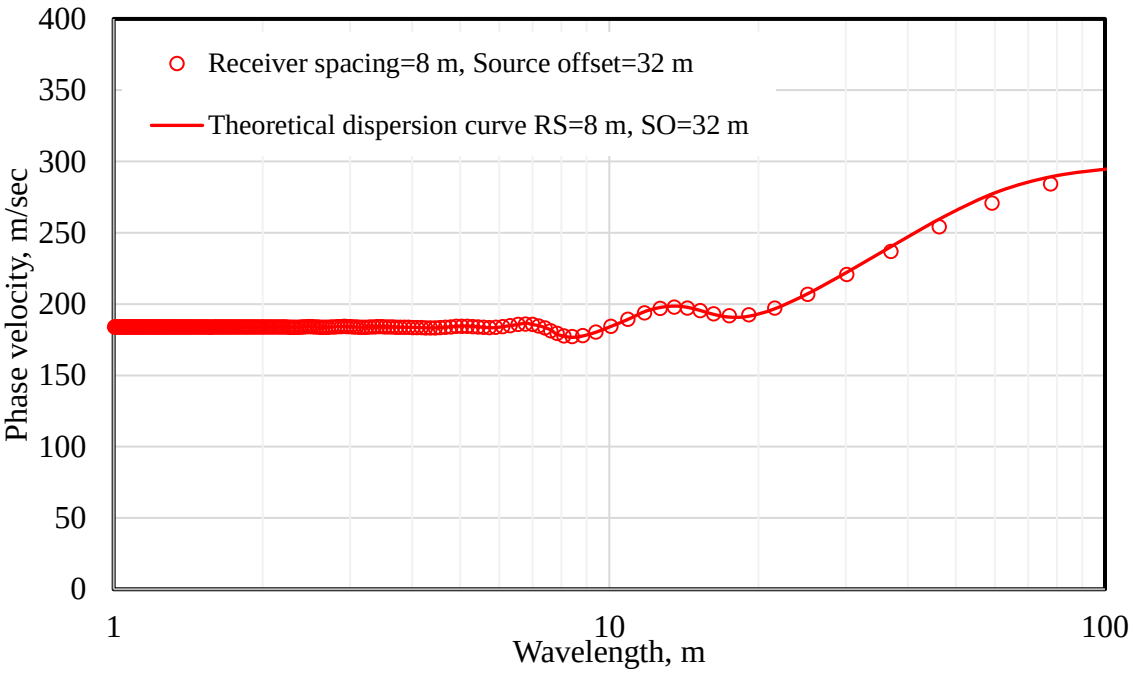

(b)

Figure B.3 Comparison of theoretical and HWAW processed phase velocity dispersion curves from Profile 1 with receiver spacing of 8 m and source offset of 32m using f_s=1875 Hz (a) Velocity versus frequency (b) Velocity versus wavelength.

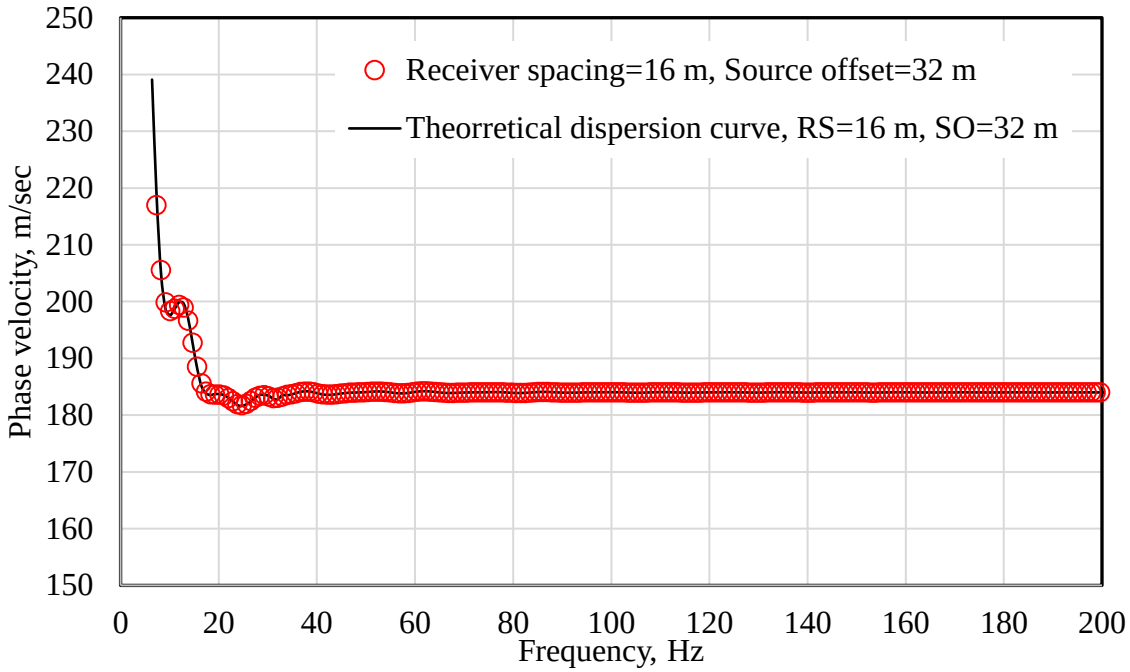

(a)

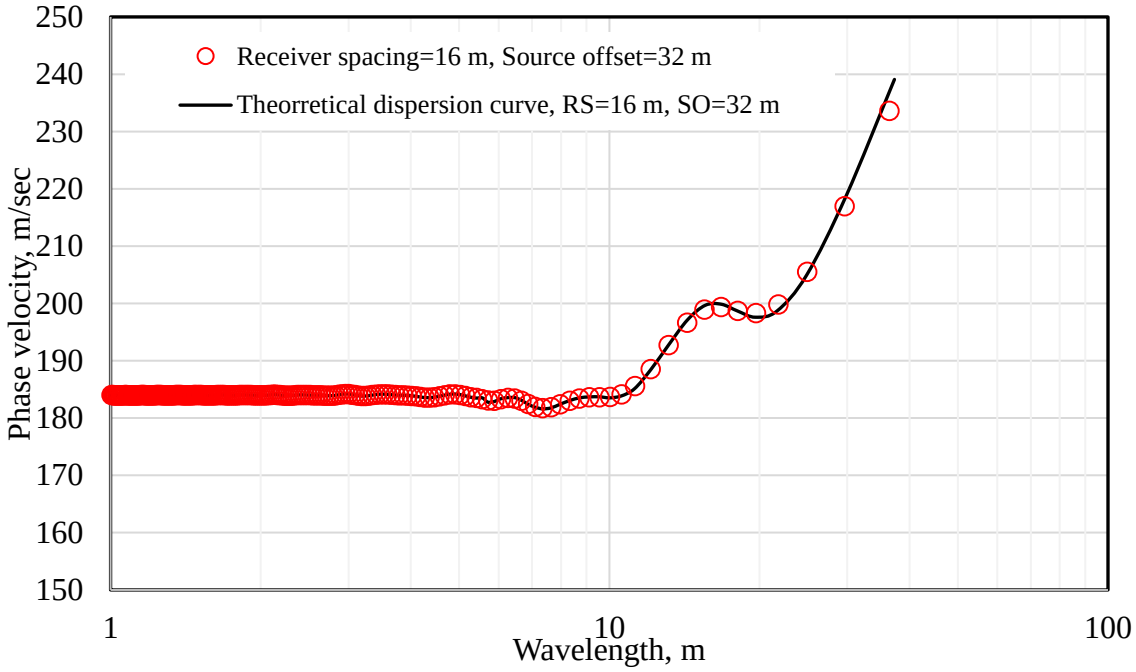

(b)

Figure B.4 Comparison of theoretical and HWAW processed phase velocity dispersion curves from Profile 1 with receiver spacing of 16 m and source offset= 32m using f_s=1875 Hz (a) Velocity versus frequency (b) Velocity versus wavelength.

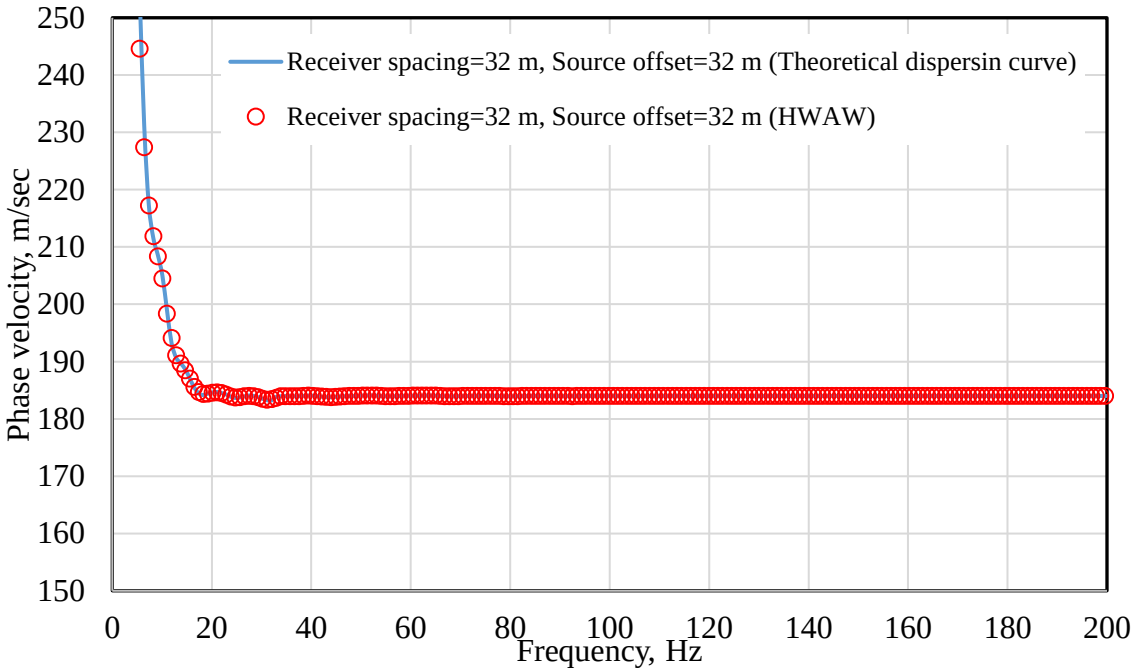

(a)

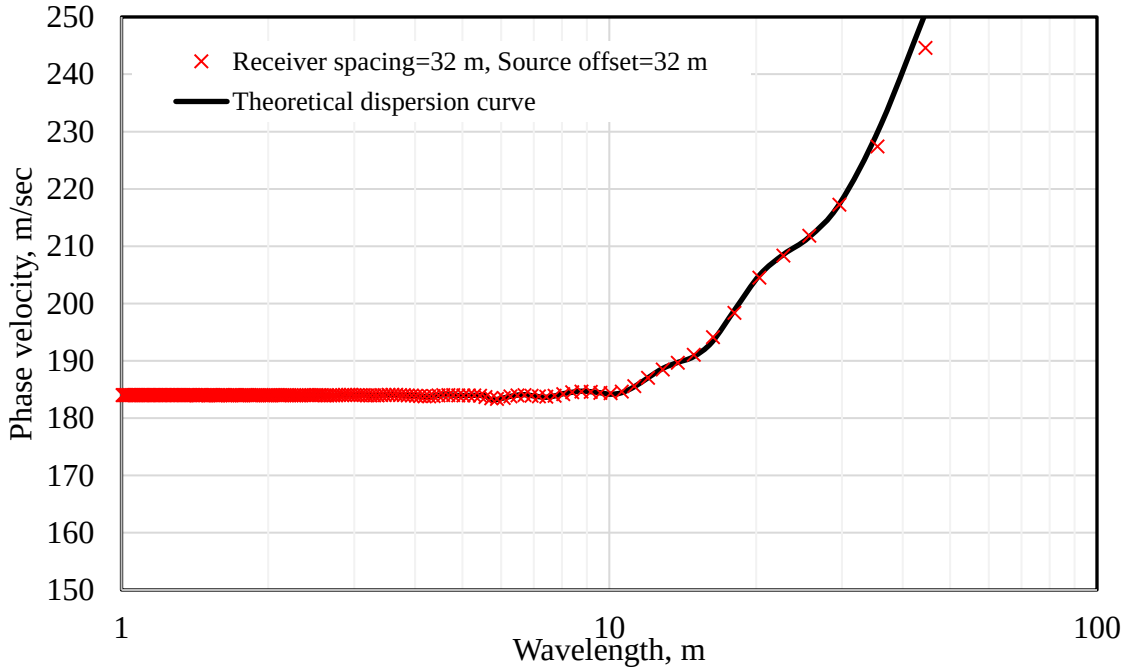

(b)

Figure B.5 Comparison of theoretical and HWAW processed phase velocity dispersion curves from Profile 1 with receiver spacing of 32 m and source offset=32m using f_s=1875 Hz (a) Velocity versus frequency (b) Velocity versus wavelength.

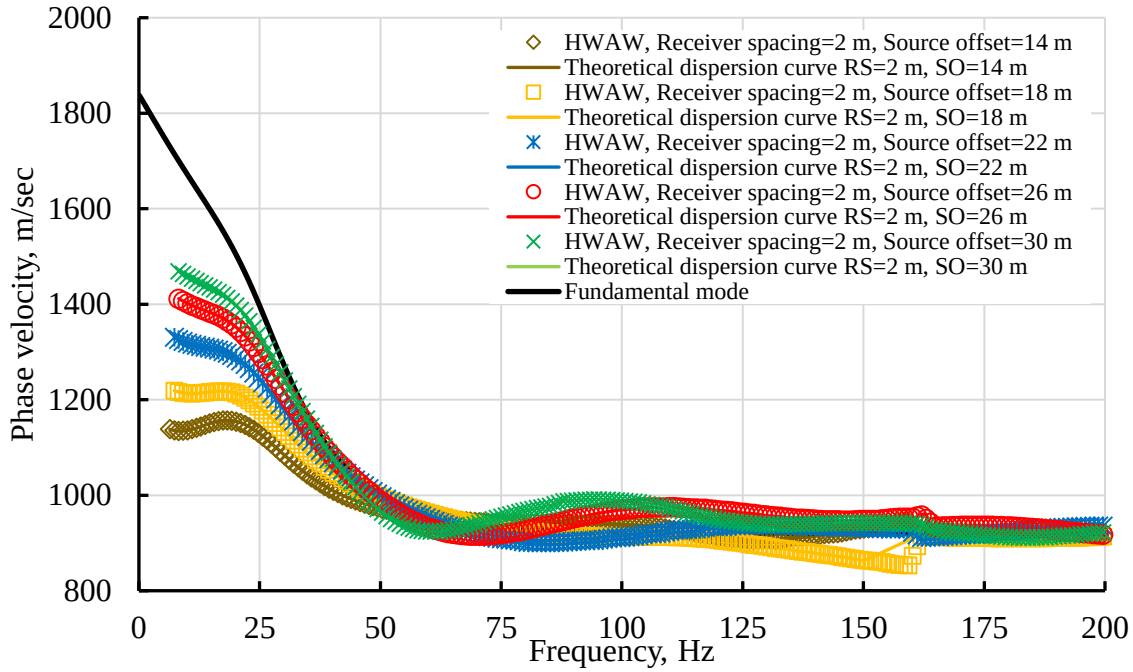

(a)

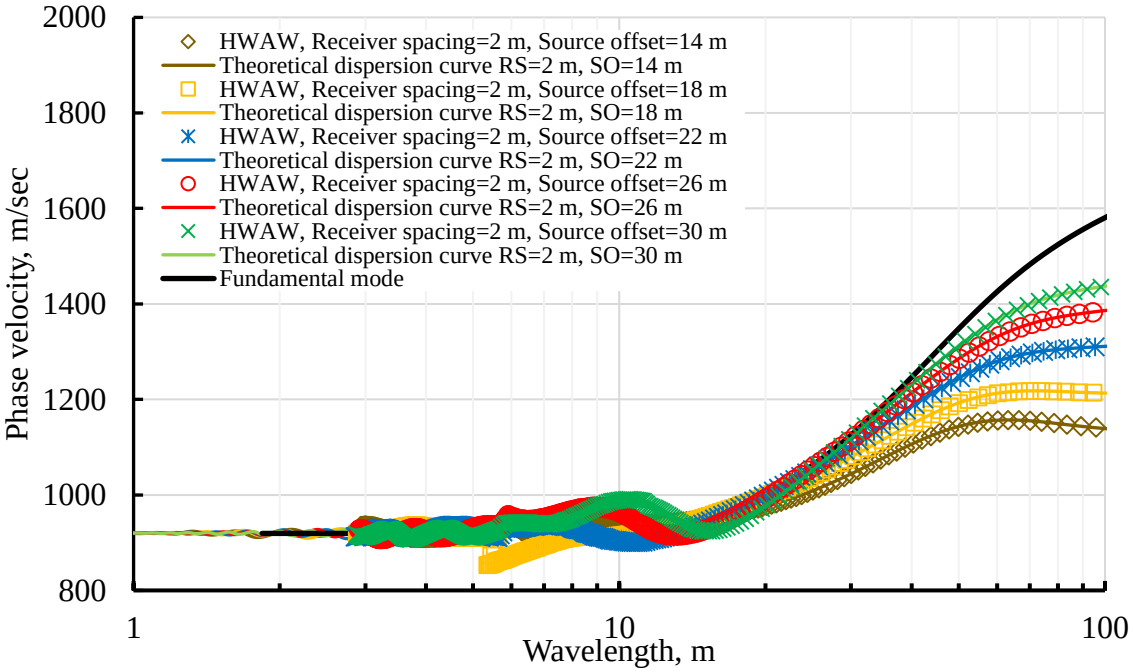

(b)

Figure B.6 Comparison of theoretical and HWAW processed phase velocity dispersion curves from Profile 3 with receiver spacing of 2 m and different source offsets using f_s=1875 Hz (a) Velocity versus frequency (b) Velocity versus wavelength.

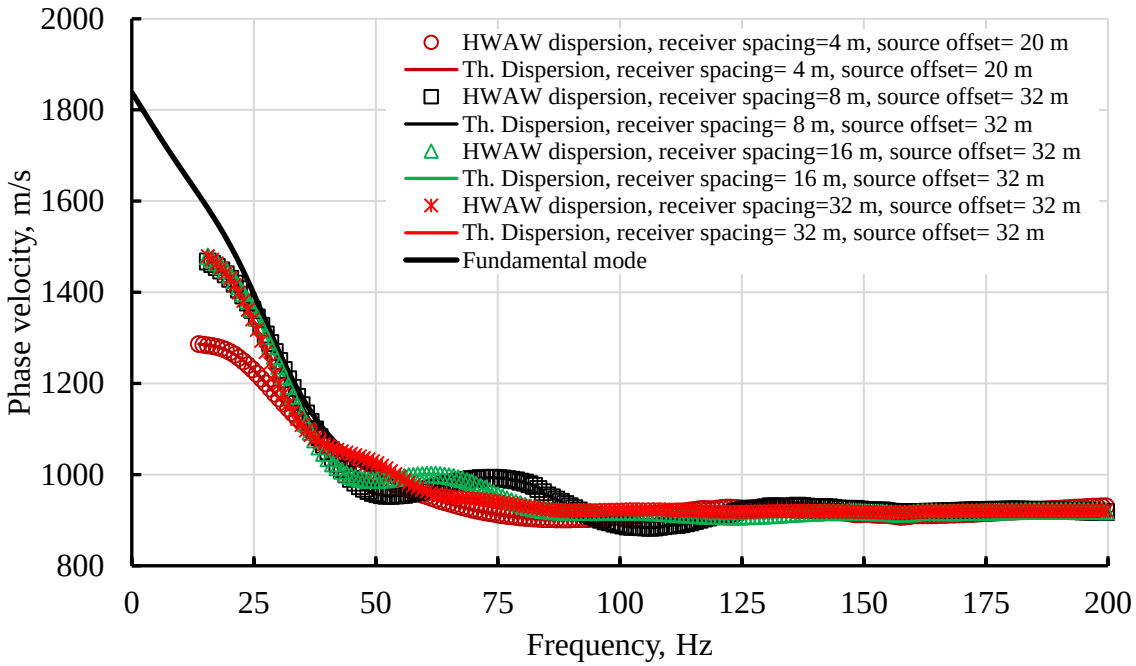

(a)

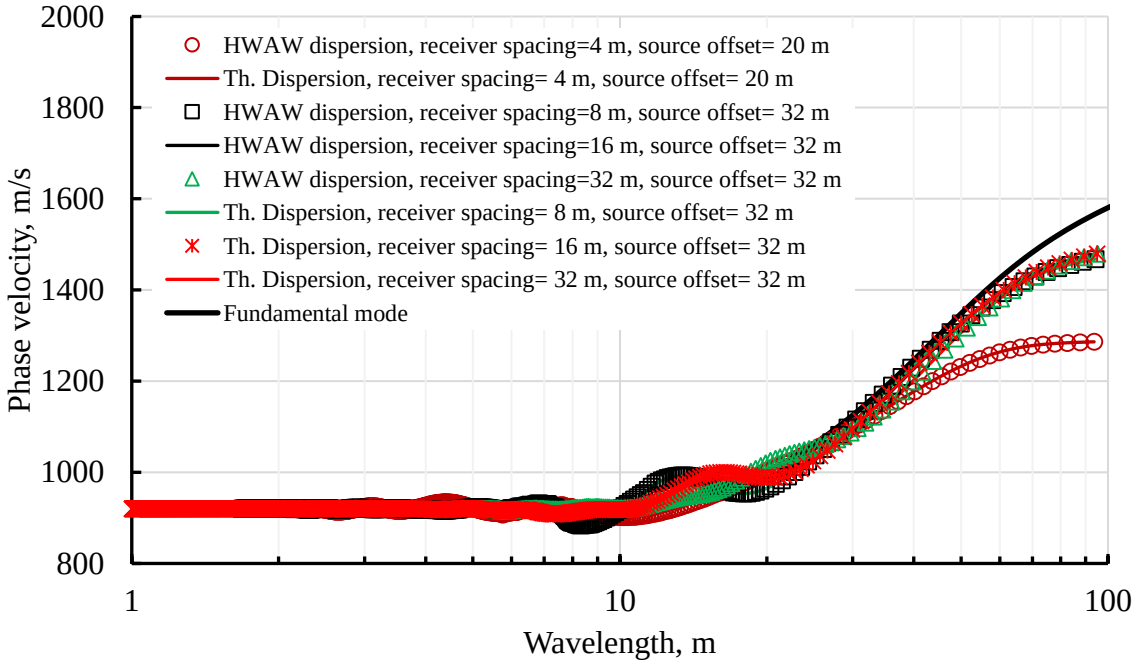

(b)

Figure B.7 Comparison of theoretical and HWAW processed phase velocity dispersion curves from Profile 3 with receiver spacings of 4m, 8m, 16m, and 32 and different source offsets using f_s=1875 Hz (a) Velocity versus frequency (b) Velocity versus wavelength.

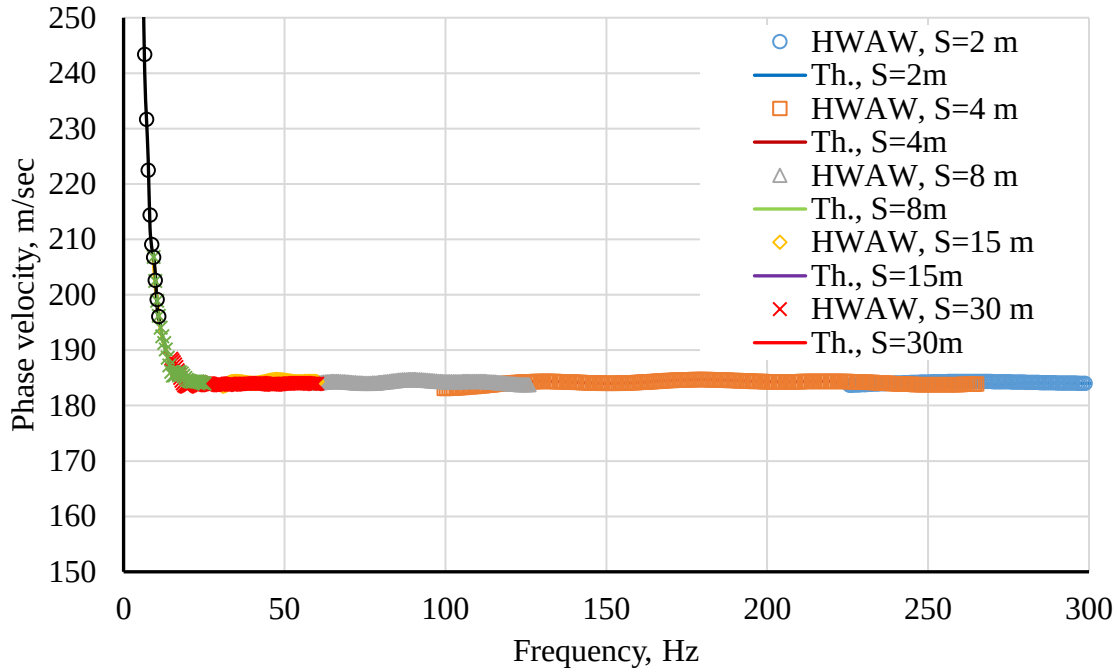

Figure B.8 Simulated data from Profile 1 using conventional SASW source and receiver spacings but processed with the HWAW method and compared to theoretical values in term of phase velocity versus frequency.

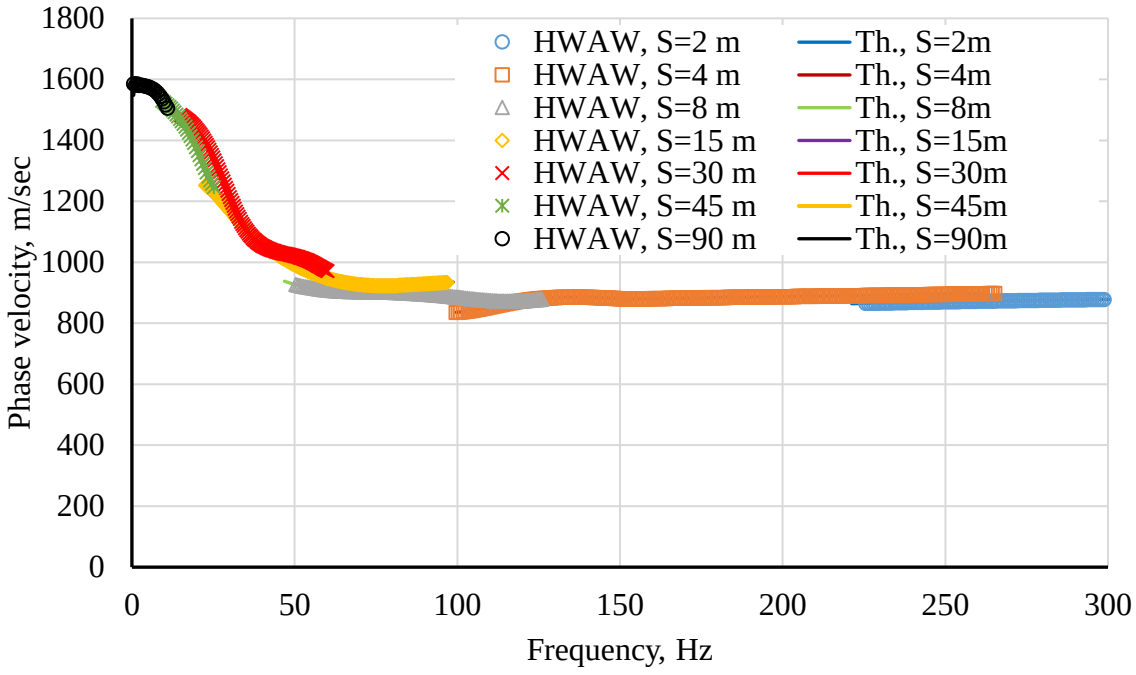

Figure B.9 Simulated data from Profile 3 using conventional SASW source and receiver spacings but processed with the HWAW method and compared to theoretical values in term of phase velocity versus frequency.

Appendix C

This appendix documents the results of Profiles 1-P25, 1-P33, 1-P40, 1-P45, 2-P25, 2-P33, 2-P40, 2-P45, 3-P25, 3-P33, 3-P40, and 3-P45. Dispersion curves are presented in terms of phase velocity versus frequency for different Poisson's ratio values and variable test setups regarding receiver spacings of 2m, 4m, 8m, 16m, 32m with various source offsets are shown in this appendix.

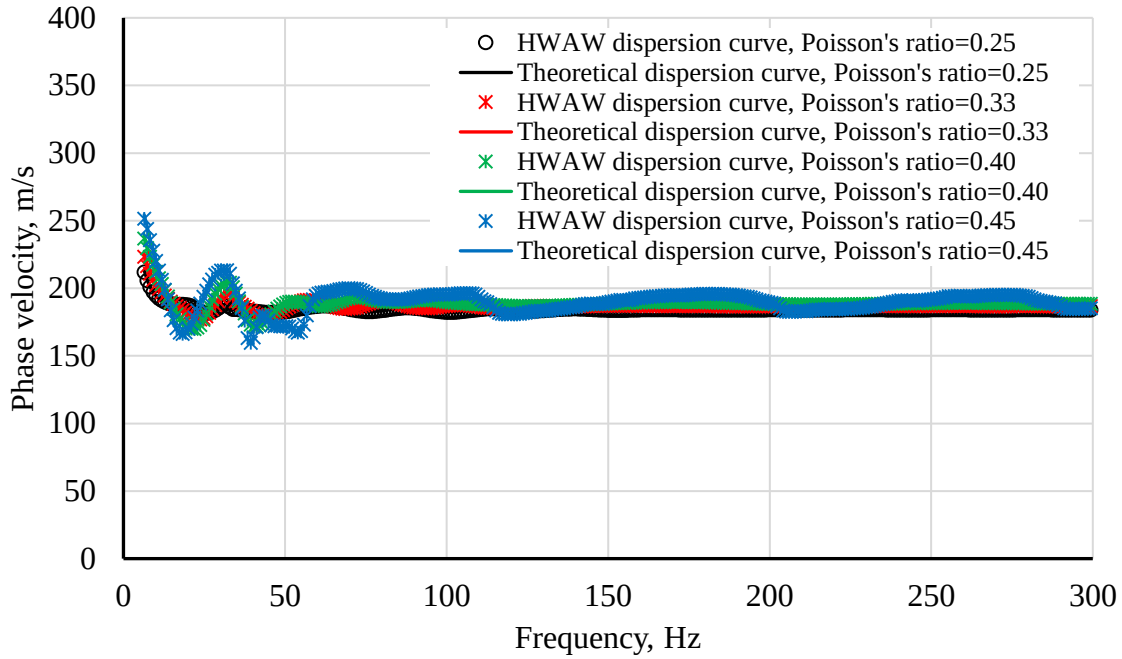

Figure C.1 Comparison of HWAW and theoretical dispersion curves for Profiles 1-P25, 1-P33, 1-P40, and 1-P45 with receiver spacing of 2m and source offset of 14m

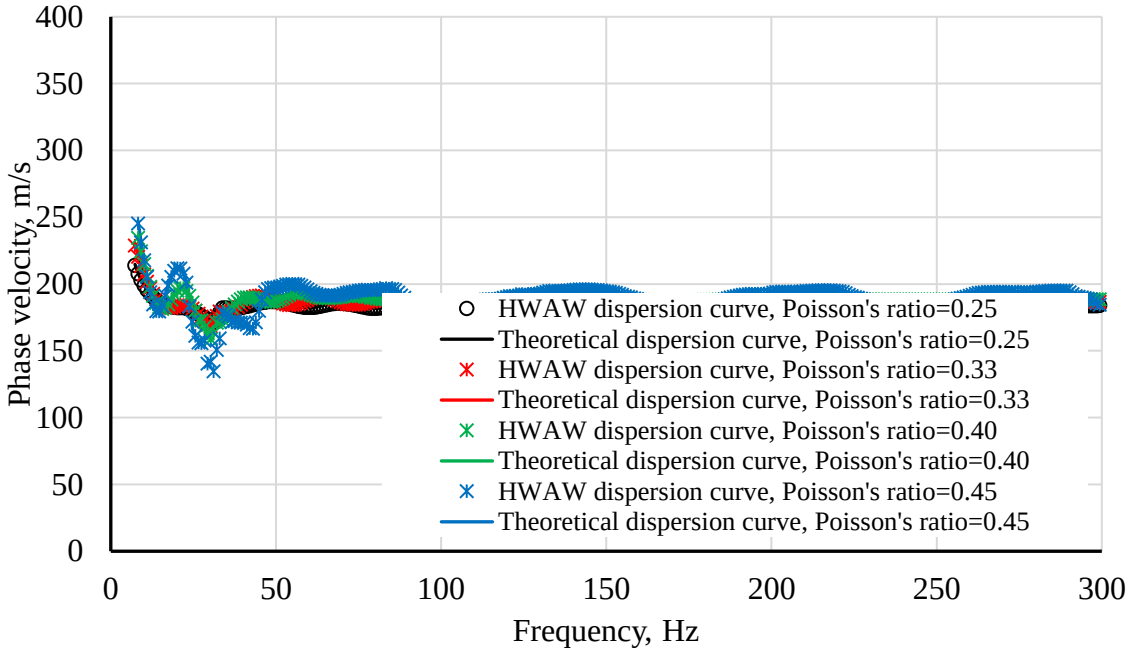

Figure C.2 Comparison of HWAW and theoretical dispersion curves for Profiles 1-P25, 1-P33, 1-P40, and 1-P45 with receiver spacing of 2m and source offset of 18m

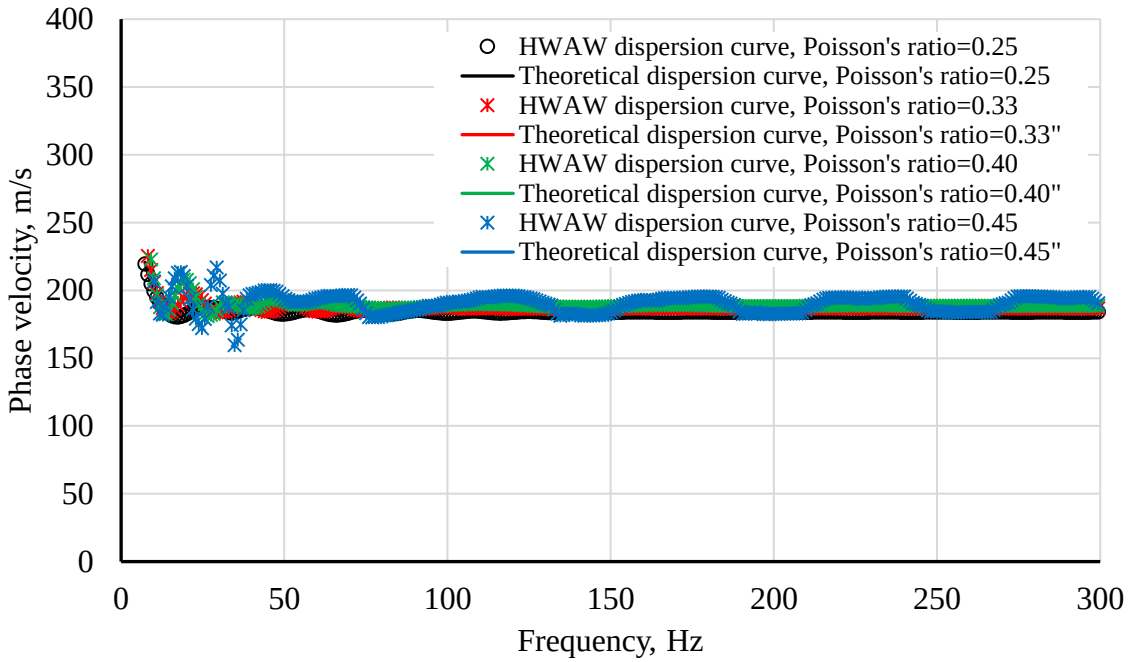

Figure C.3 Comparison of HWAW and theoretical dispersion curves for Profiles 1-P25, 1-P33, 1-P40, and 1-P45 with receiver spacing of 2m and source offset of 22m

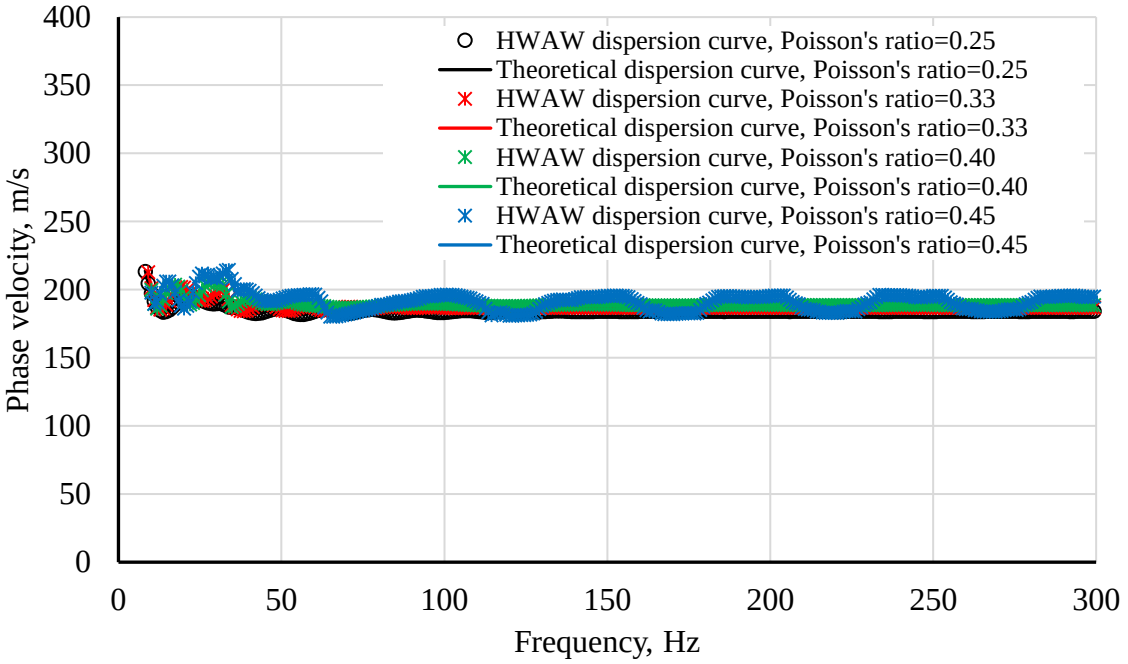

Figure C.4 Comparison of HWAW and theoretical dispersion curves for Profiles 1-P25, 1-P33, 1-P40, and 1-P45 with receiver spacing of 2m and source offset of 26m

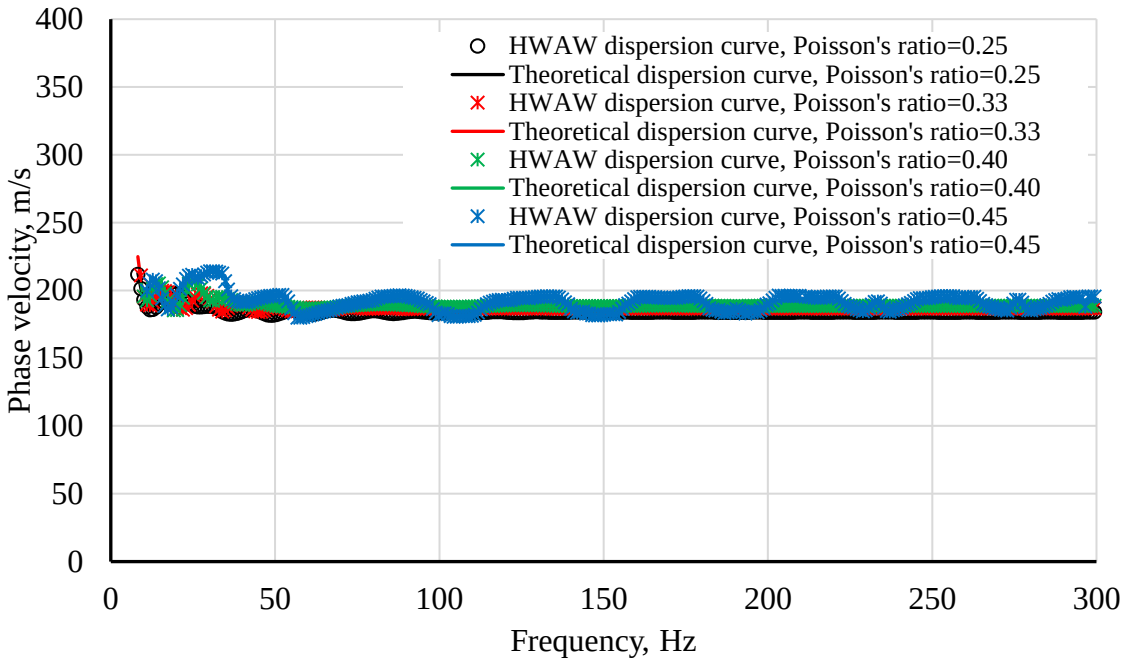

Figure C.5 Comparison of HWAW and theoretical dispersion curves for Profiles 1-P25, 1-P33, 1-P40, and 1-P45 with receiver spacing of 2m and source offset of 30m

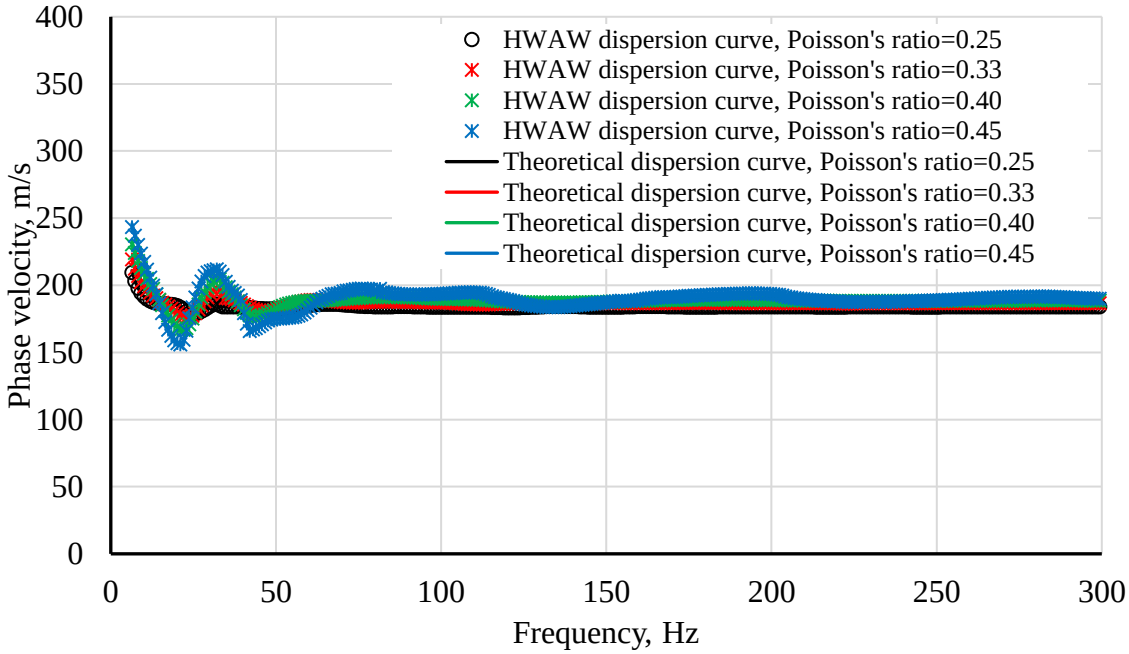

Figure C.6 Comparison of HWAW and theoretical dispersion curves for Profiles 1-P25, 1-P33, 1-P40, and 1-P45 with receiver spacing of 4m and source offset of 12m

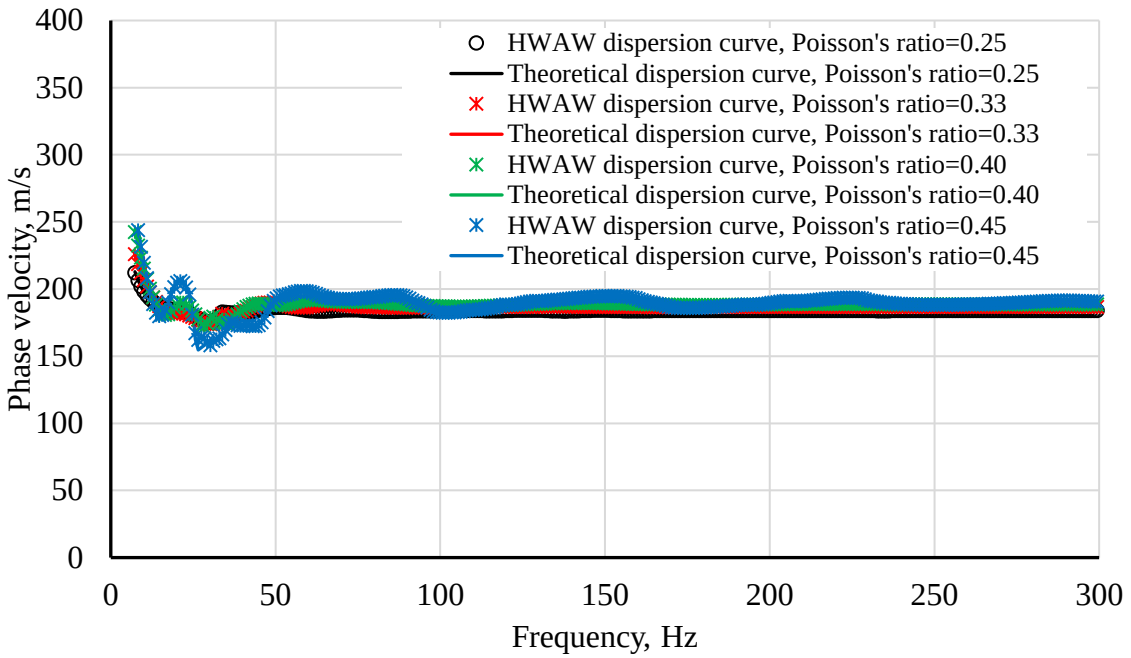

Figure C.7 Comparison of HWAW and theoretical dispersion curves for Profiles 1-P25, 1-P33, 1-P40, and 1-P45 with receiver spacing of 4m and source offset of 16m

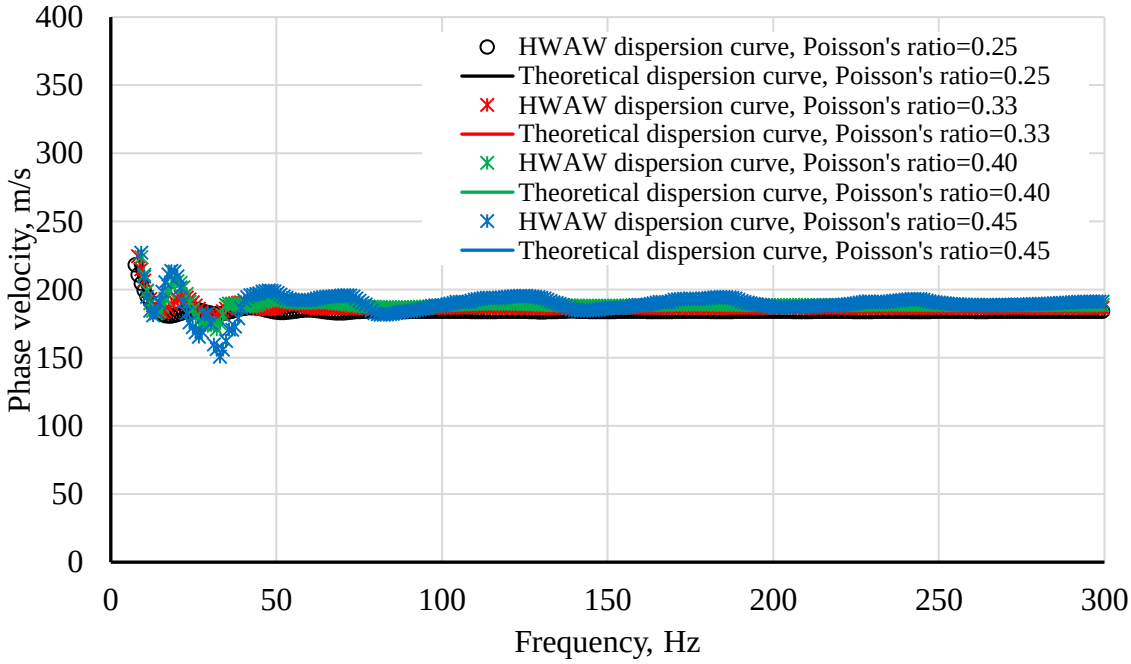

Figure C.8 Comparison of HWAW and theoretical dispersion curves for Profiles 1-P25, 1-P33, 1-P40, and 1-P45 with receiver spacing of 4m and source offset of 20m

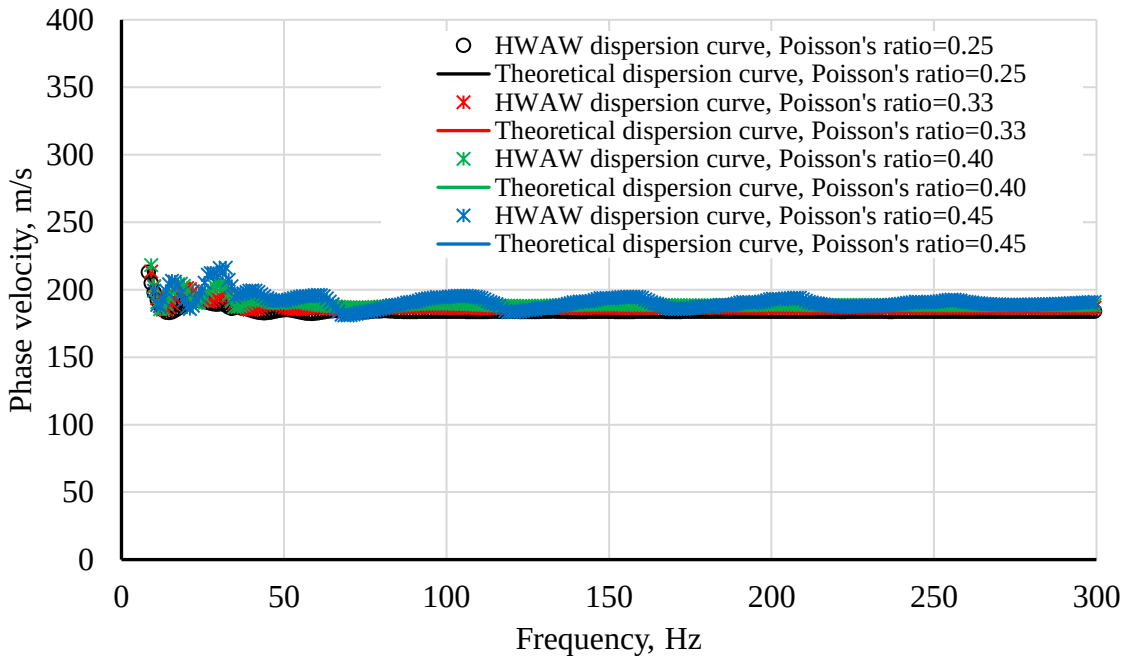

Figure C.9 Comparison of HWAW and theoretical dispersion curves for Profiles 1-P25, 1-P33, 1-P40, and 1-P45 with receiver spacing of 4m and source offset of 24m

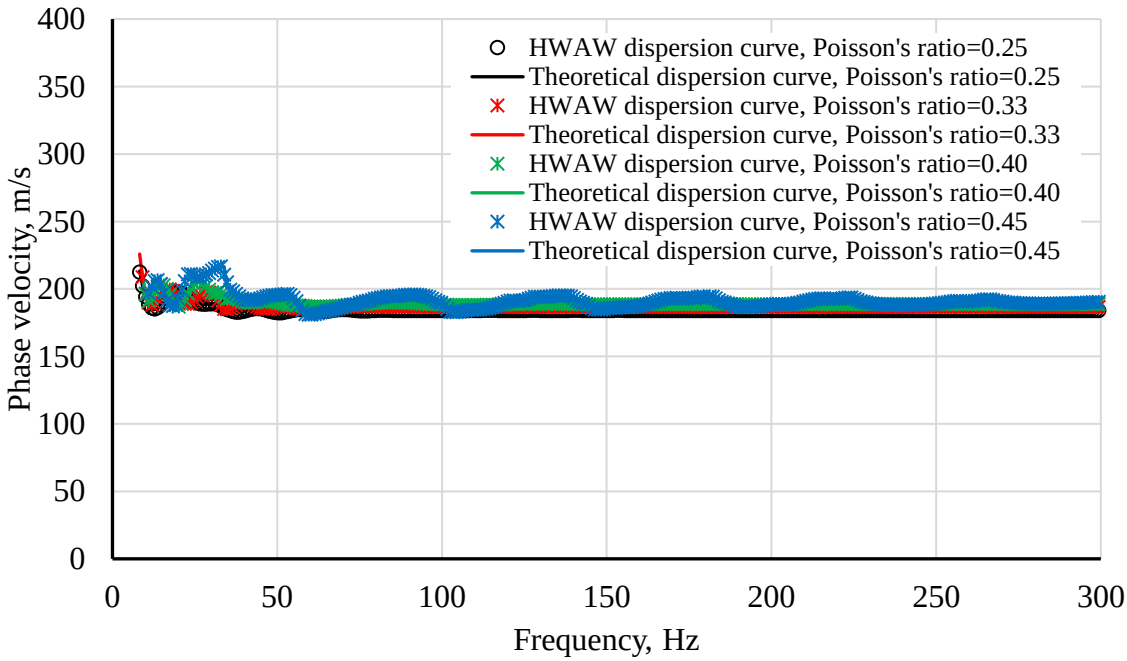

Figure C.10 Comparison of HWAW and theoretical dispersion curves for Profiles 1-P25, 1-P33, 1-P40, and 1-P45 with receiver spacing of 4m and source offset of 32m

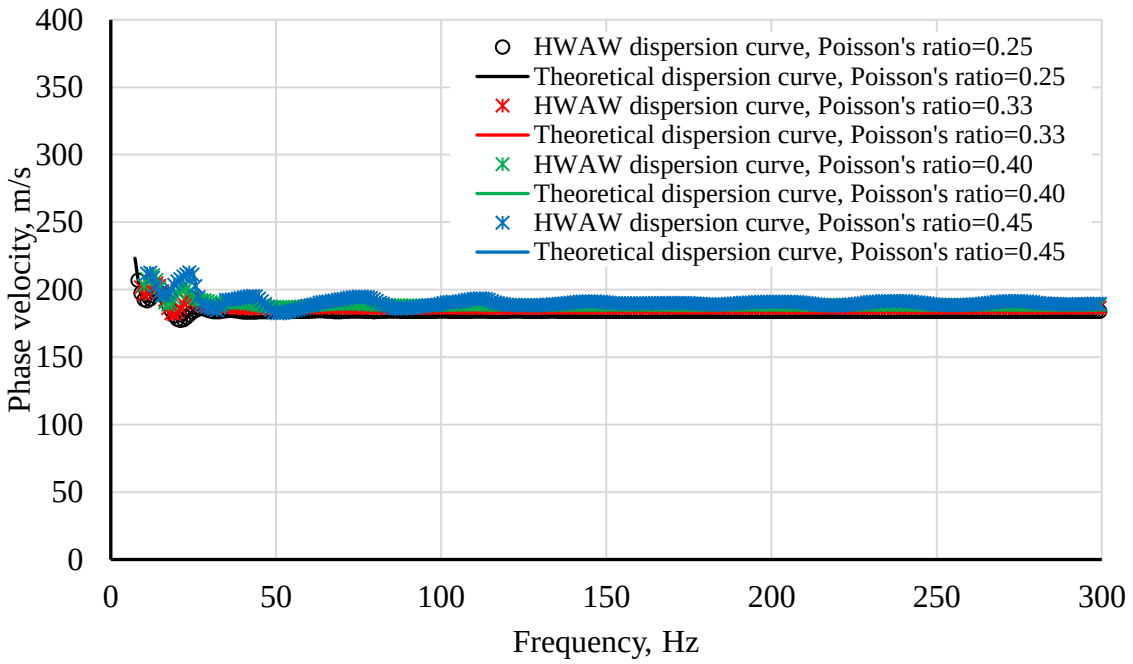

Figure C.11 Comparison of HWAW and theoretical dispersion curves for Profiles 1-P25, 1-P33, 1-P40, and 1-P45 with receiver spacing of 8m and source offset of 32m

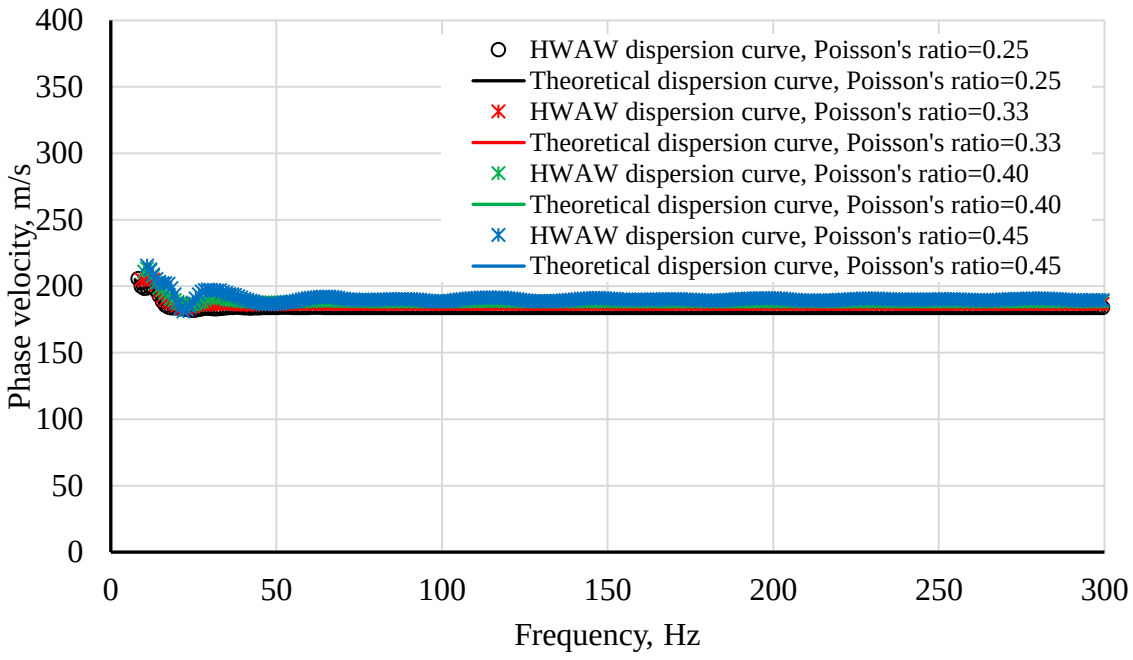

Figure C.12 Comparison of HWAW and theoretical dispersion curves for Profiles 1-P25, 1-P33, 1-P40, and 1-P45 with receiver spacing of 16m and source offset of 32m

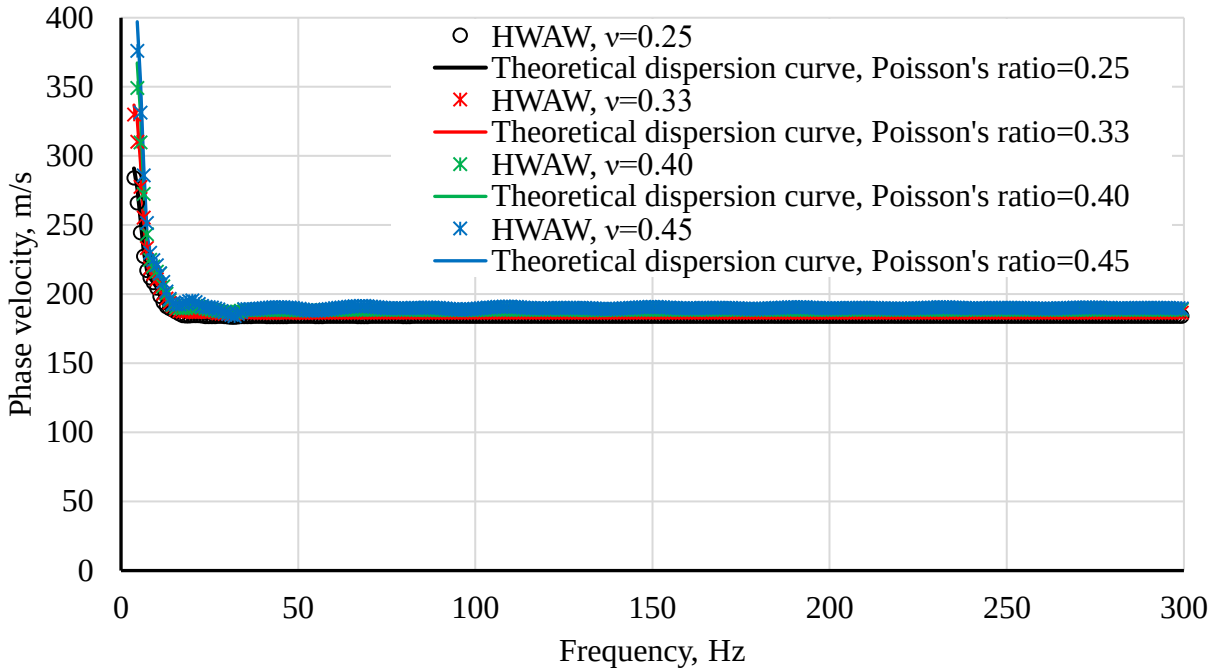

Figure C.13 Comparison of HWAW and theoretical dispersion curves for Profiles 1-P25, 1-P33, 1-P40, and 1-P45 with receiver spacing of 32m and source offset of 32m

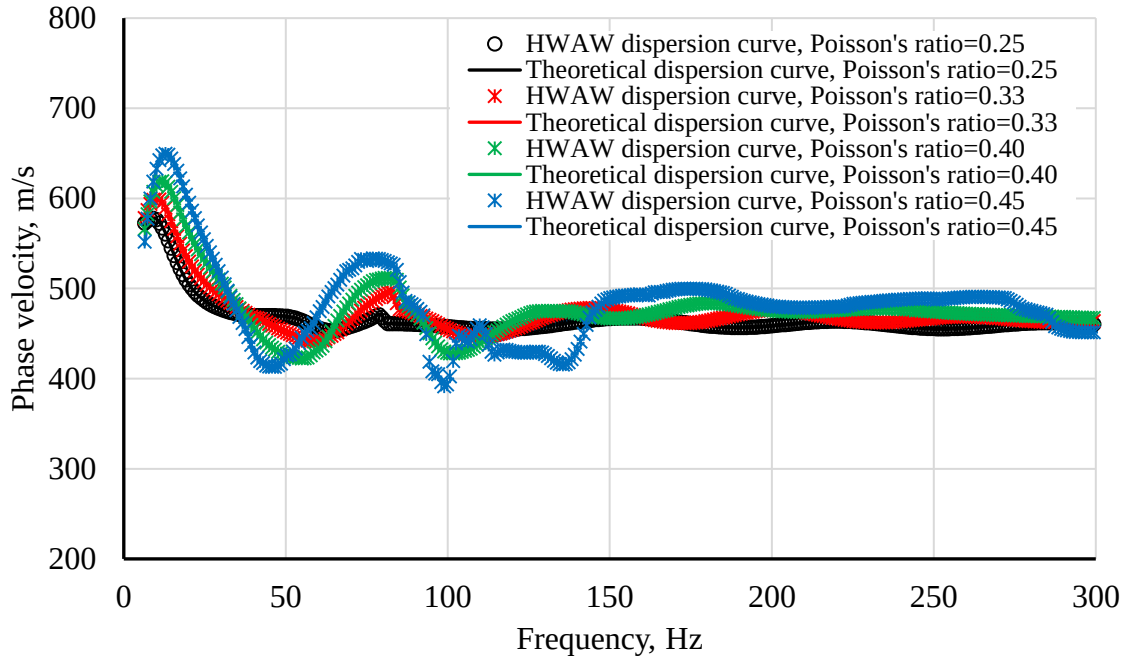

Figure C.14 Comparison of HWAW and theoretical dispersion curves for Profiles 2-P25, 2-P33, 2-P40, and 2-P45 with receiver spacing of 2m and source offset of 14m

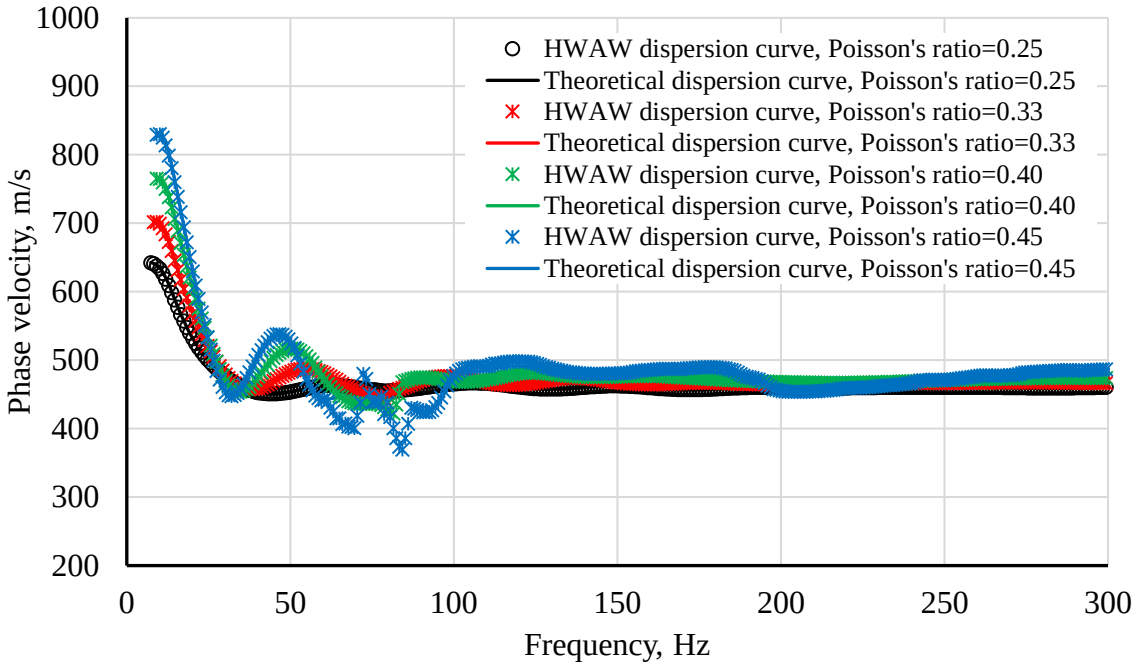

Figure C.15 Comparison of HWAW and theoretical dispersion curves for Profiles 2-P25, 2-P33, 2-P40, and 2-P45 with receiver spacing of 2m and source offset of 20m

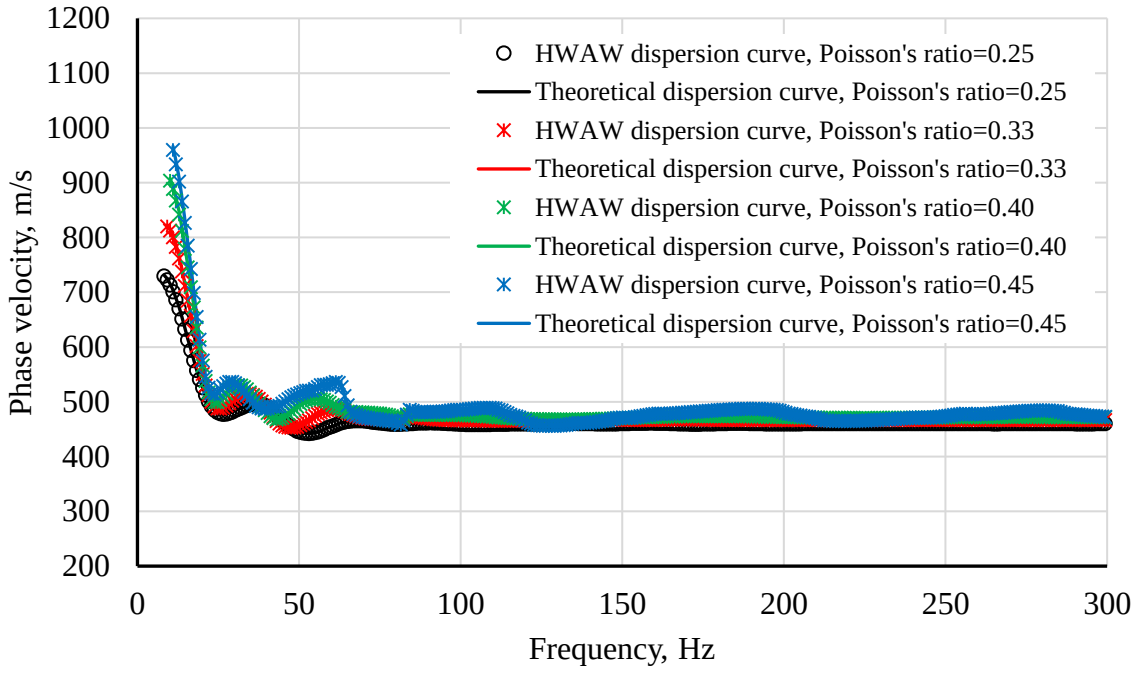

Figure C.16 Comparison of HWAW and theoretical dispersion curves for Profiles 2-P25, 2-P33, 2-P40, and 2-P45 with receiver spacing of 8m and source offset of 32m

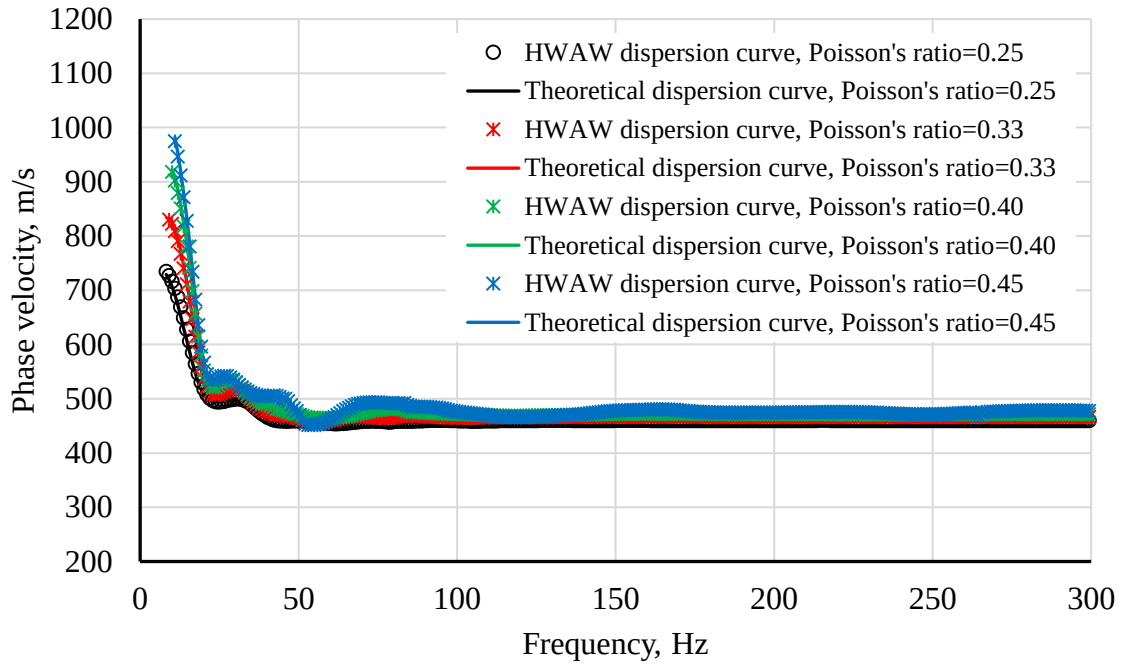

Figure C.17 Comparison of HWAW and theoretical dispersion curves for Profiles 2-P25, 2-P33, 2-P40, and 2-P45 with receiver spacing of 16m and source offset of 32m

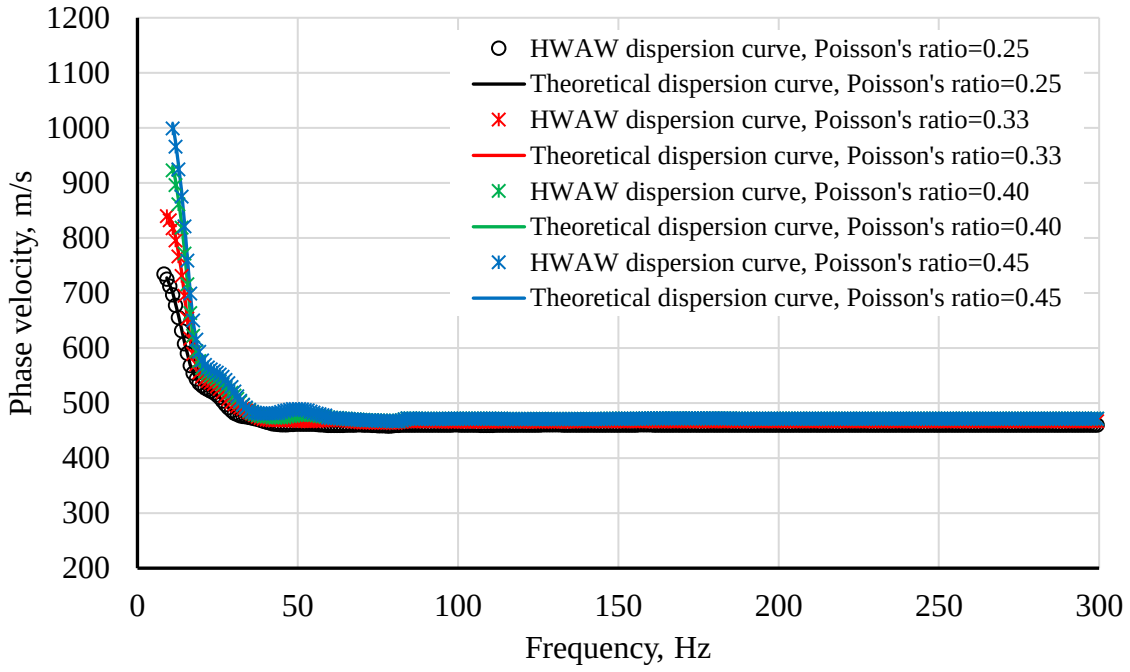

Figure C.18 Comparison of HWAW and theoretical dispersion curves for Profiles 2-P25, 2-P33, 2-P40, and 2-P45 with receiver spacing of 32m and source offset of 32m

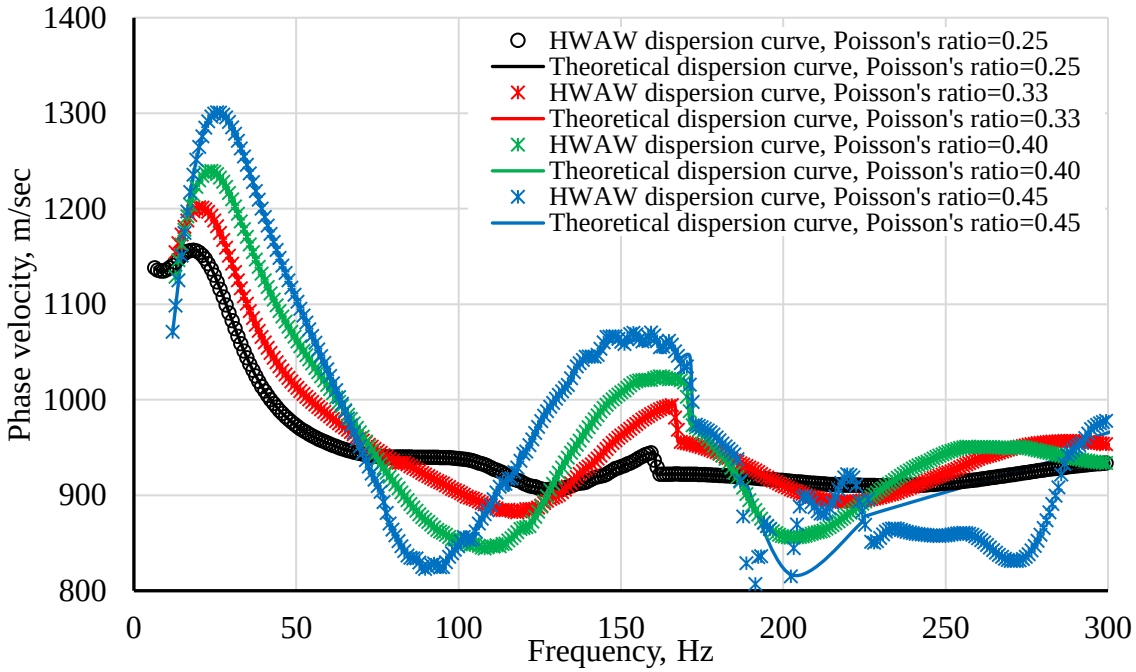

Figure C.19 Comparison of HWAW and theoretical dispersion curves for Profiles 3-P25, 3-P33, 3-P40, and 3-P45 with receiver spacing of 2m and source offset of 14m

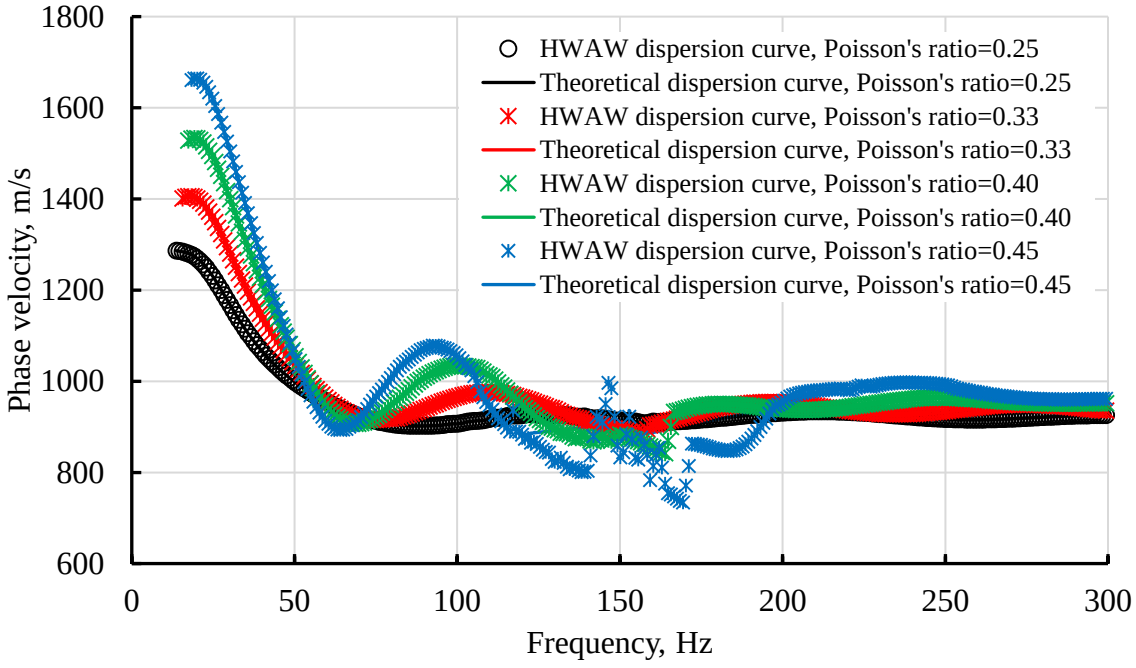

Figure C.20 Comparison of HWAW and theoretical dispersion curves for Profiles 3-P25, 3-P33, 3-P40, and 3-P45 with receiver spacing of 4m and source offset of 20m

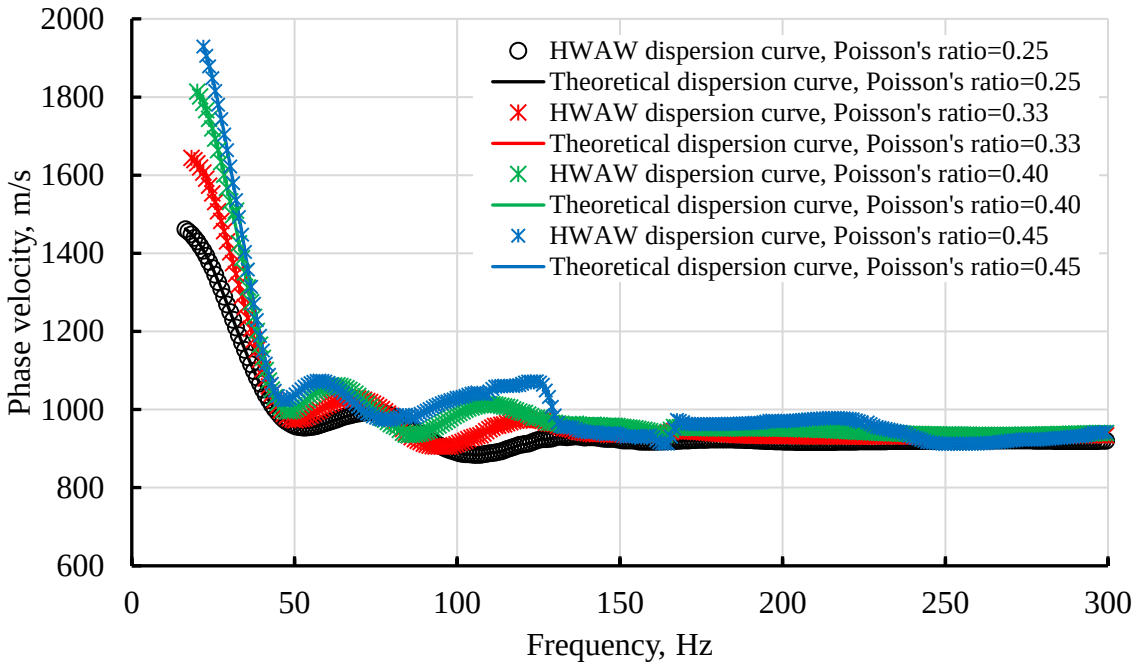

Figure C.21 Comparison of HWAW and theoretical dispersion curves for Profiles 3-P25, 3-P33, 3-P40, and 3-P45 with receiver spacing of 8m and source offset of 32m

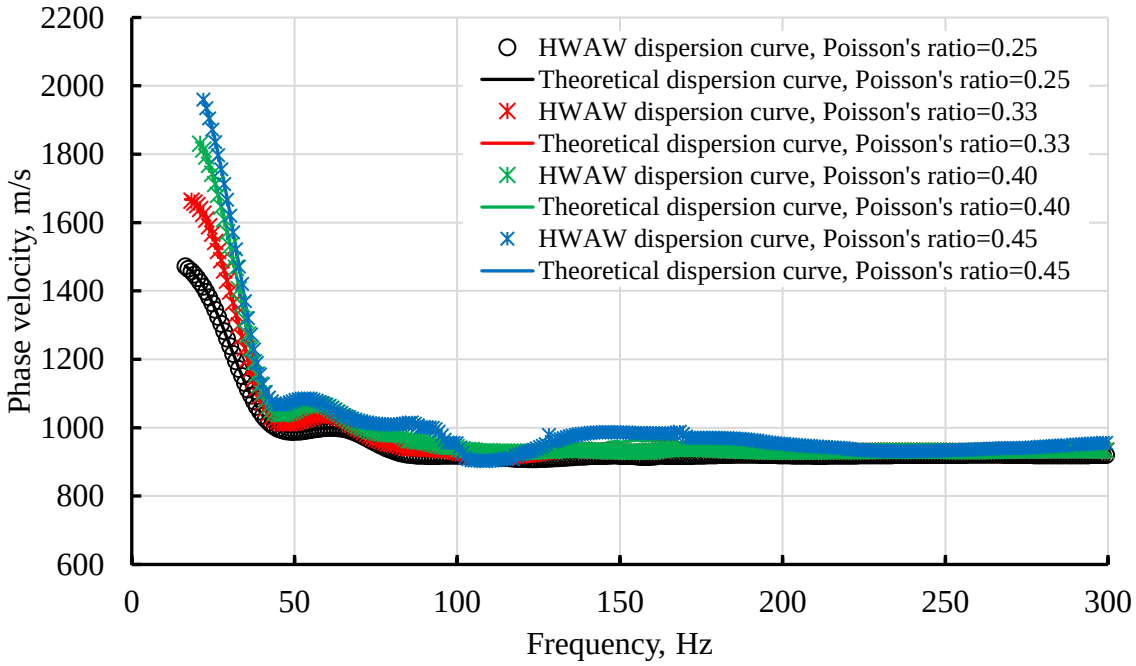

Figure C.22 Comparison of HWAW and theoretical dispersion curves for Profiles 3-P25, 3-P33, 3-P40, and 3-P45 with receiver spacing of 16m and source offset of 32m

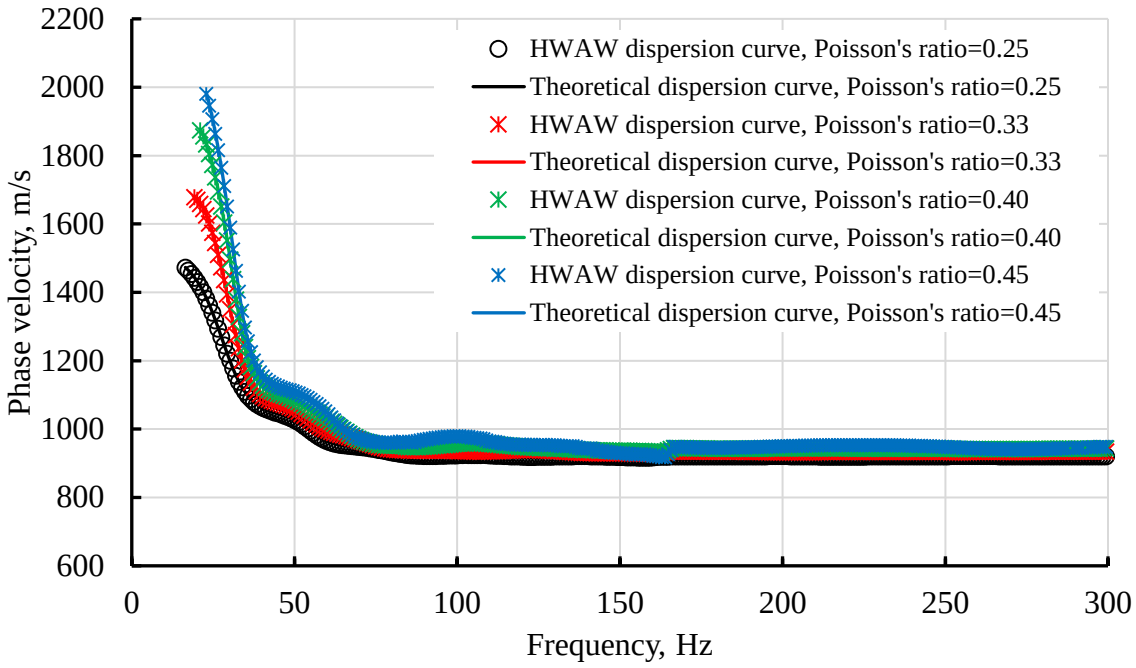

Figure C.23 Comparison of HWAW and theoretical dispersion curves for Profiles 3-P25, 3-P33, 3-P40, and 3-P45 with receiver spacing of 32m and source offset of 32m.

Appendix D

This appendix documents the phase plots for simple Profile 2 and for complex Profiles 5A and 5C.

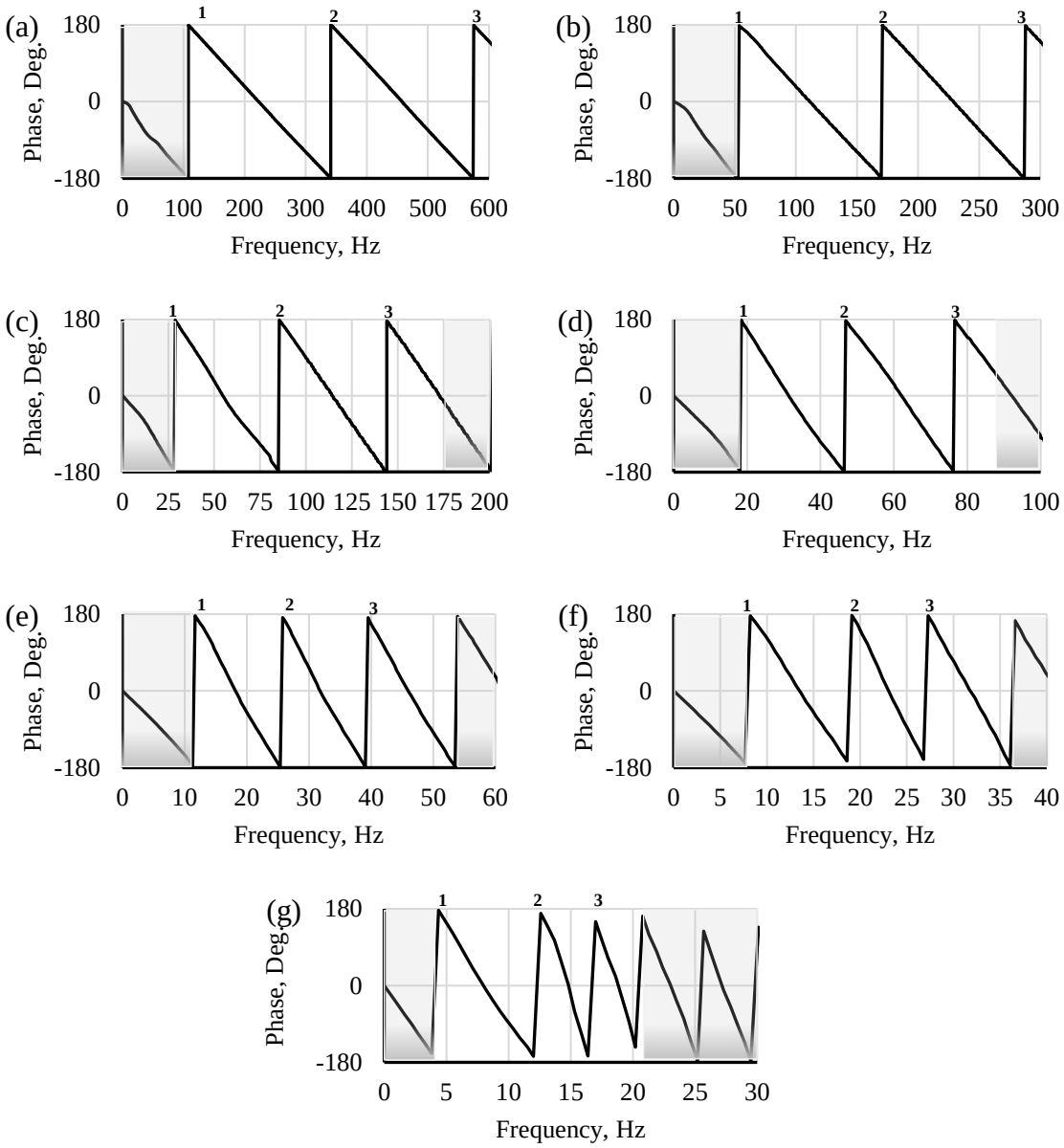

Figure D.1 Wrapped phase plots from simulated SASW measurements at Profile 2 with receiver spacings of (a) 2-2m, (b) 4-4m, (c) 8-8m, (d) 15-15m, (e) 30-30m, (f) 45-45m, and (g)60-60m. Phase unwrapping interpretation is indicated by number of 360° "jumps." Data not used in interpretation are indicated by shaded regions.

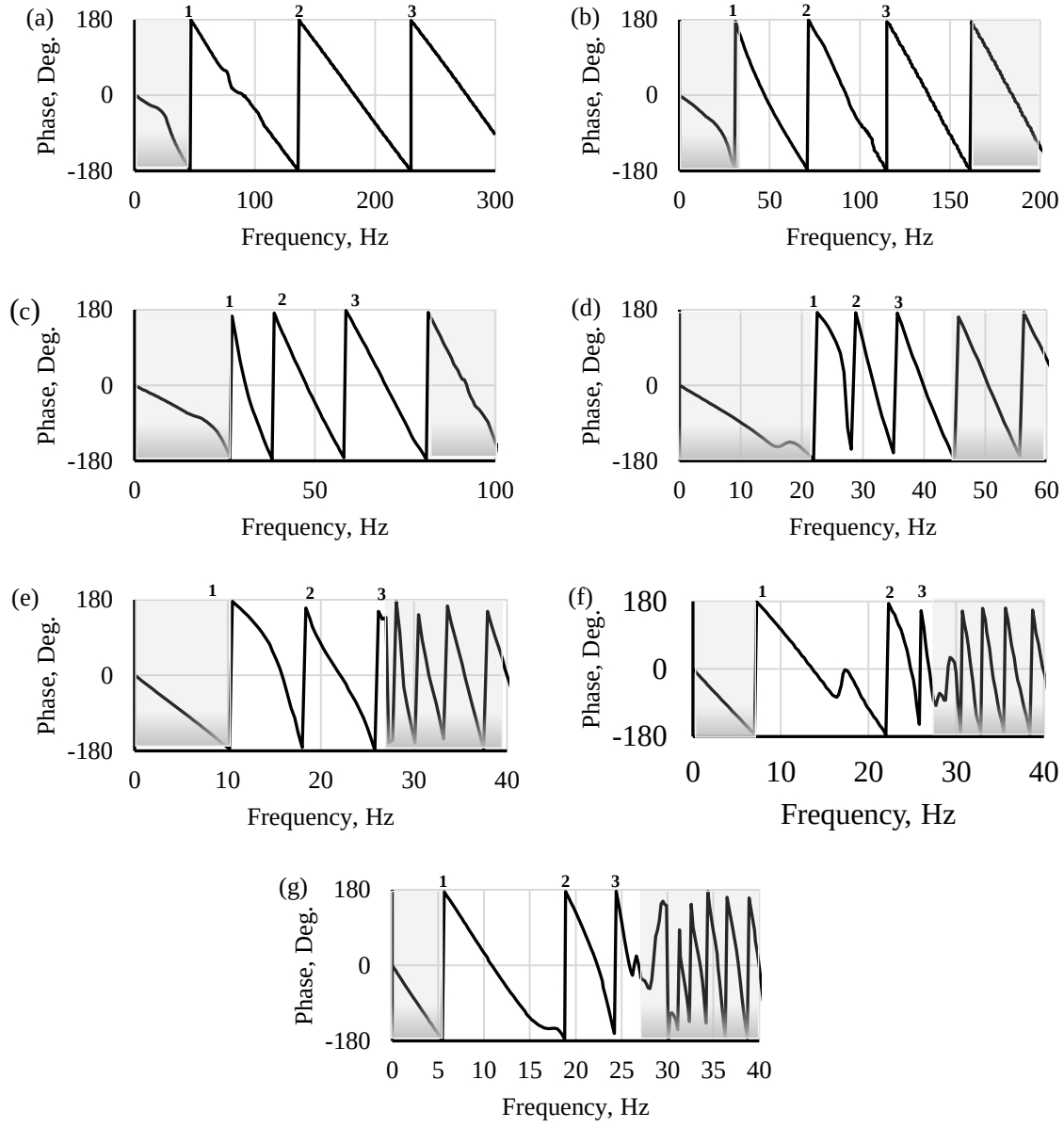

Figure D.2 Wrapped phase plots from simulated SASW measurements at Profile 5A with receiver spacings of (a) 2-2m, (b) 4-4m, (c) 8-8m, (d) 15-15m, (e) 30-30m, (f) 45-45m, and (g)60-60m. Phase unwrapping interpretation is indicated by number of 360° "jumps." Data not used in interpretation are indicated by shaded regions.

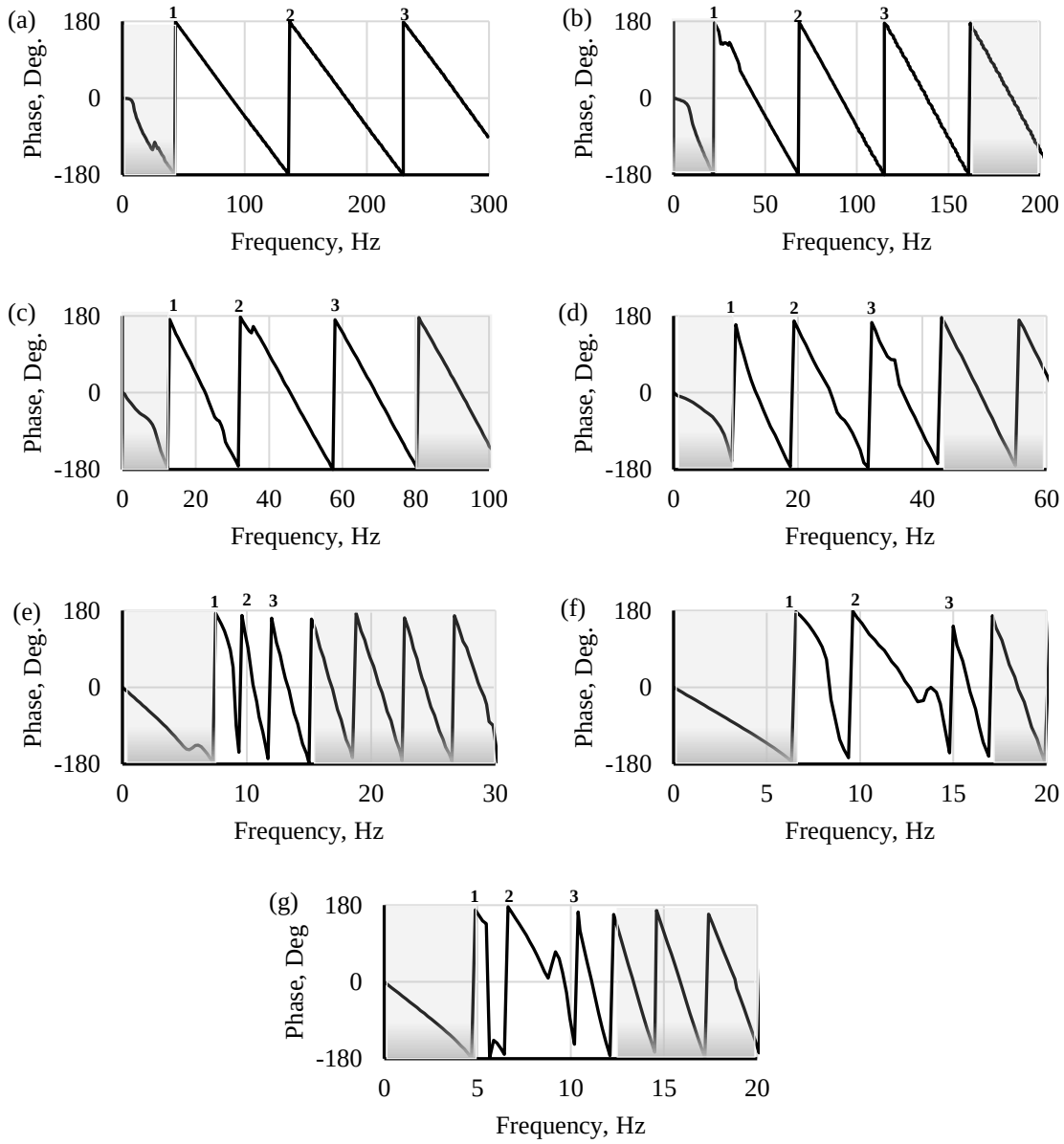

Figure D.3 Wrapped phase plots from simulated SASW measurements at Profile 5C with receiver spacings of (a) 2-2m, (b) 4-4m, (c) 8-8m, (d) 15-15m, (e) 30-30m, (f) 45-45m, and (g)60-60m. Phase unwrapping interpretation is indicated by number of 360° "jumps." Data not used in interpretation are indicated by shaded regions.

Vita

Mohammed Khan was born on July 31st, 1979, in Baghdad, Iraq. He was the youngest in a seven-child family. He studied his primary and secondary education in Baghdad. In 1997, he attended Baghdad University, and received his B.S. in Civil Engineering. Thereafter, Mohammed furthered his study in Baghdad University and, he received his M.Sc. degree in Geotechnical Engineering in 2005. Then, he worked as an assistant lecturer at Civil Engineering Department, Baghdad University on 2006. After that, he promoted to a lecturer at the same University.

In the fall of 2014, Mohammed began his Ph.D. study in the program of Geotechnical Engineering at the University of Missouri-Columbia, USA. He has been working on his dissertation research under the guidance of Prof. Brent L. Rosenblad since 2014 and passed his dissertation defense on December 3rd, 2020.